International Journal of Modern Engineering Research (IJMER)

International Journal of Modern Engineering Research (IJMER)

Contents :

An Inclusive Analysis on Various Image Enhancement Techniques

V. Hemalatha[1], P. B. Selvapriya[2], K. C. Maheswari[3]

[1,2,3] Assistant Professor, Department of CSE, N.S.N. College of Engineering and Technology, Karur, Tamilnadu, India

Abstract: *Digital Image enhancement is the process of adjusting digital images so that the results are more suitable for display or further image analysis. It provides a multitude of choices for improving the visual quality of images or to provide a "better transform representation for future automated image processing. The enhancement technique differs from one field to another field. The existing techniques of image enhancement can be classified into two categories: Spatial Domain and Frequency domain enhancement. Many images like satellite images, medical images, aerial images and even real life photographs suffer from poor contrast and noise. It improves the quality (clarity) of images for human viewing by eradicating blurs, noise, increasing contrast, and revealing image details.*
Keywords: *Geometric Corrections, Gray Scale Manipulation, Frequency based domain enhancement, Spatial based domain enhancement, Histogram Equalization.*

I. INTRODUCTION

Image enhancement is a process of enhancing the visual quality of images due to nonideal image acquisition process. It emphasizes and sharpens the image features for display and analysis. The aim of image enhancement is to improve the interpretability or perception of information in images for human viewers, or to provide `better' input for other automated image processing techniques. The enhancement doesn't increase the inherent information content of the data, but it increases the range of the selected features so that they can be detected easily. The major difficulty in image enhancement is quantifying the criterion for enhancement and therefore, a large number of image enhancement techniques are empirical and require interactive procedures to obtain satisfactory results.

II. IMAGE ENHANCEMENT

The principal objective of image enhancement is to process a given image so that the result is more suitable than the original image for a specific application. It enhances the image features such as boundaries, edges, or contrast to make a graphic display more helpful for analysis. Image enhancement methods can be based on either spatial or frequency domain techniques.

2.1 Spatial domain enhancement methods

Spatial domain techniques are performed to the image plane itself and they are based on direct manipulation of pixels in an image. The operation can be formulated as $g(x, y) = T[f(x, y)]$, where g is the output, f is the input image and T is an operation on f defined over some neighborhood of (x, y). According to the operations on the image pixels, it is separated into 2 categories: Point operations and spatial operations.

$$\text{Spatial domain } g(x, y) = f(x, y) * h(x, y) \quad \text{Equation}$$

2.2 Frequency domain enhancement methods

These methods enhance an image $f(x, y)$ by convoluting the image with a linear, position invariant operator. The 2D convolution is performed in frequency domain with DFT.

$$\text{Frequency domain } G(W_1, W2) = F(W_1, W2) \, H(W_1, W2)$$

2.3 Operations on Images

Point operations - each pixel is modified according to a particular equation that is not contingent on other pixel values. Mask operations - each pixel is modified according to the values of the pixel's neighbors Global operations - all the pixel values in the image are taken into consideration.

III. Image Enhancement Techniques

3.1 Filtering with morphological operators

Morphological image processing is a collection of non-linear operations related to the shape or morphology of features in an image, such as boundaries, skeletons, etc. Morphological techniques probe an image with a small shape or template called a structuring element. It is positioned at all possible locations in the image and it is compared with the corresponding neighborhood of pixels. Few operations test whether the element "fits" within the neighborhood, while others checks whether it "hits" or intersects the neighborhood. Morphological operations rely only on the relative ordering of pixel values, not on their numerical values, and therefore are especially suited to the processing of binary images. Fig. 1 and Fig. 2 shows that morphological operations can also be applied to greyscale images such that their light transfer functions are unknown and therefore their absolute pixel values are of no or minor interest.
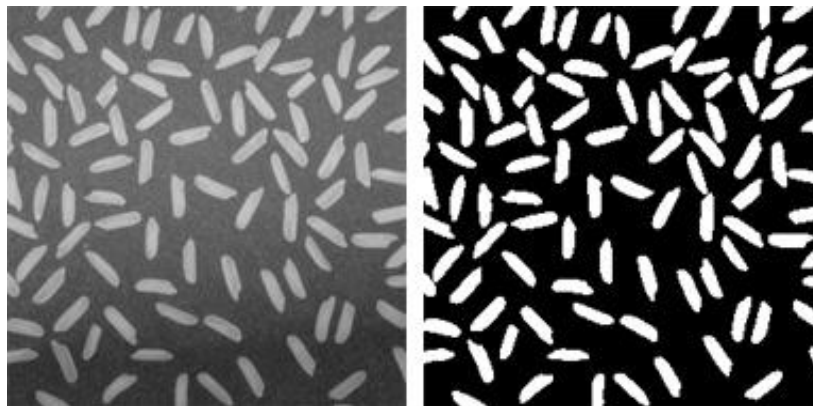
Fig. 1 Correcting nonuniform illumination with morphological operators

A - the structuring element fits the image

B - the structuring element hits (intersects) the image

C - the structuring element neither fits, nor hits the image

Structuring element
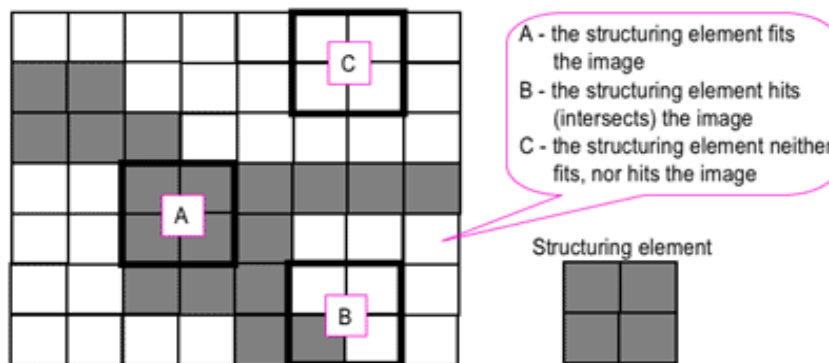
Fig. 2 Morphological filtering

3.2 Histogram equalization

Histogram equalization is a technique for adjusting image intensities to enhance contrast and it is depicted in Fig. 3 to Fig.6. Let f be a given image represented as a m_r by m_c matrix of integer pixel intensities ranging from 0 to L − 1. L is the number of possible intensity values. Let p denote the normalized histogram of f with a bin for each possible intensity. So

$$Pn = \frac{\text{number of pixels with intensity n}}{\text{total number of pixels}} \qquad \text{where n= 0, 1,..., L-1}$$

The histogram equalized image g will be defined by

$$g_{i,j} = \text{floor} \left((L-1) \sum_{n=0}^{f_{i,j}} p_n \right)$$

where floor() rounds down to the nearest integer. This is equivalent to transforming the pixel intensities, k, of f by the function

$$T(k) = \text{floor}\left((L-1) \sum_{n=0}^{k} p_n \right)$$

Fig. 3 Original Image
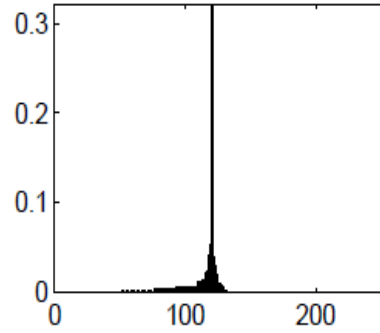
Fig. 4 Original Histogram

Fig. 5 Transformed Image
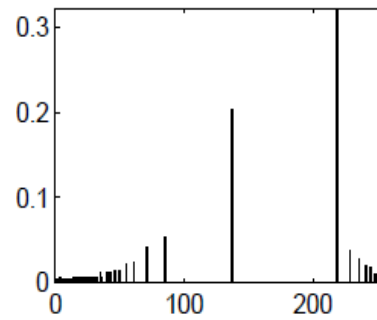
Fig. 6 Transformed Histogram

3.3 Noise removal using a Wiener filter

Wiener filter is the most important technique for removal of blur in images due to linear motion or unfocussed optics. Generally blurring due to linear motion in a photograph is the result of poor sampling. Each pixel in a photograph should represent the intensity of a single stationary point in front of the camera. If the shutter speed is too slow and the camera is in motion, a given pixel will be an amalgram of intensities from points along the line of the camera's motion as shown in Fig 7 to Fig. 10. This is a two-dimensional analogy to

$$G(u,v)=F(u,v).H(u,v)$$

where F is the fourier transform of an "ideal" version of a given image, and H is the blurring function.

Fig. 7 Original Image

Fig. 8 Blurred Image
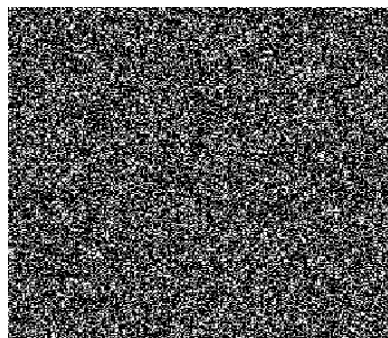
Fig. 9 Random gaussian noise

Fig. 10 Reconstructed photograph

3.4 Linear contrast Enhancement

Linear contrast enhancement, also referred to as a contrast stretching, linearly expands the original digital values of the remotely sensed data into a new distribution. The entire range of sensitivity of the display device can be utilized as shown in Fig. 11 by expanding the original input values of the image. It also makes subtle variations within the data more obvious. Such enhancements are best applied to remotely sensed images with Gaussian or near-Gaussian histograms and all the brightness values fall within a narrow range of the histogram and only one mode is apparent. The various types of linear contrast enhancement namely Minimum-Maximum Linear Contrast Stretch, Percentage Linear Contrast Stretch and Piecewise Linear Contrast Stretch.

In Minimum-Maximum Linear Contrast Stretch, the original minimum and maximum values of the data are assigned to a newly specified set of values that utilize the full range of available brightness values.

The Percentage Linear Contrast Stretch maps each grid cell value in the input raster image (z) onto a new scale that ranges from a lower-tail clip value (L) to the upper-tail clip value (U), with the user-specified number of total values (n), such that: $zn = (z - L) / (U - L) \times n$, where zn is the output value. The values of L and U are determined from the frequency distribution and the user-specified Tail clip value.

The Piecewise Linear Contrast Stretch involves the identification of a number of linear enhancement steps that expands the brightness ranges in the modes of the histogram. A series of small min-max stretches are set up within a single histogram. As piecewise linear contrast stretch is a very powerful enhancement procedure, image analysts must be very familiar with the modes of the histogram and the features they represent in the real world.
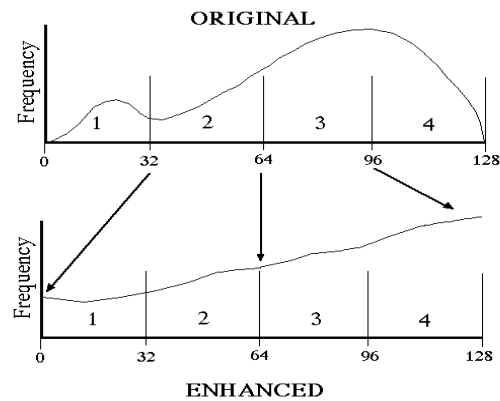
Fig. 11 Contrast Enhancement

3.5 Median Filtering

Median filtering is a nonlinear process useful in reducing impulsive or salt-and-pepper noise. It is also useful in preserving edges in an image while reducing random noise. Such noise can occur due to a random bit error in a communication channel. The median intensity value of the pixels within the window becomes the output intensity of the pixel being processed as the window slides along the image. Like lowpass filtering, median filtering smoothens the image and is thus useful in reducing noise. It preserves discontinuities in a step function and can smooth a few pixels whose values differ significantly from their surroundings without affecting the other pixels.

Figure 13 shows a 1-D sequence with two values that are significantly different from the surrounding points. Figures 14 and 15 show the result of a lowpass filter and a median filter, respectively.
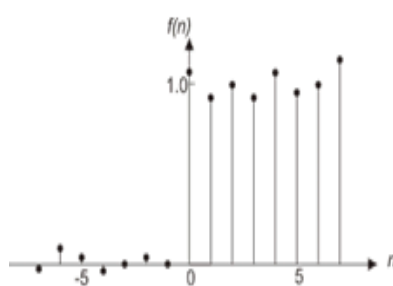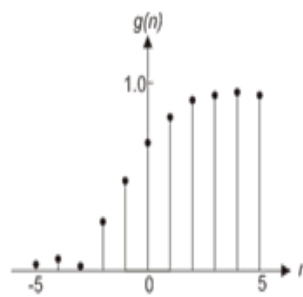
| **Fig. 12 1-D Sequence** | **Fig. 13 Lowpass filter** | **Fig. 14 Median filter** |
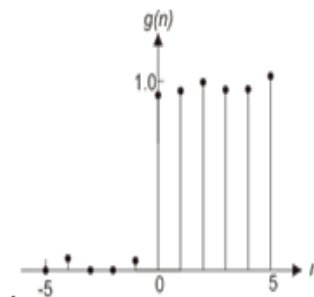
3.6 Unsharp mask filtering

The unsharp filter is a simple sharpening operator which derives its name from the fact that it enhances edges via a procedure which subtracts a smoothed or unsharp version of an image from the original image. It is commonly used in the photographic and printing industries for crispening edges. The unsharped mask is then combined with the negative image to create an image that is less blurry than the original. The resulting image may be a less accurate representation of the image's subject. It has parameters that allow it to have variable effect to affect the strong edges in the image, and to exclude the smoother low-contrast areas. The sharpening process works by utilizing a slightly blurred version of the original image. The resultant image is then subtracted away from the original to detect the presence of edges, creating the unsharp mask .Contrast is then selectively increased along these edges using this mask leaving behind a sharper final image.

Original Image	Blurred Copy	Unsharp Mask	Higher Contrast Original

Unsharp Mask	Original Image	Sharpened final Image
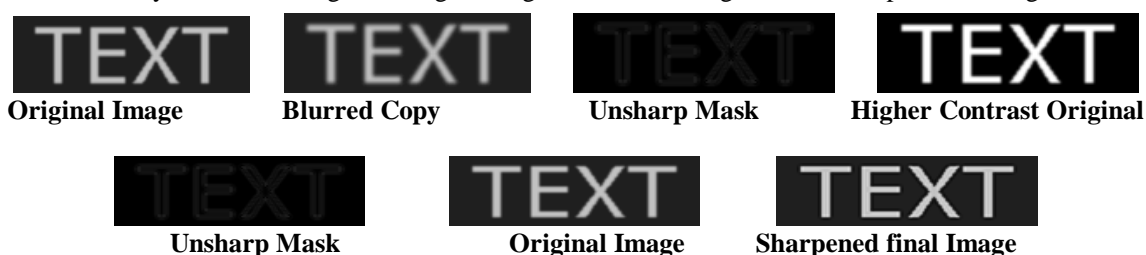
3.7 Contrast-limited adaptive histogram equalization (CLAHE)

CLAHE operates on tiles which are small regions in the image, rather than the entire image. The histogram of the output region approximately matches the histogram specified by the distribution parameter by enhancing each tile's contrast. Artificially induced boundaries are eliminated by combining neighboring tiles using bilinear interpolation. The contrast can be limited to avoid amplifying any noise that might be present in the image. It limits the amplification by clipping the histogram at a predefined value before computing the CDF. The value at which the histogram is clipped (clip limit) depends on the normalization of the histogram and thereby on the size of the neighborhood region.

3.8 Decorrelation stretch

Decorrelation Stretch is used to remove the high correlation commonly found in multispectral data sets and to produce a more colorful color composite image. The highly correlated data sets produce quite bland color images. It requires three bands for input. These bands should be stretched byte data or may be selected from an open color display. Its intended use is to highlight differences in an image that are too subtle for a human to see.

IV. CONCLUSION

In this paper, we present an image enhancement approaches based on the filtering with Morphological operators, Histogram equalization, Noise removal using a Wiener filter, Linear contrast Enhancement, Median Filtering, Unsharp mask filtering, Contrast-limited adaptive histogram equalization and Decorrelation stretch to enhance the quality of an image and help in better matching in any recognition systems. These approaches offer a wide variety of styles for modifying images to achieve visually acceptable images. The choice of such techniques is a function of the specific task, image content, observer characteristics, and viewing conditions.

REFERENCES

[1]. Feng Xiao, Mingquan Zhou, and Guohua Geng, "Detail Enhancement and Noise Reduction with Color Image Detection Based on Wavelet Multi-scale, 2011, pp. 1061-1064.
[2]. Y. He, J. Tang, X. Luo, and T. Zhang, "Image enhancement and minutiae matching in fingerprint verification," Pattern Recognition Letters, 24, 2003.
[3]. S. Greenberg, M. Aladjem, D. Kogan, I. Dimitrov "Fingerprint Image Enhancement using Filtering Techniques" submitted at Electrical and Computer Engineering Department, Ben-Gurion University of Negev, Israel.
[4]. A.K. Jain, A. Fundamentals of Digital Image Processing; Prentice Hall, 1989.
[5]. Bhabatosh Chanda and Dwijest Dutta Majumder, 2002, Digital Image Processing and Analysis.
[6]. R.W.Jr. Weeks, (1996). Fundamental of Electronic Image Processing. Bellingham: SPIE Press [3] A. K. Jain, Fundamentals of Digital Image.
[7]. R Hummel, "Histogram modification techniques", Computer Graphics and Image Processing, Vol. 4, pp. 209-224, 1975.

[8]. N. Netraveli and B. G. Haskell, "Digital Pictures: Representation and Compression," New York: Plenum, 1988.

[9]. Jinshan Tang Eli Peli, and Scott Acton, "Image Enhancement Using a Contrast Measure in the Compressed Domain", IEEE Signal processing Letters , Vol. 10, NO. 10, October 2003

[10]. 10.YunBo Rao and Leiting Chen, "An efficient contour let transform-based algorithm for video enhancement", Journal of

[11]. Information Hiding and Multimedia Signal Processing, vol. 2, no. 3, pp. 282-293, 2011.

[12]. 11. A. Nguyen, Y. P. Tan and Z. H. Chen, "On the method of multicopy video enhancement in transform domain", Proc. of the 16th IEEE International Conference on Image Processing, pp. 2777- 2780, 2009.

[13]. Scott E Umbaugh. 1998, Computer vision and image processing. Prentice Hall, NewJersey. p. 209.

[14]. Z. Chaofu, M. Li-ni, J. Lu-na ," Mixed Frequency domain and spatial of enhancement algorithm for infrared image", 2012 9th International Conference on Fuzzy Systems and Knowledge Discovery (FSKD 2012).

[15]. Raman Maini and Himanshu Aggarwal,"A Comprehensive Review of Image Enhancement Techniques", Journal of Computing, Vol. 2, Issue 3, March 2010, ISSN 2151-9617.

Bolted Joints Analysis Methods and Evaluation

G. Chaitanya[1], M. Kumara Swamy[2]

[1]*Mechanical engineering, UCEK (A)/Jawaharlal Nehru Technological University Kakinada, INDIA)*
[2]*Associate professor, Mechanical engineering, UCEK (A)/Jawaharlal Nehru Technological University Kakinada, INDIA)*

Abstract*: Calculation of accurate bolt forces is the primary requirement in many industries. All the theoretical calculations for bolt forces, includes many significant assumption based on idealized mechanical models. In this paper two models of flange joints were taken and analyzed forpretensionvariation due to internal temperature changes, And for theForces induced in the bolt due to the combined effect of external forces applied and internal temperature change. The results were utilized to gain insight into joint softening that arises from gradual, nonlinear opening of flange gap under external tension. Later these results were compared with the theoretical calculations, and our models allow relaxations for many assumptions in theoretical calculations.*
Keywords: *Bolt force,Heel gap, joint separation load, Pretension, Prying factor.*

I. Introduction

Industrial applications, structures are often uses the flange joints. The main objective of flange joint design is to provide adequate joint strength and stiffness and to minimize the fluctuating stresses induced in the bolted joint due to the thermal loads and external loads. Bolted joints are frequently analyzed using hand formulas that include many significant assumptions. In this paper, we evaluate several commonly used formulas by comparing their predictions to those of detailed finite element models. Our models allow the relaxation of many assumptions and enable a rational appraisal of these very important and widely used formulas. In addition, the FE results provide an understanding of the mechanics, which is just as important as the ability to make accurate predictions in specific cases.

The strength of the bolted joint is determined by analysis. Once the analysis is done it is clear that whether it is reaching the requirements or not. Based on the analysis results the changes have to be done in the design to increase the strength or stiffness of the joint. For the purpose of improvements to be done in the joint design, the bolt loads must be accurately calculated for the realistic design and service conditions.In this study, we analyze a bolt circle joining two flanges, to predict bolt load and joint stiffness for loads ranging up to the joint failure load. Thermal expansion is included. We compare the results from both analyses to those obtained from commonly used formulas

Using a detailed FE analysis for testing has advantages and disadvantages. The disadvantages are that the analysis may lack, or inadequately resolve, some significant effect present in the real hardware. The advantages are that the boundary conditions, material properties, geometry and loads can be precisely controlled, interesting quantities that may be impractical to measure can be recovered easily, and it is less expensive to obtain the insight that comes from observing a very large number of cases than it would be if testing were the sole approach. .
This section has two purposes:

1) to assess whether popular hand-calculation formulas for bolt and flange stiffness can be used to accurately predict the bolt load change due to thermal expansion, and
2) To gain insight into the joint mechanics when loads and displacements are perfectly axisymmetric, so that the lessons can be applied to the more realistic joint design shown.

The second purpose is arguably the more important, because bolt load changes due to thermal expansion are often only 10% or less of the total bolt load, which is of the order of typical pretension uncertainty. We study here a single, unconstrained joint consisting of a steel bolt-nut-washer set clamping two L shaped flanges of aluminum.

II. Nomenclature

Most symbols used in this document are defined below. In general, material and geometric properties are subscripted f for flange, b for bolt and nut, w for washer and m for the clamped members (flanges and washers) as a set.

P_{bolt}= bolt force,
P_{ini}= pretension given to the bolt,
P_{sep}= separation load of the joint,
Φ = joint stiffness ratio,
P_{ini}= initial pretension given to the bolt,
ΔP = change in the pretension,
k = stiffness,
δ = change in length,
ΔT = Change in the temperature,
f_{pyr} = Prying force
α = coefficient of thermal expansion
l = length,
A = cross section area,
E = young's modulus,
θ =compression frustumhalf-angle,
d = diameter of the bolt,
e_b =hole edge distance,
D = maximum diameter ofcompression frustum

III. Loads on the Bolted joint

A bolted joint is an assembly of bolt, nut, washers and flanges. In order to get the adequate joint strength pretension is to be applied on the bolt. Pretension compresses the washers, and flanges up to some extent. At the same time the pretension causes an elongation in the bolt. Pretension load is applied to the connection by stretching the fastener to a certain torque value. Torque is the turning moment of fastener or nut. Due to the many variables associated with the torque, a safety factor is calculated in determining torque value which will produce a pretension load lower than the yield point of that fastener.

Torque meter can be used to measure bolt tension. High pretension tension helps to keep joint tight, and increases the strength of a joint, and generates friction between parts to resist shear and improves the fatigue resistance of bolted connections. Generally 75% of proof strength is applied as the pretension. As a rule of thumb, the pretension should exceed the maximum load by 15% or so.

A realistic bolted joint, is subjected to thermal loads, external tensile or compressive forces. Bolted joints may be exposed to temperature changes of hundreds of degrees, as well as external loads. A change in temperature after fastener installation can induce significant stress when the bolt has a different coefficient of thermal expansion from the flanges.

The design considered here is bolt, nut and washers set made of structural steel, joining two flanges, the flanges were mounted or welded on shells circumference. However, first, the basic stiffness relationships between the fastener and the clamped material must be understood. The offset distance from the bolt centerline to the shell creates prying that obscures these basic relationships. External applied or constraint loads transmitted to the joint through the shells act at a distance from the bolt circle, tending to pry open the flanges rather than directly lifting them off one another. Even if the external load is aligned with the bolt axis using a fitting, the flanges will peel apart instead of gapping all at once, unless the fitting and flanges are unusually rigid relative to the bolt.

IV. Theoretical formulae

Most of theoretical analysis starts from an equation[1] of the form

$$P_{bolt}= \Phi P_{ext}+ P_{ini}+ \Delta P \qquad (1)$$

From the above equation (1) in the absence of external load the change in bolt length (in the grip) is equal to the sum of change in the lengths of washers and flanges. This leads to

$$\delta_b = \alpha_b l_b \Delta T + \frac{l_b}{E_b A_b}\Delta P \qquad (2)$$

$$\delta_f = \alpha_f l_f \Delta T - \frac{l_f}{E_f A_f}\Delta P \qquad (3)$$

$$\delta_w = \alpha_w l_w \Delta T - \frac{l_w}{E_w A_w}\Delta P \qquad (4)$$

From the equation (2), (3) and (4)

$$\delta_b = \delta_w + \delta_f$$

On solving the above

$$\Delta P = \frac{(2\alpha_f l_f + 2\alpha_w l_w - \alpha_b l_b)\Delta T}{\frac{l_b}{E_b A_b}+2\frac{l_f}{E_f A_f}+2\frac{l_w}{E_w A_w}} \qquad (5)$$

In the equation (1) Φ is the joint stiffness ratio. For the calculation of the stiffness several methods were proposed till now. Out of that we use two methods those are:

4.1 Method (1)

This method is from mechanical design textbook of Shigley:

I) Stiffness of any member[2] is:

$$k = \frac{AE}{l} \qquad (6)$$

II) Stiffness of a member in a bolted joint based on simple approach using fixed cone angle is[2]

$$k = \frac{\pi E_f d \tan\theta}{\ln \frac{(l_f \tan\theta + D - d)(D+d)}{(l_f' \tan\theta + D + d)(D-d)}} \qquad (7)$$

Using the equations (3) and (4)

$$A_f = \frac{\pi l_f d \tan\theta}{2\ln \frac{(l_f \tan\theta + D - d)(D+d)}{(l_f' \tan\theta + D + d)(D-d)}} \qquad (8)$$

4.2. Method (2)

This method is that of Juvinall, this is also based on compression frustum

$$A_f = \frac{\pi}{4} \left[\left(\frac{3 d_b \tan 30°}{2} \right)^2 - d_b^2 \right] \qquad (9)$$

$$k = \frac{\pi E}{4l} \left[\left(\frac{3 d_b \tan 30°}{2} \right)^2 - d_b^2 \right] \qquad (10)$$

The equation (1) is applicable when the line of action of forces coincides with the axis of the bolt. In this work the external load acting on the flanges. The line of action of forces is not coinciding with the axis of the bolt. Some prying is induced in the joint. For this purpose we modify the equation (1) by inserting the prying factor in the equation. Prying factor is a multiplier on the bolt force due to the offset bolt centerline.

$$P_{bolt} = \Phi f_{pry} P_{ext} + P_{ini} + \Delta P$$

$$= \frac{k_b}{k_b + k_f + \frac{2 k_b k_f}{k_w}} f_{pry} P_{ext} + P_{ini} + \Delta P \qquad (11)$$

$$f_{pyr} = \frac{\frac{t_f}{2} + w_b}{e_b} \qquad (12)$$

In actual joint, joint separation occurs gradually as the flanges peel apart starting at the heel. But in theoretical calculations separation occurs at all once.

$$P_{sep} = \frac{(P_{ini} + \Delta P)(k_b + k_f + \frac{2 k_b k_f}{k_w})}{f_{pyr}(k_f + \frac{2 k_b k_f}{k_w})} \qquad (13)$$

Once the theoretical value of bolt force reaches the P_{sep}, thus the bolt force is

$$P_{bolt} = \frac{k_b}{k_b + k_f + \frac{2 k_b k_f}{k_w}} f_{pry} P_{ext} + P_{ini} + \Delta P, \qquad P_{ext} \leq P_{sep}$$

$$P_{bolt} = f_{pry} P_{ext}, P_{ext} \geq P_{sep} \qquad (14)$$

V. Flange joint model

Actual bolted joints are many in types; here we are taking one common type of joint design is a flange connection between two cylindrical shells or housing. There are numbers on the circumference of cylinder in a cylindrical shell assembly. For the
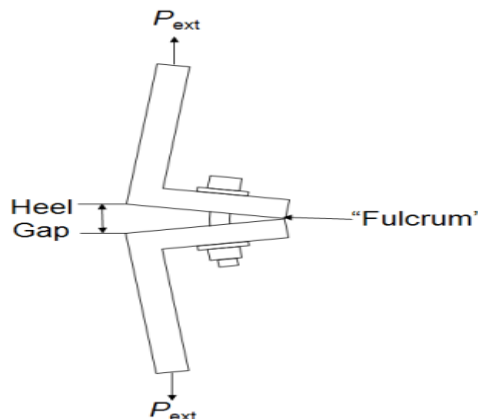

Figure (1): two dimensional model of flange joint assembly.

Analysis purposes it is sufficient to model one flange joint with carefully chosen boundary conditions. Here we have taken standard M10 bolt of class 9.8, and nut with pitch 1.5mm. Flanges are of L shape. The bolt, nut and washers are made of structural steel, and flanges are made of aluminum.

Table (1): material properties

Material	E	α	ϑ
Structural steel	2×10^{11} Pa	1.2×10^{-5} /°c	.3
Aluminum	0.71×10^{11} Pa	2.3×10^{-5} /°c	.33

Bolt and nut are modeled as per Metric Threads. The bolt belongs to class 9.8 the proof strength of bolt is 650 MPa, Yield strength is 720 MPa, and the tensile strength is 900 MPa.

VI.   Finite element analysis procedure
The detailed finite element analysis for a bolted joint presented is exemplified in the following phases:
• The first phase is modeling the joint using CREO software. The model geometry was generated using the same software and then imported as a neutral file in ANSYS WORKBENCH. Geometric details, such as chamfers, radii of connection have only a local influence on behavior of the structure.
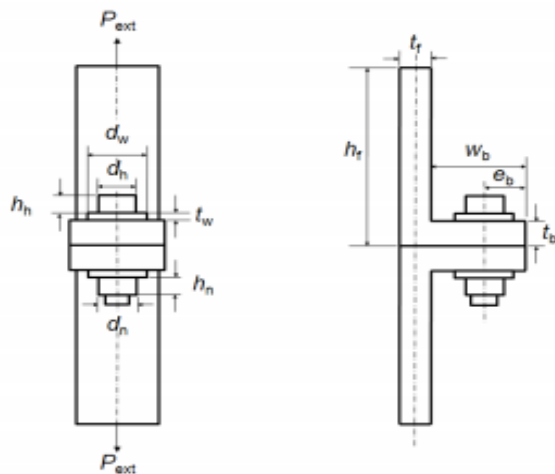
Figure (2): dimensions of the flange joint:

t_f	12.7mm	h_n	8.4mm
t_w	2.8mm	t_{ba}	12.7mm
w_b	31.3mm	h_f	100mm
w_b	31.3mm	e_b	15.65mm
h_h	6.85mm	d_b	10mm

.• Next, the prepared geometric structure is reproduced by finite elements. The finite elements are connected by nodes that make up the complete finite element mesh. Each element type contains information on its degree-of-freedom set (e.g. translational, rotational, thermal), its material properties and its spatial orientation (1D-, 2D-, 3D-element types). The mesh was controlled in order to obtain a fine and good quality mapped mesh. The assembly had 23519 nodes and 12714 elements.
• In order to solve the resulting system equation, boundary and loaded conditions are specified to make the equation solvable. These flanges were given an axial load, bolt was given a pretension of 28275 N, and total joint was subjected to a thermal load 110°c. Pretension is applied in Z axis direction.
• The last phase is interpreting the results.
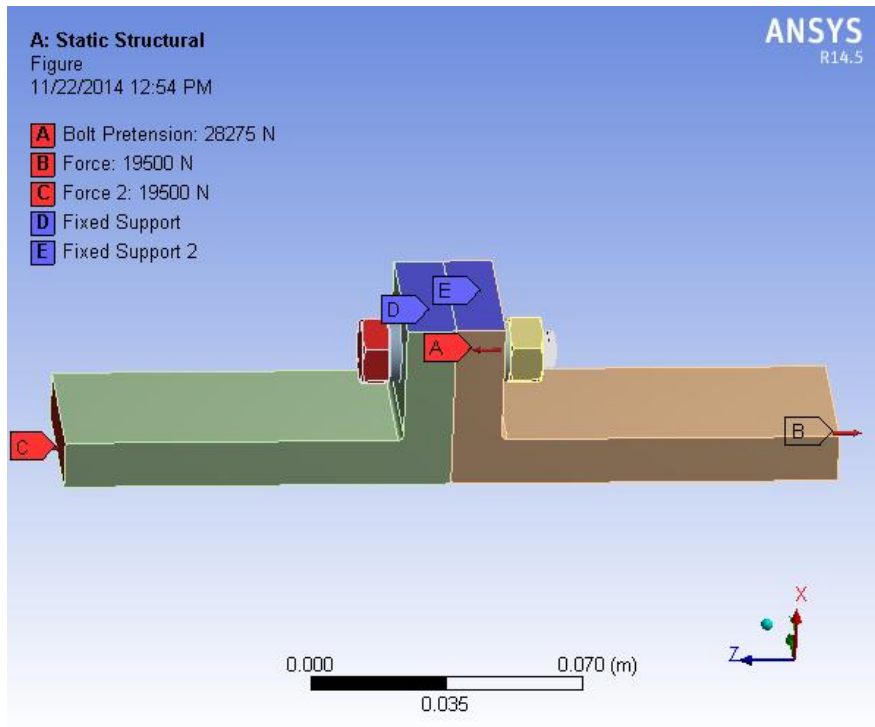
Figure (3): loads and supports given on long flange joint assembly.
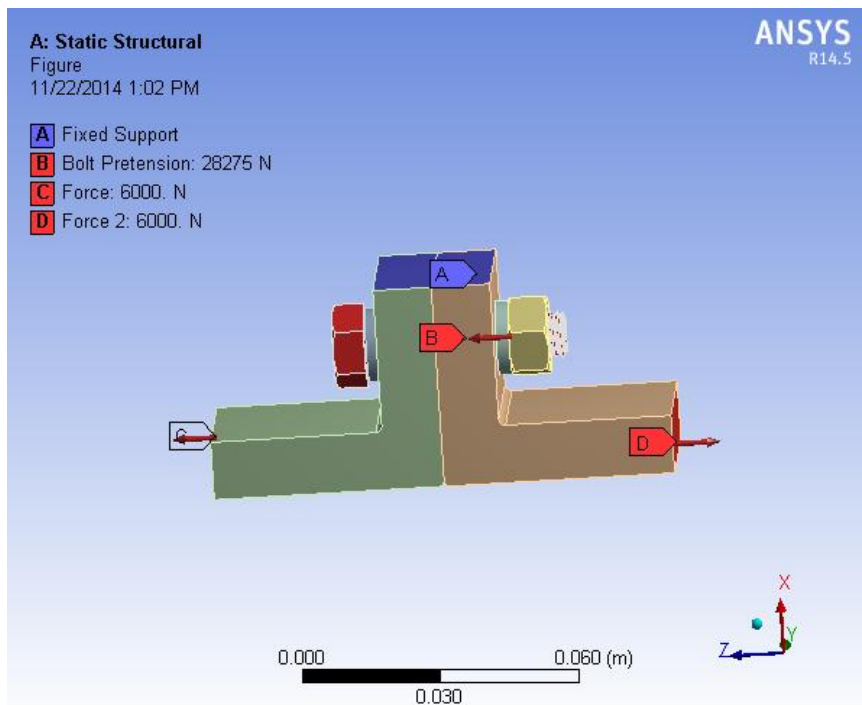
Figure (5): loads and supports given on short flange joint assembly.

VII. Results

Fig.(6) shows that results were plotted for short flange assembly bolted joint. The plot is for bolt forces versus external load for an initial pretension of 28275 N. It is clear from the plot, external load reaches near to the given pretension value, Bolt force reaches the yield strength of bolt. After this bolt forces crosses the elastic limit, that is yield criteria, the joint behavior after yielding is beyond the limitations of this study.
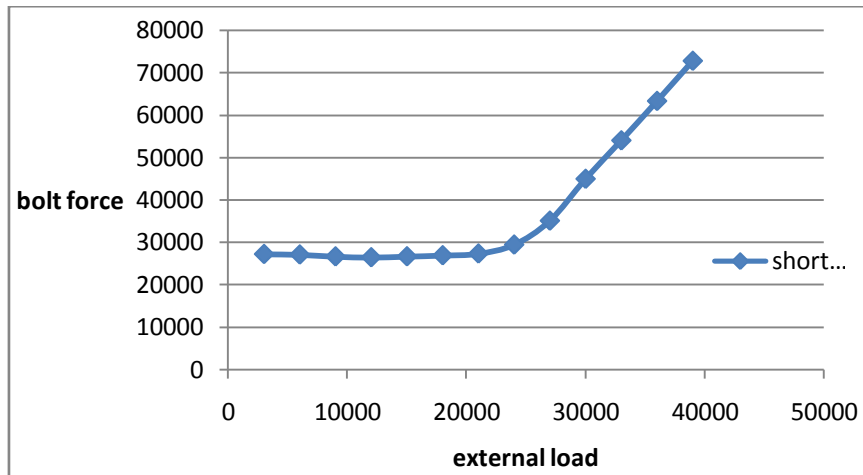
Figure (6): bolt force developed for external load in short flange model assembly

Fig.(7) shows the results of long flange assembly. From the graph it is clear that the bolt forces increases gradually unlikely in the theoretical calculations. In the Fig.(8) the bolt forces of short and long flange were compared for the purpose of better design of joint. From the graph it is very clear that there is no much difference in the bolt forces induced in the short and long flanges.
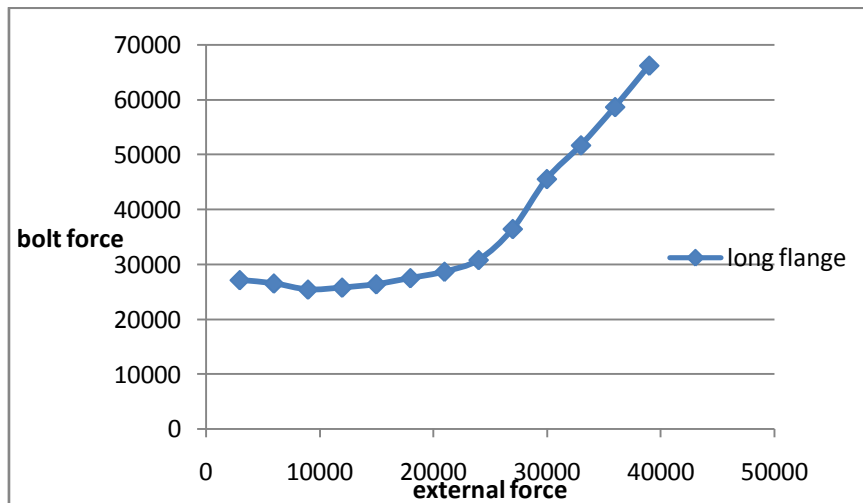
Figure (7): bolt force developed for external load in long flange model assembly**.**
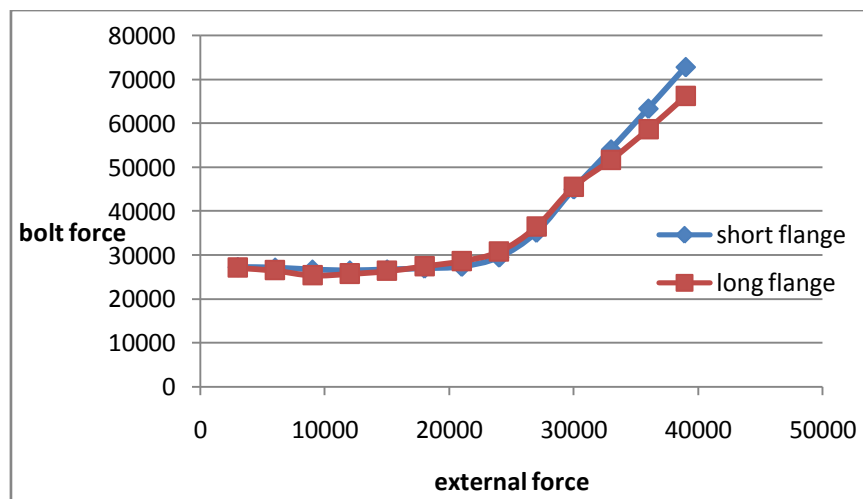
Figure (8): comparison of bolt forces developed in long and short flange assembly models.

The theoretical calculations method (1), and method (2), was used to find bolt forces. Later on the results of theoretical calculations and finite element analysis were compared. The comparison is shown in the fig.(9) and fig.(10) and it was showing that the theoretical calculations estimate a sudden change in the slope of the bolt forces curve. That sudden change in the slope of the curve, which is at the joint separation load of 19000 N. there is a steep increase in the curve with a slope of 2.405. Where as in the finite element analysis results slope of the curve is lesser than the theoretical value. It is observed thatthe theoretical values are 10 to 20% greater than the FEM results.

It is very difficult to measure the pretension applied on bolt, so there may be lot of uncertainties in applying the pretension to the bolt. If any pretension uncertainty exists in the joint, the hand calculations may over predict or lesser estimates the bolt force. This study calculated the bolt forces with hand formulae, for a pretension of $\pm25\%$ to the actual value. At the same time finite element analysis was also conducted for a pretension of $\pm25\%$ to the actual value.Both finite element analysis and theoretical calculations were compared. Comparisons were shown in Fig.(11) and Fig.(12). The observations are stating that the increase in the pretension tends to overestimate the bolt force.
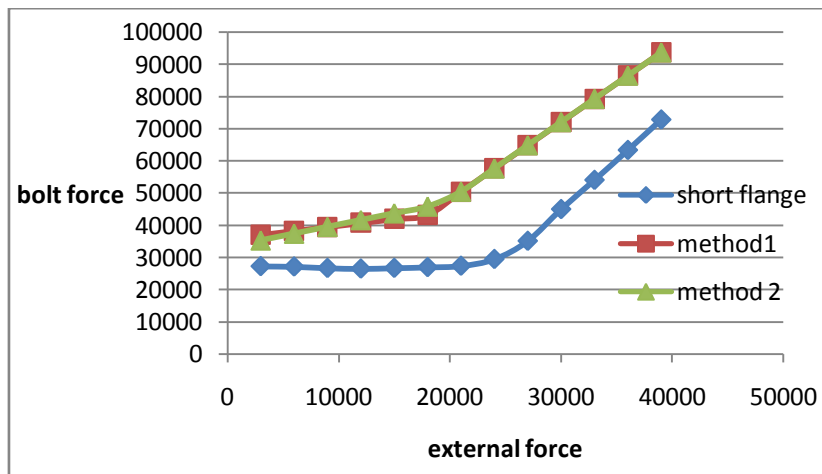
Figure (9): comparison of bolt forces developed in long and short flange assembly models with theoretical calculations method (1) and (2).
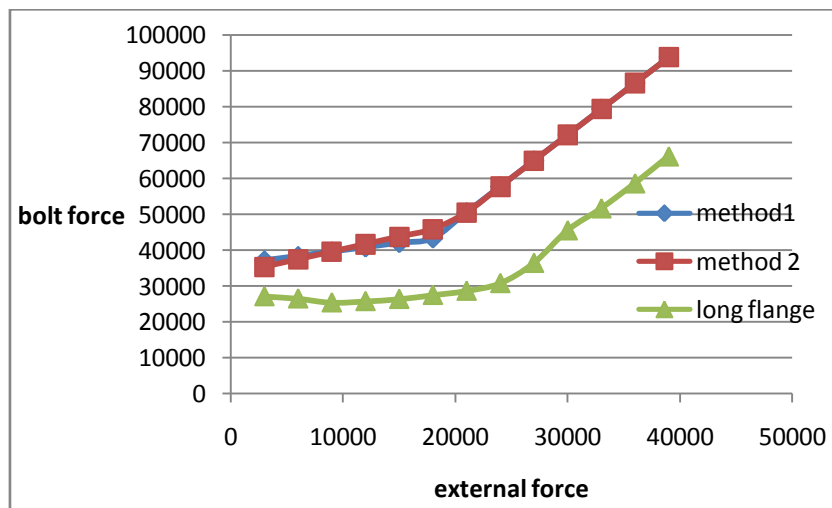
Figure (10): comparison of bolt forces developed in long flange assembly models with theoretical calculations method (1) and (2).

From the observations it was clear that the theoretical values were giving a closer fit to the finite element analysis results if the prying factor is reduced. It was shown in the Fig.(13) that a lesser prying factor value gives a closer fit to the finite element analysis values.
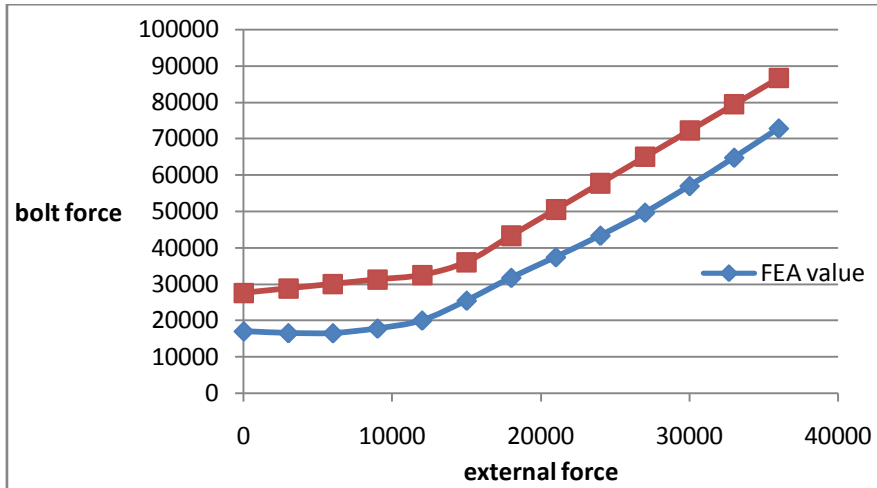
Figure (11): comparison of bolt forces developed in long flange assembly models with method 1 for the pretension value of 20000N.
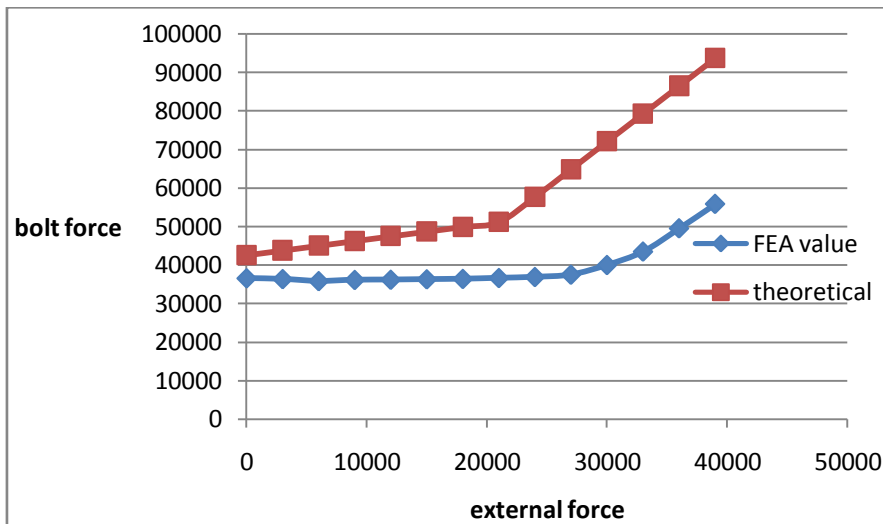
Figure (12): comparison of bolt forces developed in long flange assembly models with method 1 for the pretension value of 35000N.
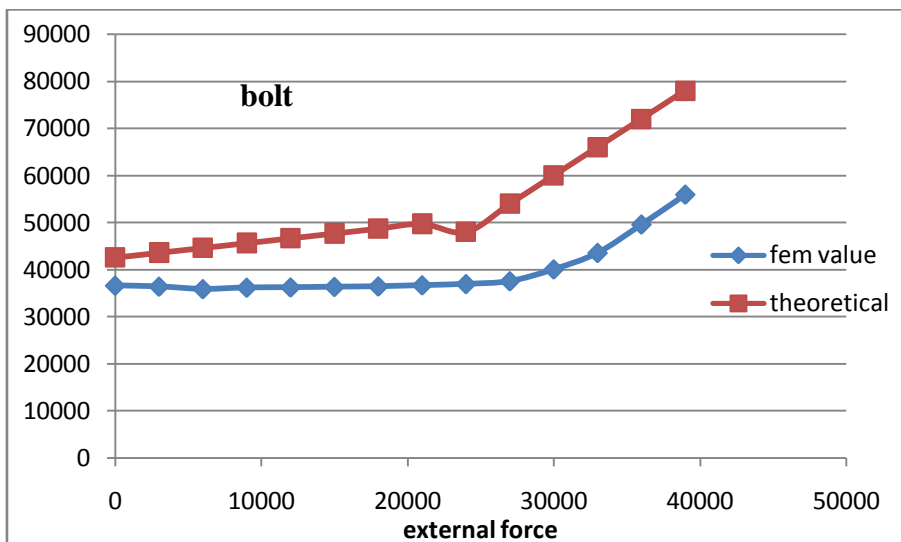
Figure (13): comparison of theoretical values with prying factor 2 to the finite element analysis values.

VIII. Conclusions

1) Theoretical calculations shows that the initial pretension applied is not having any effect on the calculation of change in the pretension due to the temperature change.
2) It is clear from the results plot; increase in the pretension increases the amount of overestimate of bolt forces.
3) Length of the flange does not have any effect on the bolt force estimation either in theoretical calculations or in the finite element analysis results.
4) Decreasing in the prying factor in the theoretical calculations gives a closer fit to the theoretical and experimental values.
5) Stiffness of the total joint is based on the initial geometry in the theoretical approach. But when the joint starts separating stiffness decreases with increase in the heel gap.
6) Because there are many assumptions in the theoretical calculations, theoretical calculations are overestimating the results up to 10-20% of actual values, for the complicated design of flange joints.

REFERENCES

[1]. "Mechanical engineering design" Shigley.
[2]. "Mechanics of materials" Punmiabc.
[3]. Anonymous, \Space Shuttle: Criteria for Pretensioned Bolts," Tech. Rep. NSTS 08307 Rev. A, NASA, Houston, 1998.
[4]. "An Evaluation of Common Analysis Methods for Bolted Joints in Launch Vehicles"51st AIAA/ASME/ASCE/AHS/ASC Structures, Structural Dynamics, and Materials Conference
18th,12 - 15 April 2010, Orlando, Florida.
[5]. "FINITE ELEMENT ANALYSIS OF BOLTED JOINT" Iuliana PISCAN, Nicolae PREDINCEA, Nicolae POP
[6]. "Engineering Fundamentals of Threaded Fastener Design and Analysis" RS Technologies, a Division of PCB Load & Torque, Inc.
[7]. Juvinall, R. C. and Marshek, K. M., Fundamentals of Machine Component Design , Wiley, 2000

OPEN ACCESS

Effect of process parameters on material removal rate during grinding of hot work steel AISI H11 under dry, wet and compressed gas environment

Deepak Kumar[1], Dr. Sanjeev Saini[2]

[1]*Department of Mechanical Engineering, M.Tech Scholar, DAVIET Jalandhar, India.*
[2]*Department of Mechanical Engineering, DAVIET, Jalandhar, India.*

Abstract: *Grinding can be described as a multi-tooth metal cutting operation in which material is generally removed by shearing and ploughing in the form of micro sized chips by the abrasive grits of the grinding wheel. This paper presents an important investigation of material removal behaviour during grinding of hot work steel AISI H11 under different working environments (dry, wet cooling and compressed gas) and process parameters (feed rate, depth of cut and wheel speed). During the experimental investigation, Aluminimum oxide grinding wheel was used to perform cutting action. It was observed that under compressed gas, increase in depth of cut and decrease in feed rate resulted in significant increase in material removal rate.*
Keywords: *Environment, Depth of cut, Feed rate, Grinding, Material removal rate.*

I. Introduction

There are several processes of manufacturing machining operations, i.e., drilling, milling, turning and grinding processes that are important for the conversion of raw materials into finished goods. Most of these processes deal with giving a new shape and form to the raw materials either by changing their state or shape. One such important process is grinding, and it is very useful technique for metal removal at fast rates and for the high level finishing of final products. Grinding is typically a finishing process where quality is important and mistakes are costly. In order to attain high quality parts and high productivity it is necessary to properly choose the correct process parameters. These parameters are usually determined through testing and experience. Grinding is a material removal and surface generation process used to shape and finish components made of metals and other materials. Grinding employs an abrasive product, usually a rotating wheel brought into controlled contact with a work surface. The grinding wheel is composed of abrasive grains held together in a binder. These abrasive grains act as cutting tools, removing tiny chips of material from the work. As these abrasive grains wear and become dull, the added resistance leads to fracture of the grains or weakening of their bond. The dull pieces break away, revealing sharp new grains that continue cutting.

Grinding has been the object of technical research for some decades now. Walton et. al.[1] have used Physical vapor deposition (PVD) coating method on low carbon steel(51CrV4) work piece with CBN grinding wheel for accurate temperature measurements even under aggressive grinding condition and environment. The obtained result shows that high pressure grinding fluid does not influence the coating performance. The temperatures estimated by the PVD-coating technique have been used to validate thermal models based on the circular arc heat source for varying specific materials removal rates. Kwak et. al.[2] presented the experimental setup to analyze effectively the grinding power and the surface roughness of the ground workpiece in the external cylindrical grinding of hardened SCM440 steel using the response surface method. The experimental results show the mathematical model. From adding simply material removal rate to the contour plot of these mathematical models, it was seen that useful grinding conditions for industrial application could be easily determined. Monici et. al. [3] have explained the concept of optimized cutting fluid application method to improve the efficiency of the process and show that combine use of neat oil and CBN wheel give better efficiency than aluminium oxide grinding wheel. Xu et. al. [4] have investigated the experimental procedure for vitreous bond silicon carbide wheel for grinding of silicon nitride. The result shows that silicon carbide grinding wheel can be used for precision form grinding of silicon nitride to achieve good surface integrity. Badger [5] has researched on the factor affecting the grindability of high speed steel(HSS) by measuring G-ratio and power consumption in surface grinding with an aluminium oxide wheel. It was found that dominant factor affecting grindability in HSS is the size of the vanadium carbides. Guo et. al. [6] have studied the effect of both wheel wear and process parameters on the grinding performance of plated CBN wheel on a nickel alloy to obtain particular model. Liu et. al. [7] have researched the stringent requirements for grinding wheels include low damage on ground surfaces, self-dressing ability, consistent performance, long wheel lives and low prices to

manufacture the silicon wafers. Anderson et. al. [8] have developed a model to predict the contact temperature with using infrared data. The infrared data showed that with increasing depth of cut numerical models were more accurate than analytical model. The obtained results suggest that use of analytical contact zone thermal model should be limited to shallow grinding while numerical models are more suited to larger depth of cut and result also showed higher Peclet number in grinding results in lower overall workpiece temperature.

Atzeni [9] et. al. have developed experimental setup to test the influence of cutting speed and feed per gain on surface roughness after grinding cycle. The observed data have been statistically processed to obtain relationship between among roughness and kinematic parameters. The obtained model shows that the roughness is mainly influenced by the feed per grain and to a lesser degree by the cutting speed. Aurich [10] et. al. have found experimental investigation of dry grinding operations of hardened heat preheated steel and then obtain data compared with wet grinding operation which is taken as reference prototype. Tawakoli et.al. [11] have investigated the effect of ultrasonic vibration on dry grinding and obtained result show that the application of ultrasonic vibration can eliminate the thermal damage on workpiece, increase the G-ratio and decrease the grinding force considerably. Nguyen [12] have investigated the performance of new segmented grinding wheel system and observed that segmented grinding wheel gives better surface integrity with minimum use of coolant as compared to standard wheel.

Brinksmeier [13] et. al. have investigated elastic bonded wheels for a grind-strengthening and super finished surface in a single step. Further, to achieve a high mechanical impact and to minimize the thermal effect of grinding process require a low cutting speed and showed that if chip thickness is constant, the chip formation mechanism shifts towards micro-ploughing and thus additionally increases the specific grinding energy. Fathallah [14] et. al. have investigated for better surface integrity of AISI D2 steel by using sol-gel grinding wheel and cooling by liquid nitrogen comparatively with conditions using aluminium oxide and cooling with oil-based. Ronald [15] et. al. have studied on the influence of grinding wheel bond material on the grindability of metal matrix composites. The obtained result showed that resin bonded wheel performed better than electroplated wheel. Herman [16] et. al. have researched radial wear of super hard grinding wheels in the process of internal grinding of bearing rings. The new developed grinding wheel is designed for bonding the abrasive grains of sub microcrystalline boron nitride using a glass-ceramic bond. This grinding wheel is compared to CBN grinding wheels composed from ceramic bonding system for roughness profile on the wheel working surface and the wear resistance. Vijayender singh [17] et. al. have developed experimental setup for grinding the composite ceramic material with cryogenic coolant. The observed result showed that cryogenic coolant (ecofriendly) in grinding gives better surface quality of material.

Ramdatti [18] et. al. have applied the Taguchi techniques to obtain an optimal setting of grinding process parameters resulting in an optimal value of material removal rate and surface roughness when machining EN-8, EN-39 and cast iron. Demirci [19] et. al. have investigated the influence of nature of bond on surface edge finishing. Experimental results showed that the grinding forces vary sensitively with bond type and wheel velocity. Using diamond grain's wheel, it was found that roughness level obtained with metallic bond is lower than that obtained with resin bond. Using a resin-bonded wheel, two mechanisms of material removal were revealed according to grain's type. (i) A partial ductile regime, i.e., ductile streaks and brittle fracture, obtained with diamond grains, and (ii) a fully ductile regime obtained with SiC grains. It was found that ground surface obtained using SiC grains' wheel has a better roughness than that obtained using diamond grains wheel. Besides, SiC grains seem to lead to more marked streaks and form defects. Demir [20] et. al. investigated influences of grain size and grinding parameters on surface roughness and grinding forces. The results showed that grain size significantly affected the grinding forces and surface roughness values.

Increasing grain size and depth of cut increased the grinding forces and surface roughness values. Pil-Ho [21] et. al. have researched grinding process for surface roughness, grinding force and tool wear. It was observed that at low air temperature decrease the magnitude of grinding force and tool wear significantly, which could result in loner tool life. Mane [22] et. al. have developed experimental setup to study for surface finish enhancement of grinding process using compressed air. From developed experimental study it is observed that, the use of air helps to improve the surface finish of machined surface. Kadirgama [23] et.al. have discussed the optimization of cylindrical grinding when grinding carbon steel (AISI 1042) and effect of three variables (work speed, diameter of workpiece and depth of cut) towards surface roughness with aluminium oxide as grinding wheel. It was found that work speed is the most dominant factors on the Ra, followed by the diameter of workpiece and depth of cut respectively. Ondrej Jusko[24] has investigated that least appropriate material for grinding wheels for cutting 14109.6 bearing steel is CBN with Aluminium oxide grains; Abral and SG grinding wheels are more suitable. A comparison of the two innovative abrasive materials shows that the performance of abral is slightly superior. Deepak pal [25] et. al. applied Taguchi parametric optimization technique to study the optimization of grinding parameters for minimum surface roughness. It was observed that surface roughness decreases as material hardness increases. It also decreases with increase in speed and changing grain size from G46 to G60, but increases changed to G80. Manimaran [26] et. al. have researched the experiment on the

grinding of AISI 316 stainless steel under dry, wet and cryogenic cooling with Alumina(SG) grinding wheel. It has been concluded that with increasing depth of cut under cryogenic cooling, the surface roughness was decreasing as compared to dry and wet cooling. Grinding force and grinding zone heat temperature also obtained less under cryogenic cooling mode.

II. Experimental Procedures

The H-11 hot work steel plate blank has been heated to a temperature of 1025^{0}C with half an hour soak time followed by quenching in a 500^{0}C hot salt bath. It was then tempered in two cycles with maximum temperature of 450^{0}C and 2 hours of soak time to obtain a final hardness of 45 HRC. Hot work AISI H11 steel have been chosen because of high hardness, excellent wear resistance, hot toughness and good thermal shock resistance properties and have wide application in die and hot-work forging, extrusion, helicopter rotor blades and shafts. The chemical composition of H11 is given in Table I.

Table I: Chemical composition of AISI H11 steel (wt %)

Constituent	C	Si	Mn	P	S	Cr	Mo	V
Composition (In %)	0.35	0.92	0.4	0.011	0.026	5.10	1.30	0.6

The same Aluminimum oxide grinding wheel was used throughout the work. Its specification was "AA46/54 K5 V8" and it was manufactured by Carborundum universal limited company. The wheel dimensions were 200 x 13.31 x 75mm. The grinding experiments were conducted on AISI H11 hot work tool steel under the three different environments of dry, wet and compressed gas. In gas environment, the compressed Nitrogen gas supplied at the grinding zone at an appropriate distance of 45 mm approximately from the cutting zone. The pressure of the compressed gas delivered to the cutting zone is maintained to fix at 3 bar in all gases environmental experiments. And, in wet grinding cooling consists of 20% coolant oil in water, applied directly at the inter-face of grinding wheel–work material at 6.5l/min. For dry grinding there is no coolant is used. The work piece material, H-11 hot die steel with 304 mm $\times$ 110 mm $\times$ 24 mm size was used and the cuts were made widthwise. During the experiments, cuts were made of 110mm length.

The schematic diagram for experimental setup is shown below in figure I. A digital weighing machine was used to measure the weight of work piece before and after each cut of grinding. To investigate the parameters of grinding, In this experimental procedure 27 Nos. of experiments by combining most robust set of different four parameters each having three levels. The different sets of combinations are obtained by as per Taguchi's L27 orthogonal array from Minitab software. The combinations of parameters with different levels are given below in table II.

Figure I: Schematic arrangement for experimental setup
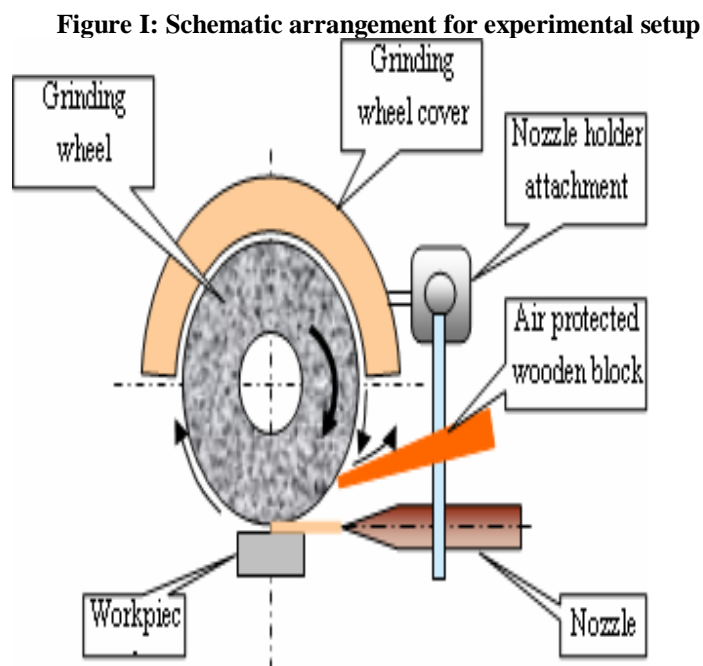
Table II: Process parameters with their values at 3 levels.

Parameters designations	Process parameters	Level-1	Level-2	Level-3
A	Environment	Dry	Wet	Gas
B	Wheel speed (rpm)	1000	1500	2000
C	Feed Rate (mm/min)	5	10	15
D	Depth of cut (mm)	0.1	0.2	0.3

As mentioned in table III, in this experimental setup total 27 Nos. of experiments have been performed on surface grinding machine. During each experiment the various parameters and its level combination are obtained as per Taguchi's L27 orthogonal array. The various levels of parameters are combined during every experiment are shown below table III.

Table III: No. of experiments (Taguchi L$_{27}$ (3^4) orthogonal array)

Exp. No.	A:Environment	B: Wheel speed (rpm)	C: Feed Rate (mm/min)	D: Depth of cut (mm)	MRR (gm/min)
1	Dry	1000	5	0.1	0.059
2	Dry	1000	10	0.2	0.363
3	Dry	1000	15	0.3	0.285
4	Dry	1500	5	0.2	0.571
5	Dry	1500	10	0.3	0.273
6	Dry	1500	15	0.1	0.095
7	Dry	2000	5	0.3	0.428
8	Dry	2000	10	0.1	0.090
9	Dry	2000	15	0.2	0.143
10	Wet	1000	5	0.1	0.095
11	Wet	1000	10	0.2	0.454
12	Wet	1000	15	0.3	0.143
13	Wet	1500	5	0.2	0.182
14	Wet	1500	10	0.3	0.571
15	Wet	1500	15	0.1	0.047
16	Wet	2000	5	0.3	0.909
17	Wet	2000	10	0.1	0.238
18	Wet	2000	15	0.2	0.285
19	Gas	1000	5	0.1	0.095
20	Gas	1000	10	0.2	0.600
21	Gas	1000	15	0.3	0.272
22	Gas	1500	5	0.2	0.800
23	Gas	1500	10	0.3	0.272
24	Gas	1500	15	0.1	0.095
25	Gas	2000	5	0.3	0.800
26	Gas	2000	10	0.1	0.091
27	Gas	2000	15	0.2	0.238

III.   Results And Discussions

Figure II: Main Effect Plot of S/N ratios for MRR
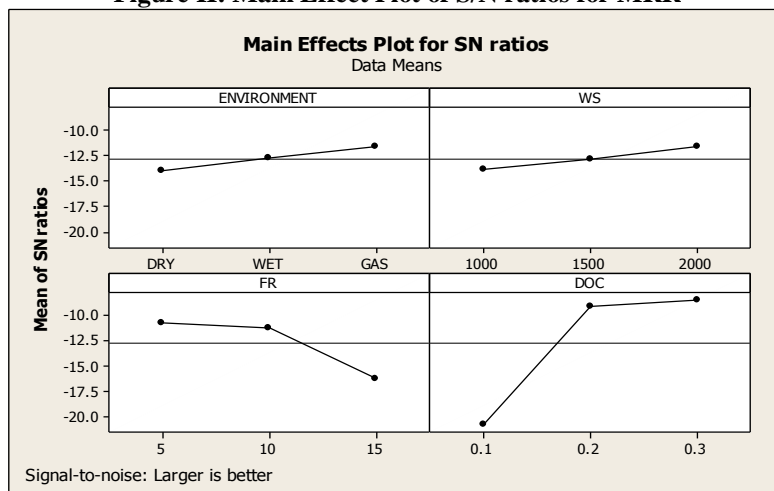
Figure III: Interaction plot of means for MRR (Larger is better)
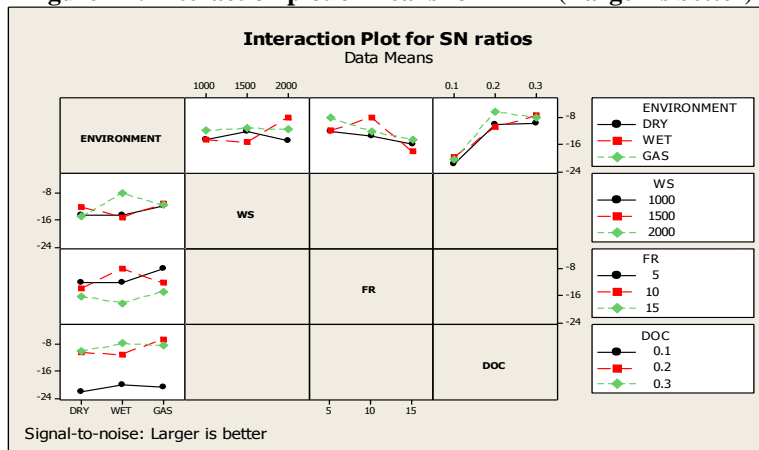
The input parameters like feed rate (FR), depth of cut (DOC), wheel speed (WS) and environment of work interface zone have considerable effect on material removal rate. Table IV and Figure II demonstrate the factor effect on material removal rate. The higher signal to noise ratio, the more favorable is the effect of the input variable on the output. The graph shows that, the optimum value levels for higher material removal rate are at a feed rate 5 mm/min, depth of cut 0.3 mm and grinding wheel speed of 2000 rpm in case of compressed gas environment. From response table V for signal to noise, it can be seen that the most influencing parameter to material removal rate for AISI H11 is depth of cut (DOC) then workpiece feed rate then followed by compressed gas environment and grinding wheel speed (WS). The fig. IV(a) shows that with increase in feed rate there is decrease in MRR, fig. IV(b) shows that compressed gas environment is more significant for MRR than wet and dry environment. Fig. IV(c) and fig. IV(d) also shows that increase in wheel speed and depth of cut result in increase in material removal rate.

Figure IV: Variations in the material removal rate with (a) Feed rate (b) Environment i.e. dry, wet cooling and compressed gas (c) Wheel speed (d) Depth of cut
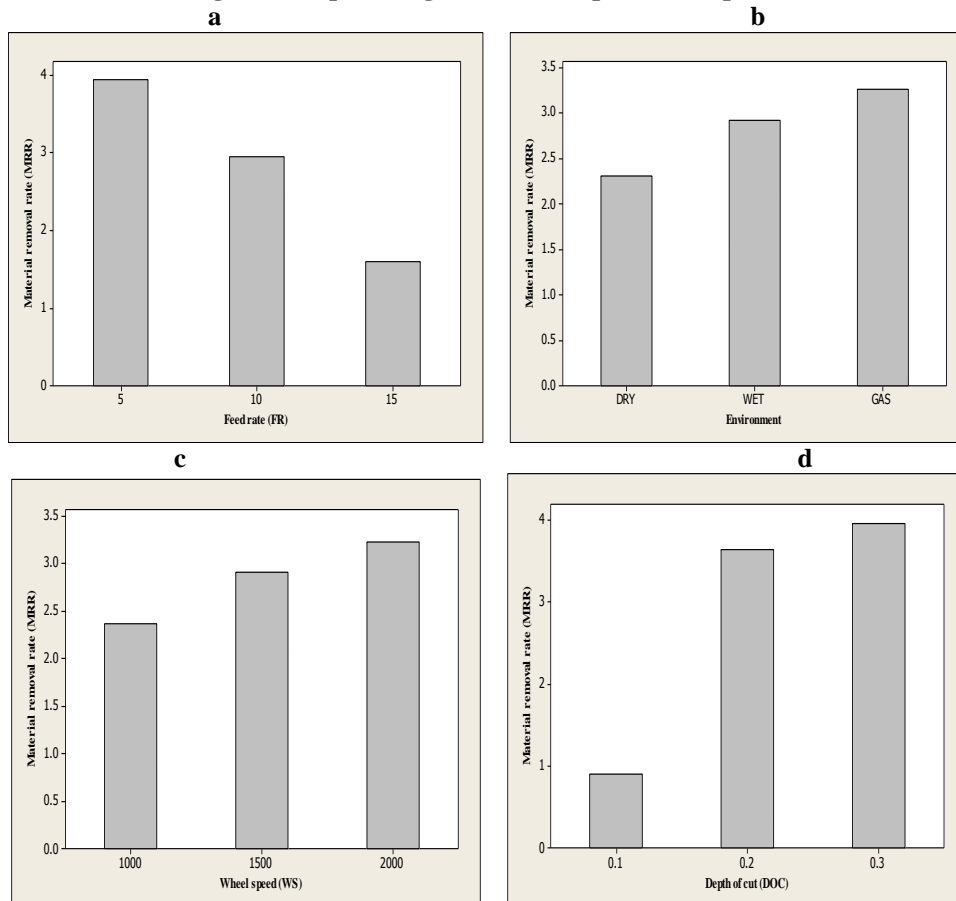
Table IV: Analysis of variance for S/N ratios (MRR)

Source	DF	Seq SS	Adj SS	Adj MS	F	P	%C
ENVIRONMENT	2	24.45	24.45	12.223	0.58	0.590	1.75
WWHEEL SPEED (WS)	2	22.64	22.64	11.319	0.54	0.611	1.62
FEED RATE (FR)	2	167.11	167.11	83.555	3.95	0.080	11.94
DEPTH OF CUT (DOC)	2	862.26	862.26	431.131	20.38	0.002	61.60
ENVIRONMENT *WS	4	92.07	92.07	23.019	1.09	0.440	6.58
ENVIRONMENT *FR	4	76.21	76.21	19.052	0.90	0.518	5.45
ENVIRONMENT *DOC	4	27.95	27.95	6.988	0.33	0.848	1.99
Residual Error	6	126.92	126.92	21.153			9.07
Total	26	1399.61					

Table V: Response Table for Signal to Noise Ratios - Larger is better (MRR)

Level	Environment	WS	FR	DOC
1	-14.006	-13.853	-10.802	-20.792
2	-12.736	-12.945	-11.306	-9.107
3	-11.679	-11.623	-16.313	-8.522
Delta	2.338	2.230	5.511	12.270
Rank	3	4	2	1

Table IV presents ANOVA results for MRR. It can be seen that the depth of cut is the most important factor affecting material removal rate. Its contribution is 61.60%. The second factor influencing material removal rate (MRR) is workpiece feed rate. Its contribution is 11.94%. For the wheel conditioning i.e., environment in which wheel was used, its contribution is 1.75%. The interaction *ENVIRONMENT×WS* is most significant. Its contribution is 6.58%. The interactions *ENVIRONMENT ×FR* and *ENVIRONMENT ×DOC* are not much significant compared to interaction *ENVIRONMENT ×FR* and their contributions are 5.45% and 1.99% respectively.

IV. Conclusion

In this paper the effect of grinding work zone environment i.e., dry, wet cooling and compressed gas and different process parameters on AISI H11 hot work steel were investigated. Experiments were carried out on the grinding of AISI H11 hot work steel with the Aluminimum oxide grinding wheel. The major conclusions from the investigation are as follows:

1. It was observed that higher material removal rate obtained under compressed gas environment than wet and dry environment, when grinding AISI H11 hot work steel under the same working parameters.
2. It was observed that depth of cut and feed rate were the most dominant factor to obtain higher MRR as compared to work zone environment condition and grinding wheel speed.

REFERENCES

[1] Walton I.M., Stephenson D.J. (2006),"The measurement of grinding temperatures at high specific material removal rates" International Journal of Machine Tools & Manufacture, vol.46, pp.1617–1625.
[2] Kwak Jae, Sim Sung (2006),"An analysis of grinding power and surface roughness in external cylindrical grinding of hardened SCM440 steel using the response surface method", International Journal of Machine Tools & Manufacture, 46, pp.304–312.
[3] Monici Rodrigo Daun, Bianchi Eduardo Carlos (2006),"Analysis of the different forms of application and types of cutting fluid used in plunge cylindrical grinding using conventional", International Journal of Machine Tools & Manufacture,46, pp. 122–131.
[4] Xu L.M., Shen Bin, (2006),"Vitreous bond silicon carbide wheel for grinding of silicon nitride", International Journal of Machine Tools & Manufacture, vol. 46, pp. 631–639.
[5] Badger J. (2007),"Grindability of Conventionally produced and powder-metallurgy high-Speed Steel", Annals of the CIRP, Vol. 56, pp.353-356.
[6] Guo C., Shi Z., Attia H. (2007),"Power and wheel wear for grinding nickel alloy with plated CBN wheels", Annals of the CIRP, Vol. 56, pp.343-346.
[7] Liu J.H., Pei Z.J. (2007),"Grinding wheels for manufacturing of silicon wafers: A literature review", International Journal of Machine Tools & Manufacture, vol. 47, pp. 1–13.
[8] Anderson D., Warkentin A. (2008),"Comparison of numerically and analytically predicted contact temperatures in shallow and deep dry grinding with infrared measurements", International Journal of Machine Tools & Manufacture, vol.48, pp.320–328.
[9] Atzen E. , Iulian L. (2008),"Experimental study on grinding of a sintered friction material", journal of materials processing technology, vol.196, pp.184-189.
[10] Aurich J.C., Herzenstiel P. (2008),"High-performance dry grinding using a grinding wheel with a defined grain pattern", CIRP Annals-Manufacturing Technology, vol. 57, pp. 357–362.

[11] Tawakoli Taghi, Azarhoushang Bahman (2008),"Influence of ultrasonic vibrations on dry grinding of soft steel", International Journal of Machine Tools & Manufacture, vol.48, pp.1585– 1591.

[12] Nguyen T., Zhang L.C. (2009),"Performance of a new segmented grinding wheel system", International Journal of Machine Tools & Manufacture, vol. 49, pp.291–296.

[13] Brinksmeier E., Heinzel C. (2009),"Superfinishing and grind-strengthening with elastic bonding system", Journal of Materials Processing Technology, vol.209, pp. 6117–6123.

[14] Fathallah Brahim Ben, Fredj Nabil Ben (2009),"Effects of abrasive type cooling mode and peripheral grinding wheel speed on the AISI D2 steel ground surface integrity", International Journal of Machine Tools & Manufacture, vol.49, pp.261–272.

[15] Ronald B. Anand, Vijayaraghavan L. (2009),"Studies on the influence of grinding wheel bond material on the grindability of metal matrix composites", Materials and Design, vol.30, pp. 679–686.

[16] Herman Daniela (2009),"Influence of vitrified bond structure on radial wear of CBN grinding wheel", International Journal of Machine Tools & Manufacture, vol.49, pp.231–242.

[17] Singh Vijayender, Ghosh S. (2010),"Grindability Improvement of Composite Ceramic with Cryogenic Coolant", Proceedings of the World Congress on Engineering 2010' Vol II, ISSN: 2078-0966 (Online).

[18] Ramdatti J.L., Popat M.A. (2010),"Some study aspect of external cylindrical grinding machine parameters using Taguchi techniques", International journal of manufacturing technology and industrial engineering (IJMTIE), vol. 1, pp.13-18.

[19] Demirci, Mezghani S., Mkaddem A., Mansori M. (2010),"Effects of abrasive tools on surface finishing under brittle-ductile grinding regimes when manufacturing glass, Journal of Materials Processing Technology, vol. 210, pp. 466–473.

[20] Demir Halil, Gullu Abdulkadir, Ciftci Ibrahim, Ulvi Seker (2010),"An Investigation into the influences of grain size and grinding parameters on surface roughness and grinding forces when grinding", Journal of Mechanical Engineering, vol.56, pp. 447-454.

[21] Lee Pil Ho, Lee S.W. (2011),"Experimental characterization of micro-grinding process using compressed chilly air", International Journal of Machine Tools & Manufacture, vol.51, pp.201–209.

[22] Mane A.B., Jadhav V.S. (2012),"Surface roughness enhancement of grinding process using Compressed air in case of dry machining", Indian journal of applied research, Vol. 2, pp.53-55.

[23] Kadirgama K., Rahman M. M. (2012),"A surrogate modelling to predict surface roughness and surface texture when grinding AISI 1042 carbon steel", Scientific Research and Essays, Vol.7 (5), pp.598-608.

[24] Jusko Ondrej (2012),"New abrasive materials and their influence on the surface quality of bearing steel after grinding", Acta Polytechnica, Vol. 52, pp.80-82.

[25] Pal Deepak, Bangar Ajay, Sharma Rajan, Yadav Ashish (2012),"Optimization of Grinding Parameters for Minimum Surface Roughness by Taguchi Parametric Optimization Technique", International Journal of Mechanical and Industrial Engineering (IJMIE), ISSN No. 2231 –6477, Vol.1.

[26] Manimaran G., Kumar M. P. (2013),"Effect of cryogenic cooling and sol–gel alumina wheel on grinding performance of AISI316 stainless steel", Archives of civil and mechanical engineering, vol.13, pp.304–312.

Thermodynamic properties and modeling of sorption isotherms for longer storage of *Urtica urens* leaves

A. Lamharrar[1], A. Idlimam[2], M. Cherkaoui[3], L. Lahnine[4], M. Kouhila[5]

[1,2,3,4,5,]*Laboratory of Solar Energy and Medicinal Plants, Ecole Normale Supérieure, Cadi Ayyad University, Marrakesh, Morocco.*
[4]*Equipe de Recherche d'Innovation de Développement Durable en Chimie Verte, Faculté des Sciences semlalia, Cadi Ayyad University, Marrakesh, Morocco*

Abstract: *Moisture equilibrium data of Urtica urens leaves by desorption and adsorption were determined at 30, 40, and 50°C. The isotherms were determined by a static gravimetric method for various temperature and humidity conditions. Five mathematical models were used to fit the experimental data. A nonlinear least-squares regression program was used to evaluate the constants of the five desorption and adsorption isotherm models GAB and Modified Halsey models were adequate to describe the sorption characteristics of the samples. Isosteric heats of desorption and adsorption were calculated by applying the Clausius-Clapeyron equation to the sorption isotherms at different temperatures. It decreased with increasing moisture content. We recognized the linear relation exists between the enthalpy and entropy of the sorption reaction.*

Keywords: enthalpy, entropy, hysteresis, mathematical models, sorption isotherm.

I. INTRODUCTION

The homeopathic remedy *Urtica urens* leaves is prepared using the entire herb known as annual nettle, while it is in blossom and is used to treat a number of health conditions, especially nettle rash or hives. Commonly known as dwarf nettle, annual nettle or small nettle, *Urtica urens* is a semi-woody plant belonging to genus *Urtica* that grows annually. Traditionally, people have been using this herb as a medication for skincare as well as alleviate skin inflammation or itchiness. In effect, scientists have especially studied the herb *Urtica urens* for its potential in supporting the skin when external irritants result in certain complaints [1].

The medicinal and aromatic plants have a great importance for both the pharmaceutical industry and the traditional. The stability of a dehydrated medicinal plant is influenced by its water activity. This stability is mainly a consequence of the relationship between the equilibrium moisture content and its corresponding water activity. Knowledge of the sorption properties of foods is of great importance in medicinal plant, especially in the quantitative approach to the prediction of the shelf life of dried medicinal plant. Equations for modeling water sorption isotherms are of special interest for many aspects of medicinal plant preservation by dehydration.

In this study, temperatures of 30°C, 40°C, and 50°C were chosen, to typify tropical storage conditions. Using an experimental approach, the equilibrium curves are determined by the saturated salt solution method. The experimental sorption curves are described by five different models to identify the most appropriate mathematical model for a better description of the product equilibrium state: GAB's model, modified Henderson's model, modified Halsey's model, modified Oswin's model. Then, we investigate from the experimental data the water activity optimal for the storage of *Urtica urens*.

Further analysis of sorption isotherm data by application of thermodynamic principals can provide information regarding differential enthalpy or the isosteric heat of sorption and differential entropy. Differential enthalpy of sorption gives an indication of the amount of bound water existing in the product. The differential entropy of material is proportional to the number of its available sorption sites at a specific energy level [2]. Subsequently we determine the thermodynamic functions (differential enthalpy, differential entropy). Moreover, we recognized the linear relation exists between the enthalpy and entropy of the sorption reaction.

II. MATERIALS AND METHODS

2.1 Experimental procedure

The plant *Urtica urens* used in our study was collected at Tahanouat, Marrakesh Morocco. The hygroscopic equilibrium could be achieved by a dynamic or static method. In the present work, a static method

is used [3]. The method is based on the use of saturated salt solutions to maintain a fixed relative humidity Rh. The mass transfers between the product and the ambient air are assured by natural diffusion of the water vapour. The atmosphere surrounding the product has a fixed relative humidity for every working temperature imposed on the system.

Six salts were chosen { KOH, (MgCl$_2$, 6H$_2$O), K$_2$CO$_3$, NaNO$_3$, KCl and (BaCl$_2$, 2H$_2$O)} so as to have a range of water activity of 0.0572-0.0898 [4]. The experimental apparatus consisted of six glass jars of 1 liter each with an insulted lid. Every glass jar was filled to quarter depth with a saturated salt solution. Duplicated samples each of 0.4 g (±0.0001g) for desorption and 0.1 g (±0.0001g) for adsorption were weighed and placed into the glass jars. The weight recording period was about 3 days. This procedure continued until the weight was constant. The equilibrium moisture content of each sample was determined in a drying oven at 105 °C for 24 h. The hygroscopic equilibrium *Urtica urens* leaves was reached in then days for desorption and eighth days for adsorption.

2.2 Modelling equations

The relationship between equilibrium moisture content, water activity, and temperature for *Urtica urens* leaves was predicted in literature by several mathematical models [5]. In our study five models have been applied: GAB's model, modified Henderson's model, modified Chung-Pfost model, modified Halsey model, and modified Oswin's model. The equations expressing those models are given below in table 1. X_{eq} represents equilibrium moisture content (%MS); a_w water activity; A, B, and C coefficients, dependant to the temperature or not, to determine by smoothing the experimental curves of sorption and θ the temperature in °C. The correlation coefficient (r) was one of the primary criteria for selecting the best equation to fit the four models to the experimental data. In addition to r, the statistical parameters mean relative error (MRE) as a percentage was used to determine the quality of the fit [6]. Levenberg-Marquardt nonlinear optimization method using appropriate software is used for the calculation of model coefficients that describe the equilibrium curves and their statistical parameters: the correlation coefficient (r) and mean relative error (MRE).

$$r = \sqrt{\frac{\sum_{i=1}^{N}\left(Xeq_{i,pred} - \overline{Xeq}_{i,exp}\right)^2}{\sum_{i=1}^{N}\left(Xeq_{i,exp} - \overline{Xeq}_{i,exp}\right)^2}} \qquad (1)$$

$$MRE = \frac{100}{N}\sum_{i=1}^{N}\left|\frac{Xeq_{i,exp} - Xeq_{i,pred}}{Xeq_{i,exp}}\right| \qquad (2)$$

Where:

$Xeq_{i,exp}$ i[th] Experimental moisture content (%d.b)

$Xeq_{i,pred}$ i[th] Predicted moisture content (%d.b)

N   number of data points.

d.b   dry basis

Table 1: Mathematical models used in our study

Model's name	Expression of the model	References
GAB	$X_{eq} = \dfrac{A\,B\,C\,a_w}{[1-B\,a_w]\,[1-B\,a_w + B\,C\,a_w]}$	[7]
Modified Henderson	$X_{eq} = \left[\dfrac{-\ln(1-a_w)}{A(\theta + B)}\right]^{1/c}$	[8]
Modified Chung-Pfost	$a_w = \exp\left[\dfrac{-A}{\theta + B}\exp(-CX_{eq})\right]$	[9]
Modified Halsey	$X_{eq} = \left[\dfrac{(-\exp(A + B.\theta)}{\ln(a_w)}\right]^{(1/c)}$	[10]
Modified Oswin	$X_{eq} = (A + B.\theta)\left[\dfrac{a_w}{1-a_w}\right]^{C}$	[11]

2.3 Determination of the optimum conditions for storage

The study of the sorption isotherms enables us to know the optimal relative equilibrium moisture for the conservation of a product as well as the water content of equilibrium to reach at the end of the drying. Also, it affords users with accurate information on how to handle a product during storage and conservation [12]. For this purpose, the optimal water activities of conservation (a_{wop}) were dogged. The whole of the experimental points is gathered on the same graph. Then, we model the isotherm of sorption by a polynomial equation of the third degree. The part closes to horizontality corresponds to the zone of better stability of the product. This process of calculation consists in making a polynomial decomposition of the equilibrium moisture content X_{eq}, for the whole of the experimental results, according to the water activity. This makes it possible to calculate the value for which the derivative second of X_{eq} is cancelled "inflection point" and consequently optimal relative humidity for conservation.

2.4 Differential enthalpy and differential entropy of sorption

The differential enthalpy or isosteric heat of sorption (ΔH_d) indicates the state of absorbed water by the solid material. The net isosteric heat of sorption (Δh_d) represents the quantity of energy exceeding the heat of vaporization of water (ΔH_{vap}) associated with the sorption process.

$$\Delta h_d = \Delta H_d - \Delta H_{vap} \tag{3}$$

The net isosteric heat of sorption can be calculated from the experimental data using the Clausius-Clapeyron equation [13]:

$$\left[\frac{d(\ln a_w)}{d(1/T)} \right]_{X_{eq}} = \frac{-\Delta h_d}{R} \tag{4}$$

This relation requires determining the isotherms at various temperatures in order to calculate the variation logarithmic curve of the water activity according to the reverse of the temperature, for a water content fixed. However, starting from the modified equations, it is possible to obtain the analytical expression of the heat of sorption Δh_d. This approach assumes that isosteric heat ΔH_d does not vary with the temperature [14]. The relationship between the net isosteric heat Δh_d and the differential entropy ΔS_d of sorption is given by:

$$(-\ln a_w)_{X_{eq}} = \frac{\Delta h_d}{R.T} - \frac{\Delta S_d}{R} \tag{5}$$

The experimental sorption isotherm data was plotting in the form of $\ln(a_w)$ versus $\frac{1}{T}$ for specific moisture content (X_{eq}). We determined Δh_d from the slope $\left(\frac{\Delta h_d}{R} \right)$ and ΔS_d from the intercept $\left(\frac{\Delta S_d}{R} \right)$. Applying this at different moisture contents allowed determining the dependence on Δh_d and ΔS_d.

2.5 Enthalpy-Entropy Compensation Theory

According to the theory of compensation, the linear relationship between the enthalpy Δh_d and the entropy ΔS_d for a specific reaction are given by:

$$\Delta h_d = T_\beta.\Delta S_d + \Delta G_\beta \tag{6}$$

The isokinetic temperature (T_β) is a characteristic property of the food surface whose dimension is absolute temperature. It represents the temperature to which all the reactions of the series proceed to the same rate. The free energy (ΔG_β) provides a criterion to evaluate if the process of the water sorption is spontaneous ($-\Delta G_\beta$) or not ($+\Delta G_\beta$). This process is repeated for several values of equilibrium relative humidity with an aim of underlining the relation between the differential entropy of sorption and the equilibrium moisture content of the studied product. The isokinetic temperature (T_β) and constant (ΔG_β)

were calculated using linear regression. The isokinetic temperature T_β represents the slope of the linear function between the differential entropy and the differential enthalpy of sorption [2].

III. RESULTAS AND DISCUSSION

3.1 Adsorption and desorption isotherms

The equilibrium moisture content increases with decreasing temperature at constant water activity (Fig 1). The sorption isotherms present the characteristic S-shaped curve (Type II), typical of sorption isotherms of many plants and food materials [3, 4, 5].
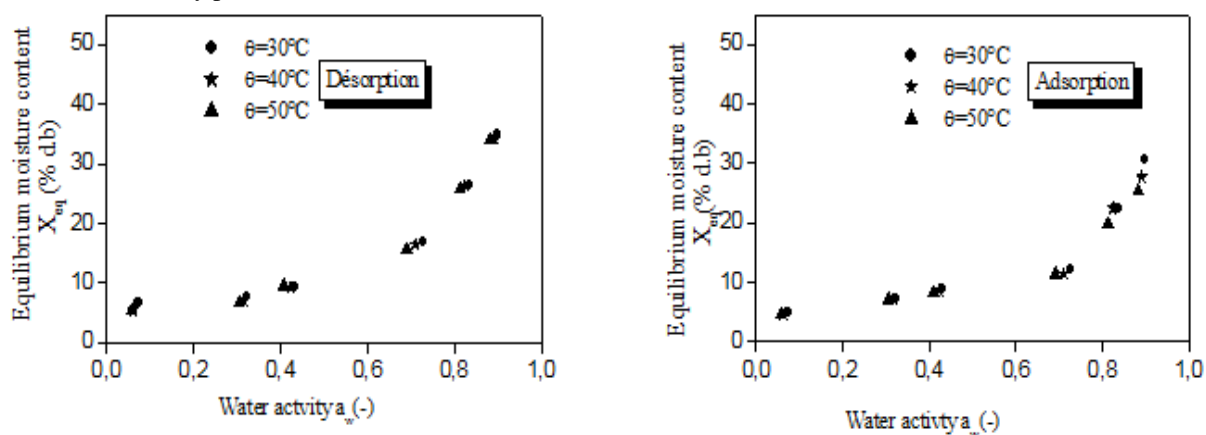
Fig. 1: Sorption isotherms of *Urtica urens* leaves at 30, 40 and 50°C

The presentation of adsorption and desorption experimental data in the same plot show that the plant does not have the same hygroscopic equilibrium behaviour (fig 2). The phenomenon of desorption-adsorption is irreversible. For the same constant relative moisture, the water content of desorption is higher than that of adsorption. Indeed, there exists a phenomenon of hysteresis. This characteristic is visible for *Urtica urens* plant.
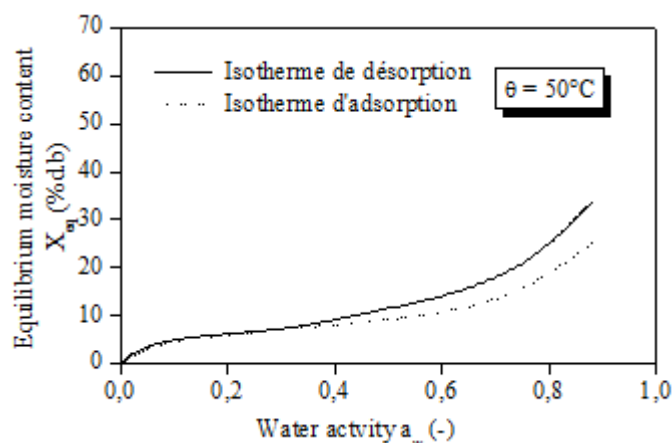
Fig.2: Sorption hysteresis phenomenon of *Urtica urens* leaves

Several hypotheses have been put to explain hysteresis. One of it is an analogy with a sponge. When the pores do not contain any more water, adsorption does not make it possible to recover the totality of initial water since this one imprisons air in the pores. Another hypothesis states that hysteresis in the sorption isotherm is a consequence of variation in the fraction of bound water present in the adsorption and desorption processes. The bound fraction being always larger on desorption than on adsorption [15].

3.2 Modelling of sorption experimental data

The results of non linear regression analysis of fitting the sorption equations to experimental data of *Urtica urens* leaves was at three temperatures are presented in Tables 2 and 3. For all the models tested, parameters A, B and C are found to be temperature dependent. For desorption isotherms, GAB model is found

---

to be the best estimator for predicting the equilibrium moisture of the *Urtica urens* leaves. This model gives the highest correlation coefficient (r) of 0.9989 and mean relative error MRE (2.7865 %) at θ = 40 °C. For adsorption isotherms, modified Halsey model is found to be the best estimator for predicting the equilibrium moisture of *Urtica urens* leaves. This models gives the highest (r) of 0.9918 and the MRE (2.8321 %) at θ = 50°C.

Table 2: Estimated model coefficients, r, MRE of five equation model fitted to desorption isotherm of *Urtica urens* leaves

Model's name	θ (°C)	A	B	C	r	MRE (%)
GAB	30°C	0.9365	151.7891	5.5773	0.9986	2.1527
	40°C	**0.9803**	**46.7567**	**7.3417**	**0.9989**	**2.7865**
	50°C	0.9485	112.8598	5.6501	0.9975	3.0121
Modified Henderson	30°C	0.0039	-17.4841	1.1021	0.9697	4.3719
	40°C	0.0023	-15.9677	1.0599	0.9791	6.7184
	50°C	0.0018	-19.4031	1.0534	0.9775	5.6338
Modified Chung-Pfost	30°C	124.4991	8.49	0.1105	0.9472	8.7143
	40°C	124.0871	9.6501	0.0633	0.9411	15.2637
	50°C	146.5175	-3.1678	0.1068	0.9492	13.6218
Modified Halsey	30°C	2.6725	0.0274	1.6101	0.9955	3.3821
	40°C	2.3441	0.0241	1.5388	0.9966	3.2581
	50°C	1.1786	0.0206	1.4927	0.9965	4.8321
Oswin Modifié	30°C	4.2552	0.2352	1.9592	0.9872	5.3127
	40°C	1.0984	0.2525	1.8779	0.9915	4.1287
	50°C	0.2431	0.2211	1.8358	0.9905	7.7385

Table 3: Estimated model coefficients, r, MRE of five equation model fitted to adsorption isotherm of *Urtica urens* leaves

Model's name	θ (°C)	A	B	C	r	MRE(%)
GAB	30°C	0.9538	756.4351	4.3744	0.9912	3.1829
	40°C	0.9351	134.8204	4.7111	0.9866	3.1815
	50°C	0.9237	282.8957	4.7116	0.9915	2.1923
Modified Henderson	30°C	0.0034	-10.9261	1.0657	0.9520	6.8457
	40°C	0.0019	-12.1797	1.1341	0.9594	8.1745
	50°C	0.0006	-9.0857	1.2814	0.9605	5.7332
Modified Chung-Pfost	30°C	112.5638	5.186	0.13	0.9302	13.7184
	40°C	136.1907	1.0462	0.1357	0.9402	12.9637
	50°C	153.7906	-9.9718	0.1523	0.9481	15.6013
Modified Halsey	30°C	2.2536	0.0193	1.5443	0.9881	3.0821
	40°C	2.4539	0.0178	1.5964	0.9847	3.3586
	50°C	**2.46**	**0.0182**	**1.6861**	**0.9918**	**2.8321**
Modified Oswin	30°C	1.9962	0.2422	1.8809	0.9769	4.3167
	40°C	0.8772	0.2146	1.9685	0.9774	6.6218
	50°C	0.7391	0.177	2.1286	0.9819	8.6253

3.3 Measurement of optimal water activity of *Urtica urens* leaves

A quality product deserves quality treatment. The heat and process engineering specialists must provide users with accurate information on how to handle a product during storage and conservation. For this purpose, the optimal water activities of conservation ($a_{w\,op}$) were determined. The sorption isotherm curve can be described as a polynomial equation of the third degree, the central part or "stage" is the best area of product stability (fig 3).
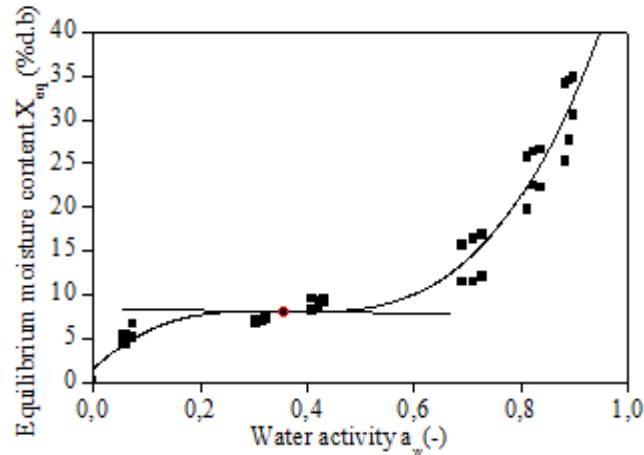
Fig.3: Determination of optimal water activity for conservation of *Urtica urens* leaves

This calculation method consists of decomposing polynomial of equilibrium moisture content Xeq, for all the experimental results for each product based on water activity (equation 7). The values of the optimal water activity conservation of *Urtica urens* leaves ($a_{w\,op}$ = 0.3532) are in perfect agreement with the results obtained for other products [16, 17]. The optimal water activities are ranged in (0.3-0.4).

$$X_{eq} = 1.6442 + 57.7527a_w - 167.6854a_w^2 + 157.38322a_w^3 \qquad (7)$$

3.4 Enthalpy and entropy of sorption

The net isosteric heat of sorption (Δh_d) values are calculated from the equilibrium moisture data at different temperatures using Clausius-clapeyron equation (4). The variation of the heats sorption of *Urtica urens* leaves with equilibrium moisture content is shown in figure 4.

The net isosteric heat of desorption an adsorption of Urtica urens leaves can be expressed mathematically as a polynomial function of equilibrium moisture content:

Desorption : $\Delta h_S = 11.753 - 1.2126\,X_{eq} + 0.0436\,X_{eq}^2 - 0.0005\,X_{eq}^3$ $\qquad (8)$

Adsorption : $\Delta h_S = 19.8186 - 3.5446\,X_{eq} + 0.2116\,M_{eq}^2 + 0.004\,X_{eq}^3$ $\qquad (9)$

The differential entropy (ΔS_d) is plotted as a function of moisture content in figure 4. Once again, the entropy data display a strong dependence on moisture content. The experimental desorption and adsorption data, respectively, conform to polynomial relation as represented by the equations:

Desorption : $\Delta S_d = 40.0995 - 4.2976\,X_{eq} + 0.1727\,X_{eq}^2 - 0.0023\,X_{eq}^3$ $\qquad (10)$

Adsorption : $\Delta S_d = 62.5820 - 10.9222\,X_{eq} + 0.6521\,X_{eq}^2 - 0.0125\,X_{eq}^3$ $\qquad (11)$
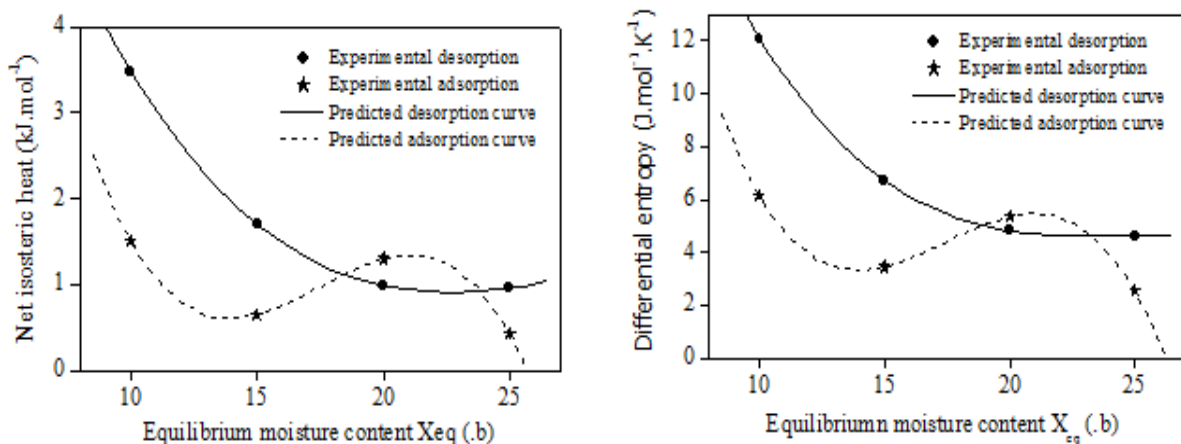

Fig.4: Net isosteric heat and differential entropy of sorption of *Urtica urens* leaves as a function of equilibrium moisture content

3.5 Enthalpy-entropy compensation theory

The Δh_d and ΔS_d values for adsorption and desorption, at given moisture contents, were calculated by linear regression equation using equation 5. It was assumed that, at specific moisture content, Δh_d and ΔS_d did not vary with temperature. Figure 5, shows a linear relation, with a correlation of determination (r =1). This indicates that the compensation exists. The parameters T_β and ΔG_β (Equation 6) were calculated from the data by linear regression, and the values are detailed in table 4
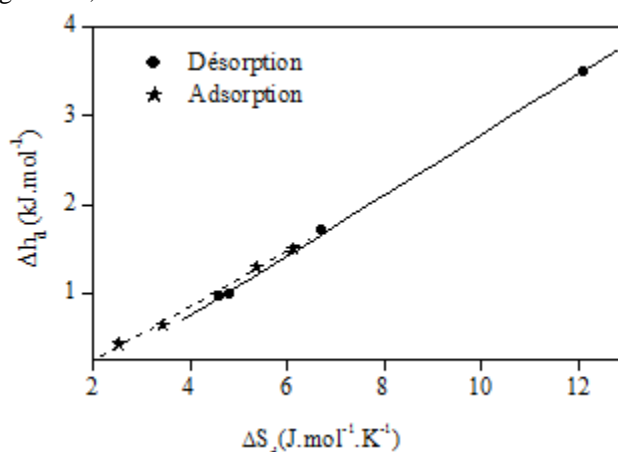

Fig.5: Compensation theory of enthalpy/entropy

Table 4: Characteristic parameters for $\Delta h_d / \Delta S_d$ Relationship

	$T_\beta (K)$	$\Delta G_\beta (J.mol^{-1})$
desorption	340.96	-623.62
adsorption	308.08	374.35

IV. CONCLUSION

It's now widely accepted that sorption data provide valuable information for industrial drying in order to preserve and store the seasonal plants and make them available to consumers all year round. The sorption data may be used not only for the identification of the optimum residual moisture content of the final product, but also for the calculation of the drying time of hygroscopic substances.

The moisture sorption curves of *Urtica urens* leaves were experimentally investigated at three temperatures 30, 40 and 50 °C. The isotherms have a sigmoid shape (Type II) which is common for many hygroscopic products. The hysteresis phenomenon was distinctly observed. Among the sorption models chosen, the GAB model was the best model describing the equilibrium moisture data for desorption, and the modified Halsey model was the most suitable to estimate adsorption isotherms. The optimal water activities of conservation were determined. Net isosteric heat of sorption and differential entropy values of *Urtica urens* leaves were found to be a polynomial function of moisture content for desorption and adsorption. Enthalpy-entropy compensation theory could be successfully applied to the moisture sorption behaviour of *Urtica urens* leaves.

REFERENCES

[1] C. Marrassini, C.Acevedo, J. Miño, G. Ferraro and S. Gorzalczany, Evaluation of antinociceptive, antinflammatory activities and phytochemical analysis of aerial parts of Urtica urens L. Phytotherapy Research, 24(12), 2010, 1807-1812.

[2] N. Arsalan, and H. Togrul, The fitting of various models to water sorption isotherms of tea stored in a chamber under controlled temperature and humidity, Journal of Stored Products research, 42(2), 2006, 112-135.

[3] A. Lamharrar A. Idlimam, and M. Kouhila, L. Themodynamic properties and moisture isotherms of Artemisia herba-alba Rev. Energ. Ren, 10(3), 2007, 311 – 320.

[4] A. Jamali, M. Kouhila, L. Ait Mohamed, A. Idlimam, and A. Lamharrar, Moisture adsorption-desorption isotherms of Citrus reticulata leaves at three temperatures, Journal of Food Engineering, 77(1), 2006, 71-78.

[5]   A. Akın, N. Özbalta, and A. Güngör, Equilibrium moisture content and equations for fitting sorption isotherms of capsicum annuum, GIDA 34 (4), 2009, 205-211

[6]   K.Y. Foo and B.H. Hameed, Insights into the modelling of adsorption isotherm systems, Chemical Engineering Journal, 156, 2010, 2–10.

[7]   C. Van den Berg, and S.Bruin, Water activity and its estimation in food systems: theoretical aspects. In L. B. Rockland & G. F. Stewart (Eds.), Water activity: influences on food quality, New York: Academic Press, 1981, 1–61.

[8]   T.L. Thompson, R.M. Peart, and G. H. Foster, Mathematical simulation of corn drying a new model, Transactions of the American Society of Agricultural Engineers, 11, 1986, 582-586

[9]   S.G. Pfost, Mourer, D.S. Chung, and G.A. Miliken, Summarizing and reporting equilibrium moisture data for grains, American Society of Agricultural Engineers, St. Josef, MI. 1976, Paper n°76-3520.

[10]   H. Iglesias, and J. Chirife, Prediction of effect of temperature on water sorption isotherms of food materials, Journal of Food Technology, 11, 1976, 109–116.

[11]   C.R. Oswin, The kinetics of package life. III. Isotherm, Journal of the Society of Chemical Industry, 65, 1946, 419-421.

[12]   H.R. Bolin, Relation of Moisture to Water Activity in Prunes and Raisin, J. Food. Sci., 46, 1980, 1190.

[13]   A. Naji, A. Idlimam, and M. Kouhila,, Sorption isotherms and thermodynamic properties of powdered milk. Chem.Eng.Comm. 197 (8), (2010, 1109-1125.

[14]   E. Tsami, Net Isosteric Heat of Sorption in Dried Fruits, Journal of Food Engineering, 14, 1991, 327-335.

[15]   E.S. Sherman, Sorption of water vapour by proteins and high polymers, J. Am. Chem. Soc, 69 (3), 1947, 646–651

[16]   H. Machhour, A. Idlimam, M. Mahrouz, I. El Hadrami and M. Kouhila, Sorption isotherms and thermodynamic properties of peppermint tea (Mentha piperita) after thermal and biochemical treatment, J. Mater. Environ. Sci. 3 (2), 2012, 232-247.

[17]   A. Idlimam, A. Lamharrar, N. Abdenouri, C.S. Ethmane Kane, S. Akkad, A. Jamali, and M. Kouhila, Thermodynamic Properties and Moisture Sorption Isotherms of Argania spinosa and Zygophyllum gaetulum, Journal of Agronomy, 7(1), 2008, 1-14.

A Review on Thermal Aware Optimization of Three Dimensional Integrated Circuits (3D ICs)

Sakshi Raghuvanshi[1], Prince Nagar[2], G.K.Singh[3]

[1]*Student,*[2]*Lecturer,*[3]*Associate Professor, Electronics and Communication Engineering,*
Sharda University, Greater Noida, Uttar Pradesh, India.

Abstract:*As the technology size has reached upto 14nm, further shrinking creates some major performance issues. Three dimensional integrated circuits (3D ICs) are gaining importance in the present arena on account of their advanced features. While stacking of die on die in 3D ICs also result in serious thermal problems. These thermal issues can be minimised at different physical design stages with the help of various techniques and algorithms. In this paper an overview of the various methods used for thermal optimization is presented including techniques at floorplanning, placement and routing. It also includes the techniques involving the use of TSVs (through-silicon-vias).*
Keywords:*Floorplanning, placement, routing, 3D-ICs, through-silicon-via (TSV).*

I. INTRODUCTION

With the growth of VLSI, continuous shrinking of technology feature size has been the demand of researchers to enhance the performance of the circuits. Also increasing the integration density leads to increased system complexity and more complex physical design. Interconnect delay is also an important issue for highly integrated circuits. Three dimensional integrated circuit (3D IC) in which multiple device layers are vertically stacked and interconnected, has emerged as a solution to alleviate these problems and enhance the performance beyond Moore's law. 3D ICs provide a means to decrease interconnect length thereby increasing speed, can also combine various technology and physical domain in a single product, therefore enhancing the capabilities. But, these benefits are achieved at cost of other factors like testing becomes difficult and complex, as the number of layers stacked increases yield also decreases. One of the major problem associated with 3D ICs is improper heat evacuation. Therefore introduction of TSVs in 3D IC designs provide a promising solution through many benefits like heterogeneous integration, reduction in wirelength and decrease in max temperature.

II. LITERATURE REVIEW

This paper follows the order of physical design stages and is organised as follows. Section 2.1 introduces with the thermal model required by 3D ICs. Section 2.2 discuss the floorplanning algorithm considering the temperature aspects too. Section 2.3 deals with the thermal aware placement in 3D ICs. Thereafter in section 2.4 TSV planning is described. And finally thermal dependent routing algorithm are discussed.

2.1 Heat Transfer Models

Several thermal analysis need to be performed for the successful application of 3D ICs in products. Development of analytical models for heat spread is required to accurately analyse thermal management of 3D ICs. **Jain Ankur**, **et.al [10]** developed finite-element and analytical models of heat transfer for stacked 3D ICs. Analytical model was developed for temperature distribution in multidie-stack with multiple heat source. This model was used to develop thermal resistance and thermal sensitivity matrices for 3D ICs which is the extension of the single-valued junction-to-air thermal resistance concept in an IC. Thermal performance of interdie bonding layer is obtained with the help of numerical simulations performed. Also due to the vertical integration of the dies has led to the reduction in die footprint area but at the cost of increased maximum temperature.

There is a great demand to perform thermal analysis involving the structure of BEOL and location of all power sources in the layout. Also the design loop to assess the thermal consequence of design iterations should include the thermal analysis and verify final design before sign-off. **Oprins H., et.al [18]** presented a method to perform a detailed fine grain thermal analysis of stacked die packages inclusive of complete back end of line structure (BEOL), interconnection between dies and complete electrical design layout of all stacked dies. By using 3D numerical techniques calculations are performed and the method allows to import the full electrical design of all dies in stack. Technique is demonstrated on a 2 stacked die structure, for which the effect of TSV on temperature distribution is studied. Experimental results indicated that the maximum error is less than 5% in the temperature peak and less than 10% in tails of temperature profile.
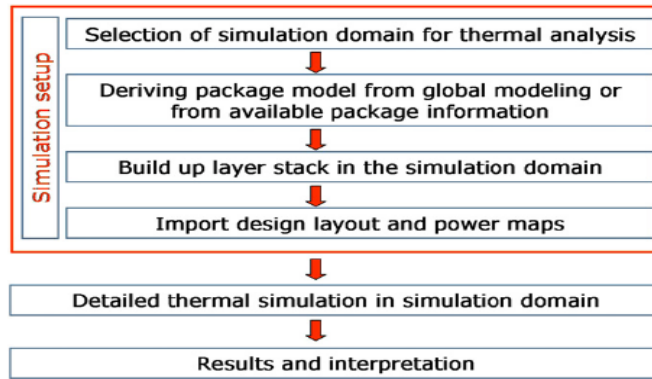
Figure 1. Flow chart for detailed thermal modeling of a stacked die structure [18]

Thermal models have usually assumed equal sized die whereas manufacturing and packaging considerations require different die size for yield and interconnection improvement. **Choobineh Leila, et.al [9]** for predicting the three dimensional temperature presented a heat transfer model for multi-die 3D IC having unequally-sized die. Three dimensional temperature fields for each die are obtained by solving the energy conservation equations with appropriate boundary conditions. Thermal performance of unequally-sized die stacks is compared with a uniformly-sized die stack with the help of this model only. It can be concluded from the experimental results that the rise in peak temperature is greater when the degree of non-uniformity is greater in the die stack.

2.2 Floor planning Algorithms For 3d Ic

Every stage of 3D IC design including the floorplanning process need to consider the thermal issues as a number of challenges are posed by thermal constraint to an efficient 3D floorplanning algorithm. For 2D circuits, floorplanning is a well-studied problem. Several works exist on thermal-driven 2D floorplanning but very few for 3D ICs. **Cong Jason, et.al[15]** proposed a thermal-driven 3D floorplanning algorithm which involved a combined-bucket-and-2D-array (CBA) an efficient 3D floorplan representation. A compact resistive thermal model (CBA-T) was integrated with the 3D floorplanning algorithm to obtain better temperature optimization. Also for faster solution generation a thermal-driven 3D floorplanning algorithm (CBA-T-Fast) based on simplified closed-form thermal model was proposed. And finally a hybrid (CBA-T-Hybrid) of resistive network and closed-form thermal model mentioned earlier was proposed to target a good trade-off between runtime and quality. For CBA-T the maximum on-chip temperature was reduced by 56% with 9X runtime when compared to non-thermal driven floorplan algorithm. Similarly, for CBA-T-Fast the maximum on-chip temperature was reduced by 40% with 2X runtime compared with the non-thermal driven 3D floorplanning algorithm. Lastly for CBA-T-Hybrid maximum on-chip temperature can be reduced by 50% with 3X runtime compared with CBA.
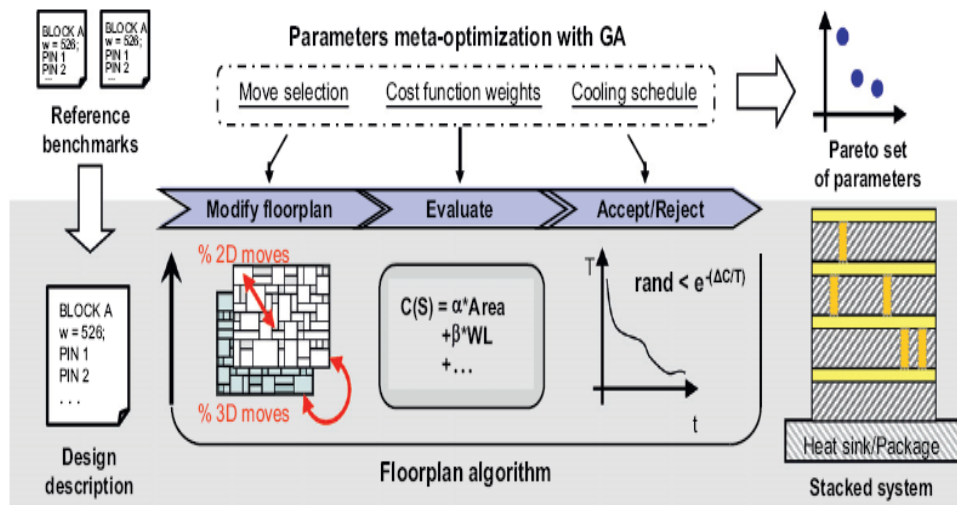

Figure 2. Workflow of floorplan algorithm and meta-optimization [11]

Multiple authors have presented thermal aware floorplanners all of them mainly focusing on minimising weighted sum of area, wirelength and peak temperature. **Frantz Felipe, et.al[11]** discuss the implementation of 3D floorplan algorithm and recognizes 17 parameters that effect its performance. Then they also proposed the use of Genetic algorithm to identify the sets of parameters which provide good floorplan. Two method for reduction of peak temperature and thermal gradients in 3D ICs used are first involving the use of smart heuristic that moves the high power density close to heat sink and other includes the use of a two-phase simulated annealing process involving two different cost function. Results help in concluding that average peak temperature and gradient was reduced by -37% and -56% respectively with an increase of 11% in area and 14% in wirelength when smart heuristic was combined with cost function.
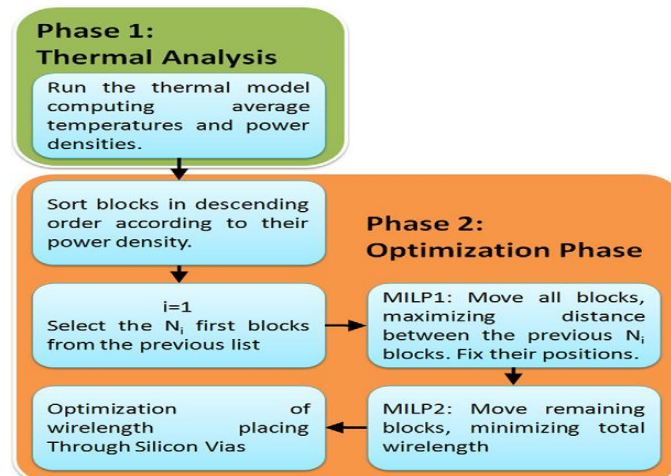

Figure 3. Iterative flow of the approach [12]

As power densities are already an issue in 2D architecture, it increases the thermal problem when moved to 3D architecture. Therefore it is necessary to devise efficient 3D floorplanning which optimize thermal profile of 3D multiprocessor architectures. **Cuesta David, et.al[12]** proposed a set of design rules for the generation of 3D thermal-aware floorplanner for Niagara architecture. The main areas of their work include (1) multi-objective formulation of the floorplanning problem in 3D multi-processor architecture with thermal constraints. (2) By using Mixed Integer Linear Programming (MILP) it performs an efficient resolution of the optimization problem by optimizing the location of functional blocks and through silicon vias. (3) Integration of this MILP model with an accurate thermal model of architecture. Based on the Niagara system experimental results showed an extensive improvement in main thermal and reliability-related metrics (peak and mean temperature, thermal gradients) along with low performance overhead.

The (linear) thermal model must be added to the topological relations when MILP [12] is used for thermal aware floorplanning thereby making the resultant algorithm becomes too complex especially when the problem size increases. **Cuesta David, et.al[13]** proposed thermal-aware floorplanner for 3D many-core single chip a more advanced than the previous one. Through the use of Multi-Objective Evolutionary Algorithm (MOEA) they thermally optimize the 3D layout. They studied the thermal aware problem and formulated the total wire length problem with two different genetic algorithms. Furthermore, this helped in eliminating hotspot, reduce peak and mean temperature and reliability issues associated with temperature. It can be concluded from the experimental results that the maximum-on-chip temperature can be reduced in 80° in the best case, for two realistic homogeneous and heterogeneous many-core single-chip architecture.

2.3 Thermal Aware Placement Algorithms

Pavlidis Vasilis F., et.al [25] examined the dependence of interconnect delay on the inter-plane via location in 3D-ICs. By optimally placing the inter-plane vias delay of interconnects can be reduced. Via locations which reduce the propagation delay are determined and the inter-plane vias locations are obtained through near-optimal heuristics and geometric programming. For implementing efficient algorithms having lower computational time along with negligible loss of optimality, proposed heuristics are used. Results indicated an improvement in delay for short point-to-point interconnects of 32% with optimally placed inter-plane vias. Also the maximum improvement in delay for optimally placed inter-plane vias is 19% for interconnect trees.

3D placement is an important stage in physical design of 3D ICs which provide the arrangement of a set of functional cells in the multi-stacked layers and offer a way to routing. Many 2D placement algorithms are extended for solving 3D placement problem but as thermal issues are critical therefore need to be solved during

physical design process. **Yan Haixia, et.al [2]** proposed a thermal aware 3D placement algorithm using a quadratic uniformity model which integrates thermal problem with placement process to reduce hotspot temperature and obtained a thermally balanced 3D placement. This algorithm include thermal aware global placement, thermal aware layer assignment and finally a detailed placement. Thermal dissipation and cell distribution are unified through DCT and integrated with wirelength optimization into a quadratic function with the help of quadratic uniformity modelling during global placement stage. This work also proposes two fast methods to estimate the temperature of each grid to update the coefficient instead of precise thermal analysis. Thereafter the distribution of cells through thermal aware layer assignment finishes assignment of cells among the stacked layers with optimum temperature. And finally detailed placement removes the overlaps and optimises the wirelength. Experimental results concluded that this algorithm helped in achieving reduced temperature with little increase in wirelength.
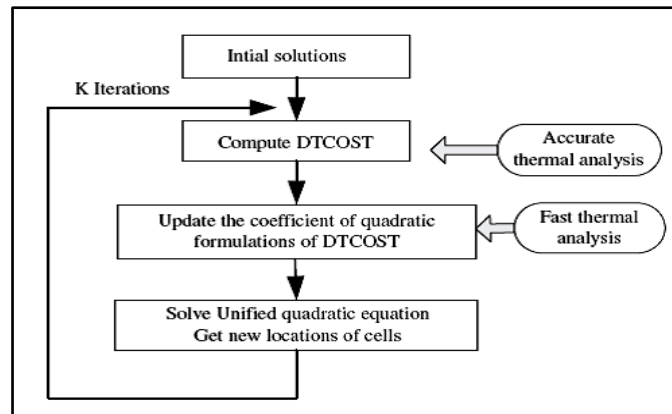
Figure 4. **Thermal aware quadratic global placement [2]**

In Yan Haixia, et.al [2] the proposed a thermal aware 3D placement algorithm based on quadratic uniformity model but it did not included the through-silicon-vias (TSVs), which are very common in 3D ICs. **Athikulwongse Krit, et.al [1]** have proposed two methods to exploit the die-to-die thermal coupling used force directed temperature aware placement in 3D ICs. First method involves the TSV spread and alignment in which TSVs are arranged only on the basis of TSV density & not on the placement density obtained from both TSV and cell area. Second method is the thermal coupling-aware placement. As based on force directed temperature aware placement, this method introduced two new forces, one that moves cells and other that moves TSVs. The movement is such that higher power cells are placed closed to TSV to heat sink path. These forces balance the power density and thermal conductivity as the area with higher difference has stronger force and weaker force for area with smaller difference.
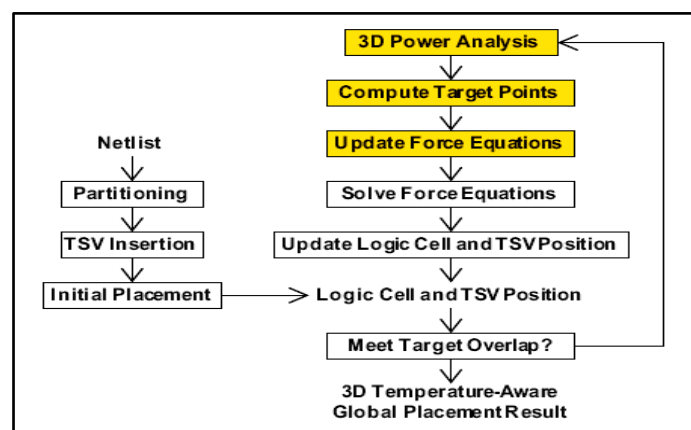
Figure 5. **Design flow for 3D IC global placement [1]**

For bus planning in 2D layout representations, concept of block alignment is successfully used but neglected for 3D layout. Also blocks are not aligned such that their position fulfil upperand lower distance limits i.e., alignment ranges are not considered. By employing different alignment methods help in structural planning of interconnects of 3D ICs as illustrated in Figure.4. **Knechtel Johann, et.al[6]** demonstrated the effective use of 2D and 3D block alignment of different interconnects for structural planning. They also introduced a 3D

layout representation Corblivar, which is based on the extended corner block list. Extension include encoding of both fixed alignment and alignment ranges along with handling inter and intra-die alignment in a unified manner. Also developed techniques for block alignment and placement. Based on CBL extension and simulated annealing (SA) an open source 3D floorplanning tool was developed. Results concluded Corblivar's applicability for structural planning of interconnects, which is block alignment along with performance competitive with classical 3D floorplanning.
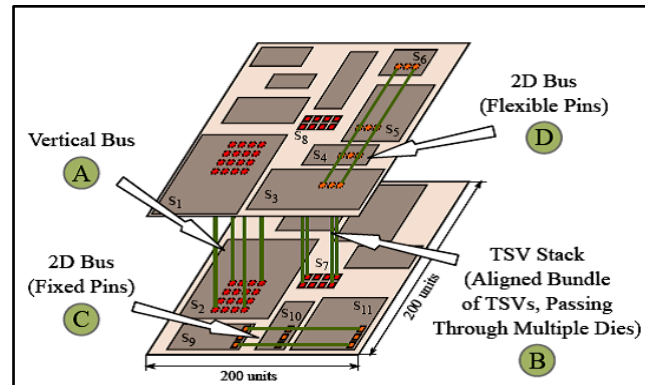
Figure 6. **Interconnect structures in a 3D IC and related block-alignment configurations [6]**

STS-via should be assigned to area which required TS-via for reducing temperature. As TS-via are only inserted into whitespaces, total wirelength of 3D ICs is affected by the STS-via position. Since placing STS-via into hot region result in wire detour leading to increased wirelength, therefore necessitates the STS-via to be integrated with pin assignment. **He Xu, et.al[4]** proposed an approach integrating STS (signal through-the-silicon) via planning with pin assignment. Authors considered STS via planning and pin assignment for two-pin nets connecting one source block to all its sink blocks. This is solved using a min-cost maximum flow based algorithm which provided an optimized solution. Their experimental results made a conclusion that temperature was reduced by 19.3% through their approach when compared to initial temperature and 1.7% when compared to algorithm not considering thermal optimization. Wirelength was also reduced by a factor of 18.9% using their algorithm.

2.4 Algorithms For TSV Planning In 3d IC

Most of the thermal via planning methods have not considered the leakage power but the via number required in the design will be under-estimated if the impact of leakage power on temperature is not taken into account. Higher temperature results to larger delay and leakage power thereby degrading the performance. Similarly increase in leakage power raises temperature resulting in more thermal vias requirement. Leakage-delay-temperature are dependent on each other therefore need to be considered together otherwise may lead to over-estimation or under-estimation for thermal-vias planning. **Wang Kan, et.al[3]** integrated the temperature-leakage-timing dependence into thermal via planning of 3D ICs. They achieved it with the help of three process: (1) Iterative TSV planning considering leakage power-delay-temperature dependence. (2) Performance aware TSV planning with resource constraints. (3) Weighted via planning with power-temperature-timing evaluation. Thus a weighted via insertion approach considers both performance and heat dissipation with resource constraint to obtain best balance among temperature-via number and delay.

Till now majority of work have concentrated on optimization of single performance criterion like power dissipation, delay and signal integrity. Based on multiple performance criterion an inclusive TSV placement and routing methods is needed to make the interconnect timing, performance and system reliability better. **Qian Libo**, **et.al[5]** first of all derived first order expressions for TSV resistance, capacitance and inductance as a function of physical dimension and material characteristics on the basis of parasitic parameter extraction model. They proposed an optimization algorithm concentrating on TSV insertion in 3D ICs with the main aim to minimize the propagation delay considering signal reflection too. Thus, their experimental results showed a 49.96% improvement in average delay and a 62.8% decrease in reflection coefficient when compared to conventional insertion algorithm. Also the effectiveness of optimization for delay increases for higher non-uniform inter-plan interconnect.
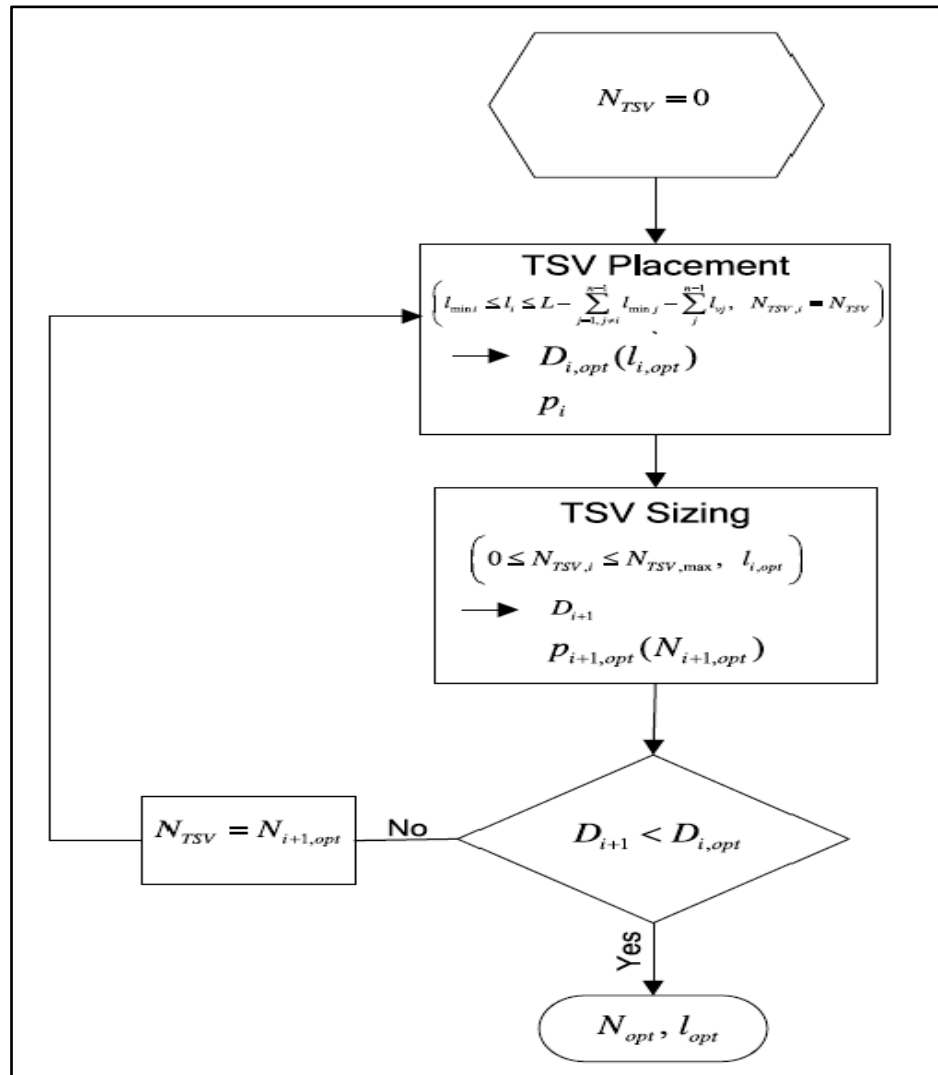
Figure 8. Design flow of interconnect iteration algorithm [5]

Only few works have examined the 3D P/G network design. Few focuses on power supply noise reduction while others concentrated on IR drop in 3D ICs during early stages. Distribution of P/G TSVs is affected by not only the power distribution but also the whitespace distribution around circuit modules as TSVs go through the silicon layer. **Li Zuowei, et.al[8]** based on a sensitivity model considering temperature-dependent leakage current this paper presented an efficient thermal aware P/G (power/ground) TSV planning algorithm with topology optimization of P/G grids. More specifically, for supporting P/G TSV planning thermal aware IR drop analysis and a sensitive model for P/G TSV insertion among layers is proposed. Also to optimize P/G network in non-uniform P/G grid topology, shorter wires are used to connect the P/G TSVs to P/G grids. Results helped in concluding that the IR drop is underestimated by 11% when thermal impacts on power delivery are neglected. Also 51.8% of additional P/G TSVs are required to overcome the severe IR drop violation than the cases without considering thermal impacts. And maximum IR drop can be reduced by 42.3% & number of violated nodes reduced by 82.4% using the P/G TSV planning based on sensitivity model.
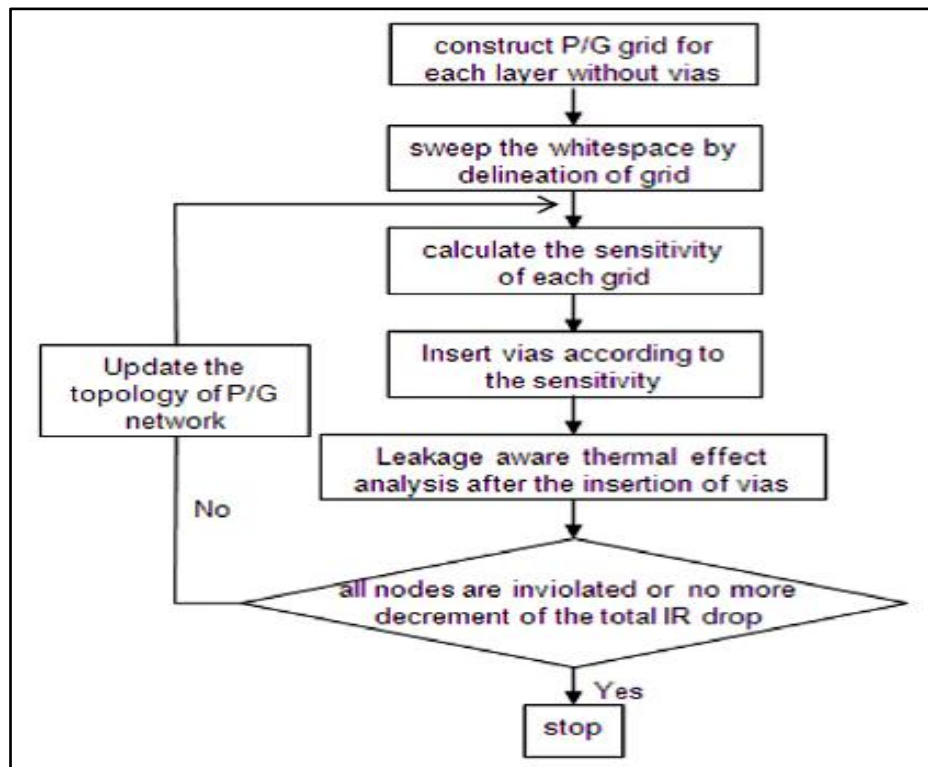
Figure 9. Overall flow of co-optimization of P/G grid topology [8]

The physical design of 3D partitioning, floorplanning and partitioning helps in determining the number of (signal) TSVs to be used. Many previous works have optimized the TSV count, wirelength and on chip temperature but have never considered the exploitation of high-level data transfer information obtained from high-level synthesis(HLS) on minimizing TSVs. **Byunghyun Lee**, **et.al[7]** proposed a set of algorithms two for TSV resource sharing and one for TSV refinement for TSV allocation optimization. Based on sharing granularity and design complexity two sharing algorithms are: (1) word-level TSV sharing and (2) bit-level TSV sharing. TSV sharing problem was resolved into a graph partitioning which employed two types of edges and solved by repetitive iterations. Whereas by using the greedy TSV splitting technique and register replication they also solved the TSV refinement. Along with this they also proposed a new TSV-aware 3D floorplanner to evaluate the wirelength more accurately. Their results showed a decrease in TSV number by 26.0% in word-level TSV with an increase in wirelength by 12.4% and a decrease in TSV count by 31.4% in bit level TSV with an increase of 18.1% in wirelength.
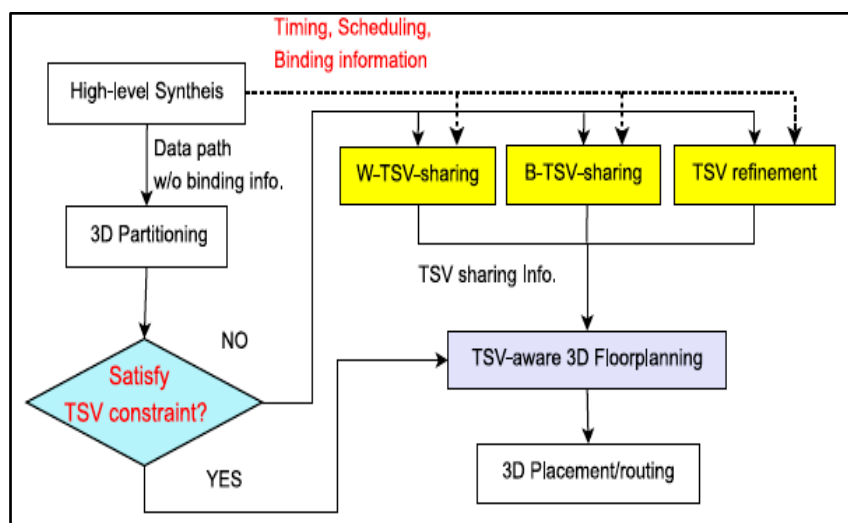
Figure 10. The algorithmic flow of the proposed word-levelTSV sharing for two layered data paths [7]
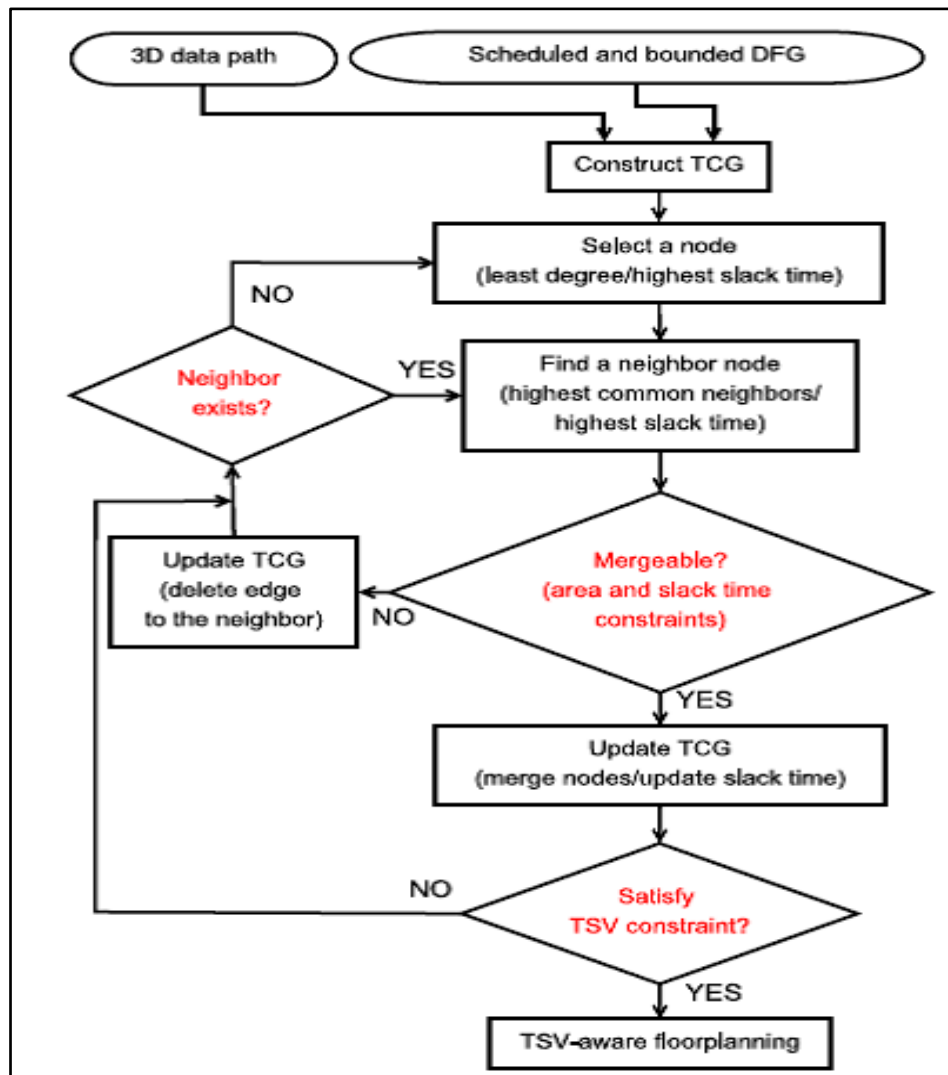
Figure 11. Algorithm flow of proposed word-level TSV sharing for two layer data paths [7]

2.5 Temperature Aware Routing Algorithms

Several 3D routing algorithms have dealt with the problems of 3D channel routing, maze routing but majority of them have not considered the thermal problem associated with 3D ICs in the routing phase. **Zhang Tianpei, et.al [17],** to lower the effective thermal resistance of material for reducing temperature of the chip, proposed a temperature-aware 3D global routing algorithm with appropriate insertion of thermal vias and thermal wires. Thermal vias and thermal wires have similar function where thermal vias are added as vertical interlayer thermal conduit having no electrical function and thermal wires conduct heat laterally within same layer. Thermal vias help spread heat paths over multiple thermal vias while vias perform conduction to heat sink. Routing scheme starts with routing congestion estimation and signal interlayer via assignment, finally followed by thermally-driven maze. Sensitivity analysis is utilized along with linear programming (LP) based thermal via/wire insertion to reduced temperature. And is repeated iteratively till temperature and routing capacity violations are resolved. Experimental result help in concluding that this routing algorithm reduces the peak temperature and remove routing congestion effectively.
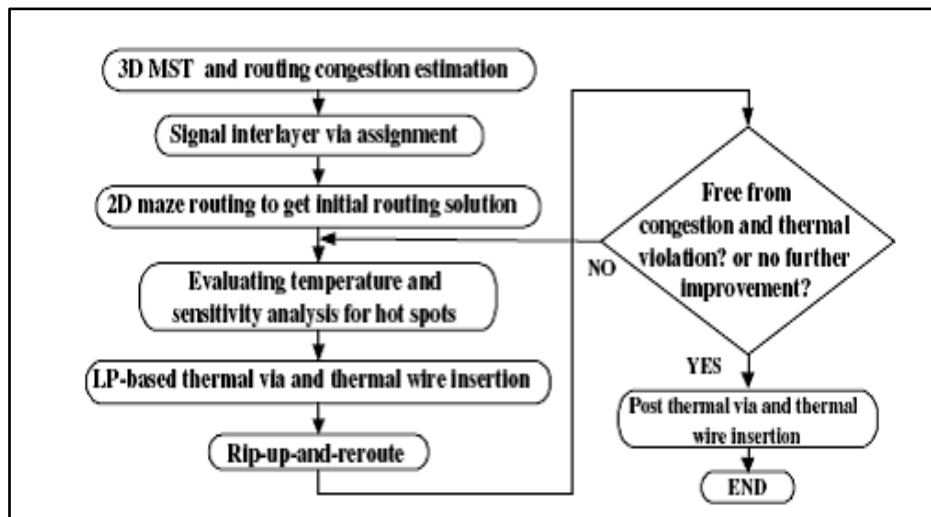
Figure 12. Flow for the temperature-aware 3D global routing algorithm

Different device layers stacked along with low thermal conductivity of bonding material leads to excessively high temperature. In a Steiner tree the location of TSVs have great impact on the overall topology as well as dealy at sink nodes of tree. In lowering temperature of chip TSVs play a vital role. **Pathak Mohit, et.al [14]** presented a thermal aware Steiner routing algorithm for 3D stacked ICs. It consisted of two main parts: tree construction and tree refinement. A delay-oriented Steiner-tree was made through the tree construction algorithm which included the minimization of Elmore delay function. Repositioning of through-silicon-vias (TSVs) used in existing Steiner tree while preserving original routing topology was done through the tree refinement algorithm for further thermal optimization. It was concluded that an improvement of 52% in performance at the cost of 15% wirelength and 6% TSV count increase for four-die stacked was reported which outperforms the 3-D maze routing.
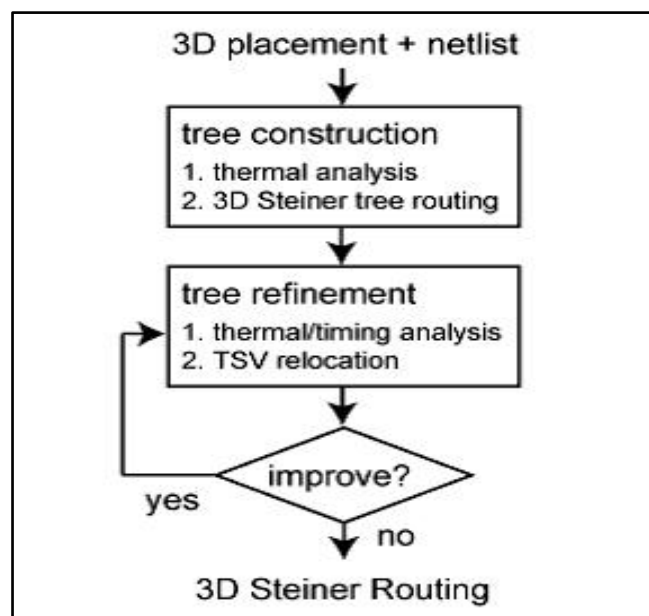
Figure 13. Overview of thermal-driven 3-D Steiner routing [14]

In the above approach [14] signal TSVs have been grouped into movable and non-movable TSVs by 3-D Elmore delay model. Movable signal TSVs don't deteriorate the performance and are placed near to hotspot region. Yet, this method does not exploit the outstanding thermal conductance of TSVs in thermal dissipation. **Hsu Po-Yang, et.al [16]** with the aim to minimize temperature with small wiring overhead, they proposed a three stage TSV locating algorithm in global routing for 3D IC. This work helps in constructing stacked signal TSV and utilize the thermal conductance of stacked TSVs to improve the thermal dissipation of the circuit. First algorithm was developed to stack signal TSVs by utilizing the thermal dissipation capabilities of stacked TSVs.

Second constructed aligned signal TSVs for the purpose of dissipating heat vertically without adding extra thermal TSVs thereby resulting in no additional area overhead for TSVs. Finally a gain function was proposed to concurrently consider interconnect wirelength and temperature profile. This gain function was utilized by the algorithm to optimize chip temperature with very small wiring overhead. Along with this, their algorithm moves TSVs on non-critical path resulting in no performance loss. Results demonstrated that a 17% temperature reduction with 3% wiring overhead and no performance loss was achieved with the help of 3-D Elmore delay model. Also in comparison to the work of Pathak and Lim [14] in which movable signal TSVs are relocated to reduce temperature, results has 8% more temperature reduction with same number of signal TSVs.
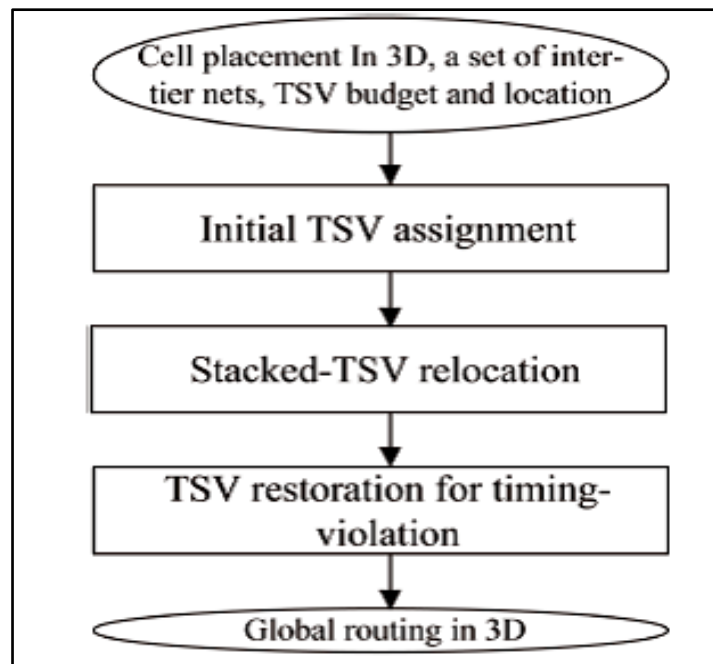
Figure 14. **Overall flow of placing signal TSVs in global routing [16]**

III. Summary

Experiments have indicated that the major issues faced by three dimensional integrated circuits, specially the thermal problems can be reduced with the help of various algorithms implemented at different design stages. Shrinking the size of ICs through vertical stacking of dies reduces the wirelength and delays but also results in increased power density along with higher on-chip temperature. Higher temperature leads to increased leakage power degrading the performance. To reduce the increased temperature TSVs are added to the 3D ICs which help in proper distribution of heat, released by various processing units and forming hotspot in the different layers. Thermal-driven floorplanning algorithm helps in reducing the on-chip temperature by 50% with low overhead. Also, the use MILP and MOEA helped in eliminating hotspot, reduce peak and mean temperature and reliability issues associated with temperature. Thermal aware 3D placement algorithm integrates thermal problem with placement process and reduce hotspot temperature to obtain a thermally balanced 3D placement. As well as a weighted via insertion approach considering both performance and heat dissipation along with resource constraint provide the best balance among temperature-via number and delay. Finally a thermal aware routing algorithm using Steiner routing for 3D stacked ICs resulted in an improvement of 52% in performance at the cost of 15% wirelength and 6% TSV count increase for four-die stacked which outperforms the 3-D maze routing.

IV. Future Scope

There are several areas in the field of thermal optimization of 3D ICs which have not been taken into consideration till yet. The impact of large interlayer vias on thermal resistance for every tile stack has not been considered. Also to speed up the thermal-driven 3D floorplanning algorithm without going through simulated annealing closed-form temperature formula need to be implemented [15]. Along with the above mentioned work, these thermal driven algorithms for different design stages can be implemented on a single 3D IC at various design stages. Implementation of the above algorithms at every design stage will enhance and improve the chip performance completely in various aspect, thereby making them more suitable for use in future.

REFERENCES

[1]   Athikulwongse Krit, Ekpanyapong Mongkol, Lim Sung Kyu, "Exploiting Die-to-Die Thermal Coupling in 3D IC Placement." Proc. Design Automation (DAC), 49th ACM/ IEEE DAC , 2012 pp.741-746.

[2]   Yan Haixia, Zhou Qiang, Hong Xianlong, "Thermal aware placement in 3D ICs using quadratic uniformity modelling approach." Integration, the VLSI Journal Vol.42 pp.175-180, 2009.

[3]   Wang K., Ma Y., Dong S., Wang Y., Hong X., Cong J., "Rethinking thermal via planning with timing-power-temperature dependence for 3D ICs," Proc. Asia and South Pacific Design Automation Conference (ASP-DAC), pp.261-266, 25-28, 2011.

[4]   He Xu, Dong Sheqin, Ma Yuchun, "Signal through-the-silicon via planning and pin assignment for thermal and wire length optimization in 3D ICs."Integration, the VLSI Jounral Vol.43 pp.342-352,2010.

[5]   Qian Libo, Zhu Zhangming, Yang Yintang, "Through-silicon-via insertion for performance optimization in three dimensional integrated circuits." Microelectronics Journal Vol.43 pp.128-133, 2012.

[6]   Knechtel Johann, Young Evangeline F.Y., Lienig Jens," Structural Planning of 3D-IC Interconnects by Block Alignment," Proc. IEEE of 19th ASP-DAC, pp.53-60, 2014.

[7]   Lee Byunghyun, Kim Taewhan, "Algorithm for TSV resource sharing and optimization in designing 3D stacked ICs." Integration, the VLSI Journal, Vol.47,pp.184-194,2014.

[8]   Li Zouwei, Ma Yuchun, Zhou Qiang, Cai Yici, Xie Yuan, Huang Tingting, "Thermal-aware P/G TSV planning for IR drop reduction in 3D ICs." Integration, the VLSI Journal Vol.46,pp.1-9,2013.

[9]   Jain Ankur, Choobineh Leila "Determination of temperature distribution in 3D ICs with unequally sized die." Applied Thermal Engineering Journal Vol.56 pp.176-184,2013.

[10]   Jain Ankur, Jones Robert E., Chatterjee Ritwik, Pozder Scott."Analytical & Numerical Modeling of the Thermal Performance of 3D ICs." IEEE Transactions on Components & Packaging Technology Vol.33, pp.56-63, March 2010.

[11]   Frantz Felipe, Labrak Lioua, O'Connor Ian."3D IC floorplanning: Automating optimization settings & exploring new thermal-aware management techniques."Microelectronics Journal Vol 43, pp.423-432, 2012.

[12]   Cuesta David, Risco-Martin Jose L., Ayala Jose L. "3D thermal-aware floorplanner using a MILP approximation." Microprocessor & Microsystems Journal Vol.36 pp.344-354,2012.

[13]   Cuesta David, Risco-Martin Jose L., Ayala Jose L., Hidalgo J.Ignacio., "3D thermal-aware floorplanner using a MOEA approximation." Integration,the VLSI Journal (Spain) Vol.46 pp.10-21,2013.

[14]   Pathak Mohit, Lim Sung Kyu, "Performance and Thermal-Aware Steiner Routing for 3-D Stacked ICs." IEEE Tans.Computer Aided Design of Integrated Circuits and Systems, vol.28, no. 9, pp. 1373-1386, Sept.2009.

[15]   Cong Jason, Wei Jie, Zhang Yan,"A Thermal-Driven Floorplanning Algorithm for 3D ICs,"International Conference on Computer Aided Design (ICCAD) IEEE Computer Society/ACM, 2004 pp.306-313.

[16]   Hsu Po-Yang, Chen Hsien-Te, Hwang TingTing, "Stacking Signal TSV for Thermal Dissipation in Global Routing for 3-D IC," *IEEE Transactions on Computer-Aided Design of Integrated Circuits and Systems, Vol.*33, no.7, 1031-1042, July 2014.

[17]   Zhang Tianpei, Zhan Yong, Sapatnekar S.S., "Temperature-aware routing in 3D ICs," Design Automation, 2006. Asia and South Pacific Conference, vol., no.6 pp.24-27 Jan. 2006.

[18]   Oprins H. , Srinivasan A. , Cupak M. , Cherman V. , Torregiani C. , Stucchi M. , VanderPlas G. , Marchal P. , Vandevelde B. , Cheng E. ," Fine grain thermal modelling and experimental validation of 3D-ICs" Microelectronics Journal Vol.42 pp.572–578, 2011.

The Coupled Effect of Nano Silica and Superplasticizer on Concrete Fresh and Hardened Properties

Mohamed I. Serag[1], Hala El-Kady[2], Muhammad S. El-Feky [3]

[1]*Material Strength Department, Faculty of Engineering/ Cairo University, Egypt*
[2]*Department of Civil Engineering, National Research Center, Egypt*
[3]*Department of Civil Engineering, National Research Center, Egypt*

Abstract: The The effect of individual and combined additions of both nano silica (NS) and polycarboxylate-ether superplasticizer (SP) admixtures on concrete mixes were studied. Twenty concrete mixes were prepared, keeping the water/cement ratio constant at w/c = 0.40, with different amounts of SP admixture, and NS. the superplasticizer was studied in the range of (0 – 0.88)% (over cement weight), nano silica additions were tested at (0 – 3.00)% range (over cement weight). Early, and late compressive strengths, as well as results of fresh concrete (slump) test of formulations were evaluated by means of design of experiments, in order to identify the primary factors and their interactions on the measured properties. The most desirable NS and SP % were determined. The results showed that regardless of the used NS percentage, the higher compressive strength results were reached at, or around SP observed saturation dosage (0.66% by weight cement). The statistical approach applied here enabled to develop relations, which could adequately describe the dependency of both the compressive strength, and slump on the composition of NS, and SP concretes. These relations were presented as contour plots, which from a practical point of view could serve as a basis for mix design.

Keywords: full factorial design, nano silica, superplastecizer

I. INTRODUCTION

Recently, nanotechnology has attracted considerable scientific interest due to the new potential uses of particles in nanometer scale. Thus industries may be able to re-engineer many existing products that function at unprecedented levels. Due to these developments in nano science and technology, various forms of nano-sized amorphous silica have become available. As these materials have higher specific surface area compared to silica fume, a considerable research effort has been attracted to investigate the influence of nano silica on the properties of cement based materials.

Although numerous papers have studied the influence of nano silica on the properties of cement composites, their effects have not been adequately characterized yet, and some discrepancies and inconsistencies in compressive strength, and workability results are witnessed. [1-5].

Since the major problem in utilizing Nano-particles is that they are highly agglomerated and if used directly in a bulk composite, they often lose their high-surface area due to grain growth. Effective means of de-agglomerating and dispersing are needed to overcome the bonding forces after wetting the powder; the ultrasonic breakup of the agglomerate structures in aqueous and non-aqueous suspensions allows utilizing the full potential of nano-sized materials, besides the addition of proper chemical dispersing admixtures.

Currently, the extended use of superplasticizer (SP) improves the workability of grouts and concretes mixtures. Superplasticizers are adsorbed onto the surface in order to de-flocculate cement particles, which release trapped water from cement flocks [6]. The mechanism behind SP mortars and concretes is associated with the adsorption of molecules onto particles surfaces, causing mainly electrostatic (e.g., polynaphtalin-sulphonate) or electrostatic/steric (polycarboxylic-ether) repulsive forces [7,8]. In this sense, it is known that mix designs containing silica as cement replacement increase the strength due to a pozzolanic and filler effect [9]. However, the compaction necessary to produce a mixture as homogeneous as possible is directly related to its rheological behavior, which depends on the chemical compatibility between the materials. In fact, the presence of mineral admixtures (MAs) in conjunction with SP additions affects the workability in the fresh state of grouts and concretes [6]. This motivates the study of optimal levels of superplasticizers and water/binder (w/b) ratios that produce an adequate balance between strength and workability. There are several qualitative and quantitative methods that can be used for these purposes. In a previous work [10], the

rheological behavior of plain and micro-SiO2 (SF) additions of plasticized cement grouts was studied based on the Marsh cone test (MCT). [11]

This study aims to estimate the optimal dosage levels of SP and w/b ratio for and nano-SiO2 (nS) additions. The program addresses the relationship between the fresh and hardened states in concrete incorporating nano silica, and SP in diverse dosages.

Typically, a trial and error approach is followed which consists in selecting and testing a first trial batch, evaluate the results, and then adjust the mixture proportions, based on deducted relationships between the mixture parameters [12] and existing knowledge or recommendations [13] and, finally, re-test the adjusted mixture.

This process is repeated until the required properties are achieved, which may involve carrying out a large and unpredictable number of trial batches. Besides, this optimization technique may not lead to a general solution of the problem. In contrast, statistical experimental design is a more scientific and efficient approach for establishing an optimized mixture for a given constraint, while minimizing the number of experimental data points [14]. Models established on the basis of a factorial design highlight not only significance of the experimental variables but also that of their interactions.

These models are valid for a wide range of mix proportioning and have a predictive capability for the responses of other points located within the experimental domain. This design approach was followed by other authors for various purposes, namely, to design and optimize the mixtures, to compare the responses obtained from various test methods, to analyze the effect of changes in mixture parameters (to evaluate SCC mixture robustness) and to evaluate trade-offs between key mixture parameters and constituent materials (for example, superplasticizer and viscosity agent) [14–21].

The influence of different combinations of nano silica-binder (NS/b), and superplasticizer-binder (SP/b) ratios on the workability (slump test) and mechanical properties (compressive strength) of 20 concrete mixtures of constant water-binder ratio (w/b) were investigated by means of design of experiments. The effects of studied parameters were characterized and analyzed using ANOVA and regression models, which can identify the primary factors and their interactions on the measured properties.

II. EXPERIMENTAL PROGRAM

2.1. Materials

Ordinary Portland Cement (OPC) conforming to ASTM C150 standard was used as received. Chemical and physical properties of used cement are given in Table 1. SiO2 nano particles with average particle size of 30 nm and 45 m2/g Blaine fineness produced from WINLAB laboratory chemicals, UK was used as received. The properties of SiO2 nano particles are shown in Table 2. Transmission electron micrographs (TEM) and powder X-ray diffraction (XRD) diagrams of SiO2 nano particles are shown in Figs. 1a,b. Crushed limestone aggregates, as well as sand free of alkali-reactive materials were used to insure producing durable Concretes; the aggregates were mixed by percentages of 65% for coarse aggregate, and 35% for fines by volume. A polycarboxylate with a polyethylene condensate de-foamed based admixture (Glenium C315 SCC) was used. Table 3 shows some of the physical and chemical properties of polycarboxylate admixture used in this study.

2.2. Samples preparation

A total of 20 mixtures were prepared as shown in table 4. Sets of 6 cubes (15*15*15 cm3) were cast to perform compression strength tests after 7, and 28 days of water curing. Cubes were consolidated in accordance to ASTM C 192 in three layers on a vibrating table, where each layer was vibrated for 10 seconds, and then the specimens were de-molded after 24 hours and cured in normal free water at room temperature until the day of testing. Five SP percentages are used in order to perform the mentioned investigation; 0%, 0.44%, 0.66%, 0.73%, and 0.88%, while four NS substitution percentages are used in parallel; 0%, 1%, 2%, and 3%. The constituents of the 20 mixtures are presented in table 4. Preparation of mixtures was performed in the following sequence: (a) Weighing components, (b) mixing the solid components inside a turn tilt mixer for 1 min, (c) adding sonicated nano silica with a portion of water and mixing for 1 min, (d) adding superplasticizer into the rest of water for helping dispersing the nano silica, and (e) finally mechanical mixing for 2.5 min.

III. RESULTS AND DISCUSSIONS

3.1. Effect of changing SP% on slump of different nano silica concrete mixes

- Saturation dosage of superplasticizer can be defined as the dosage beyond which higher contents of superplasticizer do not increase the slump value significantly.
- From figures 2 (A-D) we can conclude a saturation point of 0.66% by weight cement for all conducted mixes, either those with nano silica contents, or the plain mix.
- Increasing the superplasticizer dosage beyond the saturation point induced substantial bleeding and segregation for the control, and the 1% nano silica (NS1) mixes, while by increasing the nano silica addition above 1% (mixes NS2,and NS3), the nano silica acted as anti-bleeding and neither bleeding nor segregation occurred, this can be attributed that by increasing nano silica content , more silica particles got adsorbed on the ettringite phase of cement hydration and so more un adsorbed polymers are found free and thus resistance occurring when two neighboring polymers approach each other, this resistance increase with the increase of superplasticizer beyond the saturation point where the un adsorbed polymers increases thus increasing viscosity. As mentioned by (yamada et.al 1998) [22].
- At low superplasticizer doses, as the nano silica addition increases the slump results decreased and this can be attributed to the increase of the attractive forces that are predominant over the hydrodynamic forces exerted by the flow field and, therefore, the formation of aggregations takes place.
- While by increasing the dosage the hydrodynamic forces become higher and overcome the attractive inter-particle forces leading to breakdown of aggregations into small particles. Consequently, the liquid entrapped within aggregations is gradually released, thus increasing workability. [23]

3.2. Effect of changing SP% on compressive strength of different nano silica concrete mixes

From figures 3a-d we can conclude that regardless of the nano silica percentage used, the higher compressive strength results were reached at, or around saturation dosage (0.66%), this finding was also mentioned by [23]

The highest compressive strength result of all 20 mixes were reached using 3% NS, and 0.73% SP. The early and late compressive strengths were 540 kg/cm2, and 634 kg/cm2 respectively. The use of 3% NS, and 0.73% SP increased the late compressive strength by 135% than the non plasticized control mix. No matter the nano silica % used is the early strength results proved to be highly correlated to the late strength results with R2 values exceeding 95% for all mixes as it can be seen from figures 4 a-d, such findings were previously discussed in sections. The concrete fresh and hardened behavior cannot be predictable when SP saturation dosage is exceeded. We can finally conclude that to ensure adequate concrete fresh and hardened behavior, a percentage close to superplastesizer's saturation point should be used.

3.3. Regression model correlating NS, and SP percentage with the compressive strength and slump of concrete mixes

Based on the above mentioned results, and conclusions, the effects of studied parameters were characterized and analyzed using ANOVA and regression models, which can identify the primary factors and their interactions on the measured properties. To find out the best possible mixture under the condition of this research concept for the desired workability, and mechanical characteristics, a multi-objective optimization problem was defined and solved based on developed regression models.

Statistical design of experiments can be used for optimization of linear and non-linear systems. When non-linear effects and interactions of several different variables (factors) are anticipated, factorial designs provide the minimum number of experiments needed to investigate those effects and combine them into a property response model. the chosen k factors are set at four different levels, a 4k factorial design is created and the properties are evaluated at all combinations of those k factors and levels. A regression polynomial is then fitted to the experimental values obtained and the model is considered valid only when the differences between the experimental and the calculated values (error) are uncorrelated and randomly distributed with a zero mean value and a common variance. In what follows, the effect of NS, and SP % on the 28 days compressive strength, and slump results will be discussed statistically and the optimum percentages will be determined.

3.3.1. Evaluation of Compressive Strength Results

Based on the conducted experimental program, the following results can be drawn:

3.3.1.1. Conditional sums of squares, and analysis of variance:

The analysis of variance (ANOVA) table 5A, 5B, and 5C decomposes the total variability in the dependent variable into two components: one due to the regression, and the second due to deviations around the fitted

model. The R.-squared statistic, based upon the ratio of the model sum of squares divided by the total (corrected) sum of squares, indicates that the model accounts for 94% of the variation of the mean size percentage to the origin material. The mean squared error estimates the variance of the deviations around the model to be equal to 25.26. Since the P value corresponding to the F-ratio is less than 0.05, the model as a whole is statistically significant.

3.3.1.2. Estimation of coefficients, test of significance and confidence intervals:
The estimated coefficients for the multiple regression model are shown in Table 5C. The P values correspond to tests of the hypotheses that the coefficients are equal to zero. Values of P less than 0.05 indicate statistically significant non zero coefficients at a 95% confidence level.
The proposed equation is
28 DAYS COMPRESSIVE STREGNTH (Kg/cm2) =
{296.88 + (300.92*SP) + (34.87*NS) -15.37*(NS-1.533)*(NS-1.533)}

3.3.1.3. Test for outliers and unusual residuals:
Fig.5a shows the Standardized residuals as a function of the predicted values. The residuals show the difference between the actual values and the predictions, and the Standardized residuals, express each deviation in terms of how many deviations it is away from the fitted line. The Standardized residuals that were calculated are based on the estimated residual standard deviation if the fitting were performed without that data value. This kind of residuals is particularly useful for detecting outliers (i.e. points that do not follow the same pattern as the others). As can be seen in Fig. 5a, the plot appears reasonably random, and none of the residuals is noticeably distinct from the others. The normal probability plot the residuals, shown in Fig. 5b, can be used to judge whether the residuals could reasonably be considered to follow a normal distribution, and may also be helpful in detecting outliers. The residuals fall fairly well along a straight line, while no outliers can be observed.

3.3.1.4. Compressive strength (actual/predicted) design charts:
Figure 6 introduces helpful design chart correlating NS, and SP percentages with actual and predicted compressive strengths respectively. The NS percentages for the predicted results were chosen to be from 0% to 6% from total binder content.it should be noted that results are constrained with the proposed experimental concrete mix. Finally based on the proposed mix constituents, and without exceeding the SP saturation dosage, the most desirable NS, and SP percentages were introduced in figure 7, as well as the corresponding predicted compressive strength value.

3.3.2. Evaluation of Slump Results:
Based on the conducted experimental program, the following results can be drawn:

3.3.2.1. Conditional sums of squares, and analysis of variance:
The analysis of variance (ANOVA) table 6A, 6B, and 6C decomposes the total variability in the dependent variable into two components: one due to the regression, and the second due to deviations around the fitted model. The R.-squared statistic, based upon the ratio of the model sum of squares divided by the total (corrected) sum of squares, indicates that the model accounts for 90% of the variation of the mean size percentage to the origin material. The mean squared error estimates the variance of the deviations around the model to be equal to 2.20. Since the P value corresponding to the F-ratio is less than 0.05, the model as a whole is statistically significant.

3.3.2.2. Estimation of coefficients, test of significance and confidence intervals:
The estimated coefficients for the multiple regression model are shown in Table 6C. The P values correspond to tests of the hypotheses that the coefficients are equal to zero. Values of P less than 0.05 indicate statistically significant non zero coefficients at a 95% confidence level.
The proposed equation is
Slump (cm) = 5.495 + (23.016*SP) – (1.35*NS)

3.3.2.3. Test for outliers and unusual residuals:
Fig. 8a shows the Standardized residuals as a function of the predicted values. The residuals show the difference between the actual values and the predictions, and the Standardized residuals, express each deviation in terms of how many deviations it is away from the fitted line. The Standardized residuals that were calculated are based on the estimated residual standard deviation if the fitting were performed without that data value. This kind of residuals is particularly useful for detecting outliers (i.e. points that do not follow the same pattern as the others). As can be seen in Fig.8a, the plot appears reasonably random, and none of the residuals is noticeably distinct from the others. The normal probability plot the residuals, shown in Fig 8b, can be used to judge whether the residuals could reasonably be considered to follow a normal distribution, and may also be

helpful in detecting outliers. The residuals fall fairly well along a straight line, while no outliers can be observed.

3.3.2.4. Slump (actual/predicted) design charts:

Figure 9 introduces helpful design chart correlating NS, and SP percentages with actual and predicted slump respectively. The NS percentages for the predicted results were chosen to be from 0% to 6% from total binder content. it should be noted that results are constrained with the proposed experimental concrete mix.

Finally based on the proposed mix constituents, and without exceeding the SP saturation dosage, the most desirable NS, and SP percentages were introduced in figure 10, as well as the corresponding predicted slump value.

IV. FIGURES AND TABLES

4.1. Figures:

(a)   (b)
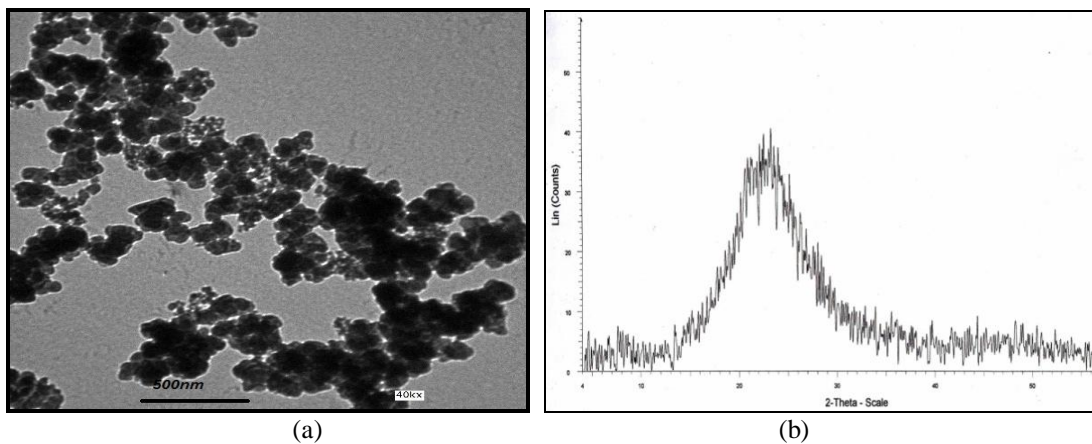
Figure 1: (a) TEM micrograph of SiO2 Nano particles, (b) XRD analysis of SiO2 Nano particles.

A) CO   B) NS1

C) NS2   D) NS3
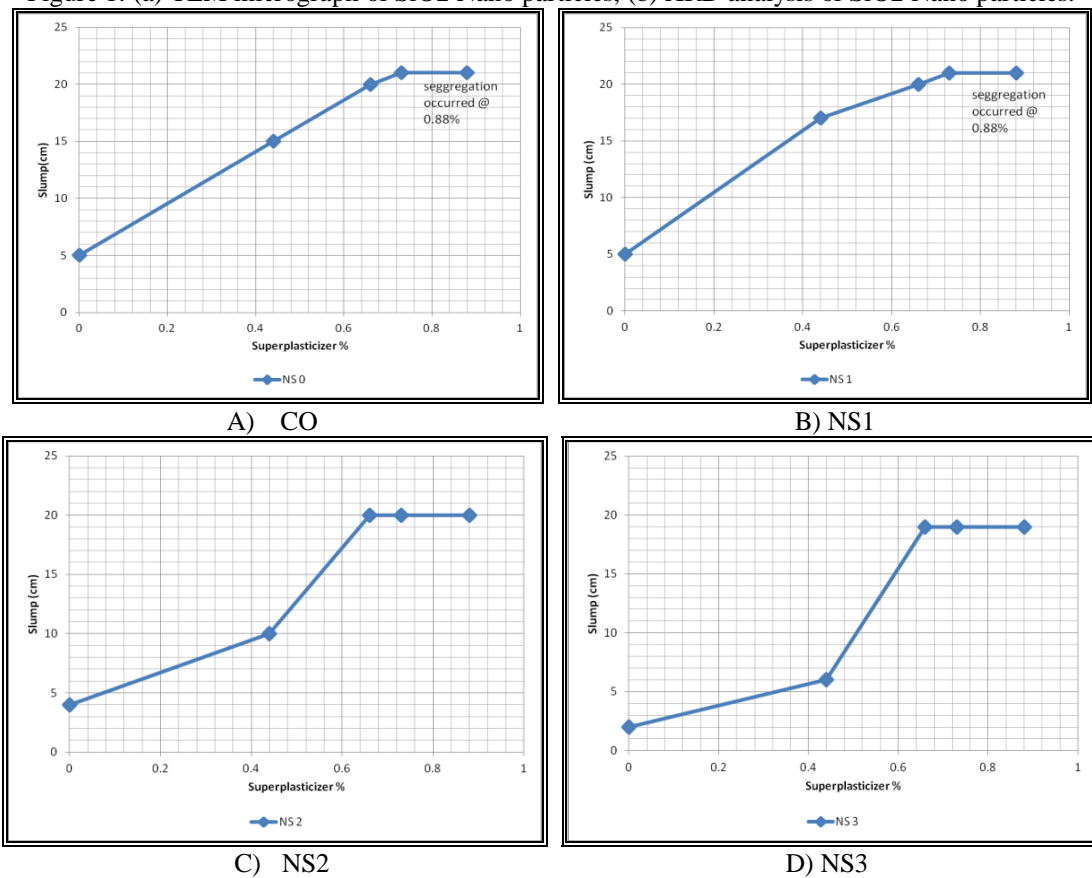
Figure 2: Effect of increasing SP on the slump of different NS concrete.

A: CO

B: NS1

C: NS2

D: NS3
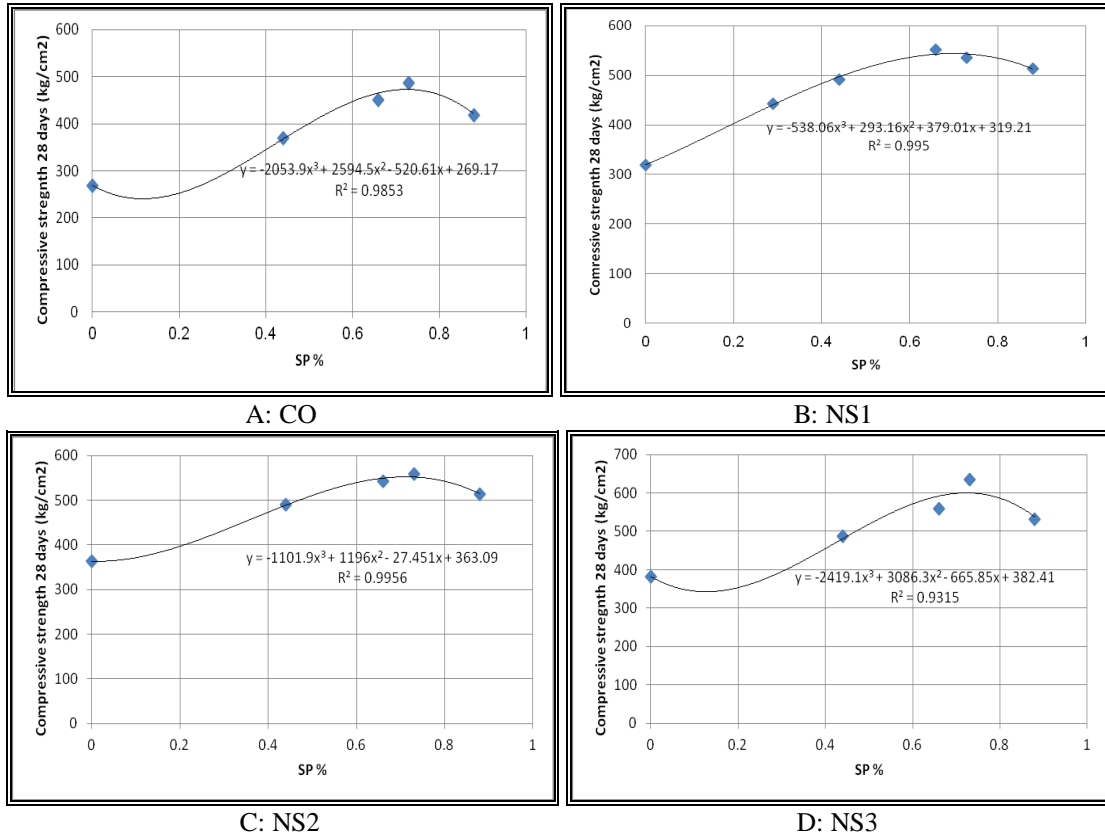
Figure 3: Effect of increasing SP on the 28 days compressive strength of different NS concrete.

A) CO

B) NS1

C) NS2

D) NS3
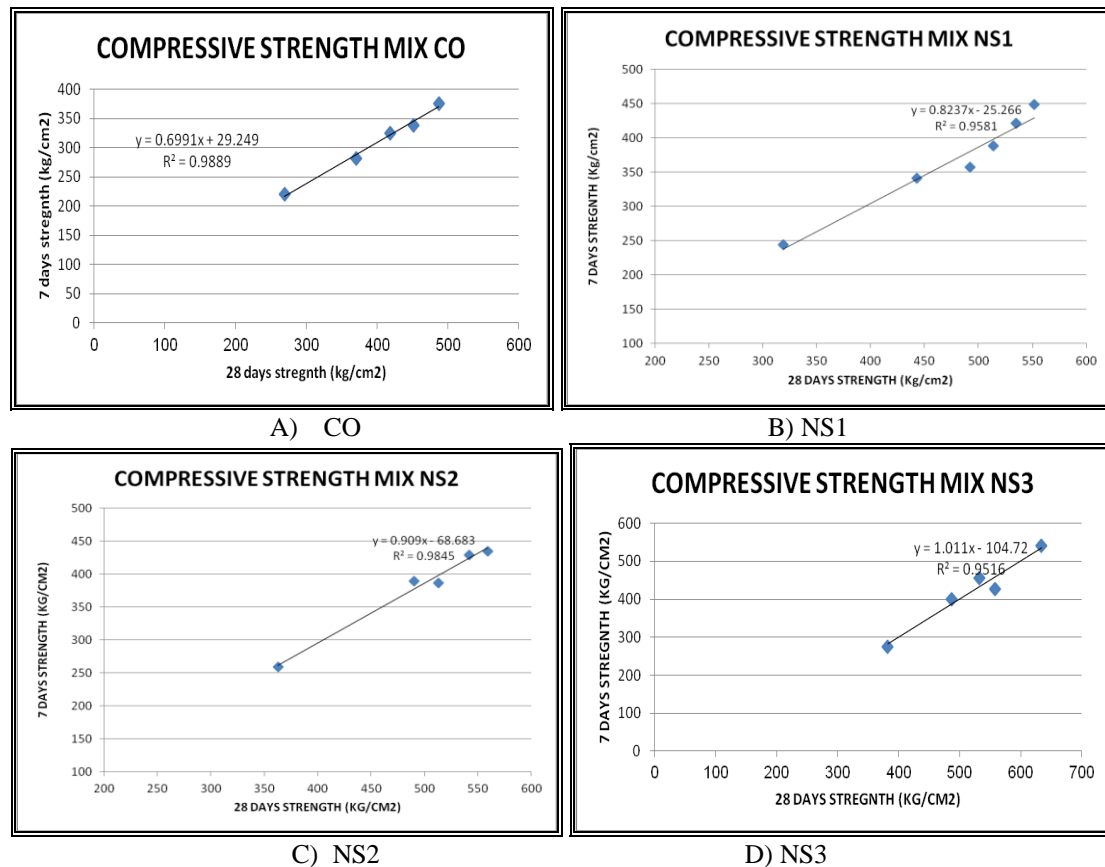
Figure 4: correlation between early and late strengths with the change of SP %.

A)

B)
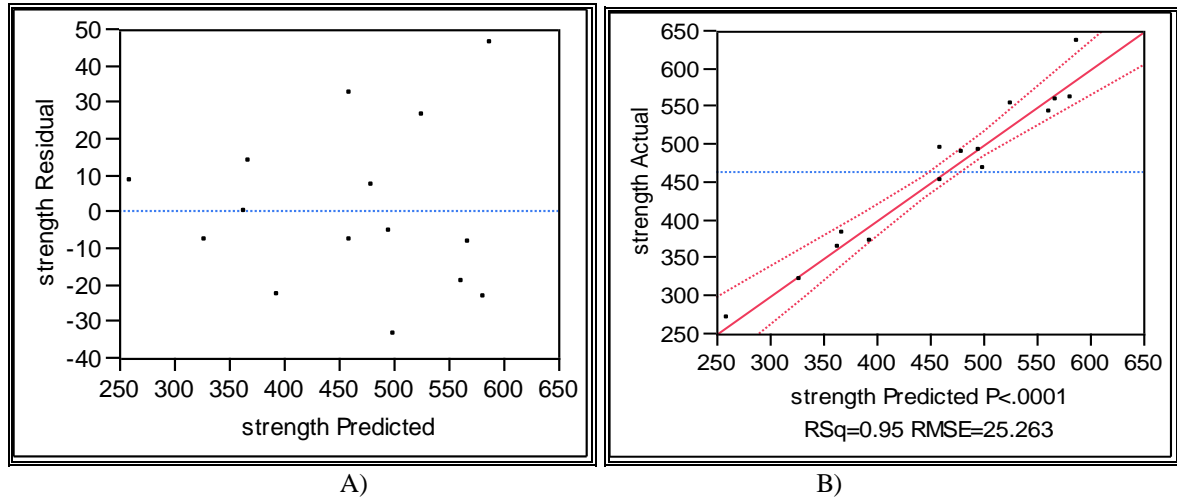
Figure 5: compressive strength A) Residual by Predicted Plot, B) Whole Model Actual by Predicted Plot
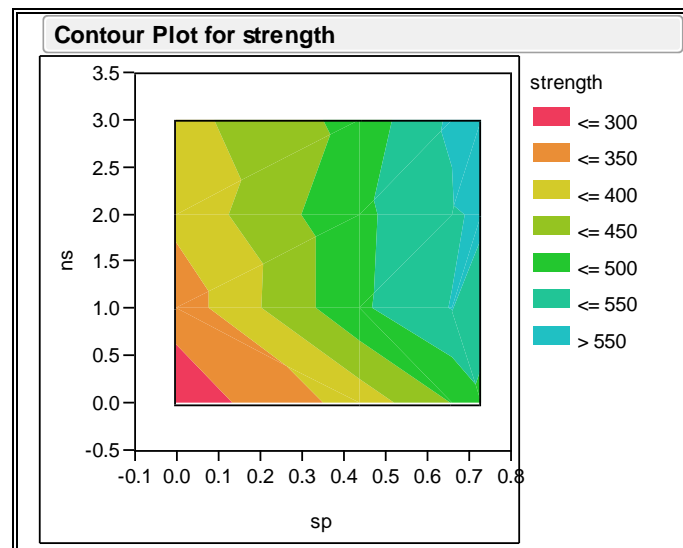
Figure 6: Contour plot correlating NS and SP with compressive strength actual results.
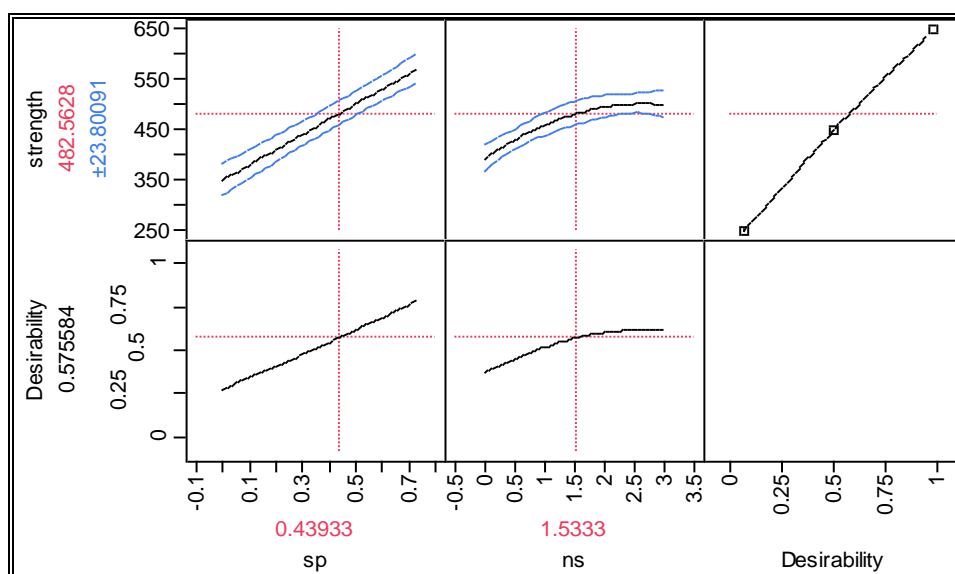
Figure 7: compressive strength most desirable NS, and SP percentages.
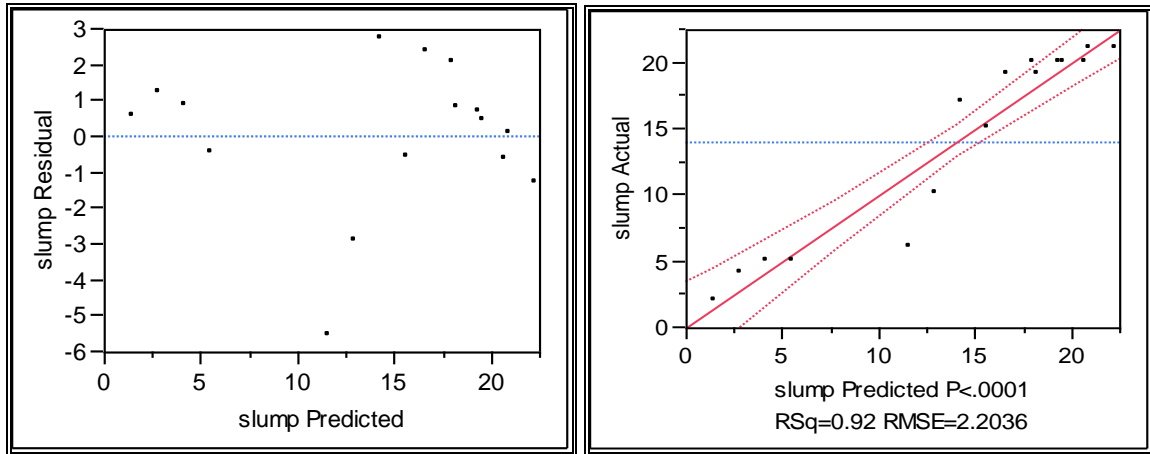
Figure 8: slump A) Residual by Predicted Plot, B) Response Whole Model Actual by Predicted Plot
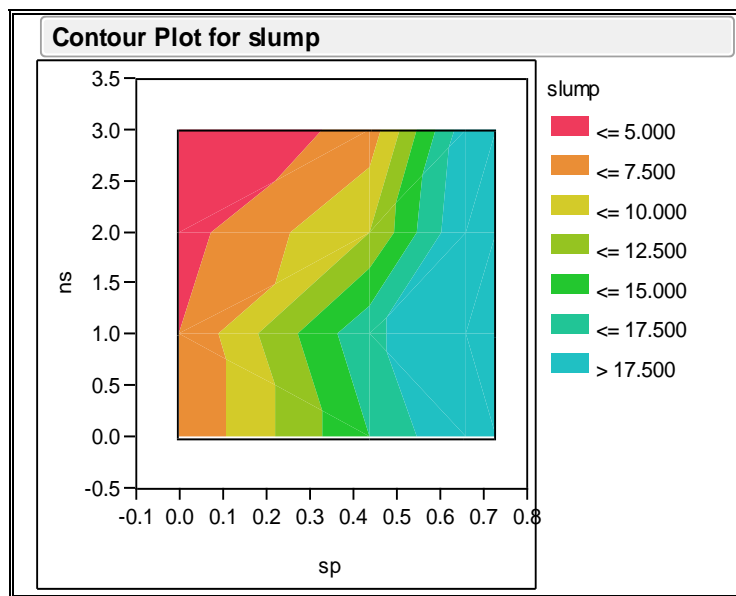
Figure 9: Contour plot correlating NS and SP with slump actual results.
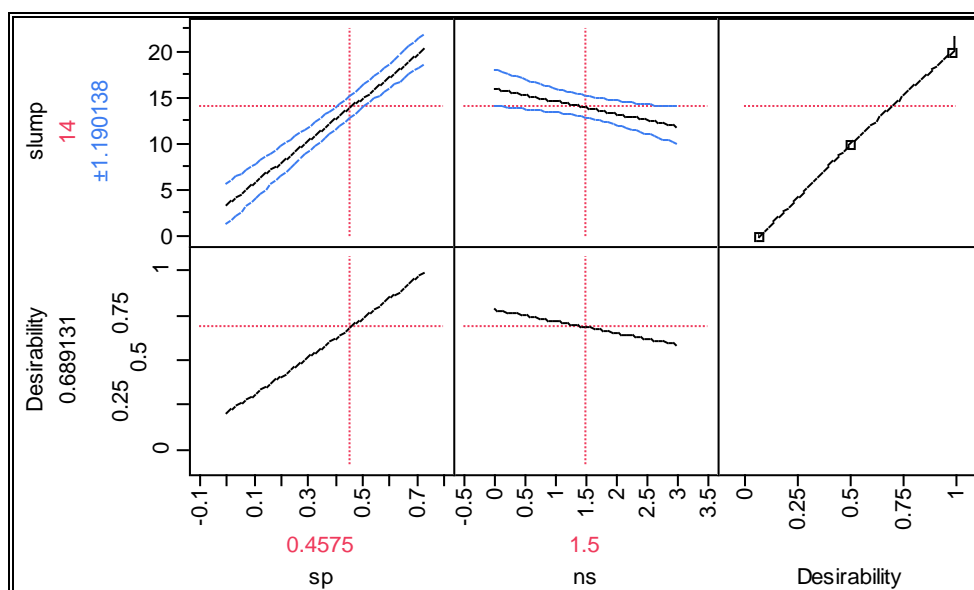
Figure 10: slump most desirable NS, and SP percentages.

The SI derived unit for **pressure** is the pascal. 1 pascal is equal to 1.01971621298E-5 kg/cm2.

4.2 Tables:

Table1. Properties of Portland cement (wt%).

Element	Sio2	Al2O3	Fe2O3	CaO	MgO	SO3	Na2O	K2O	L.O.I
Cement	20.13	5.32	3.61	61.63	2.39	2.87	0.37	0.13	1.96

Table2. Chemical composition of Nano SiO2 (wt %).

Element	SiO2	Fe2O3	Al2O3	MgO	CaO	Na2O	P2O5
NS	99.17	0.06	0.13	0.11	0.14	0.40	0.01

Table3. Physical and chemical characteristics of the polycarboxylate admixture.

Appearance	Off white opaque liquid
Specific gravity @ 20°C	1.095 ± 0.02 g/cm3
PH-value	6.5 ± 1
Alkali content (%)	Less than or equal to 2.00
Chloride content (%)	Less than or equal to 0.10

Table 4: mixtures components (kg) per 1 m³.

| MIX	CEMENT	AGGREGATE		WATER	S.P.	N.S.
		COARSE	FINE			
CO	480	1109	597	195	0	0
CO44	480	1109	597	195	2.11	0
CO66	480	1109	597	195	3.16	0
CO73	480	1109	597	195	3.50	0
CO88	480	1109	597	195	4.22	0
S1	475.2	1109	597	195	0	4.8
S144	475.2	1109	597	195	2.11	4.8
S166	475.2	1109	597	195	3.16	4.8
S173	475.2	1109	597	195	3.50	4.8
S188	475.2	1109	597	195	4.22	4.8
S2	470.4	1109	597	195	0	9.6
S244	470.4	1109	597	195	2.11	9.6
S266	470.4	1109	597	195	3.16	9.6
S273	470.4	1109	597	195	3.50	9.6
S288	470.4	1109	597	195	4.22	9.6
S3	465.6	1109	597	195	0	14.4
S344	465.6	1109	597	195	2.11	14.4
S366	465.6	1109	597	195	3.16	14.4
S373	465.6	1109	597	195	3.50	14.4
S388	465.6	1109	597	195	4.22	14.4

Where: S.P: "super plasticizer", N.S: "nano silica

Table 5: Compressive strength statistical results:
5.A. summary of Fit

Response	Value
RSquare	0.952413
RSquare Adj	0.939435
Root Mean Square Error	25.26265
Mean of Response	462.3333
Observations (or Sum Wgts)	15

5.B. Analysis of Variance

F Ratio	Mean Square	Sum of Squares	DF	Source
73.3860	46835.0	140505.12	3	Model
Prob > F	638.2	7020.22	11	Error
<.0001		147525.33	14	C. Total

5.C. Parameter Estimates

Prob>|t|	t Ratio	Std Error	Estimate	Term
<.0001	17.33	17.13187	296.88647	Intercept
<.0001	13.12	22.93379	300.92451	sp
<.0001	6.09	5.723765	34.873244	ns
0.0388	-2.35	6.556148	-15.37876	(ns-1.53333)*(ns-1.53333)

Table 6: Slump statistical results
6.A. Summary of Fit

Response	Value
RSquare	0.919892
RSquare Adj	0.907568
Root Mean Square Error	2.203584
Mean of Response	14
Observations (or Sum Wgts)	16

6.B. Analysis of Variance

F Ratio	Mean Square	Sum of Squares	DF	Source
74.6404	362.437	724.87486	2	Model
Prob > F	4.856	63.12514	13	Error
<.0001		788.00000	15	C. Total

6.C. Parameter Estimates

Prob>|t|	t Ratio	Std Error	Estimate	Term
0.0009	4.30	1.277445	5.4949307	Intercept
<.0001	11.91	1.933042	23.016545	Sp
0.0169	-2.74	0.492736	-1.35	Ns

V. SUMMARY AND CONCLUSIONS

The influence of different combinations of nano silica-binder (NS/B), and superplasticizer-binder (SP/B) ratios on the workability (slump test) and mechanical properties (compressive strength) of 20 concrete mixtures of constant water-binder ratio (W/B) were investigated by means of design of experiments. The effects of studied parameters were characterized and analyzed using ANOVA and regression models, which can identify the primary factors and their interactions on the measured properties. From the results obtained, the following conclusions can be drawn:

- A SP saturation point of 0.66% by weight cement was recognized for all conducted mixes, either that with nano silica contents, or the control mix.
- Increasing the superplasticizer dosage higher than the saturation point induced substantial bleeding and segregation for the control, and the 1% nano silica (NS1) mixes, while by increasing the nano silica addition above 1% (mixes NS2,and NS3), the nano silica thought to be acted as anti-bleeding and neither bleeding nor segregation occurred.
- At low dosages of superplasticizer, as the nano silica addition increases the slump results decreased and this can be attributed to the increase of the attractive forces that are predominant over the hydrodynamic forces exerted by the flow field and, therefore, the formation of aggregations takes place.
- While by increasing the dosage the hydrodynamic forces become higher and overcome the attractive inter-particle forces leading to breakdown of aggregations into small particles. Consequently, the liquid entrapped within aggregations is gradually released, thus increasing workability.
- Regardless of the nano silica percentage used, the higher compressive strength results were reached at, or around SP saturation dosage (0.66% by weight cement).
- The highest compressive strength results of all 20 mixes were reached using 3% of NS and 0.73% of SP by weight cement. The early and late compressive strengths were 540 kg/cm2, and 634 kg/cm2 respectively. The use of 3% NS, and 0.73% SP increased the late compressive strength by 135% than the non plasticized control mix.
- No matter the nano silica percentage used is the early strength results proved to be highly correlated to the late strength results with R2 values exceeding 95% for all mixes.
- The concrete fresh and hardened behavior cannot be predictable when SP saturation dosage is exceeded. We can conclude that to ensure adequate concrete fresh and hardened behavior, a percentage close to superplastesizer's saturation point should be used.
- The proposed regression models, correlating the NS, and SP % with both the compressive strength, and slump results proved to be highly significant.
- The R.-squared statistic, based upon the ratio of the model sum of squares divided by the total (corrected) sum of squares, indicates that the compressive strength model accounts for 94% of the variation of the mean size percentage to the origin material.
- The mean squared error estimates the variance of the deviations around the compressive strength model to be equal to 25.26. Since the P value corresponding to the F-ratio is less than 0.05, the model as a whole is statistically significant.
- The R.-squared statistic, based upon the ratio of the model sum of squares divided by the total (corrected) sum of squares, indicates that the slump model accounts for 90% of the variation of the mean size percentage to the origin material.
- The mean squared error estimates the variance of the deviations around the compressive strength model to be equal to 2.2. Since the P value corresponding to the F-ratio is less than 0.05, the model as a whole is statistically significant.
- The relationships calculated using statistical analysis of experimental results can be used as guidelines in the design of superplastecized concrete mixtures incorporating nano silica particles.
- The results obtained show that, for all properties investigated, the error of the estimate calculated using the relevant model is low when compared with the corresponding experimental value, which validates the calculated models.
- The statistical approach applied here enabled to develop relations, which could adequately describe the dependency of both the compressive strength, and slump on the composition of NS, and SP concretes. These relations were presented as contour plots, which from a practical point of view could serve as a basis for mix design.

REFERENCES

[1]. Sanchez F, Sobolev K. "Nanotechnology in Concrete – A Review". Constr Build Mater 2010; 24:2060–71.

[2]. Pacheco-Torgal, Jalali S. "Nanotechnology: Advantages and Drawbacks in the Field of Building Material". Constr Build Mater 2011; 25:582–90.

[3]. Li, H.; Zhang, M. & Ou J. "Abrasion Resistance of Concrete Containing Nano Particles for Pavement". Wear 260. 2006. P 1262 – 1266.

[4]. Byungwan Jo, Changhyun Kim, Ghiho Tae & Jongbin Park. "Characteristics of Cement Mortar with Nanosio2 Particles". Construction and Building Materials, 21 (2007) 1351–1355.

[5]. Li H, Xiao H-G, Yuan J, Ou J. "Microstructure of Cement Mortar with Nano Particles". Compos B Eng 2004; 35(2):185–9.

[6]. Chandra S, BjRnstrM J. "Influence of Cement and Superplasticizers Type And Dosage on the Fluidity of Cement Mortars-Part I". Cem Concr Res 2002; 32: 1605–11.

[7]. Zingg A, Holzer L, Kaech A, Winnefeld F, Pakusch J, Becker S, et al. "The Microstructure of Dispersed and Non-Dispersed Fresh Cement Pastes – New Insight by Cryo-Microscopy". Cem Concr Res 2008; 38:522–9.

[8]. Felekoglu B, Sarikahya H. "Effect of Chemical Structure of Polycarboxylate-Based Superplasticizers on Workability Retention of Self-Compacting Concrete". Constr Build Mater 2008; 22:1972–80.

[9]. Siddique R, Khan Mi. "Supplementary Cementing Materials". Berlin Heidelberg, Germany: Springer-Verlag; 2011.

[10]. H.J.H. Brouwers, H.J. Radix, (2005) "Self-Compacting Concrete: Theoretical And Experimental Study", Cem. Concr. Res. 35 2116–2136.

[11]. L. Senffa, D. Hotza, W.L. Repette, V.M. Ferreira, J.A. Labrincha, "Mortars with Nano-Sio2 and Micro-Sio2 Investigated By Experimental Design", Constr. Build. Mater. 24 (2010) 1432–1437.

[12]. Vera-Agullo J, Chozas-Ligero V, Portillo-Rico D, GarcِيA-Casas M, Gutiérrez- Martinez A, Mieres-Royo J, Et Al. "Mortar And Concrete Reinforced With Nanomaterials". Nanotechnology Constr 2009;3:383–8.

[13]. Gaitero J, Campillo I, Guerrero A. "Reduction Of The Calcium Leaching Rate Of Cement Paste By Addition Of Silica Nanoparticles". Cem Concr Res 2008;38(8 9):1112–8.

[14]. Rahel Kh. Ibrahim, R. Hamid ⇑, M.R. Taha, "Fire Resistance Of High-Volume Fly Ash Mortars With Nanosilica Addition", Construction And Building Materials 36 (2012) 779–786.

[15]. A.H. Shah1, U.K. Sharma, Danie A.B. Roy, and P. Bhargava, " Spalling behavior of nano SiO2 high strength concrete at elevated temperatures", MATEC Web of Conferences 6, 01009 (2013) DOI: 10.1051/matecconf/20130601009.

[16]. Efnarc. The European Guidelines For Self-Compacting Concrete. <Www.Efnarc.Org>. 15–06-2005 11:00.

[17]. Okamura H, Ozawa K, Ouchi M. "Self-Compacting Concrete". Struct Concr 2000; 1:3–17.

[18]. Nehdi Ml, Summer J. "Optimization Of Ternary Cementitious Mortar Blends Using Factorial Experimental Plans". Mater Struct 2002;35:495–503.

[19]. Khayat Kh, Ghezal A, Hadriche Ms. "Utility Of Statistical Models In Proportioning Self-Consolidating Concrete". Mater Struct 2000;33:338–44.

[20]. Bayramow F, Tasdemir C, Tasdemir Ma. "Optimization Of Steel Fiber Reinforced Concretes By Means Of Statistical Response Surface Method". Cem Concr Compos 2004;26:665–75.

[21]. Khayat Kh, Ghezal A, Hadriche Ms. "Factorial Design Models For Proportioning Self-Consolidating Concrete". Mater Struct 1999;32:679–86.

[22]. Anatol Zingg , Frank Winnefeld , Lorenz Holzer , Joachim Pakusch , Stefan Beckerb, Ludwig Gauckler, "Adsorption of Polyelectrolytes and Its Influence on The Rheology, Zeta Potential, And Microstructure Of Various Cement And Hydrate Phases", Journal Of Colloid And Interface Science 323 (2008) 301–312.

[23]. T. Mangialardi And A.E. Paolini, "Workability Of Superplasticized Micro silica-Portland Cement Concretes", Cement And Concrete Research. Vol. 18, Pp. 351-362, 1988.

Effect of process parameters on surface roughness during grinding of hot work steel AISI H11 under dry, wet and compressed gas environment

Deepak Kumar[1], Dr. Sanjeev Saini[2]

[1]*Department of Mechanical Engineering, M.Tech. Scholar, DAVIET Jalandhar, India.*
[2]*Department of Mechanical Engineering, DAVIET Jalandhar, India.*

Abstract: *The major demands in machining of parts are closely controlling both geometrical accuracy and dimensional of engineering component made up of difficult to shape material is increasing continuously. Surface roughness is the important output responses in the production with respect to quality and quantity respectively. The abrasive machining grinding process is mostly used to attain the closer tolerances with better surface finish. In this work the AISI H11 hot work steel was used to investigate the role of different working environments (dry , wet cooling and compressed gas) and process parameters (feed rate, depth of cut and wheel speed) on surface roughness. It was observed that under wet cooling environment, decrease in feed rate, depth of cut and increase in wheel speed resulted in significant increase in surface quality.*

Keywords: *Environment, Depth of cut, Feed rate, Grinding, Surface roughness*

I. Introduction

There are several processes of manufacturing machining operations i.e., drilling, milling, turning and grinding processes that are important for the conversion of raw materials into finished goods. Most of these processes deal with giving a new shape and form to the raw materials either by changing their state or shape. One of the best method to produce a part or a workpiece that the material is too hard or too brittle and it require high dimensional accuracy and surface finish is by using abrasive machining. Therefore, one such important abrasive machining process is grinding, and it is very useful technique for metal removal at fast rates and for the high level finishing of final products. Grinding is typically a finishing process where quality is important and mistakes are costly. In order to attain high quality parts and high productivity it is necessary to properly choose the correct process parameters. These parameters are usually determined through testing and experience. Grinding is a material removal and surface generation process used to shape and finish components made of metals and other materials. Grinding employs an abrasive product, usually a rotating wheel brought into controlled contact with a work surface. The grinding wheel is composed of abrasive grains held together in a binder. These abrasive grains act as cutting tools, removing tiny chips of material from the work. As these abrasive grains wear and become dull, the added resistance leads to fracture of the grains or weakening of their bond. The dull pieces break away, revealing sharp new grains that continue cutting.

Grinding has been the object of technical research for some decades now. Walton et. al.[1] have used Physical vapor deposition (PVD) coating method on low carbon steel(51CrV4) work piece with CBN grinding wheel for accurate temperature measurements even under aggressive grinding condition and environment. The obtained result shows that high pressure grinding fluid does not influence the coating performance. The temperatures estimated by the PVD-coating technique have been used to validate thermal models based on the circular arc heat source for varying specific materials removal rates. Kwak et. al.[2] presented the experimental setup to analyze effectively the grinding power and the surface roughness of the ground workpiece in the external cylindrical grinding of hardened SCM440 steel using the response surface method. The experimental results show the mathematical model. From adding simply material removal rate to the contour plot of these mathematical models, it was seen that useful grinding conditions for industrial application could be easily determined. Monici et. al. [3] have explained the concept of optimized cutting fluid application method to improve the efficiency of the process and show that combine use of neat oil and CBN wheel give better efficiency than aluminium oxide grinding wheel. Xu et. al. [4] have investigated the experimental procedure for vitreous bond silicon carbide wheel for grinding of silicon nitride.

The result shows that silicon carbide grinding wheel can be used for precision form grinding of silicon nitride to achieve good surface integrity. Badger [5] has researched on the factor affecting the grindability of high speed steel (HSS) by measuring G-ratio and power consumption in surface grinding with an aluminium

oxide wheel. It was found that dominant factor affecting grindability in HSS is the size of the vanadium carbides. Guo et. al. [6] have studied the effect of both wheel wear and process parameters on the grinding performance of plated CBN wheel on a nickel alloy to obtain particular model. Liu et. al. [7] have researched the stringent requirements for grinding wheels include low damage on ground surfaces, self-dressing ability, consistent performance, long wheel lives and low prices to manufacture the silicon wafers. Anderson et. al. [8] have developed a model to predict the contact temperature with using infrared data. The infrared data showed that with increasing depth of cut numerical models were more accurate than analytical model. The obtained results suggest that use of analytical contact zone thermal model should be limited to shallow grinding while numerical models are more suited to larger depth of cut and result also showed higher Peclet number in grinding results in lower overall workpiece temperature. Atzeni [9] et. al. have developed experimental setup to test the influence of cutting speed and feed per gain on surface roughness after grinding cycle.

The observed data have been statistically processed to obtain relationship between among roughness and kinematic parameters. The obtained model shows that the roughness is mainly influenced by the feed per grain and to a lesser degree by the cutting speed. Aurich [10] et. al. have found experimental investigation of dry grinding operations of hardened heat preheated steel and then obtain data compared with wet grinding operation which is taken as reference prototype. Tawakoli et.al. [11] have investigated the effect of ultrasonic vibration on dry grinding and obtained result show that the application of ultrasonic vibration can eliminate the thermal damage on workpiece, increase the G-ratio and decrease the grinding force considerably. Nguyen [12] have investigated the performance of new segmented grinding wheel system and observed that segmented grinding wheel gives better surface integrity with minimum use of coolant as compared to standard wheel.

Brinksmeier [13] et. al. have investigated elastic bonded wheels for a grind-strengthening and super finished surface in a single step. Further, to achieve a high mechanical impact and to minimize the thermal effect of grinding process require a low cutting speed and showed that if chip thickness is constant, the chip formation mechanism shifts towards micro-ploughing and thus additionally increases the specific grinding energy. Fathallah [14] et. al. have investigated for better surface integrity of AISI D2 steel by using sol-gel grinding wheel and cooling by liquid nitrogen comparatively with conditions using aluminium oxide and cooling with oil-based. Ronald [15] et. al. have studied on the influence of grinding wheel bond material on the grindability of metal matrix composites. The obtained result showed that resin bonded wheel performed better than electroplated wheel. Herman [16] et. al. have researched radial wear of super hard grinding wheels in the process of internal grinding of bearing rings. The new developed grinding wheel is designed for bonding the abrasive grains of sub microcrystalline boron nitride using a glass-ceramic bond.

This grinding wheel is compared to CBN grinding wheels composed from ceramic bonding system for roughness profile on the wheel working surface and the wear resistance. Vijayender singh [17] et. al. have developed experimental setup for grinding the composite ceramic material with cryogenic coolant. The observed result showed that cryogenic coolant (ecofriendly) in grinding gives better surface quality of material. Ramdatti [18] et. al. have applied the Taguchi techniques to obtain an optimal setting of grinding process parameters resulting in an optimal value of material removal rate and surface roughness when machining EN-8, EN-39 and cast iron. Demirci [19] et. al. have investigated the influence of nature of bond on surface edge finishing. Experimental results showed that the grinding forces vary sensitively with bond type and wheel velocity. Using diamond grain's wheel, it was found that roughness level obtained with metallic bond is lower than that obtained with resin bond. Using a resin-bonded wheel, two mechanisms of material removal were revealed according to grain's type. (i) A partial ductile regime, i.e., ductile streaks and brittle fracture, obtained with diamond grains, and (ii) a fully ductile regime obtained with SiC grains. It was found that ground surface obtained using SiC grains' wheel has a better roughness than that obtained using diamond grains wheel. Besides, SiC grains seem to lead to more marked streaks and form defects. Demir [20] et. al. investigated influences of grain size and grinding parameters on surface roughness and grinding forces.

The results showed that grain size significantly affected the grinding forces and surface roughness values. Increasing grain size and depth of cut increased the grinding forces and surface roughness values. Pil-Ho [21] et. al. have researched grinding process for surface roughness, grinding force and tool wear. It was observed that at low air temperature decrease the magnitude of grinding force and tool wear significantly, which could result in loner tool life. Mane [22] et. al. have developed experimental setup to study for surface finish enhancement of grinding process using compressed air. From developed experimental study it is observed that, the use of air helps to improve the surface finish of machined surface. Kadirgama [23] et. al. have discussed the optimization of cylindrical grinding when grinding carbon steel (AISI 1042) and effect of three variables (work speed, diameter of workpiece and depth of cut) towards surface roughness with aluminium oxide as grinding wheel. It was found that work speed is the most dominant factors on the Ra, followed by the diameter of workpiece and depth of cut respectively. Ondrej Jusko[24] has investigated that least appropriate material for grinding wheels for cutting 14109.6 bearing steel is CBN with Aluminium oxide grains; Abral and SG grinding wheels are more suitable.

A comparison of the two innovative abrasive materials shows that the performance of abral is slightly superior. Deepak pal [25] et. al. applied Taguchi parametric optimization technique to study the optimization of grinding parameters for minimum surface roughness. It was observed that surface roughness decreases as material hardness increases. It also decreases with increase in speed and changing grain size from G46 to G60, but increases changed to G80. Manimaran [26] et. al. have researched the experiment on the grinding of AISI 316 stainless steel under dry, wet and cryogenic cooling with Alumina(SG) grinding wheel. It has been concluded that with increasing depth of cut under cryogenic cooling, the surface roughness was decreasing as compared to dry and wet cooling. Grinding force and grinding zone heat temperature also obtained less under cryogenic cooling mode. H. Aouici [27] et. al. have investigated in hard turning of AISI H11 hot work steel and concluded that increased in feed rate and depth of cut not significant for surface quality.

II. Experimental Procedures

The H-11 hot work steel plate blank has been heated to a temperature of 1025^0C with half an hour soak time followed by quenching in a 500^0C hot salt bath. It was then tempered in two cycles with maximum temperature of 450^0C and 2 hours of soak time to obtain a final hardness of 45 HRC. Hot work AISI H11 steel have been chosen because of high hardness, excellent wear resistance, hot toughness and good thermal shock resistance properties and have wide application in die and hot-work forging, extrusion, helicopter rotor blades and shafts. The chemical composition of H11 is given in Table1.

Table I: Chemical composition of AISI H11 steel (wt %)

Constituent	C	Si	Mn	P	S	Cr	Mo	V
Composition (In %)	0.35	0.92	0.4	0.011	0.026	5.10	1.30	0.6

The same Aluminimum oxide grinding wheel was used throughout the work. Its specification was "AA46/54 K5 V8" and it was manufactured by Carborundum universal limited company. The wheel dimensions were 200 x 13.31 x 75mm. The grinding experiments were conducted on AISI H11 hot work tool steel under the three different environments of dry, wet and compressed gas. In gas environment, the compressed Nitrogen gas supplied at the grinding zone at an appropriate distance of 45 mm approximately from the cutting zone. The pressure of the compressed gas delivered to the cutting zone is maintained to fix at 3 bar in all gases environmental experiments. And, in wet grinding cooling consists of 20% coolant oil in water, applied directly at the inter-face of grinding wheel–work material at 6.5l/min. For dry grinding there is no coolant is used.

The work piece material, H-11 hot die steel with 304 mm × 110 mm × 24 mm size was used and the cuts were made widthwise. During the experiments, cuts were made of 110mm length. Surface roughness measurements in μm were repeated five times on respective cuts using a Mitutoyo SJ-201p surface roughness test machine and the average value was considered as surface roughness value for the analysis purpose. The instrument for measurement of surface roughness has been shown with the help of figure 1 and schematic arrangement for experimental setup has been shown by figure 2. To investigate the parameters of grinding, In this experimental procedure 27 Nos. of experiments by combining most robust set of different four parameters each having three levels. The different sets of combinations are obtained by as per Taguchi's L27 orthogonal array from Minitab software. The combinations of parameters with different levels are given below in table II.

**Table II: Process parameters with their values at 3 levels.**

Parameters designations	Process parameters	Level-1	Level-2	Level-3
A	Wheel Conditioning	Dry	Wet	Gas
B	Wheel speed (rpm)	1000	1500	2000
C	Feed Rate (mm/min)	5	10	15
D	Depth of cut (mm)	0.1	0.2	0.3

Figure I: Surface roughness machine

Figure II: Schematic arrangement for experimental setup
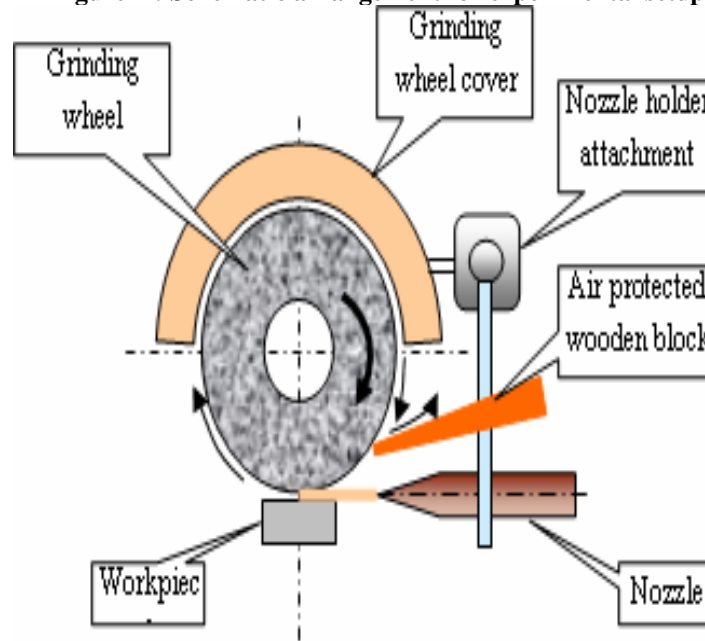
As mentioned in table III, in this experimental setup total 27 Nos. of experiments have been performed on surface grinding machine. During each experiment the various parameters and its level combination are obtained as per Taguchi's L27 orthogonal array. The various levels of parameters are combined during every experiment are shown below table III.

Table III: No. of experiments (Taguchi L$_{27}$ (3^4) orthogonal array)

Exp. No.	A:Wheel Conditioning	B: Wheel speed (rpm)	C: Feed Rate (mm/min)	D: Depth of cut (mm)	SR: Surface Roughness(µm)
1	Dry	1000	5	0.1	0.126
2	Dry	1000	10	0.2	0.186
3	Dry	1000	15	0.3	0.200
4	Dry	1500	5	0.2	0.098
5	Dry	1500	10	0.3	0.210
6	Dry	1500	15	0.1	0.180
7	Dry	2000	5	0.3	0.092
8	Dry	2000	10	0.1	0.130
9	Dry	2000	15	0.2	0.214
10	Wet	1000	5	0.1	0.104
11	Wet	1000	10	0.2	0.106
12	Wet	1000	15	0.3	0.130
13	Wet	1500	5	0.2	0.064
14	Wet	1500	10	0.3	0.100
15	Wet	1500	15	0.1	0.156
16	Wet	2000	5	0.3	0.090
17	Wet	2000	10	0.1	0.064
18	Wet	2000	15	0.2	0.120
19	Gas	1000	5	0.1	0.104
20	Gas	1000	10	0.2	0.112
21	Gas	1000	15	0.3	0.124
22	Gas	1500	5	0.2	0.104
23	Gas	1500	10	0.3	0.128
24	Gas	1500	15	0.1	0.108
25	Gas	2000	5	0.3	0.106
26	Gas	2000	10	0.1	0.078
27	Gas	2000	15	0.2	0.116

III.   Results And Discussions

Table IV and Figure III demonstrate the factor effect on surface roughness. The higher the signal to noise ratio, the more favorable is the effect of the input variable on the output. The graph shows that, the optimum value levels for best surface roughness (minimum) are at a feed rate 5 mm/min, depth of cut 0.1 mm and grinding wheel speed of 2000 rpm in case of wet grinding environment. From response table 5 for Signal to Noise, It can be seen that the most influencing parameter to surface roughness for AISI H11 is Environment i.e., the environment in which grinding wheel is using then feed rate(FR) followed by grinding wheel speed(WS) and depth of cut (DOC). Figure IV shows the interaction plots for S/N ratio for surface roughness, it shows the interaction of environment (dry, wet, gas) with grinding wheel speed, feed rate and depth of cut.

**Figure III: Main Effect Plot of S/N ratios for Surface Roughness**
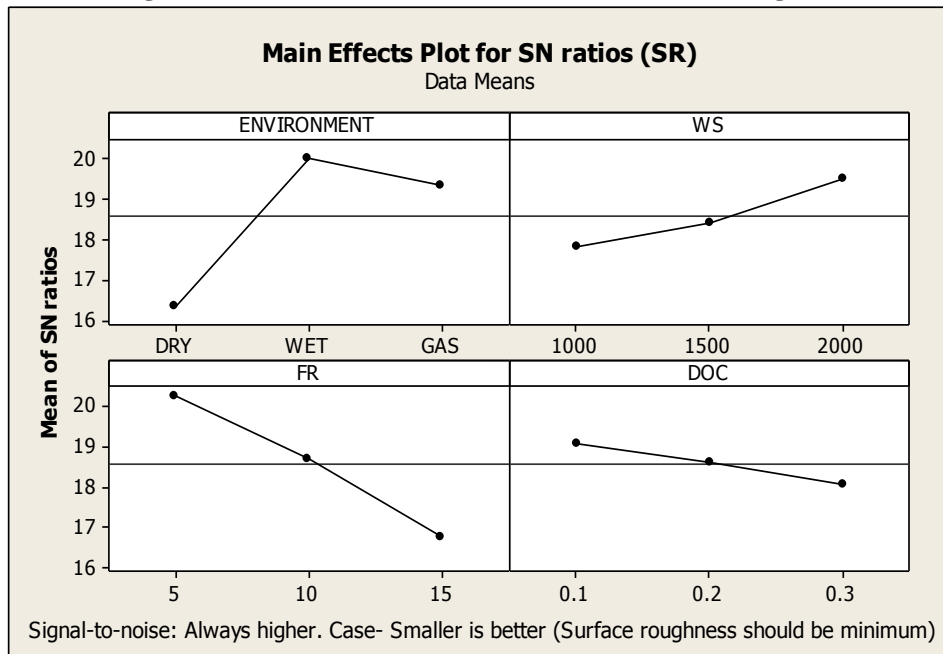
**Figure IV: Main effects plot for means for surface roughness (Smaller is better)**
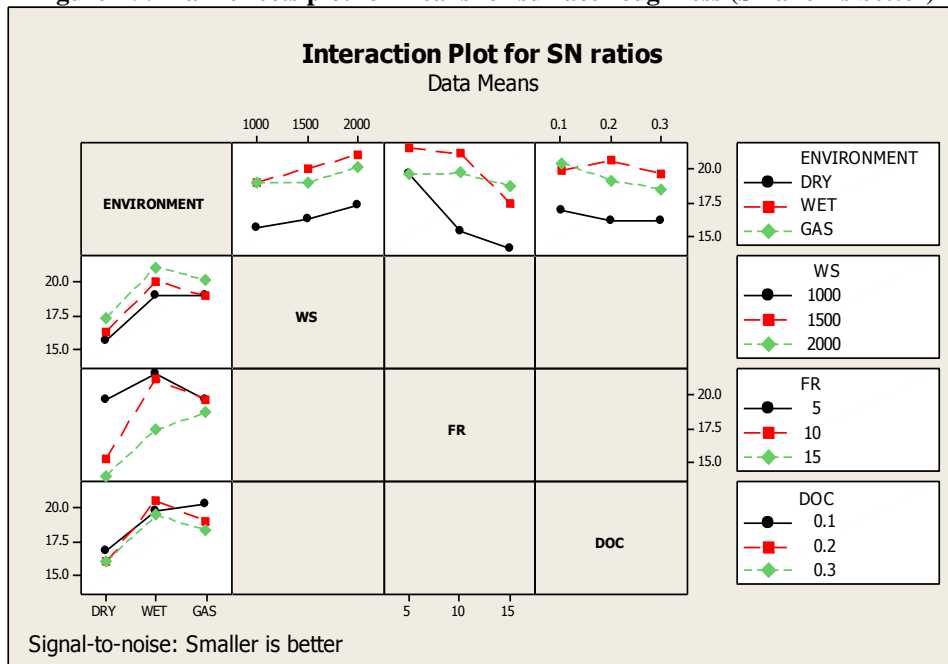
**Table IV: Analysis of variance for S/N ratios (Surface roughness)**

Source	DF	Seq SS	Adj SS	Adj MS	F	P	%C
ENVIRONMENT	2	68.772	68.7722	34.3861	7.85	0.021	34.27
WS	2	13.152	13.1520	6.5760	1.50	0.296	6.55
FR	2	55.173	55.1729	27.5865	6.30	0.034	27.50
DOC	2	4.569	4.5686	2.2843	0.52	0.618	2.28
ENVIRONMENT *WS	4	0.992	0.9919	0.2480	0.06	0.992	0.49
ENVIRONMENT *FR	4	27.760	27.7598	6.9400	1.58	0.292	13.83
ENVIRONMENT *DOC	4	3.966	3.9664	0.9916	0.23	0.914	1.98
Residual Error	6	26.275	26.2751	4.3792			13.09
Total	26	200.659					

Table V: Response table for signal to noise ratios (Surface roughness)

Level	ENVIRONMENT	WS	FR	DOC
1	16.34	17.81	20.24	19.05
2	20.01	18.39	18.70	18.59
3	19.34	19.49	16.75	18.04
Delta	3.67	1.68	3.49	1.01
Rank	1	3	2	4

From figure V(a), it is observed that wet cooling environment plays an important role and gives better surface quality as compared to dry and compressed gas environment. Figure V(b) shows that increase in grinding wheel speed also improves the surface quality of work piece. Consequently, Figure V(c) and figure V(d) show that surface roughness increased frequently with increased in feed rate and depth of cut. It is due to the reason that with increased in feed rate and depth of cut, large layer of material comes under the grinding wheel to remove large material which results greater amount of force generated between the workpiece and grinding wheel interface zone and the section of sheared chip increases because the metal resists rupture more and requires large efforts for chip removal and shows the result increased in surface roughness. It is also seen than with increased in feed rate, depth of cut leads to burn surface of workpiece material due to generation of higher temperature in grinding work zone which results in damage surface layer and produce higher surface roughness.

Figure V: Variations in the Surface roughness with (a) Environment i.e. dry, wet cooling and compressed gas (b) Wheel speed (c) Feed rate (d) Depth of cut
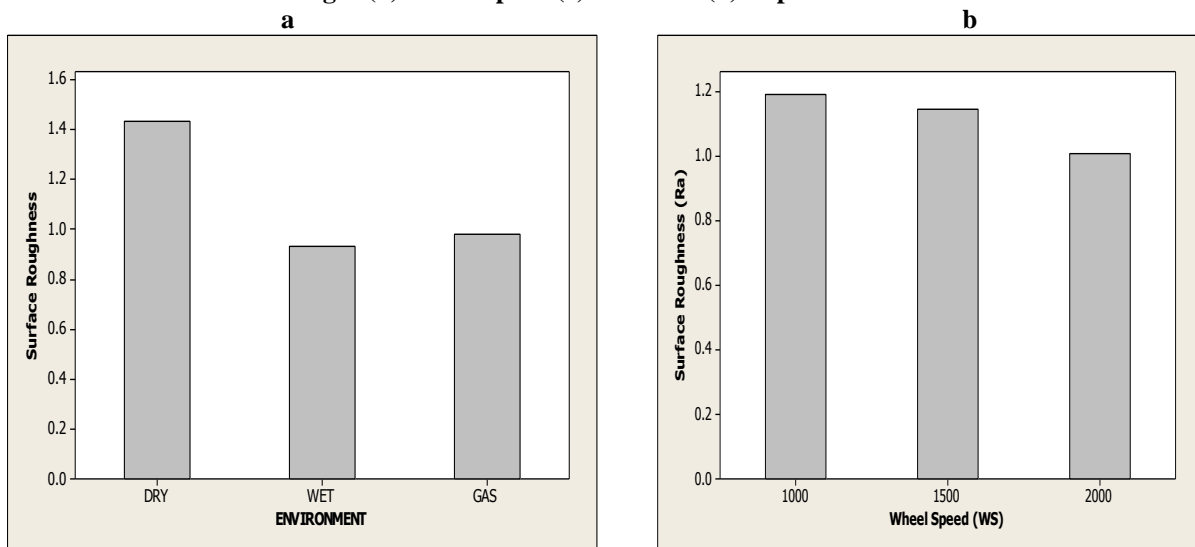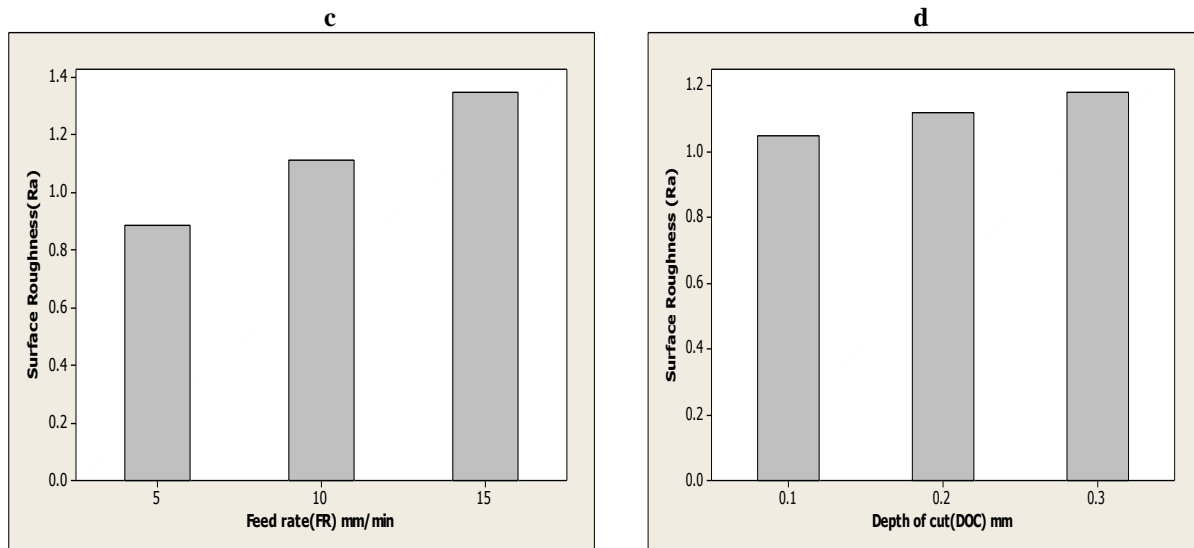
IV. Conclusion

For Surface Roughness (Ra), Experiments were carried out on the grinding of AISI H11 hot work steel under dry, wet, and compressed gas environment with the Aluminimum oxide grinding wheel. The different grinding working environment and different cutting parameters were examined and the major conclusions from the investigation are as follows:

1. It was observed that the better surface quality can be achieved under wet condition than compressed gas and dry environment, when grinding AISI H11 hot work steel with Aluminimum oxide grinding wheel.
2. The effectiveness of wet environment was due to the better lubrication provided by the coolant compared to dry and gas environment.
3. It was experimentally proved that increase in grinding wheel speed and decrease in feed rate, depth of cut produce better surface quality.

REFERENCES

[1] Walton I.M., Stephenson D.J. (2006),"The measurement of grinding temperatures at high specific material removal rates" International Journal of Machine Tools & Manufacture, vol.46, pp.1617–1625.
[2] Kwak Jae, Sim Sung (2006),"An analysis of grinding power and surface roughness in external cylindrical grinding of hardened SCM440 steel using the response surface method", International Journal of Machine Tools & Manufacture, 46, pp.304–312.
[3] Monici Rodrigo Daun, Bianchi Eduardo Carlos (2006),"Analysis of the different forms of application and types of cutting fluid used in plunge cylindrical grinding using conventional", International Journal of Machine Tools & Manufacture,46, pp. 122–131.
[4] Xu L.M., Shen Bin, (2006),"Vitreous bond silicon carbide wheel for grinding of silicon nitride", International Journal of Machine Tools & Manufacture, vol. 46, pp. 631–639.
[5] Badger J. (2007),"Grindability of Conventionally produced and powder-metallurgy high-Speed Steel", Annals of the CIRP, Vol. 56, pp.353-356.
[6] Guo C., Shi Z., Attia H. (2007),"Power and wheel wear for grinding nickel alloy with plated CBN wheels", Annals of the CIRP, Vol. 56, pp.343-346.
[7] Liu J.H., Pei Z.J. (2007),"Grinding wheels for manufacturing of silicon wafers: A literature review", International Journal of Machine Tools & Manufacture, vol. 47, pp. 1–13.
[8] Anderson D., Warkentin A. (2008),"Comparison of numerically and analytically predicted contact temperatures in shallow and deep dry grinding with infrared measurements", International Journal of Machine Tools & Manufacture, vol.48, pp.320–328.
[9] Atzen E. , Iulian L. (2008),"Experimental study on grinding of a sintered friction material", journal of materials processing technology, vol.196, pp.184-189.
[10] Aurich J.C., Herzenstiel P. (2008),"High-performance dry grinding using a grinding wheel with a defined grain pattern", CIRP Annals-Manufacturing Technology, vol. 57, pp. 357–362.
[11] Tawakoli Taghi, Azarhoushang Bahman (2008),"Influence of ultrasonic vibrations on dry grinding of soft steel", International Journal of Machine Tools & Manufacture, vol.48, pp.1585– 1591.
[12] Nguyen T., Zhang L.C. (2009),"Performance of a new segmented grinding wheel system", International Journal of Machine Tools & Manufacture, vol. 49, pp.291–296.
[13] Brinksmeier E., Heinzel C. (2009),"Superfinishing and grind-strengthening with elastic bonding system", Journal of Materials Processing Technology, vol.209, pp. 6117–6123.

[14]   Fathallah Brahim Ben, Fredj Nabil Ben (2009),"Effects of abrasive type cooling mode and peripheral grinding wheel speed on the AISI D2 steel ground surface integrity", International Journal of Machine Tools & Manufacture, vol.49, pp.261–272.

[15]   Ronald B. Anand, Vijayaraghavan L. (2009),"Studies on the influence of grinding wheel bond material on the grindability of metal matrix composites", Materials and Design, vol.30, pp. 679–686.

[16]   Herman Daniela (2009),"Influence of vitrified bond structure on radial wear of CBN grinding wheel", International Journal of Machine Tools & Manufacture, vol.49, pp.231–242.

[17]   Singh Vijayender, Ghosh S. (2010),"Grindability Improvement of Composite Ceramic with Cryogenic Coolant", Proceedings of the World Congress on Engineering 2010' Vol II, ISSN: 2078-0966 (Online).

[18]   Ramdatti J.L., Popat M.A. (2010),"Some study aspect of external cylindrical grinding machine parameters using Taguchi techniques", International journal of manufacturing technology and industrial engineering (IJMTIE), vol. 1, pp.13-18.

[19]   Demirci, Mezghani S., Mkaddem A., Mansori M. (2010),"Effects of abrasive tools on surface finishing under brittle-ductile grinding regimes when manufacturing glass, Journal of Materials Processing Technology, vol. 210, pp. 466–473.

[20]   Demir Halil, Gullu Abdulkadir, Ciftci Ibrahim, Ulvi Seker (2010),"An Investigation into the influences of grain size and grinding parameters on surface roughness and grinding forces when grinding", Journal of Mechanical Engineering, vol.56, pp. 447-454.

[21]   Lee Pil Ho, Lee S.W. (2011),"Experimental characterization of micro-grinding process using compressed chilly air", International Journal of Machine Tools & Manufacture, vol.51, pp.201–209.

[22]   Mane A.B., Jadhav V.S. (2012),"Surface roughness enhancement of grinding process using Compressed air in case of dry machining", Indian journal of applied research, Vol. 2, pp.53-55.

[23]   Kadirgama K., Rahman M. M. (2012),"A surrogate modelling to predict surface roughness and surface texture when grinding AISI 1042 carbon steel", Scientific Research and Essays, Vol.7 (5), pp.598-608.

[24]   Jusko Ondrej (2012),"New abrasive materials and their influence on the surface quality of bearing steel after grinding", Acta Polytechnica, Vol. 52, pp.80-82.

[25]   Pal Deepak, Bangar Ajay, Sharma Rajan, Yadav Ashish (2012),"Optimization of Grinding Parameters for Minimum Surface Roughness by Taguchi Parametric Optimization Technique", International Journal of Mechanical and Industrial Engineering (IJMIE), ISSN No. 2231 –6477, Vol.1.

[26]   Manimaran G., Kumar M. P. (2013),"Effect of cryogenic cooling and sol–gel alumina wheel on grinding performance of AISI316 stainless steel", Archives of civil and mechanical engineering, vol.13, pp.304–312.

[27]   Aouici H. (2010),"Machinability investigation in hard turning of AISI H11 hot work steel with CBN tool", ISBN 1392 – 1207, MECHANIKA, pp. 71-77.

Experimental Setup of Pedal Operated Centrifugal Pump for Low-lift Applications

M. Jawahar[1], G. Venkanna[2], B. Sandeep[3]

[1,2,3] Mechanical, Jayamukhi institute of technological sciences, warangal, TS, JNTUH, INDIA

Abstract: *Objective of this paper based on renewable energy , If we boost the research on pedal powered technology - trying to make up for seven decades of lost opportunities - and steer it in the right direction, pedals and cranks could make an important contribution to running a post-carbon society that maintains many of the comforts of a modern life. The possibilities of pedal power largely exceed the use of the bicycle. As the concept of* [pedal renewable energy](#) *is emerging again with the revolutionary approach to clean the environment so many inventions are before us. So we had made an attempt to design and construct pedal operated water pump which is used in small irrigation like gardening is illustrated in this paper. The pedal operated pump can be construct using local material and skill. A water system includes a Centrifugal pump operated by pedal power. The pump stand includes a housing in which a foot pedal and a drive shaft rotate. It works on the principle of compression and sudden release of a tube by creating negative pressure in the tube and this vacuum created draws water from the sump. This can be built using locally available materials and can be easily adapted to suit the needs of local people. This free the user from rising energy costs and can be used anywhere, produce pollution less environment and provide healthy exercise.*

Keywords: *centrifugal pump, gear, impeller, pedal, renewable energy.*

I. Introduction

Pedal power vehicles are becoming popular day by day. Pollution in the environment is causing serious health issue and doctors are emphasizing the use of bicycle as an exercise to be healthy. On this line Chinese are replacing their vehicles with pedal power vehicles. Indians and Bangladeshi bicycle rickshaws are the examples of such vehicles.

Pedal power energy concept is not newer just renewed in the modern times because once again there is need to shift towards is to protect the environment. It does not mean that the advancement in technology will not proceed. It provides a secure environment to do positive work. It will increase the efficiency level of man power.

1.1 What is Pedal Power?

Human are using their powers for different purposes from ancient time. Today this power is giving ways for generating power. Pedal power means transfer of human energy from one body part that is leg to power generating system. After pedaling the bicycle, energy is transferred from human body to equipments that work with electric power.

1.2 What pedal power does?

Pedal power uses bicycle power generator to lighten bulbs or supply power to many other appliances. Production of power under this method completely depends on human capabilities. As more and more appliances are attached with power generator, it becomes tough for the person to maintain the supply. Pedal power generating system is combination of different technologies including man power and bicycle as most important. Other technologies used with this system include voltage and current meters, capacitors, display board and transmitters etc. Pedal power is very easy and simple to use so a non-technical person or even a kid can also try using it.

1.3 Mention the operating principles of pedal power?

Pedal power works under three main principles, power levels, pedaling rate and gear ratios.
Power levels depend on capacity of human to pedal. Power level depends on how strong the peddler is and how long he can pedal. It is considered that a healthy non-athlete can easily generate up to 75 watts of mechanical power while an athletic person can give twice to this value. A smaller and weaker person can probably produce 50 watts in same time period. This analysis shows that power level varies with health of peddler.

Pedaling rate is another principle that influences pedal power. It counts the number of pedals a person made with pedaling speed. But some persons can produce more power at slow but consistent count of pedal. Therefore we can say that this rate varies from person to person because of physical conditions. A research shows that if a person pedal at range of 50 to 70 revolutions per minute then he can give most efficient results.

Gear ratio is relationship between rotating speed and pedaling rate. Balance between these two figure let us get beneficial results.

1.4 How pedal power is helping us in real world?

Pedal power is a reliable source of energy. It is helping humans in their survival. Worldwide more than 3.5 million people die due to water related diseases every year. To help everyone a Japanese company is developing a bicycle that purifies the water. Bicycle rider can take water from a river or lake with a hose attached with it and starts pedaling. Pedaling power pump that water through multi-unit filtration system and produces about 1.3 gallon of clean water per minute. Pedal motion is helping this world in generating electricity to run heavy machines and help home uses. But new advancement in this technology is conversion of mechanical motion. With this repetitive motion different businesses are enjoying benefits.

Pedaling does not help at business or global level but it is also helping us in maintain our physic. When you pedal at home you lose some inches from your body and generate some electric power to run your appliances at same time. You can store your produced energy into batteries as well to use it later. Human powered nebulizer technology has been developed to help patients suffering from respiratory disease. This attached with the machine, it turns liquid medicines into mist and flow it to parents lungs through a mouth piece attached with it.

II. Design And Experimental Setup Of Pedal Operated Water Pump
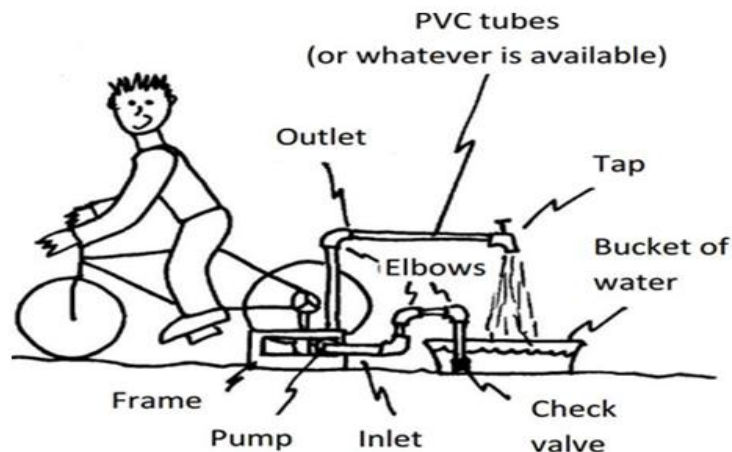
2.1 Design of Equipment

A bicycle pumping system that can be used to pump water for irrigation and small sector area like gardening, floor cleaning works etc…It is a very small mechanism on which our project is based on. The mechanism consists of single centrifugal pump which is fixed with the rear wheel bicycle. Paddling for just a minute or two is enough to pump water. Project could prove helpful for rural areas. Which are facing load shedding problem? It can be used mainly for irrigation and water drawing water from wells and other water bodies. This is a centrifugal water pump which is run by rotating the pedal of a cycle. The system comprises a bicycle, rim, impeller, pulley and inlet and delivery pipes. A wheel is connected to another gear with a smaller diameter the final supporting shaft is connected with an impeller through this process of paddling is used to lift water from a pipe into the form for cultivation. This innovation is useful for pumping water from river, ponds, wells and similar water sources thus enabling poor formers for pumping water for irrigation and cultivation. We drive a bicycle by using a paddling the wheel of the bicycle rotates a particular rpm and this wheel rotates the impellers of the centrifugal pump

2.2 Working Mechanism

The rare wheel of the bicycle is rotated with the help of driver and driven gear of the bicycle. The chain drive of the centrifugal pump is connected to the rare wheel hub of the bicycle, it also rotates when the rare wheel of the bicycle is rotated with the help of the rotation system. The shaft of the centrifugal pump rotates up to 3700rpm.With the rotation of the great speed the vacuum   is created in the centrifugal pump and this vacuum in this centrifugal pump suck the water from the water tank and it discharge the water through outlet with some amount of pressure

2.3 Main components of pedal powered water pump
The pedal powered water pump consists of the following components they are:
1. Centrifugal pump
2. Gear
3. Bicycle
4. Power transmitting unit (Chain drive from rear wheel hub to pump shaft)
5. Inlet and outlet tubes of the centrifugal pump
6. Bucket of water
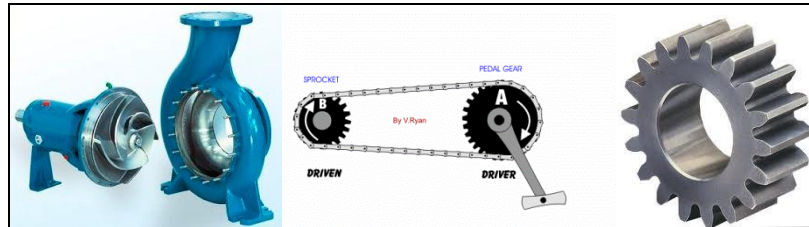
III.   Definition Of Pump

Pumps convert mechanical energy into fluid energy which can be explained as a pump is a device that moves fluids (liquids or gases), or sometimes slurries, by mechanical action.

Or

A pump is a device used to raise, compress, or transfer fluids from one place to another. When a fluid, be it hot or cold, has to be "moved" in a system, pumps are used. In other words, in a more technically appropriate manner, the pump is a machine which has the function of increasing the total (mechanical) energy of a liquid; this means that the pump transfers energy to the fluid that it receives f room the driving motor.

3.1. Classification of Pump
Pumps can be classified into two major groups according to the method by which mechanical energy is transferred to the fluid.
1. Roto dynamic typed pumps
2. Positive displacement pumps,
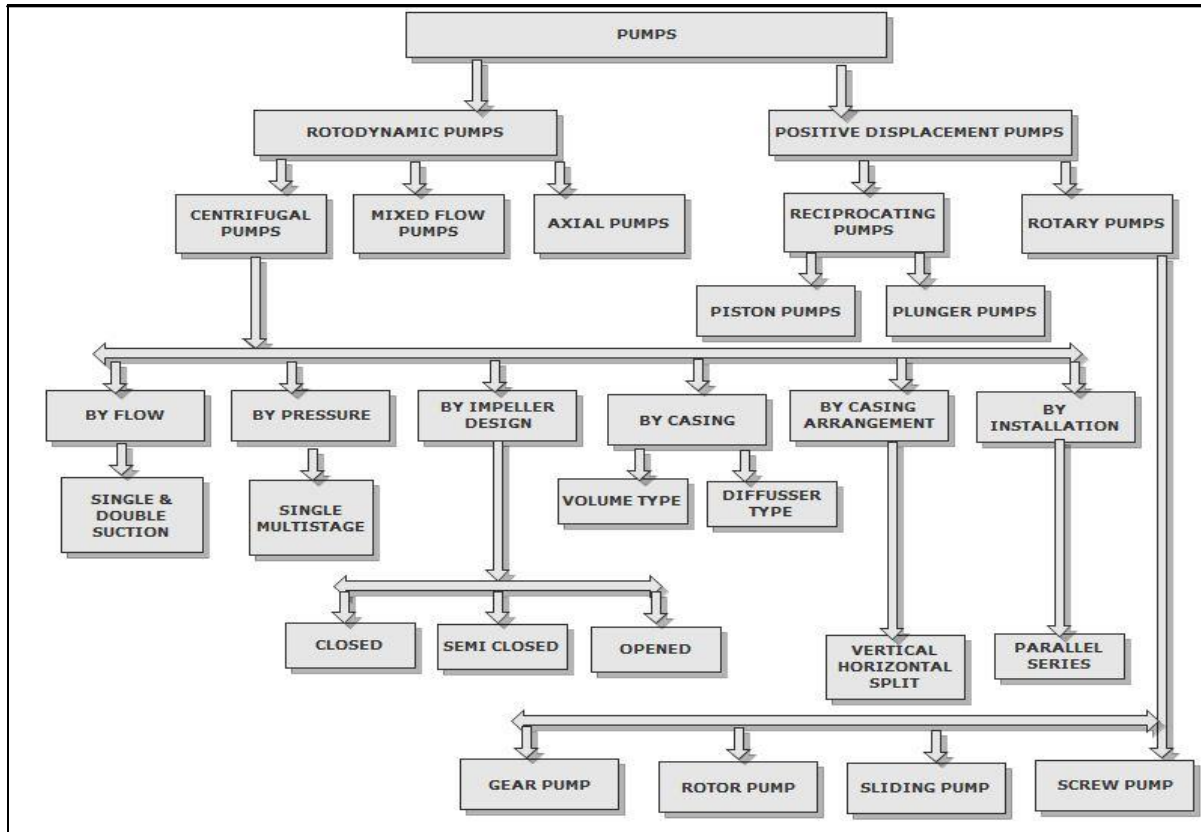
Block diagram representation of classification of Pump

3.2. Centrifugal Pump

A centrifugal pump is a rot dynamic pump that uses a rotating impeller to increase the pressure and flow rate of a fluid. Centrifugal pumps are the most common type of pump used to move liquids through a piping system. The fluid enters the pump impeller along or near to the rotating axis and is accelerated by the impeller, flowing radially outward or axially into a diffuser or volute chamber, from where it exits into the downstream piping system. Centrifugal pumps are typically used for large discharge through smaller heads. Centrifugal pumps are most often associated with the radial-flow type. However, the term "centrifugal pump" can be used to describe all impeller type rot dynamic pumps including the radial, axial and mixed-flow variations.

3.3. Main Parts

A centrifugal pump is of a very simple design. The two main parts of the pump are the impeller and the diffuser. Impeller, which is the only moving part, is attached to a shaft and driven by a motor. Impellers are generally made of bronze, polycarbonate, cast iron, stainless steel as well as other materials. The diffuser (also called as volute) houses the impeller and captures and directs the water off the impeller.
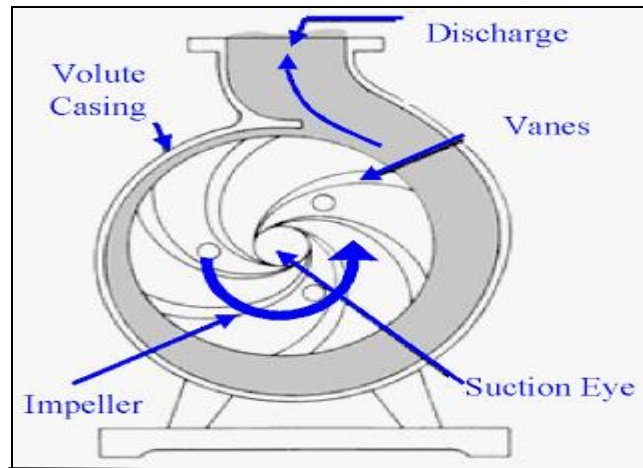
3.4. Different Types of Impellers:

IV. Calculation

Bicycle chain drive specifications
- Diameter of the driver d_1=16cm
- Diameter of the driven d_2 =7.2cm
- Maximum speed of the driver N_1=80 rpm
- Maximum speed of the driven N_2=450rpm
- Teeth of the driver T_1=40 numbers
- Teeth of the driven T_2=18 numbers
- The centre length between driver and driven x=45cm

Motor and Pump chain drive specification:
- Diameter of the motor shaft d=1.3cm
- Length of the motor shaft l=22cm
- Pump type: single stage type
- Type of pump: centrifugal type
- Power of the pump:1.5HP

- Suction diameter of the pump=3cm
- Discharge diameter of the pump=2cm
- Diameter of the driver d_1=20cm
- Diameter of the driven d_2=5.5cm
- Maximum speed of the driver N_1=2100rpm
- Maximum speed of the driven N_2=3700rpm
- Teeth of the driver Td_1=50 numbers
- Teeth of the driven Td_2=12 numbers
- The center length between driver and driven x=47.5cm

4.1 *MODEL* CALCULATION:

$L_1 = \pi(r1 + r2) + 2x + (r1 - r2)^2/x1$ (for cycle)

Where,

R_1= radius of the driver= 8cm
R_2=radius of the driven=3.6cm
X1=the centre length between driver and driven=45cm

$L_1 = \pi(8+3.6) + 2*45 + (8+3.6)^2/45$

L_1=126.42 cm
Where
$L_2 = \pi(r1 + r2) + 2x + (r1 - r2)^2/x2$ (for pump)

R_1= radius of the driver=10cm
R_2=radius of the driven=2.75cm
X_2=the centre length between driver and driven=47.5cm
$L_2 = \pi(10 + 2.75) + 2 \times 47.5 + (10-2.75)^2/47.5$

L_2=138.9cm

Speed ratio :- (for cycle chain drive)
Speed of the driver/speed of the driven= number of teeth on the driven/no. of teeth on driver=
$N_2/N_1 = d_1/d_2 = t_1/t_2$
=450/80=16/7.2=40/18
Speed ratio= 56.25: 2.2: 2.2
Where

N_1=Speed of the driven =450rpm
N_2=Speed of the driver=80rpm
D_1=diameter of the driver=16cm
D_2=diameter of the driven=7.2cm
T_1=teeth of the driver=40numbers
T_2=teeth of the driven=18numbers

Speed ratio (for pump chain drive):
Seed of the driver/speed of driven=number of teeth on driven/number of teeth on driver=
$$N_2:N_1 = d_1:d_2 = t_1:t_2$$

3700/2100=20/5.5=50/12
Speed ratio= 1.3: 3.6: 4.1
- Power (p) =$2\pi NT/60$ KW
Where

N=speed of the motor shaft=3700 rpm
T=total torque produce in the motor shaft

4.2 Assembly of Pedal Powered Water Pump

The pedal powered water pump includes the pump chain drive with driver and driven. The driver of the pump chain drive consists of 50 numbers of teeth and it is placed on the centre hub of the rare wheel of the bicycle and the driven gear is consisting of 18 number of Teeth's. It is connected to the shaft of the centrifugal pump the single station stage pump of 1.5 hp. The shaft diameter of 1.3 cm and length of the shaft 22 cm without electric winding is placed on the carriage of the bicycle. The carriage of the bicycle is placed on the rare wheel of the bicycle.

Advantages of pedal powered water pump

1. It is renewable as well as sustainable. As it is needed till the human existence on this planet and the ultimate source is the human himself.
2. Pedal renewable is cost-effective so everyone can access to its advantages. There is only need to set pedal with crank system attached to the drive.
3. It is pure energy zero percent carbon emission so clean and healthy surroundings.
4. It keeps the body system well and increases the efficiency level if used to a certain extent. Excess use of anything is bad for health.
5. It does not harm the socio-political benefits as it is the personal property of every individual.
6. The conventional centrifugal pump needs either electricity or diesel engine, but the present innovation works on pedaling.

This is a non-polluting and environment friendly device. Since it is made of commonly available materials and costs less. It is affordable to common people. It requires less maintenance Minimum input energy is required to get the maximum output of water. This device can be transported easily from one place to another.

V. Results And Discussions

The below Figure gives the variation of discharge with rotor shaft rpm of Pedal power centrifugal pump. It is observed that the discharge increases uniformly with the rpm. Experimental result shows that discharge of about 0.0025m3/sec can be obtained for around 140rpm. The variation in the obtained plot is due to errors in observation and due to power transmission losses.
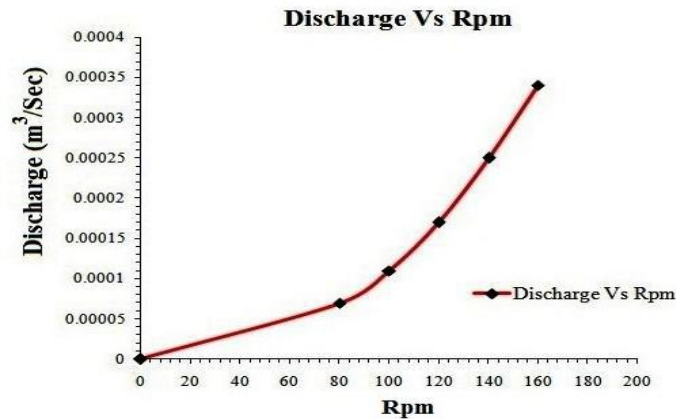
Figure: Variation of Discharge with Rpm

Figure .shows the variation of head with discharge of PPCP. It is observed that the head decreases uniformly with discharge. Experimental result shows that head of 8m can be obtained with discharge of about 0.00007m3/sec. The variation in the obtained plot is due to errors in observation and due to power transmission losses.
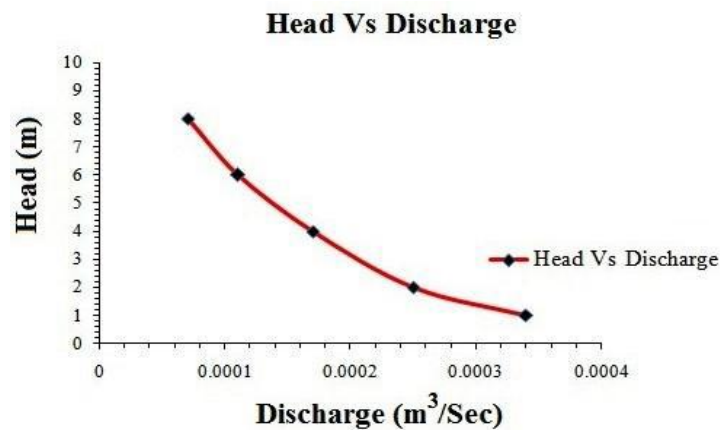
Figure: Variation of Head with Discharge

VI.   Applications

➢   Pedal Power Applications The following, mostly agricultural related, mechanical application have used pedal power technology: chain trencher, weeding/harvester rider, frontend loader, thresher, weedier (paddy), rot tiller, grain reaper, oil seed press, forklift, huller/Sheller, soy grinder, reel mower, bulldozer, dumptrike, grain drill, rice separator, tri- and quadric-cycle (with interchangeable units: cargo, flatbed, tanker, stake bed, dumper, pickup, animal, garden tools), sickle bar mower, crawler tractor, wildflower seed harvester, rice polisher, grain winnower and seeder.

➢   Various applications of standard bicycle with Pedal power attachments are shown

Operating a Circular

Rice Threshin

Winnowing

Corn Shelling

Water Pumping from a Shallow Well

VII. Conclusion

At a time when there is energy crisis casting its shadow all over the world, one has to look into alternate renewable energy resources. One such alternate way to generate power is presented in this paper. The Kinetic energy of the gear in terms of velocity ratio is generated by pedaling, which can be used to operate small powered devices. The various applications where this power could be used are also discussed in this paper. Villagers who use bicycles are going to be benefited the most.

We had successfully proven the calibration and working of centrifugal pump with pedal power of bicycle type for gardening purpose and it is also suitable for small scale work.

REFERENSES

[1]   "Fluid mechanics and Hydraulic Machine" By DR. R.K. Bansal laxmi publication (p) ltd.
[2]   "Non conventional sources of energy" fourth edition 2008By G.D.RAI Khanna publisher.
[3]   "Machine Design" (S. I. Units) By R.S. Khurmi & J. K.Gupta
[4]   Atul.P.Ganorkar, K.S.Zakiuddin, H.A.Hussain, "An Experiment on Development of Pedal Operated Water Pump", IOSR,e-ISSN:2278-1684,(2014).
[5]   Vishal Garg, Neelesh Khandare, Gautam Yadav, "An Experimental Setup and Design of Pedal Powered Water Pump", International Journal of Engineering Research and Technology (Vol.2, Issue.1) (2013).
[6]   Ademola Samuel Akinwonmi, Stephen Kwasi Adzimah, Fredrick Oppong, "An Experiment on Pedal Powered Centrifugal Pump for Purified Water Supply Device" ISDE (Vol.3, No.11) (2012).

AUTHOR

Mr. M.JAWAHAR. is working as Associate Professor in Dept of Mechanical Engineering Jayamukhi institute of technological sciences, narsampet, Warangal,(TS)-506332.India. He received B.Tech degree (2004) in Mechanical Engineering from JNTUH University, TS, India. He obtained M.Tech degree (2006) in Design Engineering from Kakatiya University , Warangal,TS, India. He has been teaching for the past 8 years. He has attended many International Seminars and Conferences. He has published seven papers in International Journals and presented five papers in International and National conferences. His research interests are in the areas of Design,Vibrations and FEM Analysis etc.

CO-AUTHORS

Mr. G.VENKANNA. is working as Assistant Professor in Dept of Mechanical Engineering Jayamukhi institute of technological sciences, narsampet, Warangal,(TS)-506332.India. He received B.Tech degree (2014) in Mechanical Engineering from VBIT, Warangal, TS, India.. His research interests are in the areas of Design and Thermal.

Mr. B.SANDEEP. is working as Assistant Professor in Dept of Mechanical Engineering Jayamukhi institute of technological sciences, narsampet, Warangal,(TS)-506332.India. He received B.Tech degree (2013) in Mechanical Engineering from VAAGDEVI COLLEGE OF ENGG, Warangal, TS, India .He is pursuing M.Tech in CAD/CAM. His research interests are in the areas of CAD/CAM and Thermal.

Crack Detection of Ferromagnetic Materials through Non Destructive Testing Methodology

Pawan Sharma[1], Amit Kumar[2], Mandeep Singh Sidhu[3],
Prof. (Dr.) B. K. Sharma[4]

[1,2,3,4] *Department of Mechanical Engineering, Vivekananda Institute of Technology (East), Jaipur, India-303012*

Abstract: *The real components have so many defects in the material, which acts as a crack. In fact, manufacturing of a component is not ideal. In manufacturing several kinds of defects are generated like voids and inclusions. Thus, it must be check all the critical components through non-destructive techniques (NDT) to detect the potential dangerous cracks. In Certain crucial components such as Airplanes, Space Vehicles, Nuclear Plants, Heavy Machinery, Dams, Concrete etc., online monitoring of defects is necessary. Concrete is different from other construction materials. Concrete can be made from combination of different materials. Its final properties depend on its treatment at construction site. To achieve this, sophisticated technologies are used. Ferromagnetic Composite Iron (FCI) is used in power generating devices and DC brushless Motors. Laminations can be substituted by Ferromagnetic Composite Iron (FCI) materials which offer a great manufacturing advantage. Non Destructive testing (NDT) is a major part of quality control. In Non-Destructive testing (NDT) different materials are tested for surface, volumetric and internal defects present in it. Non Destructive testing (NDT) is also an assurance that the proposed product is good and reliable. To apply these techniques, a certain level of skills is very necessary so that maximum amount of information is fetched related to the proposed product during testing. This paper deals with the Non Destructive Testing Methodology Used for crack detection in ferromagnetic materials.*

Keywords: *Crack, Ferromagnetic Materials, Non Destructive Testing, CAI, CAT, CAOC,*

I. Introduction

In industries it is impossible to synthesize product which is totally immune to crack(s). Crack may occur during manufacturing, testing or use. The products so developed are usually subjected to fatigue loading. During fatigue loading, the component may develop crack due to cyclic loading. Crack is simply defined as to fail or to give up. Crack may also be defined as break/rapture without complete separation of parts. Crack generally occurs with a sharp or a sudden sound. In industries the structures are generally subjected to fatigue or cyclic loading. Manufacturing Failure is indicated by cracks which occur in different kind of materials such as metals, composite, plastics and minerals. During production, time to time checking of product is necessary to avoid any kind of damage to the product by cracks during its manufacturing. Inadequate crack detection may result in various hazards which may cost human life at top. The crack when propagated to a high level develops into fracture which ultimately causes the whole structure to collapse.

The materials which exhibit a much high level of saturation magnetization are generally referred to as ferromagnetic materials. Ferromagnetic materials have a enamors applications in industry and in other places.

The ferromagnetic materials have vast applications in industries and power plants. In some places ferromagnetic materials are also used for creating and distributing electricity.

The ferromagnetic materials are based on the property of Bohr Magneton. Bohr Magneton is defined as the moment which is associated with the electronic property of spin.

$$m = \pm \frac{e}{m} \frac{1}{2} h$$

Here, $\frac{e}{m}$ is the Ratio of electronic charge to mass

h is the Planck's constant whose value is $1.05*10^{-34}$ joule-sec

II. Literature Review

L. Boni, et. al. [1], has mentioned in his paper that metal pads which have thin bonds are more effective to achieve damage tolerance in case of cracks present in structures**.** Four different tests are performed based on four different configurations to know about the residual strength and the growth of crack. It is observed that a minor role is played in case of thin bonded metals by pads debonding.

A.chudnovsky [2], has discussed in his paper about the empirical equations. Under the conditions of creep and fatigue, these equations are used to calculate the slow growth of the crack. Energy release rate or stress intensity factor are the basic functions in terms of which the propagation rate of crack is generally expressed. Under varying load conditions, the crack behavior is determined using crack stability analysis. Also the crack growth resistance technique is used to determine the crack behavior. A constant crack resistance is assumed for stable crack propagation.

J.C.Newman, et. al. [3], has mentioned in his paper about various ways to determine the growth of crack. The most used, easy and reliable method used is the FASTRAN life-prediction code. On testing, cracks were developed on open ends and the thus the test data was obtained.

Lei Ma, et. al [4], has mentioned in her paper about the crack propagation through cyclic loading. Using molecular dynamic simulation, the test specimen was put under cyclic loading and was observed. The cracks propagated and brittleness was observed in crack propagation.

Haiying Zhang, et. al [5], has mentioned in his paper about the crack-layer concept for the slow growth of crack. The estimation of lifetime and fracture growth is done by modeling of crack-layer model. This method has been applied to a numerous engineering materials in past few decades for the brittle fracture. Finite Element Methods are used to calculate the driving forces of crack-layer.

III. Crack

Crack is nothing but simply a failure of material. Crack can also be understood as breakdown of component without complete separation of its adjoining parts. Areas in low shear and where bending plays a major role usually have flexural cracks. Bending stresses and shear stresses are the key features for a crack to propagate and finally resulting in fracture. For a safe structure, detection of crack is must otherwise the structure may collapse as a result of propagation of crack. Crack could be symmetrical or asymmetrical. When determination of crack is done in a rotor, then a spare rotor is used for the substitution of cracked rotor otherwise the consequences may be hazardous. Cracks are classified as deep cracks or semi-deep cracks. Semi deep cracks are the results of varying pressure and humidity conditions followed by the type of material used. Due to sudden movement of structures as a result of earthquakes, semi-deep cracks are developed into deep cracks. Complex Variable Approach is used to derive the general equation of crack in anisotropic bodies. Stress functions are used to determine the value of stress-intensity factor which represents the conditions of crack and its extension. Microscopic techniques are used to determine and locate cracks and to study their nature. Ultrasound, X-Ray etc. is used to identify the cracks and structural damage. Then microscopic techniques are used to analyze the damage done to the structure. A high level of precision is achieved using high powerful tools such as inverted microscopes. The Worn out part is removed and analyzed under high resolution magnification to get more information about that part.

IV. Non Destructive Testing (NDT) Methodology

The known Full Form of NDT to a person is Non Destructive Testing. As the name suggests, it is a testing without destroying the elements or components used in testing. In modern world, structures are subjected to high pressure and high load conditions. The main purpose of Non Destructive Testing (NDT) is to make sure that the structure, component, material or element doesn't fail within the pre-determined time.

Non Destructive Testing (NDT) is also used to check the quality of raw material before processing the part and is used until the final inspection of product.

Apart from all the above mentioned uses, Non Destructive Testing (NDT) for condition monitoring, energy level monitoring, residual life assessment.
There are four main criteria for Non Destructive Testing (NDT) techniques
- Type of Material
- Type of Defect
- Size of Defect
- Location of Defect

V. Common Non Destructive Testing (NDT) Methods

5.1 Volumetric Examination Method
- **Ultrasonic Testing-UT**
In this method sound waves of high frequency are used to detect the changes in the properties of materials. It is used to determine the thickness of metallic and non-metallic materials whose only one side is accessible.

- **Radiography Testing-RT**

    In this method the source of radiation is an X-Ray device or Radioactive Isotope. X-rays are passed through the material and are captured on film just like in a simple X-ray. Digital Devices are also used to capture X-Rays. After the film is processed an image is obtained which shows Variation in density. The density change depicts the imperfections.
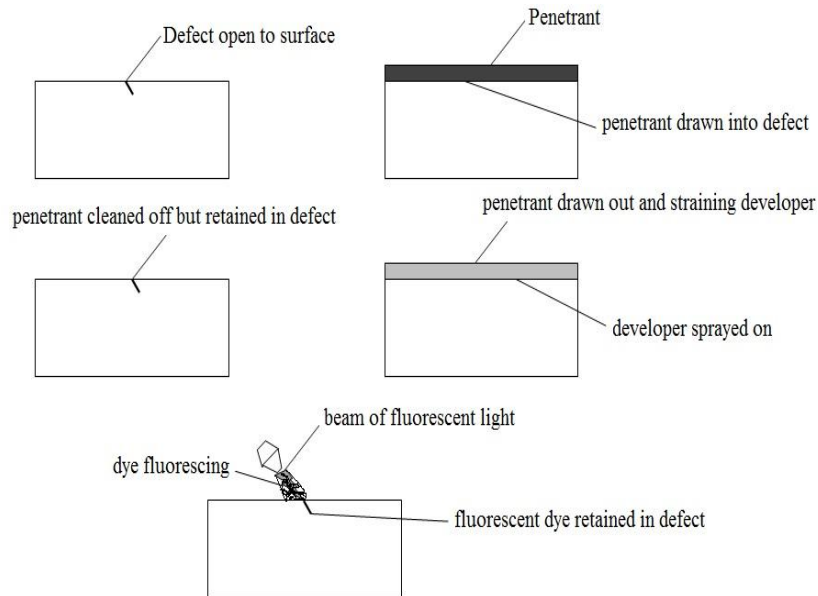
Fig. 1: Non Destructive Evaluation (NDE) Principles

5.2 Surface Examination Method
- **Visual Inspection-VT**

    It is the oldest method. A component is scanned using high power lens or Cameras to determine the Surface condition of that component.
- **Liquid Penetrant-LP**

    In this method visible or fluorescent dye solutions are used to coat the test object. The dye in excess is removed. Penetrant is made to flow out of the imperfections. With the naked eyes, the change in color between the penetrant and developer is used. In case the imperfection is not visible with the naked eyes, ultraviolet lamp is used to see the imperfections.
- **Magnetic Particle-MP**

    Magnetic particle is a fast and easy method used in iron and steel materials for the detection of surface irregularities. Magnetic flux lines and magnetic particles are used to detect the defects in components. Wherever the magnetic flux lines changes, discontinuity is located.
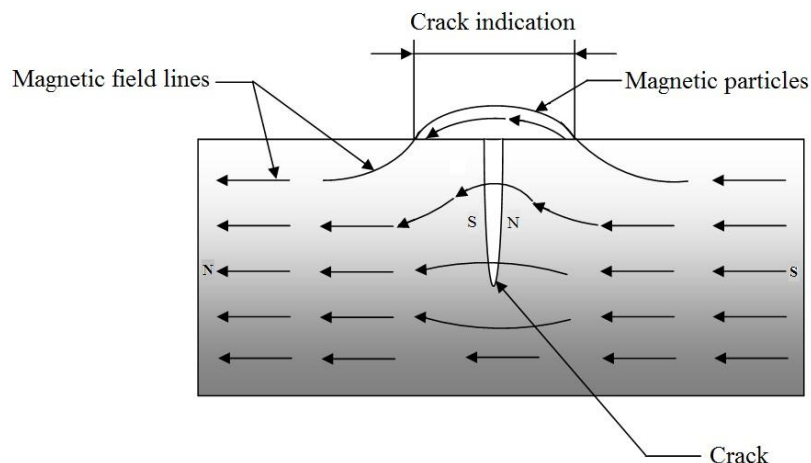
Fig. 2: Magnetic Particle Inspection Method

- **Eddy Current-EC**

It is a non-contact method. In eddy current testing, induced magnetic flux is responsible for the generation of electric current in conductive materials. Imperfections cause the change in properties of material and change the induced magnetic field. When detected, these changes indicate the imperfections in test material.

5.3 Integrity Examination Method
- **Leak Testing-LT**

Pressure gauges, Soap bubble test, electronic listening devices, Liquid and gas penetrant are used to detect the leak. In pressure Vessels, pipelines and other pressure retaining components, several other technologies are used to detect the leak.
- **Acoustic Emission Testing-AET**

Emission is defined as during stressing a solid material the imperfections grows and if short bursts of acoustic energy are emitted by material, these are known as "Emissions". Special Receivers are used in ultrasonic testing to detect the acoustic emissions. The source of emission is evaluated by studying the intensity, rate and other characteristics of emitted ray. Triangular technique is used to locate the defect.

5.4 Condition Monitoring Method
- **Thermography-Infrared Testing-IR**

The thermal profile of any item, building or machine is generated using thermography in graphic form so that a working temperature assessment is derived. The difference in the component temperature is identified by doing this.
- **Vibration Analysis-VA**

Vibration noise is produced by the rotary machines. The condition of the machine is estimate by monitoring the frequency, amplitude etc. of the vibrations. The vibrations cause some parts of machine to crack or rapture.

VI. Conclusion

Non Destructive testing (NDT) techniques have these common features:
- Some degree of disassembly is used in many cases of machines or structures.
- Thickness measurement would be an exception.
- Real Time monitoring is not offered by any of the techniques.
- Operator skill is required for the interpretation of results.
- Operator must have access to equipment to perform tests.

REFERENCES

[1]. Crack propagation in flat panels stiffened by bonded pads, International Journal of Fatigue, Volume 68, November 2014, Pages 1-9
[2]. Slow crack growth, its modeling and crack-layer approach: A review, International Journal of Engineering Science, Volume 83, October 2014, Pages 6-41
[3]. Predicting crack growth in specimens with overloads and cold-worked holes with residual stresses, Engineering Fracture Mechanics, Volume 127, September 2014, Pages 252-266
[4]. Molecular dynamic simulation of fatigue crack propagation in bcc iron under cyclic loading, International Journal of Fatigue, Volume 68, November 2014, Pages 253-259
[5]. Applying the crack-layer concept to modeling of slow crack growth in polythene, International Journal of Engineering Science, Volume 83, October 2014, Pages 42-56

Review on Techniques for Total Throughput Maximization of Two-Way Relay Networks Using At Cooperative Protocol

Bondar V. S.[1], Sudhir S. Kanade[2]

[1]*Department of electronics and Telecommunication Engineering, TPCT'S College Of Engineering, Osmanabad*
[2]*Head of electronics and telecommunication Department,TPCT'S College of Engineering, Osmanabad*

Abstract: With the integration of Internet and multimedia applications in next generation wireless communications, the demand for wide-band high data rate communication services is growing. In recent years, multiple transmitter and receiver antennas are employed in the wireless communications systems to adapt various demands of high speed wireless links and improved signal to noise ratio . In order to take full advantage of the Multi Input Multi Output (MIMO) systems, relay selection technique is needed at the transmitter & receiver side. Many relay selection techniques exist in literature. In this paper a brief review of previous work which done with relay selection for mimo system is disscussed.
Keywords: Multi Input Multi Output(MIMO), Relay Selection, Resource Allocation, Joint Optimization

I. Introduction

Future wireless networks are expected to provide much higher data rates, energy efficiency,and reliability in a cost-effective manner. To meet the ever increasing demand for higher data rates and longer battery life, a promising approach to furtherimproves the energy and bandwidth efficiency is diversity reception. Multi input multi output (MIMO) is one of the promising techniques which can offer diversity and successful in fighting against channel fading. However, it requires more than one antenna at the transmitter and/or receiver which is not feasible on small, handheld devices in ad hoc network, sensor network or up-link of cellular networks. [1-3] Cooperation among a group of users to re-transmit each other's data can emulate a multiple transmit antennae environment to achieve spatial diversity gains. With the broadcast nature of the wireless channel, when a source transmits signals to a destination, neighboring users can also receive the signals. These neighboring users can relay the signals to the destination. As a result, diversity gain can be achieved without implementing multiple antennas or using costly RF chains. Popular against channel fading.

However, it requires more than one antenna at the transmitter and/or receiver which is not feasible on small, handheld devices in ad hoc network, sensor network or up-link of cellular networks. [1-3] Cooperation among a group of users to re-transmit each other's data can emulate a multiple transmit antennae environment to achieve spatial diversity gains. With the broadcast nature of the wireless channel, when a source transmits signals to a destination, neighboring users can also receive the signals. These neighboring users can relay the signals to the destination. As a result, diversity gain can be achieved without implementing multiple antennas or using costly RF chains. Popular cooperative schemes used by relays are (i) amplify and forward (AF) and (ii) decode and forward (DF). In AF, cooperating node simply amplifies the signal and transmits towards destination.

In DF, the relay, decode and re-encode the information before sending it to destination. Cooperative protocols normally require two phases. In first phase Source broadcasts the information which can be received by relays and destination. In second phase, relays transmit it to destination.[4-5] .Due to broadcast nature of the wireless channel, at any given instant, many nodes would receive the signal transmitted by the source of the message. To include each of them in cooperation is the wastage of resources. Many replicas of the same signal re-transmitted by the relay increase traffic and hence induce interference in the channel. Researchers have proved that limited number of relays or partners participating in cooperation enhances the performance of the link. If direct channel between source and destination is satisfactory, then the cooperation of relay may not be needed. Looking at the time varying nature of the wireless channel, required number of relay is also variable. Therefore, the relay or partner selection is the crucial issue for implementing fruitful cooperative communication. The remainder of the paper is arranged to

1) Provide overview of various relay selection schemes
2) Highlight their benefits and challenges

II. Relay Selection Methods

Relay selection is the process of selecting the 'best' partner or partners to achieve the goal within given constraint. Goal and constraint – both depend on the type of the wireless network. Wireless networks have variety of architectures- from cellular to sensor and infrastructure based to infrastructure less, from high profile devices to low cost low power tiny nodes. Different applications have different constraints like for sensor network, power is most important while for cellular voice communication has real time constraint and for data networks, through put is of main concern. Infrastructure based networks are centrally controlled while ad-hoc networks have distributed control. Considering variety of wireless networks, there cannot be a single technique of relay selection. Vast variety of techniques can be found in recent publications. They can be put under the category as shown below:

1. Threshold based relay selection [6-10]
2. Multiple relay beamforming [11]
3. Cross layer relay selection [12]
4. Distributed relay selection [13]
5. Delay optimized relay selection[14]
6. Joint relay selection and resource optimization [15-20]
7. Joint up-down relay selection [21]

Selection of partner or relay can be done before transmitting the signal (proactive) or it can be done as and when required (reactive). The generic approach of relay selection involved three steps: Measurement, Comparison and Selection. The decision of selection can either be done by source or destination. The criteria for selection can be received SNR, end-to-end delay, bit error rate, packet error rate, frame error rate. With the relay, there are two (or more) channels involved in completing the path between the source and destination. Channel between S-R and R-D are independent. It is therefore becomes essential to consider the statistical parameter who take the effect of both the channel into account.

At the same time, it is also important to optimize the resources utilized in cooperation. As a result, relay selection and resource optimization problem is undertaken simultaneously. The methods of selection and optimization jointly are employed based on power minimization, data rate (or through put) maximization, delay minimization or overhead minimization. For full duplex applications, the selection of relay can be done jointly for uplink as well as down link considering the reciprocal channel. This results in reduced overheads of election. As the wireless channel is dynamic in nature, the selection of relay has to be adaptive. The frequency of adaptation depends on the nature of the channel. Relay selection is conveniently done centrally in case of infrastructure based network, while it can be distributed in case of ad-hoc network Centralized technique is optimum but requires more overheads while in distributed technique, fewer overheads are required for selection but it may be sub-optimal.

A. Threshold based techniques

In [6-10], destination driven arbitrary multiple relay selection technique is presented in which relays are selected such that the combined SNR of direct path and relays path exceeds preset threshold as shown in Fig.2. In broadcast phase, the signal send by the source is received by the destination. It compares received SNR with threshold. If not satisfied, it selects the relay arbitrarily to send signal in next slot and combines the SNR and compare with threshold. This process continues till the received SNR exceeds the threshold. Once it happens, no more relays are selected.

In this technique, channel state information is not derived by the destination by receiving the training signal but the relays are selected randomly so as to exceed the combined received SNR. Here, relay selection time depends on the channel condition as for bad channel, more relays need to get selected one after the other. In the process of decision making, the threshold is very important. In [10], optimization of decision threshold is done as a function of power and BER. This method is simplified in [9] in which the first relay with the instantaneous channel gain larger than the threshold is selected to cooperate with the source.

In [7], four methods are proposed based on statistical parameters. (1) Best relay selection in which the relay with max. SNR is selected. (2) Nearest Neighbor selection in which selection is not based on spatial position but relay with the best channel with S or D is selected (3) Best worst channel selection in which relay having best worse channel out of all S-R and R-D channels is selected (4) Best harmonic mean method in which harmonic mean of both the channels of the relay i.e. S-R and R-D is considered for selecting the relay.
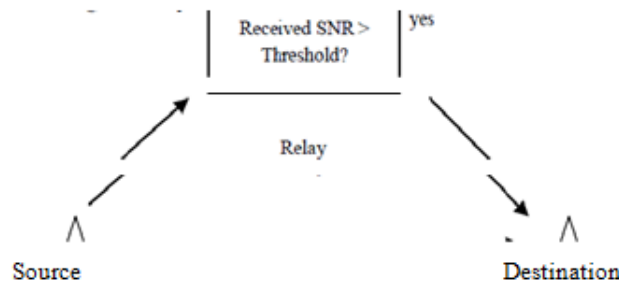
Fig.1 Threshold Based relay relay selection

B. Multiple Relay Beam forming

In [4], multiple relay beamforming is discussed in acquiring CSI in the absence of the direct path between source and destination. As number of selected relays increase, it further increases the energy for feedback but the energy for data transmission reduces as more relays do beamfor increases for acquiring CSI increase with the number of total relays available. Hence, number of participating relay is also limited by energy. Here, feedback and training overheads are significant.

C. Cross Layer Relay Selection

Timer based single relay selection technique involves network layer in the process of selecting relay.employed to avoid contention. Source send RTS message when it has data to send which is received by destination and all the relays. Destination responds by sending CTS which is also received by all relays. From RTS-CTS, all relay nodes adjust the power level necessary for cooperation based on some predetermined policy. All relays set the timer. The relay with best channel will have the shortest timer. Then source send data which is received by the destination. Destination stores it for later use. In contention stage, when timer ends, th channel. Relay send message to destination with DF protocol. Destination jointly decodes the signal.

D. Distributed Relay Selection

Distributed relay selection approaches are presented and compared with the techniques in [5]. In distributed control mechanism, nodes have knowledge of receive SNR but not transmit SNR or no feedback mechanism I selection (1) Simple selection (2) Selection based on out In simple selection, selection of partner is done randomly. but some node would remain without any partner. In second method, selection of partner is done to minimize outage probability. To do so, each node hears one another's transmission and selects the partner whose transmission can be detected correctly by him with the highest received SNR technique leads to better performance but for that each node to overhear message. In fixed priority selection, each node has fixed priority list and it helps N partners starting top of that list. Compared to no-cooperation, fixed priority cooperation performs better and as number of cooperating partners increases, outage probability reduces significantly particularly in high SNR region.
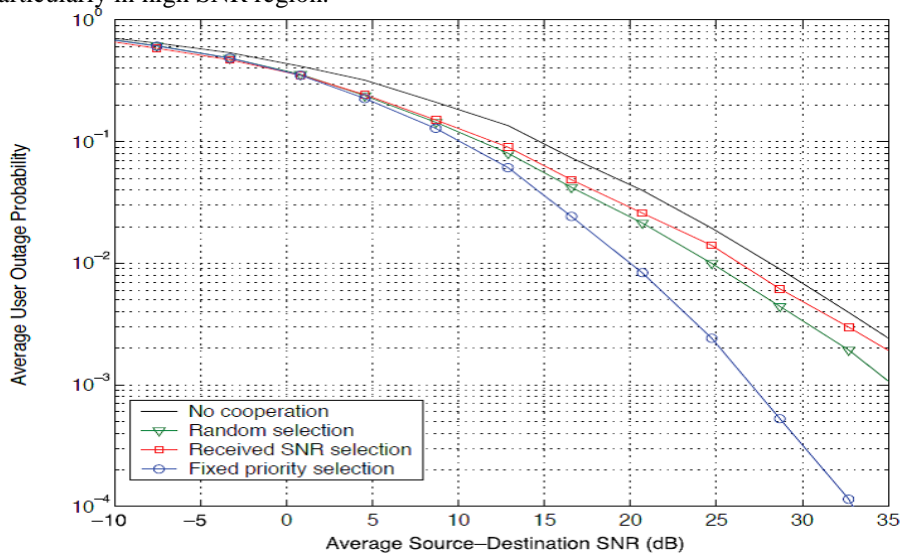

Figure: 2 Comparison of outage probability comparison of distributed & centralized techniques

Fig.2 shows that fixed priority outperforms in high SNR. Centralized control method improves the performance as distributed system chooses the optimum while centralized system chooses the best solution. Fixed priority method for selecting cooperating partner is advantageous. Centralized control improves performance but requires channel information between each node pair and the same is to be communicated to all the nodes which increase the overheads.

E. Delay optimized Relay selection

Relay selection based on minimization of total transmission time for fixed data rate systems is presented in [18]. Transmission time or end-to-end delay is important criteria for time sensitive applications. Total Time is estimated as summation of the time to decode the data for the worst case relay plus time for cooperation. If channel condition is not good, more time is needed to decode the message. After decoding, relay re-encode the message and sent. Two methods are proposed (1) Best expectation method in which the expectation of cooperation time is considered for calculating the total transmission time (2) Best-m method in which the source predetermined the number of relays depending on the channel statistic needed for cooperation for minimizing total transmission time i.e. fixed number of relays is employed. In both the methods, more than one relays are selected. Here, the advantage is overhead reduces significantly. As statistical channel distribution is considered for calculating number of relays, the solution may be sub-optimal if channel variances are large.

F. Joint relay selection and resource optimization

Relay selection process can be more fruitful if it is augmented with the resource optimization techniques. Resources in wireless networks are power, data rate (bandwidth), frequency or channel (in case of FDMA), no. of time slots (in case of TDMA), codes (in case of CDMA) or subcarriers (in case of OFDMA). For example, when the relays are selected, their powers are adjusted in such a way that the combined signal at the destination has sufficient power to just get detected. If power is not controlled at the relays, it leads to wastage of power and increased interference in the network. In [7], [8], [15] and [17] relay selection with power optimization is presented. In [9], pricing variable is introduced to optimize power and bandwidth both along with relay selection. Maximizing the minimum data rate among all the S-D pairs is considered while selecting the relay in [12]. There are M sources and N relays in the system. Let Ps and Pr be the source and relay power respectively. Pout be the outage probability and e is the maximum tolerable outage probability. The optimization problem is formed as [8].

$$\min\left(\sum_{i=1}^{M} Psi + \sum_{j=1}^{N} Pri\right)$$

In case of data rate optimization, the relay with the best channel condition is selected so that it can support higher data rate transmission. For this, the optimization problem can be formulated as [9].

$$\text{maximize}\sum_{i=1}^{M} Ui(Ri)$$

Where, Um is the utility function which reflects user satisfaction and Rm is the data rate associated with relay i. The relays are selected to maximize the data rate under the constraint of the total maximum power available.

III. Conclusion

Proper selection of Relay or partner is very important for achieving the benefits of cooperative communication. Variety of relay selection schemes from the literature is studied and compared. Although single-relay selection is attractive due to its simplicity, it may fail to meet the QoS performance required by users due to the limited diversity gain. To enhance the service quality by increasing the cooperative diversity order, more than one relay should be favored to be involved, which leads to the multiple relay selection. Resource allocation issue can be clubbed together with relay selection results in joint relay selection and resource allocation techniques. The parameters of main concern are power, data rate, QoS, end-to-end delay and overheads. The decision of selection can either be taken centrally or in distributed manner. The centrally controlled techniques results in the "best" solution but at the cost of more processing power and significant amount of overheads. On other hand, distributed control schemes are more suitable for ad-hoc wireless network where relay selection decision is left on the individual relays, which may be sub-optimal but can be taken without much complexity and with fewer overheads.

REFERENCES

[1]   A. Sendonaris, E. Erkip, and B. Aazhang, "User cooperation diversity–part I: system description," IEEE Trans. Commun., vol. 51, no. 11, pp. 1927–1938, Nov. 2003.

[2]   A. Sendonaris, E. Erkip, and B. Aazhang, "User cooperation diversity–part II:implementation aspects and performance analysis," IEEE Trans. Commun., vol. 51, no. 11, pp. 1939–1948, Nov. 2003.

[3]   J. N. Laneman, D. N. C. Tse, and G. W. Wornell, "Cooperative diversity in wireless networks: Efficient protocols and outage behavior," IEEE Trans. Inf. Theory, vol. 50, no. 12, pp. 3062–3080, Dec. 2004.

[4]   A. Bletsas, A. Khisti, D. P. Reed, and A. Lippman, "A simple cooperative diversity method based on network path selection," IEEE J. Sel. Areas Commun., vol. 24, no. 3, pp. 659–672, Mar. 2006.

[5]   Y. Zhao, R. Adve, and T. J. Lim, "Improving amplify-and-forward relay networks: optimal power allocation versus selection," IEEE Trans.Wireless Commun., vol. 6, no. 8, pp. 3114– 3123, Aug. 2007.

[6]   G. Amarasuriya, M. Ardakani, and C. Tellambura," Adaptive Multiple Relay Selection Scheme for Cooperative Wireless Networks", in Proc. IEEE WCNC 2010, pp. 1-6

[7]   Y. Jing, H. Jafarkhani," Single and Multiple Relay Selection Schemes and Their DiversityOrders", in the proc. ICC 2008 workshop

[8]   F.Atay Onat1, Y. Fan, H. Yanikomeroglu1, H. Vincent Poor, "Threshold Based Relay Selection in Scheme for Cooperative Wireless Networks", in Proc. IEEE WCNC 2010, pp. 1-6

[7]   Y. Jing, H. Jafarkhani," Single and Multiple Relay Selection Schemes and Their Diversity Orders", in the proc. ICC 2008 workshop

[8]   F.Atay Onat1, Y. Fan, H. Yanikomeroglu1, H. Vincent Poor, "Threshold Based Relay Selection in Cooperative Wireless Networks", in Proc. IEEE Global telecommunication Conference GLOBECOM 2008.

[9]   H. Niu, T. Zhang, Li Sun, "Performance Analysis of a Threshold-Based Relay Selection Algorithm in Wireless Networks", Int. Jour. of Communication & Networks, Scientific Research, Vol.2 No.2, May2010

[10]   W. Pam Siriwongpairat, T. Himsoon, W. Su, K. J. Ray Liu, "Optimum Threshold-Selection Relaying for Decode-and-Forward Cooperation Protocol", in Proc. IEEE Wireless Networking and Communication Conference, WCNC2006

[11]   R. Madan, N. B. Mehta, A. F. Molisch, J. Zhang, "Energy-Efficient Cooperative Relaying over Fading Channels with Simple Relay Selection", in Proc. IEEE Global telecommunication Conference GLOBECOM 2006

[12]   Z. Zhou1, S. Zhou, J. Cui1, S.Cui, "Energy-Efficient Cooperative Communication Based on Power Control And Selective Relay In Wireless Sensor Networks", IEEE Trans.Wireless Commun., vol. 7, no. 8, pp. 3066 - 3078 , Aug. 2008.

[13]   A. Nosratinia and T. E. Hunter, "Grouping and partner selection in cooperative wireless networks," IEEE J. Sel. Areas Commun., vol. 25, no. 2, pp. 369–378, Feb. 2007.

[14]   S. Nam, M. Vu, V. Tarokh, "Relay Selection Methods for Wireless CooperativeCommunications", in Proc. IEEE Conf. on Information sciences & Systems CISS 2008, pp- 859- 864

[15]   M. Islam, Z. Dziong, K.Sohraby, M. Daneshmand, R.Jana, "Joint Optimal Power Allocation and Relay Selection with Spatial Diversity in Wireless Relay Networks", in proc. Mobile VCE Green Radio, Software Defined Radio - WINCOMM, 2011

[16]   J.Bo SI, Z. LI, L DANG, Z. LIU, "Joint Optimization of Relay Selection and Power Allocation in Cooperative Wireless Networks", in Proc IEEE int. conf. on Communication Systems, ICCS2008, pp. 1264 – 1268

[17]   Z.Qian-qian, GAO Wei-dong, PENG Mu-gen, WANG Wen-bo, "Partner selection strategies in cooperative wireless networks with optimal power distribution", Journal of China Universities of Posts and Telecommunications, Science Direct- Elsevier, Sep2008

[18]   K.Vardhe, D.Reynolds, B. Woerner, "Power Allocation and Relay Selection in Cooperative Wireless Networks", in Proc IEEE Military Conf. MILCOM 2010 pp. 2108 - 2112

[19]   T.Chiu-Yam Ng, Wei Yu et al," Joint Optimization of Relay Strategies and Resource Allocations in Cooperative Cellular Networks", IEEE J. Sel. Areas Commun., vol. 25, no. 2, pp. 328 - 339 ,Feb 2007.

[20]   S. Sharma, Yi Shi, Y. Thomas Hou, S. Kompella, "An Optimal Algorithm for Relay Node Assignment in Cooperative Ad Hoc Networks", IEEE/ACM Trans on Networking, vol. 19, no. 3,pp. 879 - 892 June 2011

[21]   Wei Yang_, Lihua Li_, Gang Wu†, Haifeng Wang†, and Ying Wang, "Joint Uplink and Downlink Relay Selection in Cooperative Cellular Networks", in proc. Vehicular Technology Conf. VTC 2010.

[22]   Jaafar Adhab Aldhaibani, A. Yahya , R.B. Ahmad, N. A. Al-Shareefi and M. K. Salman, "Effect of Relay Location on Two-Way Df and Af Relay in Lte-A Cellular Networks", International Journal of Electronics and Communication Engineering & Technology (IJECET), Volume 3, Issue 2, 2012, pp. 385 - 399, ISSN Print: 0976- 6464, ISSN Online: 0976 –6472.

[23]   Prachi R. Shinde, Madhura Gad and Prof. S.U. Kulkarni, "Genetic Algorithm Approach into Relay Co-Ordination", International Journal of Electrical Engineering & Technology (IJEET),Volume 4, Issue 3, 2013, pp. 35 - 42, ISSN Print : 0976-6545, ISSN Online: 0976-6553.

[24]   Sohrab Alam and Sindhu Hak Gupta, "Performance Analysis of Cooperative Communication Wireless Network", International Journal of Electronics and Communication Engineering & Technology (IJECET), Volume 3, Issue 2, 2012, pp. 301 - 309, ISSN Print: 0976- 6464, ISSN.

International Journal of Modern Engineering Research (IJMER)

Contents :

Application of Intuitionistic Fuzzy Soft Matrices in the Analysis of the Expectations of Old Age People

Dr. A. Praveenprakash[1], Kanimozhiraman[2]

[1]*Professor, Department of Mathematics, Hindustan University, Chennai, India*
[2]*Assistant Professor, Department of Mathematics, KCG College of Technology, Chennai, India*

Abstract: *In our real life, we are facing the situations involving uncertainty, imprecision and vagueness. To deal with these situations the concept of Soft set was developed. To enhance the flexibility of its applications the parametrization tool of soft set theory was used. It has been said that "we start dying the day we are born". The whole life of a person is dedicated for the welfare of his family. At his old age, when his health deteriorates, he starts to expect the support from his family. When the family members are not able to support him, problems arise. This situation forces him to old age home which affects him, his family and also the society. Though all the expectations can't be satisfied by the family members, some of the vital expectations may be fulfilled. In this paper we find out the major expectation of the old age people using Intuitionistic Fuzzy Soft Matrices (IFSM).*

Keywords: *Intuitionistic fuzzy soft set, Intuitionistic fuzzy soft matrices, Old age people, Old age home.*

I. Introduction

In 1999 Molodtsov [1] introduced Soft set theory as a general mathematical tool for dealing with uncertainty. The concept of Intuitionistic fuzzy sets (IFS) was proposed by Atanassov [2, 3]. After the introduction of the concept Intuitionistic fuzzy soft sets by P.K. Maji [4] et al, Jiang et al [5] extended the methods to intuitionistic fuzzy soft theory. Intuitionistic Fuzzy Soft Matrices (IFSM) was proposed by B. Chetia et al [6] in the year 2012 and Rajarajeswari et al[7-9]. Proposed some definitions for Intuitionistic soft matrices (IFSM) and its types. In this paper the expectations of the old age people was analyzed using IFSM. This paper is organized as follows. In Section 2 the preliminaries are given. In Section 3, the problems of the old age people are elaborated based on the information which is collected from the experts using linguistic questionnaire. In Section 4, the IFSM is applied to analyze the expectations of the aged people. And in final section, conclusions are derived based on our study.

II. Preliminaries

Definition2.1.[10]A fuzzy set (class) A in X is Characterized by a membership (characteristic) function $f_A(x)$ which associates with each point in X a real number in the interval [0,1], with the value of $f_A(x)$ at x representing the "grade of membership" of x in A.

Definition 2.2. [15] Let U be a non-empty set, called initial universal set of objects and E is a set of parameters in relation to U which is often the set of attributes, characteristics or properties of objects. Let P(U) denotes the power set of U. A pair (F,E) is called a soft set over U, where F is a mapping given by $F : E \rightarrow P(U)$.

Definition 2.3.[11]. Let U be a non-empty set, called initial universal set of objects and E is a set of parameters in relation to U which is often the set of attributes, characteristics or properties of objects. Let $A \subset E$. A pair (F, A) is called fuzzy soft set over U where F is a mapping given by $F : A \rightarrow I^U$ and I^U denotes the collection of all fuzzy subsets of U.

Definition 2.4. [12] Let $U = \{x_1, x_2, ..., x_n\}$ be the initial universe of elements and $E = \{e_1, e_2, ..., e_m\}$ be the set of parameters. The pair (U,E) will be called a soft universe. Let $F : E \rightarrow I^U$ and μ be a fuzzy subset of E, i.e., $\mu: E \rightarrow I = [0, 1]$, where I^U is the collection of all fuzzy subsets of U. Let F_μ be a mapping $F_\mu : E \rightarrow I^U \times I$ defined as follows:

$F_\mu(e) = (F(e), \mu(e))$, where $F(e) \in I^U$. Then F_μ is called generalized fuzzy soft set over the soft universe (U, E).

Here for each parameter e_i, $F_\mu(e_i)$ indicates not only the degree of belongingness of the elements of U in $F(e_i)$ but also the degree of possibility of such belongingness which is represented by $\mu(e_i)$.

Definition 2.5. [13] Let U be an initial universal set , E be the set of parameters. Let IF^U denotes the collection of all intuitionistic fuzzy subsets of U. Let $A \subseteq E$. A pair (F, A) is called all intuitionistic fuzzy soft set over U, where F is a mapping given by $F : A \to I\,F^U$.

In other words, Let I^U ($I = [0, 1] \times [0, 1]$) denote the power set of all intuitionistic fuzzy soft subsets of U, A pair (F, E) is called intuitionistic fuzzy soft set over U , where $F : E \to I^U$ is a mapping from parameter set E to U, that is to say, for

$$\forall e \in E, F(e) = \left\{ < x, \mu_{F(e)}(x), \gamma_{F(e)}(x) >: x \in U \right\} \in I^U, \ \mu_{F(e)}(x) \in [0,1], \ \gamma_{F(e)}(x) \in [0,1] \text{ denote}$$

membership and non-membership degrees of an element $x(\in U)$ regard to intuitionistic fuzzy set $F(e)$,

respectively, which satisfying $\mu_{F(e)}(x) + \gamma_{F(e)}(x) \le 1$.

Let *IFS(U)* denote all intuitionistic fuzzy soft sets over initial universal set U . IFSs is represents according to initial universal set U is continuous or discrete.

(1) If U is continuous, we denote $(F, E) = \int_U \left[\mu_{F(E)}(x), \gamma_{F(E)}(x) \right] / x$.

(2) If U is discrete, we denote $(F, E) = \sum_{i=1}^m \left[\mu_{F(E)}(x_i), \gamma_{F(E)}(x_i) \right] / x_i$ where $|U| = $ m.

Definition 2.6[14](Inclusion relation). Suppose (F, E) and $(G, E) \in IFS(U)$, we say that (F, E) is a intuitionistic fuzzy soft subset of (G, E), If for $e \in E$, we have $F(e) \subset G(e)$, that is to say , for $\forall e \in E, \forall x \in U$, we have $\mu_{F(e)}(x) \le \mu_{G(e)}(x)$ and $\gamma_{F(e)}(x) \ge \gamma_{G(e)}(x)$ denoted by $(F, E) \widetilde{\subset} (G, E)$.

Definition 2.7(Equation relation). Suppose (F, E) and $(G, E) \in IFS(U)$, we say they are intuitionistic fuzzy soft equal if and only if $(F, E) \widetilde{\subset} (G, E)$ and $(F, E) \widetilde{\supset} (G, E)$, namely for $\forall e \in E, \forall x \in U$, $\mu_{F(e)}(x) = \mu_{G(e)}(x)$ and $\gamma_{F(e)}(x) = \gamma_{G(e)}(x)$ denoted by $(F, E) \cong (G, E)$.

Definition 2.8(Complement operation) Suppose $(F, E) \in IFS(U)$, $(F, E)^c \cong (F^c, E)$ is defined as intuitionistic fuzzy soft complementary set of (F, E), where $F^c : E \to I^U$, for $\forall e \in E, \ F^c(e) = \left\{ < x, \mu_{F(e)}(x), \gamma_{F(e)}(x) >: x \in U \right\}$. Obviously (F^c, E) is also an IFSs over the same initial universal set U.

Definition 2.9 (Union and Intersection operation). Suppose (F, E) and $(G, E) \in IFS(U)$,

(i) The Intuitionistic fuzzy soft union of these two IFSss can be defined as $(F, E) \widetilde{\cup} (G, E) \cong (M, E)$ where for $\forall e \in E,$ we have

$$M(e) = F(e) \cup G(e) = \left\{ < x, \mu_{M(e)}(x) = \mu_{F(e)}(x) \vee \mu_{G(e)}(x), \gamma_{M(e)}(x) = \gamma_{F(e)}(x) \wedge \gamma_{G(e)}(x) >: x \in U \right\}$$

(ii) The Intuitionistic fuzzy soft intersection of these two IFSss can be defined as $(F, E) \widetilde{\cap} (G, E) \cong (H, E)$ where for $\forall e \in E,$ we have

$$H(e) = F(e) \cap G(e) = \left\{ < x, \mu_{H(e)}(x) = \mu_{F(e)}(x) \wedge \mu_{G(e)}(x), \gamma_{H(e)}(x) = \gamma_{F(e)}(x) \vee \gamma_{G(e)}(x) >: x \in U \right\}$$

Definition 2.10.(IFSM) Suppose $(F, E) \in IFS(U)$, denote $|U| = m$, $|E| = n$, Intuitionistic fuzzy soft matrix is defined by $\tilde{F} = (f_{ij})_{m \times n}$, where $f_{ij} = (\mu_{F(e_j)}(x_i), \gamma_{F(e_j)}(x_i))$, $i = 1, 2, \ldots, m$, $j = 1, 2, \ldots, n$. The concrete form of IFSM is as follows:

$$\tilde{F} = \begin{pmatrix} & e_1 & e_2 & \cdots & e_n \\ x_1 & (\mu_{F(e_1)}(x_1), \gamma_{F(e_1)}(x_1)) & (\mu_{F(e_2)}(x_1), \gamma_{F(e_2)}(x_1)) & \cdots & (\mu_{F(e_n)}(x_1), \gamma_{F(e_n)}(x_1)) \\ x_2 & (\mu_{F(e_1)}(x_2), \gamma_{F(e_1)}(x_2)) & (\mu_{F(e_2)}(x_2), \gamma_{F(e_2)}(x_2)) & \cdots & (\mu_{F(e_n)}(x_2), \gamma_{F(e_n)}(x_2)) \\ \vdots & \vdots & \vdots & \cdots & \vdots \\ x_n & (\mu_{F(e_1)}(x_m), \gamma_{F(e_1)}(x_m)) & (\mu_{F(e_2)}(x_m), \gamma_{F(e_2)}(x_m)) & \cdots & (\mu_{F(e_n)}(x_m), \gamma_{F(e_n)}(x_m)) \end{pmatrix}$$

IFSM over initial universe could be denoted by *IFSM(U)*.

Definition 2.11. Suppose $\tilde{G}, \tilde{F} \in IFSM(U), \lambda > 0,$ then some operations about IFSM could be defined as follows:

(1) $\tilde{F} \oplus \tilde{G} = (\mu_{F(e_j)}(x_i) + \mu_{G(e_j)}(x_i) - \mu_{F(e_j)}(x_i) \times \mu_{G(e_j)}(x_i), \gamma_{F(e_j)}(x_i) \times \gamma_{G(e_j)}(x_i))_{m \times n}$;

(2) $\tilde{F} \otimes \tilde{G} = \left(\mu_{F(e_j)}(x_i) \times \mu_{G(e_j)}(x_i), \gamma_{F(e_j)}(x_i) + \gamma_{G(e_j)}(x_i) - \gamma_{F(e_j)}(x_i) \times \gamma_{G(e_j)}(x_i) \right)_{m \times n}$;

(3) $\lambda \tilde{F} = \lambda \left(\mu_{F(e_j)}(x_i), \gamma_{F(e_j)}(x_i) \right)_{m \times n} = \left(1 - \left(1 - \mu_{F(e_j)}(x_i)^{\lambda}, \gamma_{F(e_j)}(x_i) \right)^{\lambda} \right)_{m \times n}$;

(4) $\tilde{F} = \left(\mu_{F(e_j)}(x_i), \gamma_{F(e_j)}(x_i) \right)_{m \times n}^{\lambda} = \left(\left(\mu_{F(e_j)}(x_i) \right)^{\lambda}, \left(1 - \left(1 - \gamma_{F(e_j)}(x_i) \right)^{\lambda} \right) \right)_{m \times n}$.

Proposition 2.1. Suppose $\tilde{G}, \tilde{F} \in IFSM(U)$, *and* $\lambda, \lambda_1, \lambda_2 > 0,$ we have

(1) $\tilde{F} \oplus \tilde{G} = \tilde{G} \oplus \tilde{F}$;

(2) $\tilde{F} \otimes \tilde{G} = \tilde{G} \otimes \tilde{F}$;

(3) $\lambda \left(\tilde{F} \oplus \tilde{G} \right) = \lambda \tilde{G} \oplus \lambda \tilde{F}$;

(4) $\left(\tilde{F} \otimes \tilde{G} \right)^{\lambda} = \tilde{F}^{\lambda} \otimes \tilde{G}^{\lambda}$;

(5) $\lambda_1 \tilde{F} \oplus \lambda_2 \tilde{F} = (\lambda_1 + \lambda_2) \tilde{F}$;

(6) $\tilde{F}^{\lambda_1} \otimes \tilde{F}^{\lambda_2} = \tilde{F}^{(\lambda_1 + \lambda_2)}$.

Definition 2.12. Let U be a finite universe, $\tilde{F}_k \in IFSM(U), (k = 1, 2, \ldots K),$ and

$w = (w_1, w_2, \ldots, w_k), \sum_{k=1}^{K} w_k = 1$ is a weight vector, then the weighted arithmetic average operator is defined as follows:

The weighted arithmetic average operator $f_w = IFSM(U) \rightarrow IFSM(U)$, namely

$$f_w(\tilde{F}_1, \tilde{F}_2, \ldots, \tilde{F}_k) = \bigoplus_{k=1}^{K} w_k \tilde{F}_k \qquad (1)$$

Algorithm for multi expert group decision making problems:

Step 1: Input the IFSM (given by the experts) over a finite universe U and a finite parameter set E.

Setp 2: Calculate collective IFSM $\tilde{F}^*$ using the weighted arithmetic average operator by formula (1)

Step 3: Compute the threshold vectors based on median $\lambda_{med}(E)$ by using the formula,

$\lambda_{med}(E) = \left\{ \lambda_{med}(e_j) | 1 \le j \le n \right\} = \left\{ \left(\mu_{med}(e_j), \gamma_{med}(e_j) \right) | 1 \le j \le n \right\}$, where for $\forall e_j \in E, \mu_{med}(e_j)$ is the median by ranking membership degree of all alternatives according to order from large to small (or from small to large), namely

$$\mu_{med}(e_j) = \begin{cases} \mu_{e_j}\left(x_{\left(\frac{m+1}{2}\right)}\right) & , \textit{if } m \textit{ is an odd number}, \\ \left(\mu_{e_j}\left(x_{\left(\frac{m}{2}\right)}\right) + \mu_{e_j}\left(x_{\left(\frac{m}{2}+1\right)}\right)\right)\Big/2 & , \textit{if } m \textit{ is an even number}, \end{cases}$$

and $\gamma_{med}(e_j)$ is also median by ranking membership degree of all alternatives according to order from large to small (or from small to large), namely

$$\gamma_{med}(e_j) = \begin{cases} \gamma_{e_j}\left(x_{\left(\frac{m+1}{2}\right)}\right) & , \textit{if } m \textit{ is an odd number}, \\ \left(\gamma_{e_j}\left(x_{\left(\frac{m}{2}\right)}\right) + \gamma_{e_j}\left(x_{\left(\frac{m}{2}+1\right)}\right)\right)\Big/2 & , \textit{if } m \textit{ is an even number}, \end{cases}$$

Step 4. Calculate choice value(c_i) of all alternatives.
Step 5. Rank all alternatives according to choice value and select the optimal decision by $c_k \ \max_{1 \le i \le m} c_i$.

III. Old Age People

We have conducted a survey in various old age homes in Chennai during May to June 2014. We framed a linguistic questionnaire and administered the same to 100 old aged persons living under different difficult circumstances. Based on our study , Here we listed some of the problems of the old age people, and the solutions to overcome these problems.

Table 1.

Problems of the old age people	Needs
Isolation	Inclusion
Boredom	Be usefully occupied
Neglect	Care
Abuse	Protection
Fear	Reassurance
Economical Insecurity	Economical security
Failing Health	Doing exercise ,healthy food
Lack of respect	Respect and love
Lack of self esteem	Self confidence
Lake of preparedness for old age	Preparedness of old age

Five important attributes are given by the three experts which is obtained based on the data given above.
The attributes given by experts are as follows
x_1 - Economic security
x_2 - Inclusion
x_3 - Care
x_4 - Respect and Love
x_5 - Be usefully occupied

Family status
e_1 - Poor
e_2 - Middle Class
e_3 - Rich

Economic security

Retirement is not "golden" for all older adults. Post retirement period is the dependence period on their children. These older adults struggle each day with rising housing and health care bills, inadequate nutrition, lack of access to transportation, diminished savings, and job loss. So they need some regular income and be prepared financially . The children should give them money without hesitation. They should realize that it is their duty to spend money for their parents.

Inclusion

It is important that the older adults must feel included in the happenings around them, both in the family as well as in the society. So the children should try their best to make them comfortable and get them involved in family and society related activities so that they can spend the rest of their life happily.

Care

For a plant to grow, atleast in starting stage somebody should take care of it. Without any care, even a pet will not stay with us. Parents are the epitome for their children's life, they spend their whole life for their children, so children should take care of them.

Respect and Love

"We make them cry,
who care for us.
We cry for those,
who never care for us."
This is the truth of life. Its STRANGE but TRUE!"

Parents play an important role in our lives. They brought up their children despite of having so many socio-economic difficulties. They fulfill our every demand & never complain for anything. In return its our duty to give respect, love & care to them.

Be usefully occupied.

A person who is not usefully occupied tends to physically and mentally decline and this in turn has a negative emotional impact. Most people who have reached the age of 60 years or more have previously led productive lives and would have gained several skills during their life-time. Identifying these skills would be a relatively easy task. Motivating them and enabling them to use these skills is a far more challenging process that requires determination and consistent effort by dedicated people working in the same environment as the affected elders.

IV. Application Of IFSM

$U = \{x_1, x_2, x_3, x_4, x_5\}$ is the set of attributes, $E = \{e_1, e_2, e_3\}$ is the set of family status , $\tilde{F}_k \, (1 \le k \le 3)$ is the IFSM given by three experts, where the experts weights are $w = \{0.5, 0.3, 0.2\}$

Table 2. The evaluation value of $\tilde{F}_1$

	e_1	e_2	e_2
x_1	(0.8,0.1)	(0.6,0.3)	(0.2,0.1)
x_2	(0.6,0.3)	(0.4,0.3)	(0.4,0.3)
x_3	(0.5,0.3)	(0.5,0.4)	(0.5,0.2)
x_4	(0.7,0.2)	(0.7,0.2)	(0.7,0.1)
x_5	(0.7,0.1)	(0.3,0.2)	(0.2,0.2)

Table 3. The evaluation value of $\widetilde{F}_2$

	e_1	e_2	e_3
x_1	(0.7,0.1)	(0.4,0.5)	(0.3,0.5)
x_2	(0.5,0.2)	(0.3,0.2)	(0.5,0.3)
x_3	(0.5,0.3)	(0.4,0.5)	(0.6,0.3)
x_4	(0.8,0.1)	(0.7,0.3)	(0.9,0.2)
x_5	(0.3,0.4)	(0.6,0.2)	(0.3,0.2)

Table 4. The evaluation value of $\widetilde{F}_3$

	e_1	e_2	e_3
x_1	(0.6,0.2)	(0.7,0.2)	(0.6,0.2)
x_2	(0.4,0.1)	(0.3,0.3)	(0.7,0.1)
x_3	(0.5,0.2)	(0.3,0.5)	(0.3,0.1)
x_4	(0.8,0.1)	(0.6,0.1)	(0.5,0.1)
x_5	(0.3,0.5)	(0.3,0.4)	(0.4,0.2)

Table 5.Collective IFSM $\widetilde{F}^*$ and the threshold vector $\lambda_{med}(E)$.

	e_1	e_1	e_1
x_1	(0.7405,0.1149)	(0.5735,0.3224)	(0.3309,0.1862)
x_1	(0.5362,0.2132)	(0.3519,0.2656)	(0.5055,0.2408)
x_1	(0.5000,0.2766)	(0.4351,0.4472)	(0.4998,0.1966)
x_1	(0.7551,0.1414)	(0.6822,0.1966)	(0.7610,0.1231)
x_1	(0.5417,0.2091)	(0.4082,0.2297)	(0.2744,0.2000)
$\lambda_{med}(E)$	(0.5417,0.2091)	(0.4351,0.2656)	(0.4998,0.1966)

Table 6 .T he choice value of all alternatives

	e_1	e_2	e_3	c_i
x_1	1	0	0	1
x_2	0	0	0	0
x_3	0	0	1	1
x_4	1	1	1	3
x_5	1	0	0	1

Rank all alternatives x_i (i = 1,2,…,5) in accordance with choice value $x_4 > x_1$,x_3, $x_5 > x_2$. This shows that the very important need of the old age people is respect and love.

V. Conclusion

We found that the most important need of the aged persons is respect and love. Even though they were in different family status, they are expecting the love and respect from their children and grandchildren. Why do some of us leave them in Old-age Homes? Why they had to struggle all alone there? God has given human beings the quality to take care of their old ones. Hence, we should not ignore Almighty's reward. To eradicate this problem parents should set an example before their children by serving their parents & grand parents. Once the children get this precious quality in their genes we wouldn't have such inhumanity in our society.

REFERENCES

[1]. D. Molodtsov, Soft set theory-First results, Computers and Mathematics with Application 37 (4-5) (1999) 19-31.

[2] K. Atanassov, Intuitionistic fuzzy sets, Fuzzy Sets and Systems 20 (1986) 87–96.

[3] K. Atanassov, More on intuitionistic fuzzy sets, Fuzzy Sets and Systems 33 (1989) 37–46.

[4] P.K. Maji, R. Biswas, A.R. Roy, Intuitionistic fuzzy soft sets, J. Fuzzy Math. 9 (2001) 677–692.

[5] Yuncheng Jiang, Yong Tang, Qimai Chen, An adjustable approach to intuitionsitic fuzzy soft sets based decision making, Appl. Math. model. 35 (2011)824–836.

[6] Chetia.B,Das .P.K.,2012, "Some results of Inuitionistic Fuzzy Soft matrix theory" Advances in Applied science Research,3(1):412-423.

[7] P. Rajarajeswari, P. Dhanalakshmi,"Intuitionistic Fuzzy Soft Matrix Theory and its application in Decision Making",International Journal of Engineering Research and Technology, vol.2(4) pp.1100-1111, 2013.

[8] P. Rajarajeswari, P.Dhanalakshmi, "Intuitionistic fuzzy soft matrix theory and its application in medical diagnosis", Annals of Fuzzy Mathematics and Informatics, vol.2, pp. 1-11, 2013

[9] P.Rajarajeswari, P.Dhanalakshmi,"Similarity measures of intuitionistic fuzzy soft sets and their application in medical diagnosis", International journal of mathematical archive, vol.5(5), pp. 143-149, 2014.

[10]. L.A.Zadeh, Fuzzy sets, Information and Control , 8,(1965),338 – 353.

[11] P. K. Maji, R. Biswas, A. R. Roy, Fuzzy soft sets, The Journal of Fuzzy Mathhematics 9 (3) (2001) 589-602.

[12] P. Majumder, S. K. Samanta, Generalised fuzzy soft sets, Computers and Mathematics with Application 59 (4) (2010) 1425-1432.

[13] P. K. Maji, R. Biswas, A. R. Roy, Intuitionistic fuzzy soft sets, The Journal of Fuzzy Math- hematics 9 (3) (2001) 677-692.

[14] Junjun Mao et al,Group decision making methods on intuitionistic fuzzy soft matrices, Applied Mathematical Modelling,37,(2013)6425-6436

[15] P. K. Maji, A. R. Roy, R. Biswas, An application of Soft set in a decission making problem, Computers and Mathematics with Application 44 (2002) 1077{1083.

Management operation system techniques (MOST) replaces PERT and CPM in construction scheduling

Shailla

RGPM College Bhopal INDIA

Abstract: *The Management Operation System Technique (MOST) invented in 1961, replaces PERT and CPM on construction projects and in program management. Since its inception, MOST has gained popularity and is now widely used in both large and small construction projects. Its use has been equally effective on projects ranging from several thousand dollars to $193 million so far. It is a combination of several traditional and modern planning techniques like bar chart, Gantt chart, CPM and PERT. The advantages of these have been extracted and disadvantages have been eliminated. Few of the advantages are: it is very helpful for repetitive works in both real and infrastructure projects and uses backward integration which helps in knowing the ground realities very easily. It gives the project manager visibility and identifies potential trouble areas requiring management action. This paper deals with application of MOST for construction activities of a 25 Kms Road project and drawing of MOST schedules. In the end the limitations of MOST are mentioned.*
Keywords: *(PERT, CPM, MOST, Bar chart, Gantt chart, MPS)*

I. Introduction

Intelligent planning, scheduling and control are absolutely essential to the success of any project: research and development, construction, manufacturing, bids, proposal etc. The Management Operation System Technique (MOST) invented in 1961, replaces PERT and CPM on construction projects and in program management. Since its inception, MOST has gained popularity and is now widely used in both large and small construction projects. Its use has been equally effective on projects ranging from several thousand dollars to $193 million so far. Elements of several traditional and modern planning techniques (bar chart, Gantt chart, PERT, CPM etc.) are combined in this newest management tool, MOST. The advantages of each of these methods have been extracted and the disadvantages of each have been eliminated .MOST not only contributes to single project R & D, construction, bids, and proposals, but also to Multi-Project Scheduling (MPS) either in production short runs or R & D. MOST's contribution to MPS has added another management tool to help satisfy the ever increasing need for better multi-project scheduling methods .MOST has been developed to give the project manager visibility; presenting all information necessary for good project control simply and clearly, and in time to allow effective management action. Its early warning system identifies potential trouble areas requiring management action and pin-points long-lead-time tasks. It also provides well-organized data for timely and comprehensive reporting. MOST can be particularly useful in monitoring programs that cross company, division or department lines, making it an extremely helpful tool for the general manager. MOST has the added advantage of presenting a graphic picture of a project status, manpower loading, costs and any related weak spots in an easily read schedule

II. What Is Management Operation System Techniques?

When planning a project of any size, CPM can be used, if desired, to establish milestones and float (or slack) time become apparent as the MOST schedule begins to take shape. Float in MOST will be determined without any calculation, such as the forward and backward passes which are needed in CPM.

If one prefers to use an existing CPM or other computer scheduling method to supply the schedule logic and dependencies, they may continue to do so. In that case, they will be simply converting the network diagram into MOST to provide all the benefits to be gained by MOST's unique graphic monitoring capabilities in a schedule that never needs to be redrawn. MOST converts CPM paths into bars keyed to working days, so that progress against scheduled deadlines can be checked easily by project supervisors.

In any case, once MOST is mastered, the planner can go directly to MOST without the use of either CPM or anything else
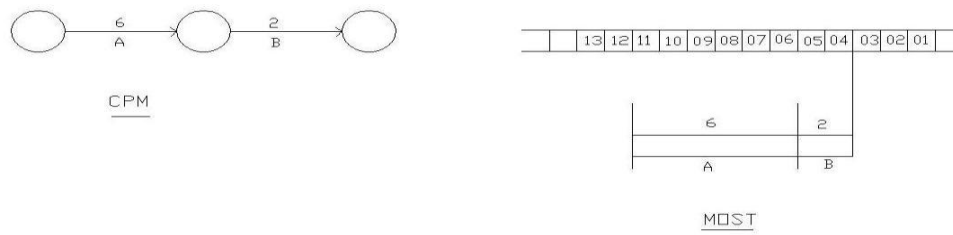
FIGURE 1

A MOST schedule is divided vertically into calendar periods. Programmed activities are displayed as segments of hollow bars, with events appearing as flags at the appropriate time bar continues along the chart. An arrow is drawn vertically from the tail-end of each discontinued bar to the surviving path, to show the relationship between them.Thus, a MOST user can see at a glance when a job-and-path is scheduled to begin and end, and what other jobs hinge on its completion. In addition to displaying deadlines, a MOST chart also shows how far a job has actually gone. This is done by a unique method of blocking in the hollow bars. To check progress, a vertical reporting line is placed on the schedule from the calendar scale periodically, to highlight all the activities scheduled to progress as of the reporting date. Bars filled in right up to the reporting lines are on schedule; those filled in short of the line are behind schedule; and those blocked in solidly to a point beyond the reporting line are behind of schedule.

The MOST schedules differs from PERT and CPM in that when the critical sequence(s) of activities is (are) established, MOST completes the schedule by working backwards from the contract completion date. But before constructing a MOST schedule, we must first decide on the level of detail required to monitor the program. This will vary, depending upon the size and type of projects being monitored.

Since the schedule is time-oriented, there is less initial effort in preparing the first MOST draft (diagram). After the MOST is drawn and coordinated with management and department supervision, actual reporting begins. MOST clearly shows a project's day-to-day status. Critical paths and float times are shown at a glance. The MOST is laid out to show the latest date that a job can start without jeopardizing the schedule. All the updating is done manually, although the system can feed a computer, should the, need arise. But in any case, manually updating MOST will take one hour or less, regardless of project size or complexity. This is because reporting centers around those activities to be monitored during the reporting period bar continues along the chart. An arrow is drawn vertically from the tail-end of each discontinued bar to the surviving path, to show the relationship between them.

III. How To Use Management Operation System Technique
MOST schedules are generally drawn on 22X34 inch or 24X36 inch paper for standardisation. The paper should be reproducible in order to convert to blue prints for normal distribution. The Vellum paper will become the schedule master which can be updated weekly, reproduced and stored. The following figures will illustrate the technique in preparing a MOST schedule.

FIGURE 2

The time estimate for shop drawing 20 days is entered immediately above the bar and to the right of the starting flag (sees Figure 3).
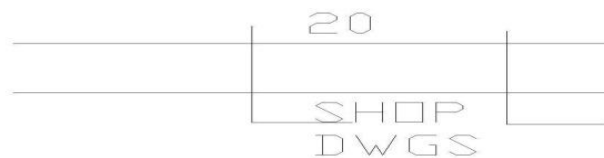

FIGURE 3

In construction schedules, the time estimates are shown in days, not weeks, because that is the language generally used. When applying the calendar to the top of the schedule, the normal calendar (4-1/3 weeks to a month) is used. All of the construction holidays are deleted in order to reflect the normal 40-hour work week. (see Figure 4).
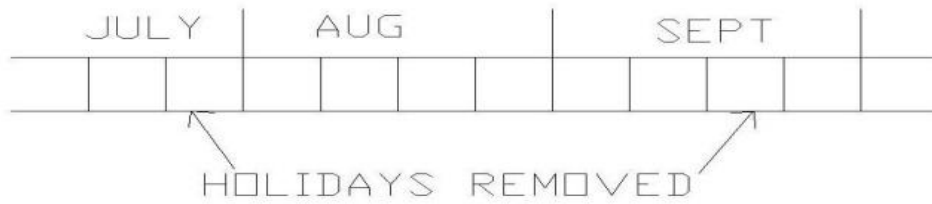
FIGURE 4

Figure 5 illustrates the designation of time, and the duration in days. As shown in Figure 6, jobs can occur in a series, overlap, or but parallel, depending upon their time and project relationships.
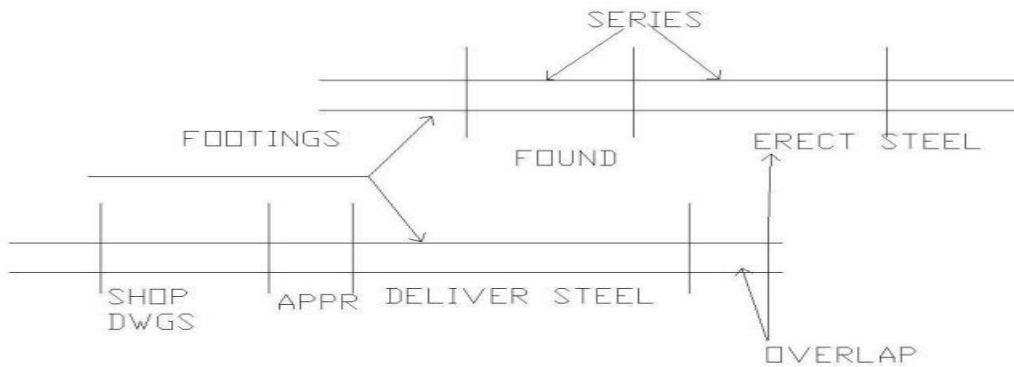

FIGURE 6

The basic MOST schedules (Figure 7) include jobs, delay notes, title block, and trend analysis.
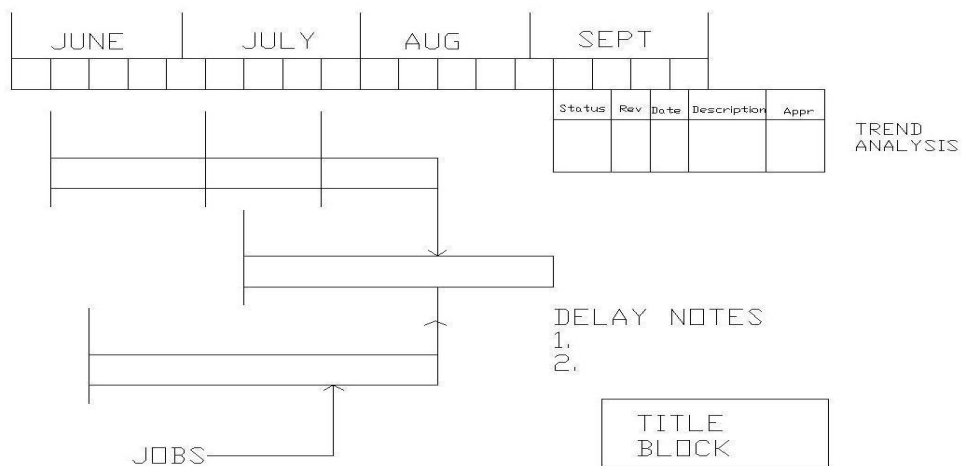

FIGURE 7

IV. Case Study

Construction Activities of the a road Project considered for a Length of 25 Km

Activity	Duration (weeks)
Possession of Obstruction Free Site	2
Stump Removal	6
Clearing & Grubbing	7
Taking OGL	3
Submission & Approval of Cross section	5
Excavation	9
Embankment Filling	3
Sub Grade	13
Drainage Layer	14
Wet Mix Macadam (WMM)	15
Dense Graded Bituminous Macadam (DBM)	8
Bituminous Concrete (BC)	4.8

Typical Job Listing

Beginning the scheduling the first few activities in figure 18. In this example Activity 1 includes getting clearances from Forest department and other necessary NOC from other departments.

01 02 03 04 05 06 07 08 09 10 11 12 13 14 15 16 17 18 19 20 21 22 23 24 25 26 27 28 29 30 31 32 33 34
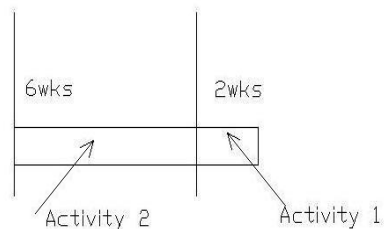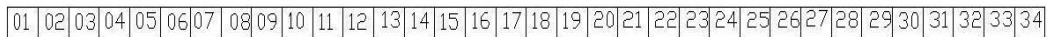
LISTING OF ACTIVITY IN MOST
FIGURE 18

In the following figure 19 the clearing grubbing includes the shifting of pipe line of water and sewerage if any, and any other building that exists in the Right of Way. Since the Activity 3 i.e. Clearing and Grubbing can be started after removal of stumps that are there after cutting of trees. So the Clearing and Grubbing can be done with a lag of one week from the start of Activity 2.

CONTINUE OF ACTIVITY LISTING
FIGURE 19

In the above figure it might be seen that the all the activities are starting after the start of first activity. If there are any activities which can be started before the start of the project then it creates a dilemma in finalization of critical path.In construction scheduling with MOST for a conventional road project proceeds from Possession of Obstruction Free site to getting the clearances from all the authorities like forest and environment ministry, any land acquisition that is to be made, demolishing of existing buildings coming in the way of Right of way, and the most important rehabilitation and resettlement of the Project affected People.By using the MOST system as described above the scheduler will develop a realistic schedule. It will not only show what jobs are necessary to construct a road to satisfy easy and comfortable journey, but it will also illustrate the latest start of all constraint jobs so as not to jeopardize the schedule or the contract date.Figure 20, illustrates a road construction being done till the level of Wet Mix Macadam (WMM). In this figure we can see the activities having a relationship between the activities and their constraints. All other jobs will be shown in their respective schedule positions to clearly display the relationship of parallel and overlapping jobs. If the start up of jobs illustrates too many of the same type of jobs or trades in parallel, the MOST visibility will highlight this potential problem. Figure 20 shows a "success-oriented" schedule. In other words, all jobs must be completed on the time frame against the calendar; there is no room for error. There is also no free time to allow for down time or inclement weather. Since construction is most often depending upon the weather, it is advisable to allow for at least two days per month during the winter months for contingencies or downtime. During the spring or summer months allow one day per month for rain. In many instances, some schedulers may allow two to three weeks per years for inclement weather. It's important to allow for these contingencies when preparing the Baseline Schedule.

MOST MODEL TILL SUBGRADE
FIGURE 20

MOST MODEL – UPDATED
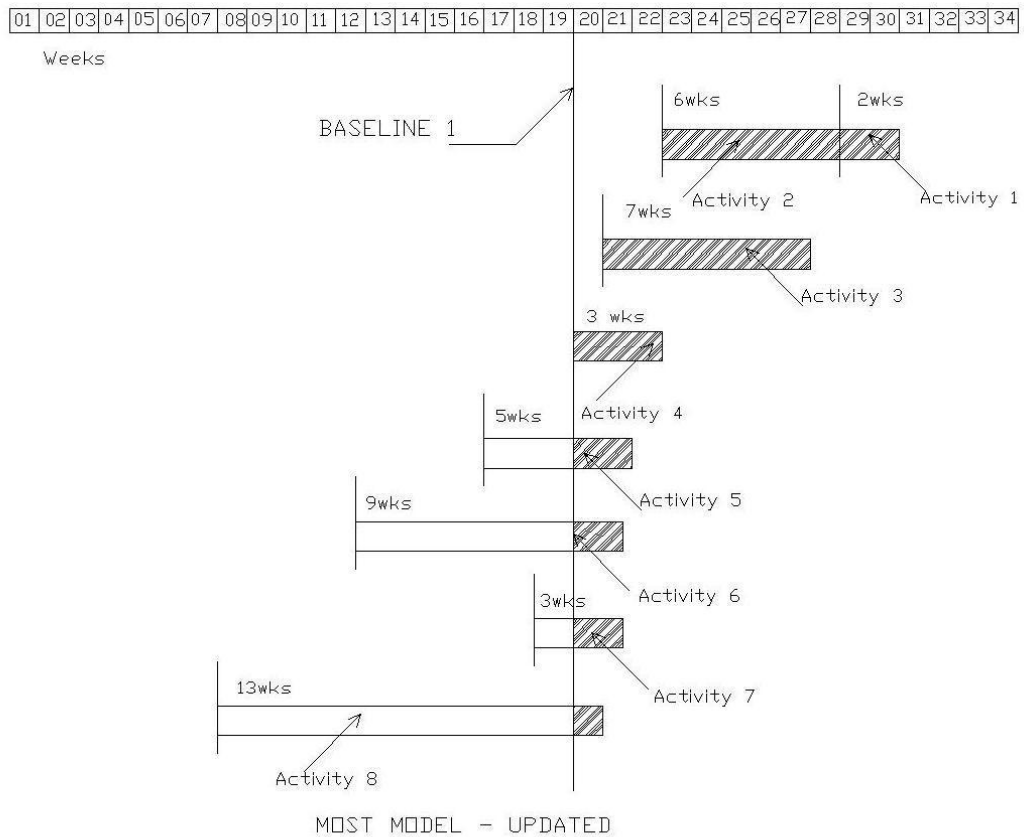
FIGURE 21

Figure 21 then, shows an update. The update figure can be seen the activities 1, 2, 3 and 4 completed and rest of the activities in different stages. From this figure it can seen whether the activity is on schedule/ behind schedule/ahead of schedule. From this we can know the criticality of the activity and in turn of the project. It is important to display all the slippages and delays completely and honestly to avoid suffering the consequences behind it too late to correct.

Now to figure 22 and add the remaining jobs which will complete the MOST schedule for this road project and activities such as laying of top layer and additional activities. Figure 21 shows a could be kept on baseline schedule we can now commence tracking progress weekly. A copy of all revisions should be kept on file until the project is completed, all payments have been received and made, and all required waivers and releases obtained. It's also recommended the original reproducible vellum be stored in the event a similar project is bid at a later date. This schedule will then be of some use if a bid schedule is required

```
|01|02|03|04|05|06|07|08|09|10|11|12|13|14|15|16|17|18|19|20|21|22|23|24|25|26|27|28|29|30|31|32|33|34|
```
Weeks

COMPLETE MOST DIAGRAM FOR THE PROJECT
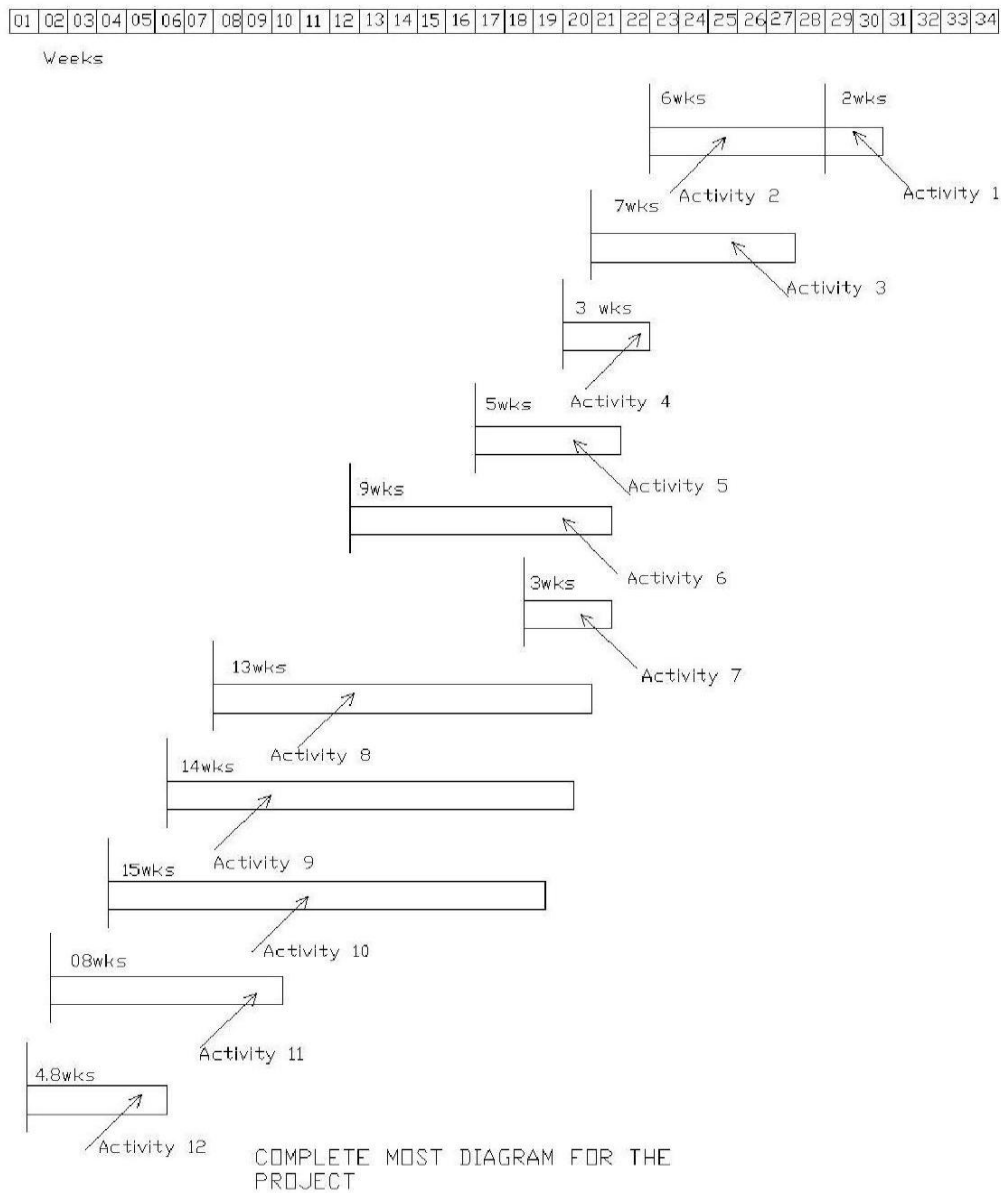
FIGURE 22

V. Conclusion

The Management Operation System Technique (MOST) replaces PERT and CPM on construction projects and in program management. Since its inception, MOST has gained popularity and is now widely used in both large and small construction projects. It is very helpful for repetitive works in both real and infrastructure projects. The use of percentage completion makes the monitoring of progress very easy. MOST uses backward integration which helps in knowing the ground realities very easily. The redrawing without rescheduling of activities is done in a simple manner. It is easy to update and is useful in cases of arbitration. The monitoring task by weekly updating is very easy. No forward and backward pass are required since MOST diagram describes it in detail. In-numerous baselines can be used for monitoring, which is very helpful in tracking of progress with tight control. Elements of many traditional and new planning techniques have been incorporated in MOST. MOST's contributes to MPS as an added management tool. It identifies potential trouble areas requiring management action

VI. Limitations

MOST becomes complicated when the number of activities is more. It is convenient for macro level planning.

VII. Recommendations

The breaking of project into activities should be done cautiously to prevent confusion and complexity. The use of weeks instead of days as calendar duration is easier to work with. The updating becomes less tedious.

REFERENCES

[1]. Anthony L. Lannone, And M Civitello, Jr.- Prentice-Hall ,1989. Construction Scheduling Simplified.
[2]. Project planning and control with PERT & CPM Dr. B.C.Punammia
[3]. www.springer.cou/cda/content
[4]. www.mindtoul.com
[5]. www.edu.twfurang/cho5.ppt

Tranformerless H6 Grid Tied Inverter For Photovoltaic Generation

Syed Sha Mohammed

Department of electrical and electronics, Visvesvaraya Technological University, India

Abstract: *Transformer less inverter is widely used in grid-tied photovoltaic (PV) generation systems, due to the benefits of achieving high efficiency and low cost. Various transformer less inverter topologies have been proposed to meet the safety requirement of leakage currents, such as specified in the VDE-4105 standard. In this paper, a family of H6 transformer less inverter topologies withlow leakage currents is proposed, and the intrinsic relationship betweenH5 topology, highly efficient and reliable inverter concept(HERIC) topology, and the proposed H6 topology has been discussedas well. One of the proposed H6 inverter topologies is takenas an example for detail analysis with operation modes and modulationstrategy. A universal prototype is built for H6 topology mentionedfor evaluating their performances in terms of power efficiency and powerquality characteristics. Experimental results show that inthe proposed H6 topology, it has been found that with the increase in the switching frequency, the magnitude of higher order harmonics increases and that of lower order harmonics reduces. The size and cost of filter reduces as the order of harmonics increases, so a tradeoff must be done between the switching frequencies and the cost of filter the system*

I. Introduction

The Photovoltaic generation is extensively increasing, since it is an essential inexhaustible and broadly available energy resource. For economic development of any country, energy is one of the critical inputs. Now a day's most of the energy is generated with fossil fuels which are non-renewable and cause environmental degradation by emission of carbon dioxide and other greenhouse gases, which are harmful to the environment. This has paved the way for research on renewable energy technology and other researches in the fields of power electronics and hence, the cost of utilizing the renewable energy is at an ever decreasing rate [1].

PV cells have an advantage of being maintenance and pollution free, but the cost of installation is high and in most of the power application they require a power converter for load interference. Also PV modules have relative low conversion efficiency. The overall system cost can be reduced by using high efficiency power converter[2]. Rapid advancement in the technology which extends from the field of renewable energy generation to the power supply of a portable digital device, impose great challenges on power electronics. The need of high efficiency, power density and reliability of power supply forcing power electronics engineers and researchers to find new way of power conversion with high efficiency and low losses. Ideally zero losses are aimed. But it is impossible to have lossless systems. Hence the power converters evolved from the earlier high loss, large linear power supplies to today's highly efficient and compact converters. In highly competitive industrial environment designers strive for improvement in efficiency, size and weight. In the recent past, various different inverter topologies have been proposed and are currently utilized for low power, single-phase grid-connected photovoltaic (PV) systems. A full-bridge inverter in combination with a line-frequency transformer is a familiar and common topology [3]. The transformer, however, is not a necessity or requirement and inverters avoiding transformers provide various advantages. Inverters without transformers outmatch those with presence of transformers with respect to higher efficiency, reduced cost, weight, embodied energy and minuscule size.When transformer is not used in the topology there is no method of increasing the inverter output voltage V_{inv} to the required RMS grid voltage value. Therefore, high DC bus voltage is required to guarantee the power flow from the PV array to the grid [3]. The system can only function when the DC bus voltage is more than the total amplitude of the grid voltage at all time. This constraint decides the minimum power rating of the system.

1.1 Common Mode Voltage Description

The common mode voltage of any circuit is the average of the voltages between the outputs and a common reference.
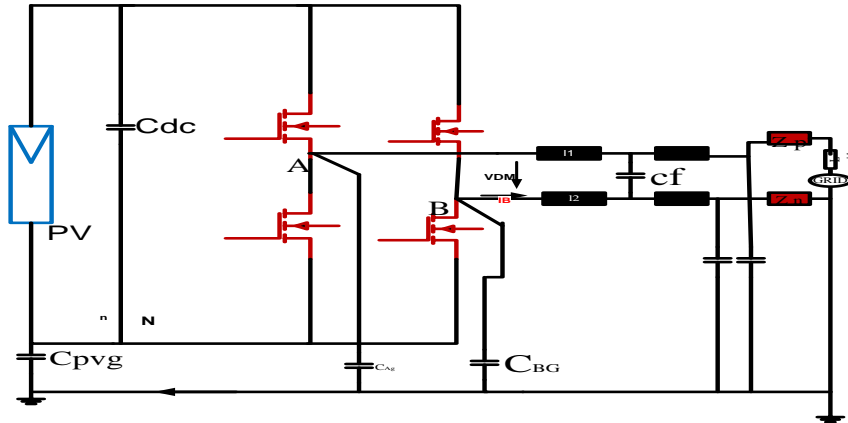
Fig: 1 Full Bridge Grid Tied Inverter

For the full-bridge inverter topology shown in Fig: 1.5 the negative terminal of the DC bus's point N is used as common reference. Therefore, the common-mode voltage, V_{cm} is given as:

$$V_{CM} = \frac{V_{AN} + V_{BN}}{2} \quad (1.1)$$

$$I_{cm} = I_A + I_B = C_{PVg}\frac{dVcm}{dt} (1.2)$$

The differential mode output voltage, V_{dm} is the voltage between both outputs :

$$V_{dm} = V_{AN} - V_{BN} = V_{AB} \quad\quad (1.3)$$

Combining equations (1.1) and (1.3) we get

$$V_{AN} = \frac{Vdm}{2} + V_{cm} \quad\quad (1.4)$$

$$V_{BN} = \frac{-Vdm}{2} + V_{cm} \quad\quad (1.5)$$

In addition to the common-mode voltage V_{cm}, two other sources, V_1 and V_2 are generated due to the asymmetries in the differential mode impedances [9][11]. Therefore, it is possible to have common-mode currents if any impedance asymmetry exists.

Inverters are the most important power electronics equipment in grid tied PV systems. Inverter interfacing PV modules with the grid ensures that the PV modules are operated at the maximum power. Their major role is to convert DC power into AC power. Based on the photovoltaic arrays output voltage, output power level and applications, the photovoltaic grid-connected system can adopt different topologies. These configurations describe the evolution of grid-connected inverters as from past, present and future technologies. There are different technologies and topologies available for transformer-less grid connected PV systems. In PV plants applications, various technological concepts are used for connecting the PV array to the utility grid. Each technology has its advantage and/or disadvantages compared to other, in terms of efficiency and power quality.

II. H5 Topology

The principle of H5 inverter topology can be explained with the help of fig: 2.1. It consists of five switches. And there are four operation modes in each period of the utility grid of the H5 topology, as shown in fig: 2.2. It can be seen that in the active modes, the inductor current of H5 topology is always flowing through three switches due to its extra switch $S5$ in dc side. In the freewheeling modes, the inductor current of H5 topology is flowing through two switches.
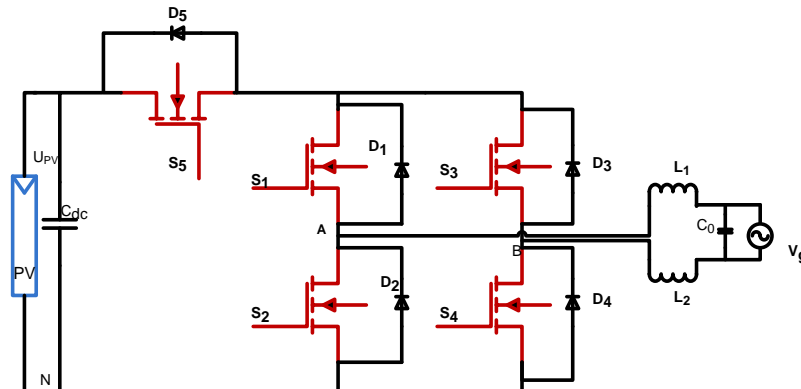
Fig: 2 H5 Topology

The basic operation of H5 inverter is illustrated by means of Fig: 3. Here all the four modes of operation of H5 inverter topology can be seen. During mode one gate pulses are given to switches S1, S4 and S5. When these switches are turned on there will be positive voltage V+ across the output end of the inverter. The direction of flow of current (clock wise) is as shown in the above Fig: 3.
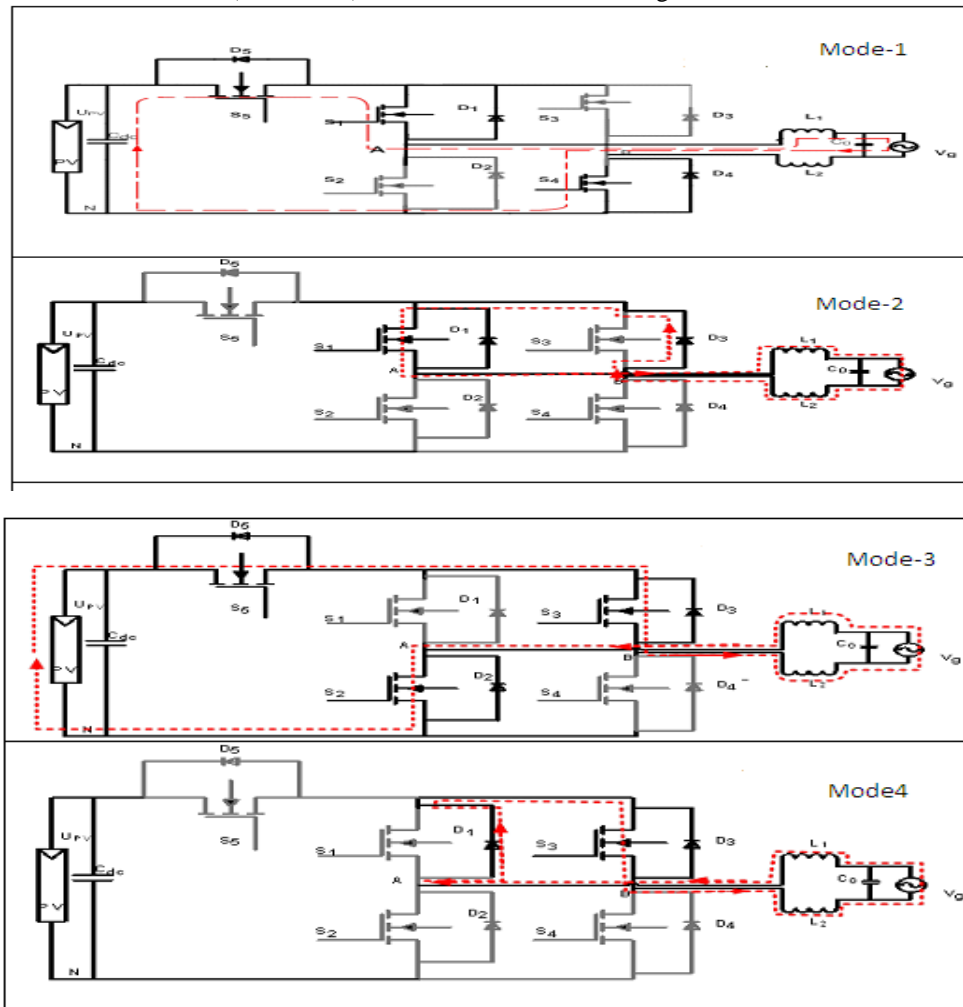
Fig: 3 Four modes of operation of H5 inverter topology
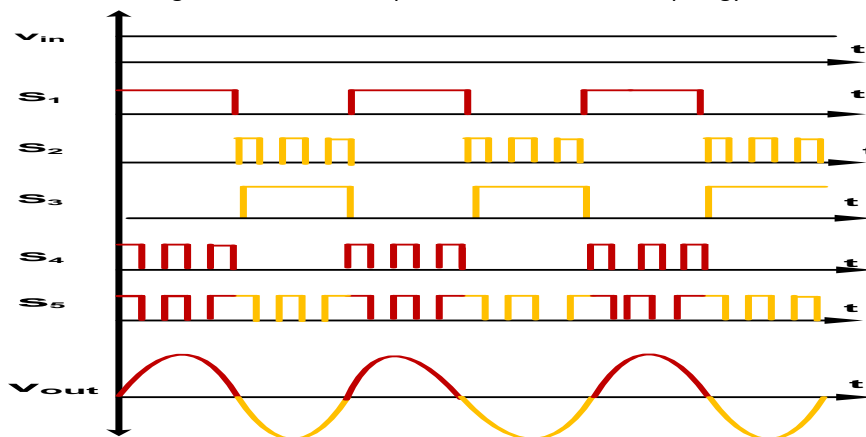
Fig: 4 Switching waveforms of H5 Inverter Topology

Figure two of the Fig 3 shows the second mode of operation of the H5 inverter, in the second mode gate pulse is given only to switch S1. This mode of operation is the first freewheeling mode. In the third mode of operation gate pulses are given switches S2, S3 and S5. When switches S2, S3 and S5 are turned on the direction of flow of current reverses (anti- clock wise) as shown in the Fig: 3 and the output voltage will be –V.

Finally in the fourth mode the (2nd freewheeling mode) during this mode gate pulse is only given the 3rd switch hence the energy stored freewheels through the switch S3 and diode D1. Here we can see that during both the active modes switch S1 is kept on.

III. Heric Topology
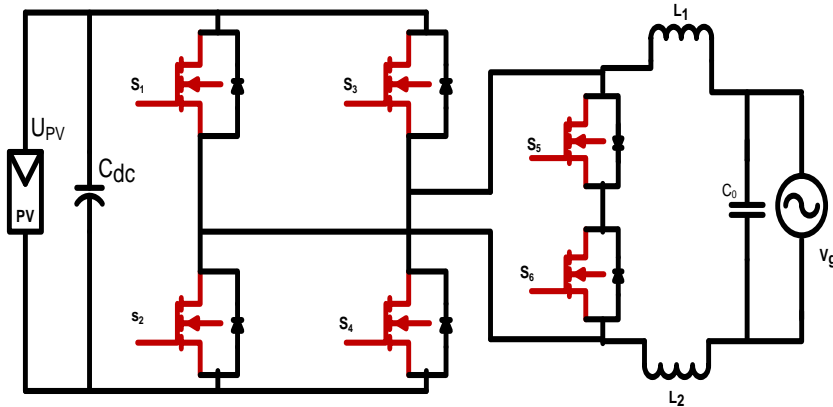

Fig: 5 HERIC Topology

The above Fig: 5 show HERIC topology, the basic operation of HERIC inverter is illustrated by means of Fig 6. Here all the four modes of operation of HERIC inverter topology can be seen. In the first mode of operation gate pulses are given to switches S1, S4 and S5. When these switches are turned on there will be positive voltage V+ across the output end of the inverter. The direction of flow of current (clock wise) is as shown in the above Fig 6.The waveforms of the gate drive signals for HERIC topology are shown in Fig: 7.
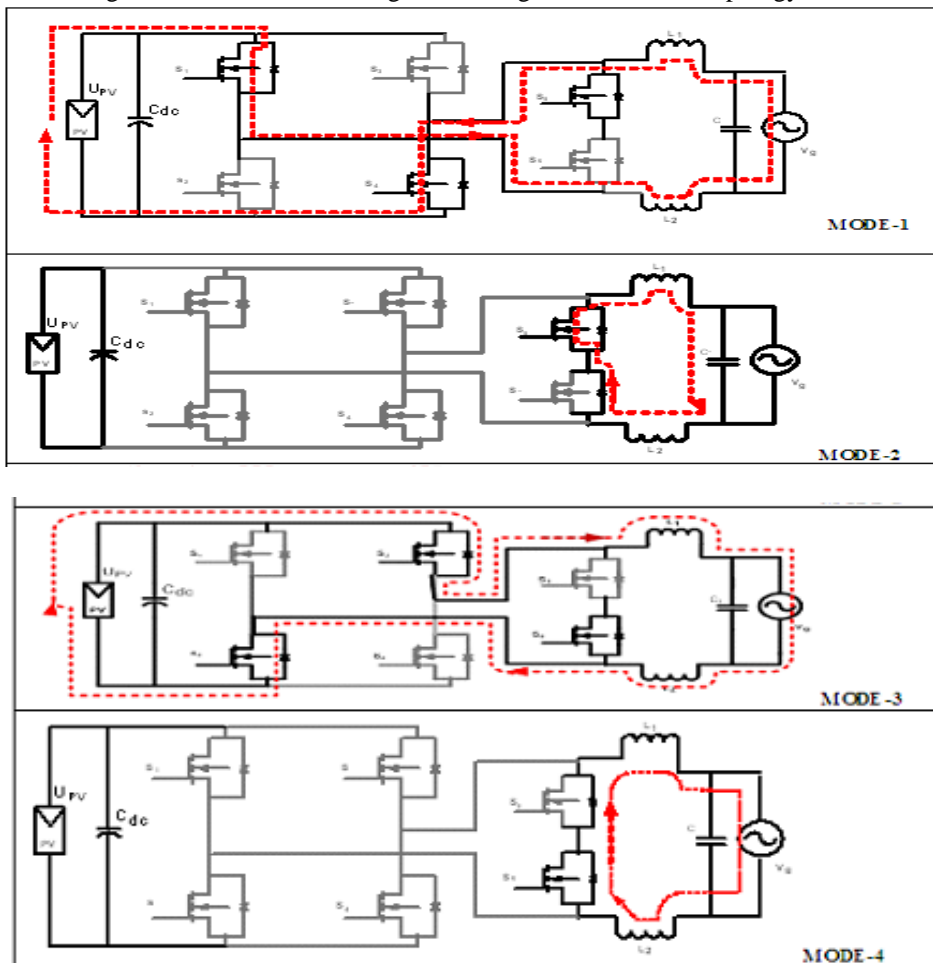
Fig: 6 Shows Different Operation Modes of HERIC Topology

Here it can be seen that there are six switches in this topology, even though gate pulses are given to three switches in the active mode, inductor current flows only through two switches, so on state losses are reduced to some extent as the conduction loss of one switch is reduced.

Figure two of the Fig: 6 shows the second mode of operation of the HERIC inverter, in the second mode, gate pulse is given only to switch S5. This is the first freewheeling mode, here the stored energy flows through switch S5 and the diode D6. In the third mode of operation gate pulses are given switches S2, S3 and S6. When switches S2, S3 and S5 are turned on the direction of flow of current reverses (anti- clock wise) as shown in the Fig: 6 and the output voltage will be –V. Finally in the fourth mode the (2nd freewheeling mode (dissipate) during this mode gate pulse is only given to 6th switch. Hence the energy stored freewheels through the switch S6 and diode D5.
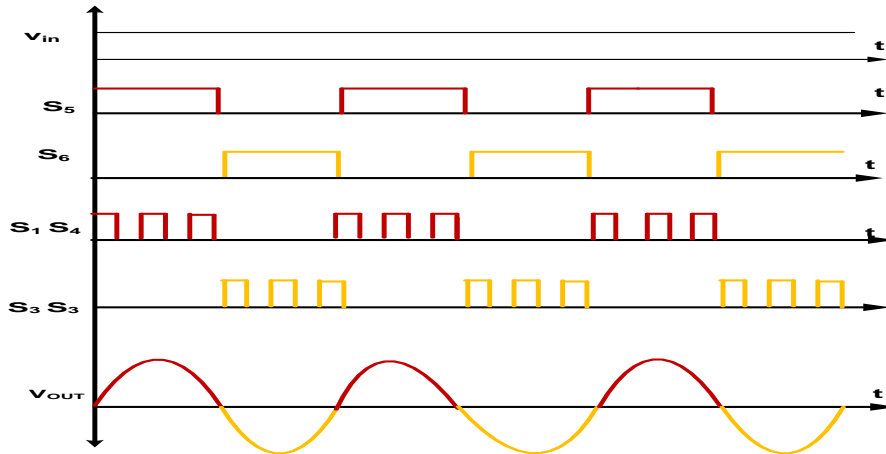

Fig:7 Switching waveforms of HERIC Inverter Topology

The above waveforms show the operation of HERIC topology; here we can see that during first active mode switches S_1, S4, S5are conducting.

IV. H6 Topology
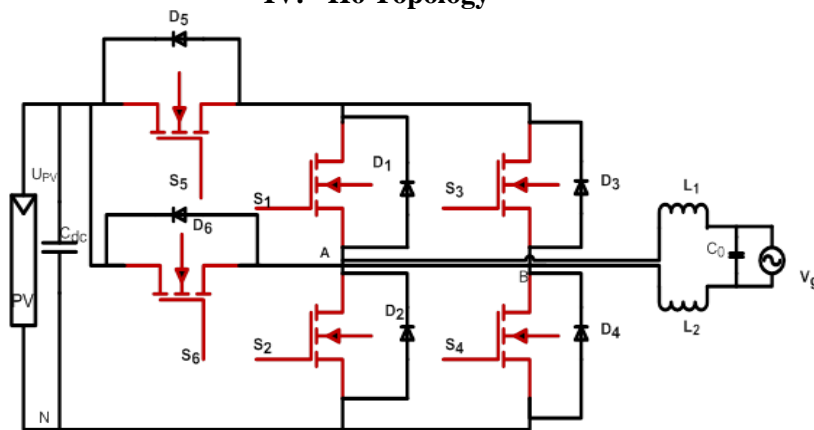
Fig: 8 Transformer-Less H6 Grid Tied Inverter Topology

The circuit structure of Transformer-less H6 grid tied inverter topology is shown in Fig: 8. From the aforementioned analysis, an extra switch *S6* is introduced into the H5 inverter topology between the positive terminal of the PV array and the terminal (B) to form a new current path. As a result, a novel H6 transformer-less full-bridge inverter topology is derived.

There are four operation modes, as shown in Fig: 9. In the first mode of operation switches S1,S4 and S5 are given gate pulse, this is the first active mode of operation a positive voltage V+ across the output end of the inverter is obtained. In the second mode of operation switch S1 is left on and all the other switches are kept off. This mode is the first freewheeling mode; the energy stored is freewheeled through diode D3 and switch S1.
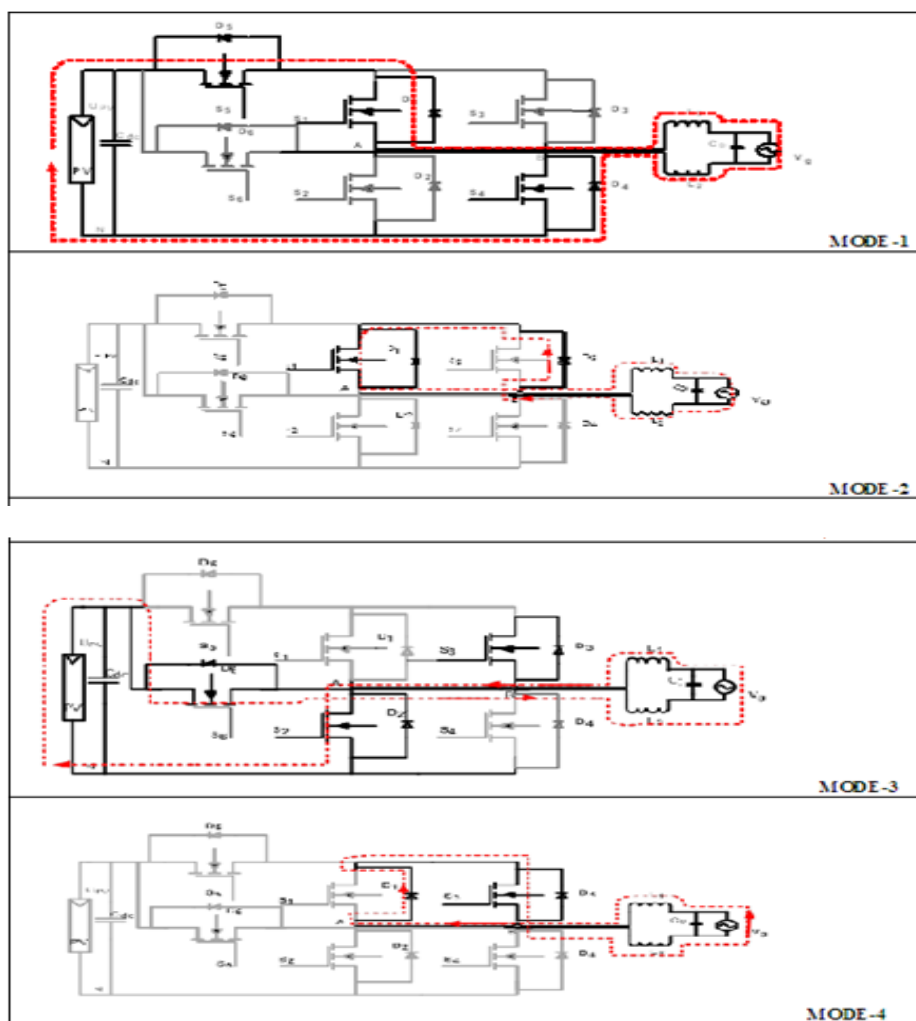
`Fig: 9 Shows Different Operation Modes of H6 Inverter Topology

In the third mode of operation switches S2, S3 and S6 are given gate pulse the other switches are turned OFF. The inductor current is flowing through *S*2 and *S*6. Although *S*3 is turned ON, there is no current flowing through it, and the switch *S*3 has no conduction loss in this mode.Nevertheless, in the H5 topology, the inductor current flows through *S*2*, S*3 and *S*5. Therefore, the conduction loss of proposed topology is less than that of H5 topology, this is the second active mode of operation, and a voltage (V-) across the output end of the inverter is obtained. In the last mode of operation switch S3 is left on and all the other switches are kept off. This mode is the second freewheeling mode; the energy stored is freewheeled through diode D1and switch S3.

Based on the above mentioned analysis, the PV array can be disconnected from the utility grid when the output voltage of the proposed H6 inverter is at zero voltage level and the leakage current path is cut off. The CM voltage of the proposed topology in each operation mode is equals to $0.5U_{PV}$, and it results in low leakage current characteristic of the proposed H6 topologies. The proposed H6 topology with unipolar SPWM method not only can achieve unity power factor, but also has the ability to control the phase shifts between voltage and current waveforms. The drive signal is in phase with the grid-tied current. Therefore, it has the capability of injecting or absorbing reactive power, which meets the demand for VDE-4105 standard.

V. Hardware Implementation
After all the studies and design process the prototype of the H6 grid tied inverter is developed. The layout of the prototype developed is as shown in the Fig: 10. The switches used in the inverter are MOSFETs having part number IRF540N. To generate gating pulses a 16 bit RENESAS microcontroller (RL78_R5f102aa) is used and TLP 250 is used as gate driver.

Fig: 10 Hardware implementation of H6 inverter

VI.   Experimental Results

Developed prototype is tested under various conditions. Main objective is to study the behavior of the inverter under various switching frequencies and duty cycle, and to check the amount of harmonics it injects into the system. To judge the quality of voltage generated by the inverter, a detailed harmonics analysis of voltage waveform is done. The following Fig: 11 show the Experimental setup of H6 inverter circuit for measurement of harmonics. The plot of harmonics for different duty cycle and switching frequencies are plotted.

Output Voltage $V_0 = V_{IN} \times Duty\ cycle$ (5.1)

$$Efficiency = \frac{V_{0\ practical}}{V_{0\ ideal}} \times 100 \ (5.2)$$

Fig: 11 Experimental setup of H6 inverter circuit for measurement of harmonics

Table I showing THD at different duty cycle for H6 topology

Sl no	Duty cycle	Input voltage	Output voltage	Efficiency	Switching Frequency	THD
1	10 %	15 V	1.2	80%	1Khz	19.0
2	20 %	15V	2.4	80%	1Khz	19.1
3	30 %	15V	3.6	80%	1Khz	19.2
4	40 %	15V	4.8	80%	1Khz	19.3
5	50 %	15V	6.2	82.6%	1Khz	19.4
6	60 %	15V	7.4	81.6%	1Khz	19.6
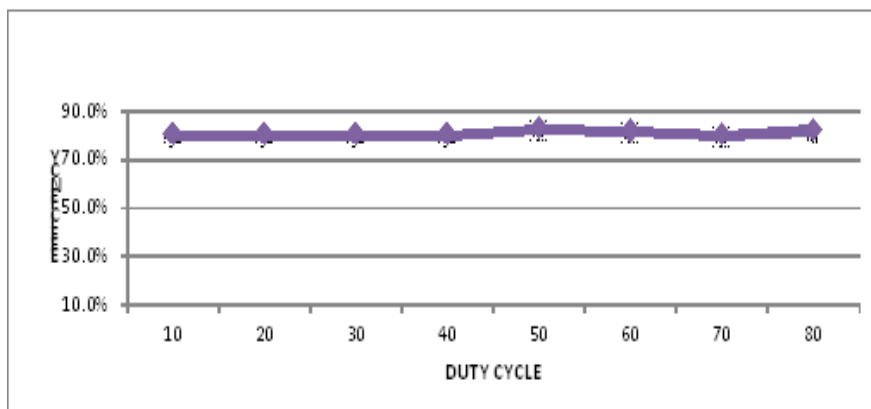
Fig: 12Graph showing duty cycle v/s. efficiency
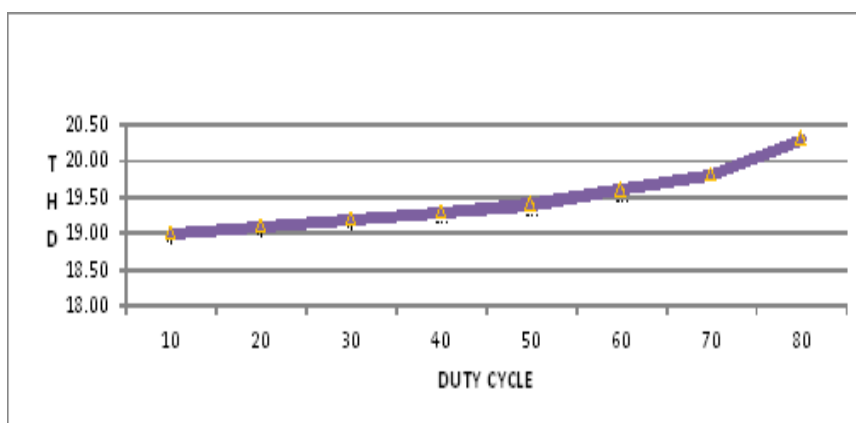
Fig: 13 Graph showing duty cycle v/s THD

Table II showing harmonics at different frequencies for H6 topology

S l n o	Switching frequency	Input voltage	Output voltage	Duty cycle	3rd order harmonics	5rd order harmonics	7rd order harmonics	9rd order harmonics	11rd order harmonics	%THD	%losses
1	500 Hz	15V	7.6	60%	17%	5%	4%	2%	1%	19.6	15.5
2	1KHz	15V	7.5	60%	15%	6%	5%	5%	2%	19.4	16.6
3	2khz	15V	7.4	60%	12%	11%	4%	5%	2%	19.3	17.7
4	5khz	15V	7.2	60%	7%	12%	7%	7%	2%	19.1	20.0
5	10khz	15V	7.1	60%	5%	4%	17%	7%	2%	19.0	21.1
6	15khz	15V	7.0	60%	2%	1%	4%	17%	4%	18.6	22.2
7	20khz	15V	6.9	60%	1%	1%	3%	5%	17%	18.6	23.3
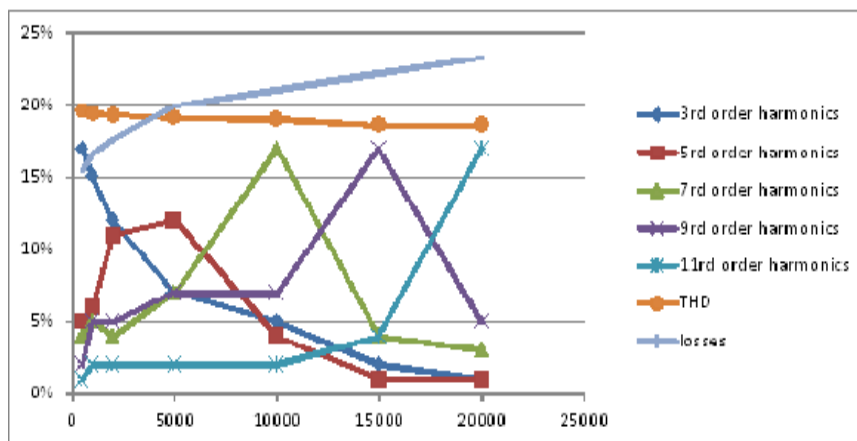
Fig: 14 showing comparison betwween different harmonicsat different switching frequencies

VII. Conclusion

The increased penetration of renewable energy sources into the power grid will help ease our dependence on fossil fuel-based energy sources. This paper is focused on the design of the PV-grid connected inverter power stage that supports the proposed PV system. In this project various grid tied inverters were studied and a H6 grid tied inverter is modeled. The behavior of grid tied inverter circuit is studied under different duty cycle and switching frequency.A H6 inverter is designed and to study the various properties of the converter the prototype of rating V_o= 12V, V_{in}=15V and f_s=10000 Hz was developed.It has been found that with the increase in the switching frequency, the magnitude of higher order harmonics increases and that of lower order harmonics reduces. The size and cost of filter reduces as the order of harmonics increases, but with high switching frequency, switching losses in the inverter increases, so a tradeoff must be done between the switching frequencies (efficiency) and the cost of filter the system.

REFERENCE

[1]   S. B. Kjaer, J. K. Pederson, and F. Blaabjerg, "A review of single-phase grid-connected inverters for photovoltaic modules," IEEE Trans. Ind. Appl., vol. 41, no. 5, pp. 1292–1306, Sep/Oct. 2005.
[2]   F. Blaabjerg, Z. Chen, and S. B. Kjaer, "Power electronics as efficient interface in dispersed power generation systems," IEEE Trans. Power Electron., vol. 19, no. 5, pp. 1184–1194, Sep. 2004.
[3]   B. Sahan, A. N. Vergara, N. Henze, A. Engler, and P. Zacharias, "A single stage Module integrated converter based on a low-power current source inverter," IEEE Trans. Ind. Electron., vol. 55, no. 7, pp. 2602–2609, Jul. 2008.
[4]   M. Calais, J. Myrzik, T. Spooner, and V. G. Agelidis, "Inverters for single phase grid connected photovoltaic systems—An overview," in Proc. IEEE PESC, 2002, vol. 2, pp. 1995–2000
[5]   F. Blaabjerg, Z. Chen, and S. B. Kjaer, "Power electronics as efficient interface in dispersed power generation systems," IEEE Trans. Power Electron., vol. 19, no. 5, pp. 1184–1194, Sep. 2004.
[6]   Q. Li and P. Wolfs, "A review of the single phase photovoltaic module integrated converter topologies with three different dc link configuration," IEEE Trans. Power Electron., vol. 23, no. 3, pp. 1320–1333, May 2008.
[7]   O. Lopez, F. D. Freijedo, A. G. Yepes, P. Fernandez-Comesana, J.Malvar, R. Teodorescu, and J. Doval-Gandoy, "Eliminating ground current in a transformer less photovoltaic application," IEEE Trans. Energy Convers., vol. 25, no. 1, pp. 140–147, Mar. 2010.
[8]   R. Gonzalez, J. Lopez, P. Sanchis, and L. Marroyo, "Transformer less inverter for single-phase photovoltaic systems," IEEE Trans. Power Electron., vol. 22, no. 2, pp. 693–697, Mar. 2007.
[9]   H. Xiao and S. Xie, "Leakage current analytical model and application in single-phase transformer less photovoltaic grid-connected inverter," IEEE Trans. Electromagn.Compat., vol. 52, no. 4, pp. 902–913, Nov. 2010.
[10] VDE-AR-N 4105: Power Generation Systems Connected to the Low- Voltage Distribution Network—Technical Minimum Requirements For the Connection to and Parallel Operation with Low-Voltage Distribution Networks, DIN_VDE Normo, 2011–08.
[11] B. Yang, W. Li, Y. Gu, W. Cui, and X. He, "Improved transformer less inverter with   common-mode leakage current elimination for a photovoltaic grid-connected power system," IEEE Trans. Power Electron., vol. 27, no. 2, pp. 752–762, Feb. 2012.
[12] R.Gonzalez, E. Gubia, J. Lopez, and L.Marroyo, "Transformer less single phase multilevel-based photovoltaic inverter," IEEE Trans. Ind. Electron., vol. 55, no. 7, pp. 2694–2702, Jul. 2008.
[13] H. Xiao and S. Xie, "Transformer less split-inductor neutral point clamped three-level PV grid-connected inverter," IEEE Trans. Power Electron., vol. 27, no. 4, pp. 1799–1808, Apr. 2012.
[14] L.Zhang, K. Sun, L. Feng, H.Wu, and Y. Xing, "A family of neutral point clamped full-bridge topologies for transformer less photovoltaic grid-tied inverters," IEEE Trans. Power Electron., vol. 28, no. 2, pp. 730–739, Feb. 2012.
[15] Y. Gu,W. Li,Y. Zhao, B.Yang, C. Li, and X. He, "Transformer less inverter with virtual DC bus concept for cost-effective grid-connected PV power systems," IEEE Trans. Power Electron., vol. 28, no. 2, pp. 793–805, Feb. 2012.

Significancy Test For The Control Parameters Considered In Weld Bead Geometry Optimization For Gas Metal Arc Welding Process Using Taguchi Method And Anova Technique

Arka Sen [1], Dr. Sudip Mukherjee [2]

[1]*Assistant Professor, Department of Mechanical Engineering, Surendra Institute of Engineering & Management, Siliguri ,West Bengal, India*
[2]*Professor, Department of Mechanical Engineering, Jalpaiguri Government Engineering College, Jalpaiguri, West Bengal, India*

Abstract: *Here in this work, an attempt has been made to find the interaction between control parameters and weld bead geometry for fillet welding in mild steel specimen using Gas Metal Arc Welding process. Accordingly control parameters have been adjusted to find the optimal bead geometry. Initially the equations involving control parameters and bead geometry were developed by multiple regression analysis method. The ANOVA technique is then employed to calculate the significant difference between the means of the control parameters ,Also this justifies the range of the control parameters considered for the experiment.*
Keywords: *ANOVA, GMAW process, Bead width, Left leg length, Re-inforcement height, Right leg length.*

I. Introduction

Nowadays Gas Metal Arc welding process (GMAW) has been widely used as a welding technique throughout the industrial world. GMAW uses a welding torch, an electric power source, shielding gas & a wire pool with wire drive control. GMAW process can be used to weld thicker metal plates with high productivity. Shielding gas is used to protect the weld pool from oxidation. The shielding gas used is either inert gas or carbon dioxide.

GMAW process is done in butt joints as well as fillet joints. The quality of weld is determined by the weld bead geometry characteristics (physical parameters); i.e., the weld bead width, weld bead penetration, weld re-inforcement height, weld left leg length and weld right leg length. This weld bead geometry characteristics is a function of input variables (control parameters) which are welding current, welding voltage, welding speed, wire tip distance, weld joint position, wire diameter, shielding gas composition, gas flow rate, material composition and material thickness. These control parameters affect the quality of the weld. Here for simplification the most influencing parameters welding current, welding voltage and welding speed are considered. Using ANOVA technique, the comparison of means of the control parameters are done. This technique is widely used nowadays to determine the significant difference of the means of the control parameters considered for the experiment. Also the calculation of F-ratio, the percentage contribution of control parameters on the effect of weld bead and the error calculation of the experiment are done in this study.

II. Experimental Work

The experimental work for predicting the relationship between control parameters & the weld bead geometry is done systematically by a defined process. Gas metal arc welding (GMAW) was conducted on mild steel plates. Three most important control parameters are identified which mostly determine the weld bead profile. These parameters are welding current, welding voltage & the welding speed. The operating range of each of the parameters is taken in accordance with the normal operating range for such kind of operation. The assigned control parameters are listed in the Table. 1

Table 1 : Control factors and their levels

PARAMETERS	SYMBOL	LEVEL		
		LOW	MIDDLE	HIGH
WELDING CURRENT (Amp)	I	160	220	280
WELDING VOLTAGE (Volt)	V	20	22.5	27
WELDING SPEED (mm/sec)	S	1.97	3.57	5.17

The mechanical and chemical properties of the base metal are given below.

Table 2: Mechanical properties of base metal

Ultimate Tensile Strength, Kpa	439885.514464
Yield Strength, Kpa	370248.465936
Elongation	15.00%
Rockwell Hardness	B71

Table 3: Chemical properties of base metal

Material	% Composition
Iron (Fe)	98.81 - 99.26%
Carbon (C)	0.18%
Manganese (Mn)	0.6 - 0.9%
Phosphorus (P)	0.04% max
Sulphur (S)	0.05% max

The weld bead geometry is shown in Fig 1.
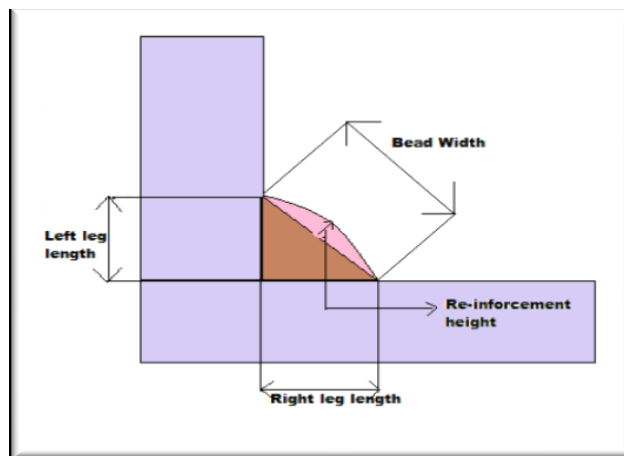
Fig 1. Weld bead geometry

III. Experimental Data Analysis

From the Taguchi design of experiment, a conclusion is made that for three number of independent experimental parameters, i.e, welding current, welding voltage & welding speed and three different levels of each parameter, i.e. low , mid & high, there has to be nine different observation sets.

Table 4: Measured Experimental Data as per Taguchi Design of Experiment

Experiment No	Welding Current (A)	Welding Voltage (V)	Welding Speed (mm/sec)	Bead Width (mm)	Re-inforcement Height (mm)	Left Leg length (mm)	Right leg length (mm)
1	160	21	1.97	10.2	0.5	7.4	7.4
2	180	20	2.58	10.1	0.7	6.3	5.8
3	190	21	2.30	10.4	0.9	8.6	8.1
4	200	23	2.88	11.1	1.2	8.0	8.4
5	210	24	1.97	10.1	1.5	7.1	7.2
6	220	22	2.02	12.1	1.5	9.0	8.6
7	240	22	2.72	10.5	0.9	7.1	8.4
8	250	26	4.28	11.0	1.3	7.6	7.2
9	280	27	5.17	12.5	1.1	9.1	8.6

From the experimental observations, multiple regression analysis is done to find the relationship between control parameters & physical parameters. The equations obtained are as follows:

Bead Width (BW) $= 0.0123 + 0.0095 *I + 0.35005 * V + 0.00981 * S + 0.00092764* I^2 + 0.000561 * V^2 - 3.8726 * S^2 - 0.4 *I * V + 0.01329 *I*S +0.035 *V*S$--(1)

Re-inforcement height (RH) = -0.0035197 + 0.003848444 *I + 0.0017637334 *V +0.077151088 *S + 0.000048641* I^2 + 0.0000545898 *V^2 – 14.186 * S^2 + 0.0283 *I*V -0.000778671* I* S + 0.026906535 *V*S
--(2)

Left leg length (LLL) = -0.044638867 + 0.281959034 * I + 2.840262884* V – 5.583572 * S + 0.00001485 * I^2 + 0.001725776 * V^2 + 527.541 * S^2 -14.07151286* I * V + 12.19315 *I*S+ 0.039817247 *V* S
--(3)

Right leg length (RLL) = -0.0154 + 0.0900 * I + 0.8077 * V + 1.7139* S - 0.0002 * I^2 – 0.0004 * V^2 - 322.5063 * S^2 - 3.3705 * I * V + 0.0034 * I* S -0.0088 * V* S--(4)

IV. Anova Calculation And Result

In performing the ANOVA test, it is assumed that the means of different samples are equal. To do that, the différences of the sample means are compared with the variability within the sample observations. The test statistic is the ratio between the sample variation (MSB) and within the sample variation (MSW). If this ratio is close to 1, there is evidence that the means are equal which indicates that there is no difference between the sample means of the physical parameters. If the ratio F-ratio (calculated) > F-ratio (critical) then the null hypothesis is rejected which indicates that there is a significant difference between the means of the four physical parameters.

Table 5: Anova Data Table

WELDING CURRENT(KA)			WELDING VOLTAGE(KV)			WELDING SPEED (MM/SEC)		
A	B	C						
160	160	160	20	20	20	1.97	1.97	1.97
160	220	220	20	22.5	22.5	1.97	3.57	3.57
160	280	280	20	27	27	1.97	5.17	5.17
220	160	220	22.5	20	22.5	3.57	1.97	3.57
220	220	280	22.5	22.5	27	3.57	3.57	5.17
220	280	160	22.5	27	20	3.57	5.17	1.97
280	160	280	27	20	27	5.17	1.97	5.17
280	220	160	27	22.5	20	5.17	3.57	1.97
280	280	220	27	27	22.5	5.17	5.17	3.57

ANOVA calculation requires that a null hypothesis is to be taken which represents that there is no significant difference among the means of the four physical parameters. Let us consider, null Hypothesis $H_0 = U_1$ which represents no significant difference between the means of the four physical parameters for different possible combinations of control parameters

Table 6 : Anova calculation table for welding current   Table 7: Anova calculation table for welding voltage

Level 1	Level 2	Level 3	Treatment Mean	Estimated Effects
160	160	160	160	-60
160	220	220	200	-20
160	280	280	240	20
220	160	220	200	-20
220	220	280	240	20
220	280	160	220	0
280	160	280	240	20
280	220	160	220	0
280	280	220	260	40

Level 1	Level 2	Level 3	Treatment Mean	Estimated Effects
20	20	20	20	-3.166
20	22.5	22.5	21.66666667	-1.499333333
20	27	27	24.66666667	1.500666667
22.5	20	22.5	21.66666667	-1.499333333
22.5	22.5	27	24	0.834
22.5	27	22	23.83333333	0.667333333
27	20	27	24.66666667	1.500666667
27	22.5	20	23.16666667	0.000666667
27	27	22.5	25.5	2.334

Table 8: Anova calculation table for welding speed

Level 1	Level 2	Level 3	Treatment Mean	Estimated Effects
1.97	1.97	1.97	1.97	-1.6
1.97	3.57	3.57	3.036666667	-0.533333333
1.97	5.17	5.17	4.103333333	0.533333333
3.57	1.97	3.57	3.036666667	-0.533333333
3.57	3.57	5.17	4.103333333	0.533333333
3.57	5.17	1.97	3.57	0
5.17	1.97	5.17	4.103333333	0.533333333
5.17	3.57	1.97	3.57	0
5.17	5.17	3.57	4.636666667	1.066666667

Referring Table: 6 at 1% significant level F-ratio 2, 24 (critical) = 5.6136 (From table of Fisher`s distribution) & at 5% significant level F-ratio 2, 24 (critical) = 3.4028 (from table of Fisher`s distribution). Therefore for both 1% and 5% significant level F-ratio (calculated) is greater than F-ratio(critical) ; hence the null hypothesis is rejected which indicates that there is a significant difference among the means of the four physical parameters. The critical region for welding current is less than 3.4 and greater than 5.61.   F- Ratio (calculated)   is 6 which fall in the critical region. Thus it is concluded that, by varying the range of current from 160 A to 280 A for different possible combinations, there has been a significant difference in the physical parameter measurement.

Referring Table: 7 at 1% significant level F-Ratio 2, 24 (critical) = 5.6136 at 5% significant level F-ratio 2, 24 (critical) = 3.4028. Therefore for both 1% and 5% significant level F-ratio (calculated) > F-ratio (critical); hence the null hypothesis is rejected which indicated that there is a significant difference between the means of the three different levels of voltage. The critical region for welding voltage is less than 3.4 and greater than 5.61 . F- Ratio (calculated)   is 5.99 which fall in the critical region. Thus it is concluded that, by varying the range of voltage from 20 V to 27 V, there has been a significant effect in the result.

Referring Table: 8 at 1% significant level F-ratio 2, 24 (critical) = 5.6136 & at 5% significant level F-ratio 2, 24 (critical) = 3.4028. Therefore for both 1% and 5% significant level F-ratio (calculated) > F-ratio (critical); hence the null hypothesis is rejected which indicated that there is a significant difference between the means of the physical parameters. The critical region for welding voltage is less than 3.4 and greater than 5.61. F- Ratio (calculated)   is 5.9960 which fall in the critical region. Thus it is concluded that, by varying the range of voltage from 20 V to 27 V, for different possible combinations, there has been a significant difference in the physical parameter measurement.

Table 9: Anova result for welding current

CAUSE OF VARIATION	DEGREES OF FREEDOM(df)	SUM OF SQUARES (SS)	MEAN OF SQUARES (MS)	F-RATIO (calculated	F-RATIO (CRITICAL) at 1% significant level	F-RATIO (CRITICAL) at 5% significant level
Treatment	2	21600	10800	6	5.6136	3.4028
Residual	24	43200	1800			
Total	26	64800				

Table 10: Anova result for welding voltage

CAUSE OF VARIATION	DEGREES OF FREEDOM(df)	SUM OF SQUARES (SS)	MEAN OF SQUARES (MS)	F-RATIO (calculated	F-RATIO (CRITICAL) at 1% significant level	F-RATIO (CRITICAL) at 5% significant level
Treatment	2	75.48	37.74	5.998410596	5.6136	3.4028
Residual	24	151	6.291666667			
Total	26	226.48				

Table 11: Anova result for welding speed

CAUSE OF VARIATION	DEGREES OF FREEDOM(df)	SUM OF SQUARES (SS)	MEAN OF SQUARES (MS)	F-RATIO (calculated	F-RATIO (CRITICAL) at 1% significant level	F-RATIO (CRITICAL) at 5% significant level
Treatment	2	15.35	7.675	5.99609375	5.6136	3.4028
Residual	24	30.72	1.28			
Total	26	46.07				

The percentage contribution of the control parameters to affect changes in physical parameters is found to be as follows:

Table 12: Percentage contribution of control parameters

CONTROL PARAMETERS	TOTAL DEGREES OF FREEDOM	TOTAL SUM OF SQUARES BETWEEN TREATMENT GROUPS	% CONTRIBUTION
Welding current	64800	21600	33.33333333
Welding voltage	226.48	75.48	33.32744613
Welding speed	46.07	15.35	33.3188626

Total Error (%) in experiment = 100 - sum of % contribution of control parameters
$$= 100 - 99.9796 = 0.02035\%$$

V. Conclusion

It can be concluded that the control parameters have nearly equal contributions on the effect of the physical parameters with .02% of error, which is very less.

Also from the ANOVA, it can be concluded that the calculated F-ratio falls in the critical region and there has been a significant difference between the means of the control parameters considered for the experiment which justifies the range of control parameters considered.

REFERENCES

Journal papers:
[1]   A New Approach for Predicting and Optimizing Weld Bead Geometry in GMAW by Farhad Kolahan, Mehdi Heidari, World Academy of Science, Engineering and Technology 2:2 2010
[2]   Optimization of GMAW process parameters using Particle Swarm Optimization by Sreeraj , T Kannan , Subhashis Maji / Mechanica confab.
[3]   Achieve to desired weld bead geometry for the vessel fillet joints in mobile robotic welding by M. Golestani Sehat, Kh. Farhangdoost Mechanical Engineering Department Ferdowsi University, mashhad, Iran; Published inTehran International Congress on Manufacturing Engineering (TICME2005) December 12-15, 2005, Tehran,Iran.
[4]   Effect of Welding Parameters on Dilution and Weld Bead Geometry in Cladding by M.Nouri, A.Abdollah-zadehy and F.Malek Department of Materials Engineering, Tarbiat Modares University; J. Mater. Sci. Technol., Vol.23 No.6, 2007.
[5]   Optimization of weld bead geometry in TIG welding process using grey relation analysis and taguchi method by Ugur Esme, Melih Bayramoglu, Yugut Kazancoglu, Sueda Ozgun: UDK 621.791.05 Original Scientific Article : ISSN 1580-2949, MTAEC9, 43(3)143(2009).

Ensuring Know-how Protection in Production

Günther Schuh[1], Matthias Kreimeier[2]

[1]*Department of Technology Management, Fraunhofer Institute for Production Technology, Aachen, Germany*
[2]*Department of Technology Management, Fraunhofer Institute for Production Technology, Aachen, Germany*

Aabstract: *While many different product protection measures have been developed and established in recent years, there is still a great risk posed by the leakage of knowledge in production. These risks are often downplayed by companies, although they directly relate to their own production and engineering know-how. The various company-specific protection measures in production span a wide range, and they can be applied both to production relocation (e.g. to China) and to existing facilities. A systematic approach for identifying critical damage scenarios, and the methodically supported development and selection of individual protection measures are required for effective protection of critical company know-how in production.*

Keywords: *know-how protection measures, outsourcing, product piracy, production processes, risk assessment.*

I. Motivation and Challenges

The damage to the Gkerman mechanical engineering sector caused by product piracy has been growing steadily in recent years, and reached approximately 7.9 billion Euros in 2013[[1]]. According to a study by the VDMA (association of the German mechanical engineering industry) conducted with companies in Germany, more than 71 percent of the participants are affected by product and/ or brand piracy. Nowadays, not only designs, but also components and entire machinesare being plagiarized. The majority of plagiarism originates from the People's Republic of China (72%), followed by Germany (23%), Turkey (20%), and India (19%). Overall, the percentage of plagiarism from other countries has also been increasing [[1]].

Despite these developments and the high number of plagiarism cases from countries such as India and China, the trend to outsource production to these countries continues to develop [[2]]. Although the "outsourcing hype" has decreased in recent years, the absolute number of outsourced production continues to rise further. The main motive behind this remains the reduction in personnel costs. Therefore, the companies that seek "price leadership" are primarily those who outsource their production. Additionally, companies are increasingly tending to outsource their non-core production in order to focus on core products and components. Of course, the rapid growth of the market in China, and the requirement of having local production also play a crucial role. In addition to the electrical and textile industry, companies in the automotive and mechanical engineering industries continue to outsource their production capacities [[2]]. Technological and organizational measures can be taken to protect know-how while establishing the production and onsite throughout the production process itself. Effective protection is particularly necessary and important in cases where specific technological knowledge is necessary for production.

Many protective measures against product piracy have been developed in the past, and have already become standard (e.g. special product labelling). Similarly, methods have already been developed for the evaluation and selection of protective measures. The Product Piracy Conflict (PPC) matrix is an example [[3]]. However, the protection of a company's own production know-how has not receivedsufficient attention yet. With a systematic approach to assess possible damage scenarios and to identify and develop effective protection measures, the risk of a leakage of knowledge can be sustainably minimized [[4], [5], [6]].

II. Methodology For Establishing Knowledge-Protected Production

The procedure for developing effective knowledge protection in production includes three essential elements. After the identification of critical damage scenarios, appropriate safeguards should be researched and/ or developed. A reassessment of damage scenarios while taking the developed protective measures into consideration then forms the basis for establishing a plan of action and the development of further protective measures. The implementation and periodic review of the effectiveness of protective measures can then be carried out. Figure 1shows the entire procedure with further sub-steps in accordance with the process proposed

by Marxen et al. forconducting a piracy risk and measures analysis (PRMA) to systematically identify potential hazards caused by product piracy [[7]].
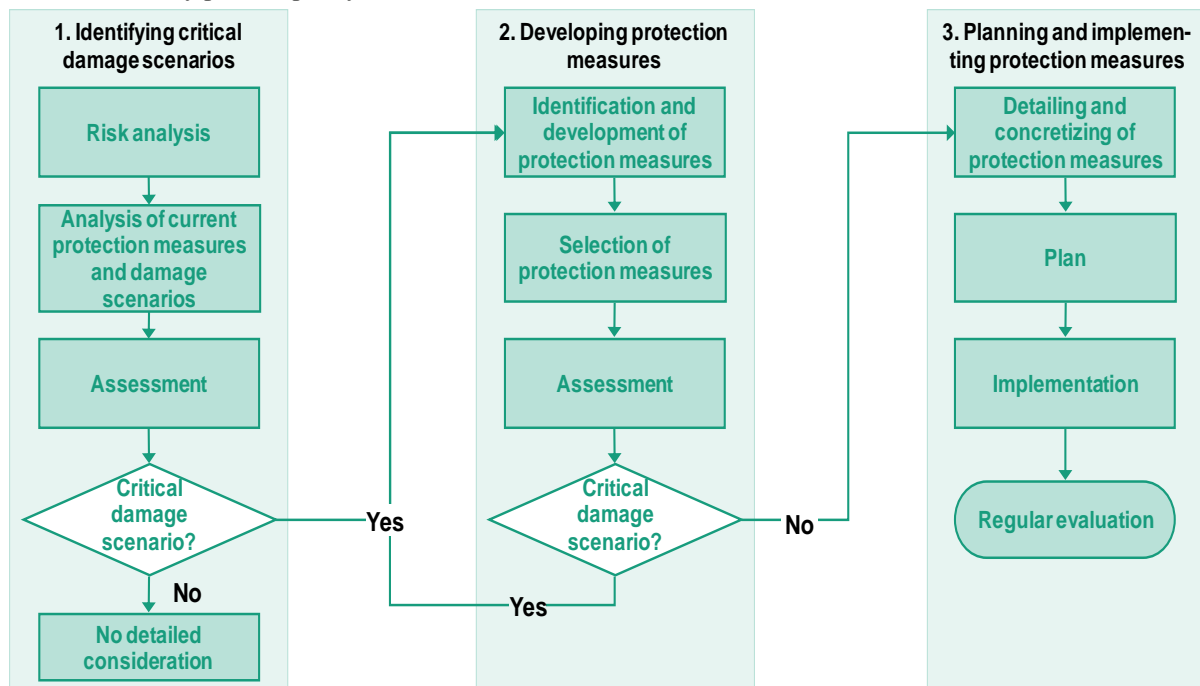

Figure 1: Methodology for developing a know-how protection concept in production

III. Identifying Critical Damage Scenarios

A risk analysis of the entire product production process serves as the starting point for identifying possible critical damage scenarios. To this extent, the individual process steps must be identified, starting with the procurement of required production goods such as raw materials. Existing process documentation can be of help here. It is important to record internal and external information flows, as well as dependencies and interactions between individual stages. Similarly, the machinery, equipment, and tools required for production should also be considered. All relevant holders know-howsuch as employees, documents, and software such as machine programs must be identified.

Based on the production process, critical aspects which are relevant to product and knowledge protection can be identified in the next step along with their corresponding risk areas. Then, damage scenarios which could potentially lead to a know-how leakage are sought within each area, andthe possible causes and reasons for the loss of knowledge should be identified. The aim of this analysis is to collect all potential and hypothetical damage scenarios, also the unlikely ones.

In order to cover damage scenarios that are not directly obvious or known, the method of "Six Thinking Hats" [[8]] can be applied. This creative technique is used as an instrument to take different positions and viewpoints on an issue and therefore the simulation of various approaches. In this case, the method can be used to switch one's own point of view. It is possible to gain several points of view for detecting damage scenarios through targeted questioning techniques (e.g. "Imagine that you supplyto plant xy. Which information do you receive about your customers and their products?"). Similarly, the know-how protection measures and activities which are currently implemented should alsobe identified and assigned to the risk categories and damage scenarios.

Subsequently, the identified loss scenarios must be evaluated. The probability that a damage scenario occurs is assessed on a points scale (refer to [[7]]). Also, the significance of the risk must be evaluated on a similar scale (e.g. 1 point = no expected consequences, whereas 5 points = very serious consequences expected). The probability of occurrence is then multiplied by the risk significance, as done by Marxen et al., to generate a risk ratio which serves as an indicator of the know-how leakage risk [[7]]. To evaluate whether appropriate measures should be developed for a particular damage scenario, it is necessary to establish critical values for the probability of occurrence, the risk significance, and the risk ratio. Plotting this evaluation in a portfolio reveals the scenarios for which protection measures must be developed (Figure 2, shaded area).
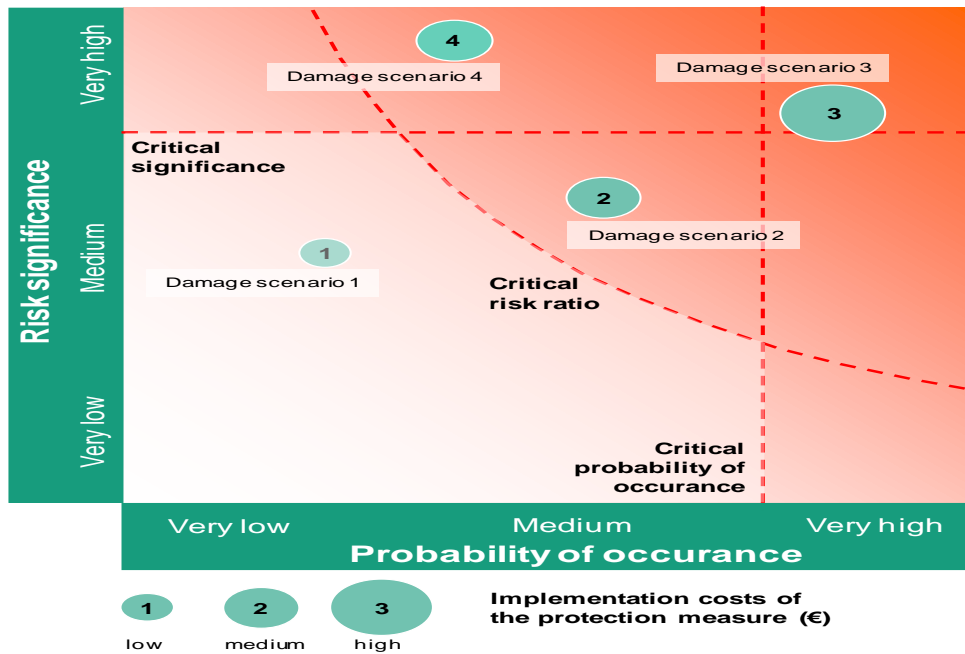
Figure 2: Identification and evaluation of critical damage scenarios

IV. Developing Protection Measures

Individual measures should be identified for each critical damage scenario in order to develop a comprehensive approach for securing production knowledge. Measures which are principally possible to implement in specific cases and scenarios are selected from a catalog of already known measures. Furthermore, it must be checked whether the development of new safety measures for each damage scenario makes sense.

In order to identify appropriate prevention measures, the applicability of established standard measures will be examined as a first step. Additionally, an evaluation of the possible effectiveness of the measures for the specific company will be performed. The measures' applicability is to be evaluated either as "meaningful", "possibly meaningful" or "not meaningful".An overview of all meaningful measures will therefore be available for the company. For example, a wide range of standard protection measures involves the encryption or securing of data related to machine control systems [[9], [10]]. However, small- and medium-sized companies often have older machines with no Windows-based machine control, rendering this measure ineffective.

Creative techniques, such as the TRIZ method [[11]], used throughout facilitated workshops with interdisciplinary participants from a company have been deemed to be effective for the development of new protective measures or the modification of existing ones. Further support for the development of individual protection measures poses the following central questions:

- Which protective measures come first to mind?
  - Raising awareness
  - Making plagiarized products unattractive
  - Complicating marketing
  - Managing human resources
  - Making access to production processes less transparent
  - Limiting access to critical company know-how
- Which conditions must be met?
- With which mechanisms/ other measures can the idea be combined?
- Which challenges are associated with the idea? Which consequences would the protection measure have (e.g. effects on material properties or the overall process)?
- What are the advantages and disadvantages of the measure?

After this step, a variety of potentially applicable measures can be developed. This is followed by a second step which involves a systematic selection of measures which have the highest benefit for the company in question.The protection potential, implementation costs, and the impact on existing production processes will be evaluated. This supports a need-based selection and prioritization of the individual protective measures based on the company's restrictions.
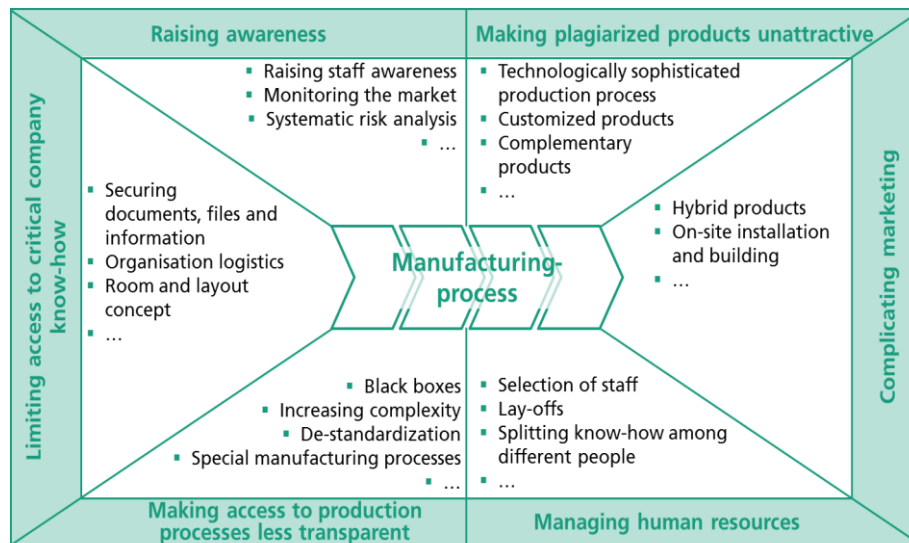
Figure 3: Know-how protection concept with six basic factors

The critical damage scenarios are subsequently evaluated based on the selected protection measures once again with regard to risk significance and probability of occurrence. This should be done through a detailed discussion of the individual damage scenarios in a workshop with participants from different departments and hierarchical levels of the company. Can the selected measures reduce the risk and significance of the damage scenario so that it is no longer in the critical region of the portfolio (seeFigure 2), or are additional measures needed? This question should be answered at the workshop. The protection potential and the effect of the selected measuresare therefore defined for the respective critical damage scenario.

If the selected measures ensure sufficient protection for all critical potential damage scenarios, the planning and implementation of the measures can be done in the next phase. If the reevaluation reveals further critical damage scenarios, another iteration of the second phase "developing protection measures" (seeFigure 1) is necessary.

A sustainable concept for knowledge protection in production consists of a systematic combination of different individual measures [[12]]. To maximize the protection potential, measures with different protection functions should be implemented. An overview of the six components of a protection concept and exemplary protective measures are shown inFigure 3.

The particularly critical categories for know-how protection in production form the following three areas:

- Limiting access to critical company know-how
- Making access to production processes less transparent
- Managing human resources

The first category includes individual protection measures which limit the access to critical company know-how. An example of such a measure is an adapted room concept. The development of a special room concept for production allows the separation of sensitive process steps or keeping specific process parameters hidden from the machine operators. One possible form of implementation is the encapsulation of machine components, which can only be accessed by authorized employees.

For the second category, measures that decrease transparency or the use of de-standardized components serve to decrease the risk of leaking critical production information. The actions associated with an increase in process complexity include, for example, the integration of unneeded components/ supplies in various production processes, or the performance of unnecessary process steps. The use of de-standardized components in production leads to significantlyimpeding unauthorized replica. For a large part of the potential plagiarists, the de-standardization of components is not obvious at first glance. A replica of the products with standard components inevitably leads to a significant reduction in functionality or the lifetime of the product. The complicated procurement of de-standardized components discourages a lot of potential plagiarists [[12]].

The third category of know-how protection relates to human resources management. The aim is to scrutinize employees deployed in critical areas of production. If it is found that an employee has connections to competitors, or an above average tendency to change jobs, then particular attention needs to be paid while selecting the tasks to be assigned to this employee, and his/ her setting. In addition, access to critical areas of production should only be granted to employees with long years of service.

V. Planning and Implementing Protection Measures

After selecting all measures for the development of a comprehensive protection concept, the third phase consists of supporting the planning and implementation of the measures. The first step is to detail and concretize the selected protection measures. This includes appointing responsible employees, identifying development costs, and coordinating with potential suppliers. Asensible and responsibledealing with suppliers is of particular importance in the implementation of protection measures.

It must be ensured that business partners will not transmit any critical documents or information [[13], [14]]. Communication rules for disclosingcompany information to third parties form an important part of the protection strategy. These rules should be set and agreed upon in advance with all departments. The unintentional transmission of sensitive information to external business partners can therefore prevented. Additionally, the procurement of components and modules which should be protected should not be done through a systems supplier, but rather through several independent suppliers.The knowledge of the individual components of the protected product is therefore divided, and no single vendor has all of the information concerning the product.

If the measures are worked out in detail, and the necessary implementation efforts are approved, each activity can be converted into an action plan. In addition to assigning the responsible employees, a time planning of the different activities should be carried out. Once this planning step is completed, the implementation of the protective measures should be started.

It is very important to periodically review of the protection concept including all its components. Companies currently operate in a highly dynamic competitive environment, and are confronted with ever-changing factors. A static protection concept therefore cannot guarantee long-term protection. Continuously updating the risk analysis and reviewing the identified damage scenarios are therefore a prerequisite for ensuring sustainable know-how protection [[12]].

VI. Conclusion

Sustainable know-how protection in production is especially important if the uniqueness of the product depends on manufacturing skills and unique features [[15]]. A systematic approach is essential to identify critical damage scenarios. Technological and organizational protection measures can be developed through a creative, methodically supported process. Effective protection is provided by measures individually developed for each damage scenario, where already existing standard measures forpiracy protection can be used, as well their further development to suit the individual needs of the company.

REFERENCES

[1]   VDMA workinggroup "Produkt- und Know-how-Schutz": VDMA Studie Produktpiraterie, 2014
[2]   Kinkei, S.; Maloca, S.: Produktionsverlagerung und Rückverlagerung in Zeiten der Krise. Modernisierung der Produktion, Mitteilungen aus der ISI-Erhebung Nr. 52. Fraunhofer ISI, Karlsruhe 2009, p. 12
[3]   Schuh, G.; Haag, C.: How to Prevent Product Piracy Using a New TRIZ-Based Methodology - TRIZ Future Conference 2008. Procedia Engineering (2011) 9, p. 391-401
[4]   Abele, E.; Kuske, P.; Lang, H.: Schutz vor Produktpiraterie. Springer-Verlag, Berlin, Heidelberg 2011
[5]   Wildemann, H.: Produktpiraterie. TCW-Verlag, München 2010
[6]   Abele, E.; Kuske, P.; Lauer, B.: Know-how Schutzstrategien im Maschinenbau implementieren. ZWF 106 (2011) 6, p. 444-448
[7]   Marxen, L.; Geiger, R.; Meyer-Schwickerath, B.: Systematische Risiko- und Maßnahmenidentifikationund strategische Verankerung im Unternehmen. In: Abele, E.; Albers, A.; Aurich, J.C.; Günther, WA. (Hrsg.): Wirksamer Schutz gegen Produktpiraterie im Unternehmen. Piraterierisiken erkennen und Schutzmaßnahmen umsetzen. VDMA-Verlag, Frankfurt am Main 2010, p. 25 -63
[8]   De Bono, Edward. Six thinking hats. Penguin, 1999.
[9]   Birkhold, M.; Verl, A.: Post-Stuxnet: Sicherheitslücken bedrohen weiterhin Produktionsanlagen. ZWF 106 (2011) 4, p. 237 - 240
[10]   Jessenberger, S.: Detaillierte Lösungskonzepte für mehr IT-Sicherheit in industriellen Netzwerken. ZWF 104 (2009) 2, p.94-97
[11]   Altshuller, GenrikhSaulovich. The innovation algorithm: TRIZ, systematic innovation and technical creativity. Technical Innovation Center, Inc., 1999.
[12]   Neemann, Chr. W: Methodik zum Schutz gegen Produktimitationen. Dissertation, RWTH Aachen, 2007. Berichte aus der Produktionstechnik 2007, Nr. 13, Shaker Verlag, Aachen 2007
[13]   Meier, H.; Siebei, C.; Nahr, M.: Auswahlstrategie von Kooperationspartnern im Kontext der Produktpiraterie. ZWF 104 (2009) 12, p. 1093 -1096
[14]   Kafitz, W: Sicherheit und Plagiatschutz beim automatisierten Datenaustausch. ZWF 104 (2009) 6, p. 513-517
[15]   Gausemeier, J.: Produktpiraterie – Bedrohung für Innovationskraft und Wettbewerbsfähigkeit. ZWF 105 (2010) 5, p. 403-404.

An Experimental Investigations of Nusselt Number for Low Reynolds Number in an Agitated Helical Coil

K. Ashok Reddy[1], M. Bhagvanth Rao[2], P. Ram Reddy[1]

[1]*Professor,Dept.of Mechanical Engineering,Guru Nanak Institutions Techanical Campus, Ibrahimpatnam, R R Dist, Telaganna State.*
[2]*Director, CVSR College of Engineering Uppal Road, Greater Hyderabad Telaganna*
[3]*Director, Malla Reddy College of Engineering, Masimaaguda, Hyderabad, Telaganna*

Abstract: *In this paper, we present results of measured heat transfer coefficients for each sodium carboxymethyl cellulose concentration at two different lengths of coil L=2.82m, L=2.362m and with two different heat inputs 1.0kW and 1.5kW. Test solutions of sodium carboxymethyl cellulose concentrations of 0.05%, 0.1%, 0.15% and 0.2% were used in our experimental runs. A four flat blade paddle impeller was used to verify the mixed fluid, under steady heating of Newtonian and non-Newtonian fluids in an flat bottom agitated vessel. A Kanthal Heating Element Equipment have been design and fabricated to optimize the heating of the fluids in an agitated vessel. The rehogical properties like flow behavior index, consistency index and viscosity data were carried experimentally using Rotating Cylinder Method for all the test solutions. A correlations have been presented for Newtonian and non Newtonian fluids in laminar flow conditions.*

I. Introduction

Tube coils offer substantial amount of heat transfer area at a considerably low cost. Coils have lower wall resistance and show better performance in achieving the better heat transfer rates. Due to turn of helix angle, centrifugal force is generated inside the coil and hence the heat transfer rates with helical coil arrangement is better than the corresponding straight coil.

The tubes are coiled into helices in which inlet and outlet are conveniently located side by side. When such coils are used with impeller, they tend to increase the side wall heat transfer rates. For ordinary use, it is suggested that the straight tube equation such as Sieder-Tate [1] relation can be used, when the value of h so obtained is multiplied by $[1 + 3.5(d/d_c)]$ where d is the inside diameter of the tube and d_c is the diameter of the coil helix.

As far as mechanical agitation is concerned, heat transfer through conducting surface improves with agitation as contact with the heat transfer area is improved. As far as the inside coefficient for the coil is concerned the increased turbulence due to circulatory path, the heat transfer coefficient will be greater than those calculated for straight tubes. Helical coils arrangements in a agitated vessel show significant experimental results for unsteady state of bulk temperature profiles leading to higher heat transfer rates compared to the jacketed agitated vessel.

During 50's, many – a - papers were published in evaluating the heat transfer coefficients in agitated vessel with a helical coil. In their studies, they were able to correlate the experimental data with dimensionless parameters like Reynolds number, Nusselt number and Prandtl number with different impeller geometries. Krishnan and Pandya[2],Jha and Raja Rao [3] have conducted experiments with non-Newtonian fluids and correlated the rheological properties with dimensionless quantities in obtaining the heat transfer coefficients in a coil agitated vessel.

Seth and Stahel [4] have discussed the merits and demerits of the immersion coils used to evaluate the heating, cooling and isothermal and non-isothermal temperature distribution in an agitated vessel. In their successive publications, the authors pointed out that the heat transfer rates depend upon the coil location, vessel size and shape and type of impeller used in experimentation, rheological properties and degree of mixing. Skelland and Dimmick [5] have studied heat transfer in agitated vessel with heating coils. Shetty and Jayakumar[6] have presented heat transfer for half-coil jacket around the vessel. The overall heat transfer coefficient has been investigated for different initial temperatures of hot liquid inside the vessel by varying the flow rate of coolant through the half-coil. Dhotre et al [7] have investigated modeling and dynamic studies in half coil jackets.

Pedrosa and Nunhez [8] extended the work of Oldshue and Gretton[9] to understand the experimental data by using Computational Fluid Dynamics software to study improvement in heat transfer rates in a helical

coil agitated vessel . The experiments were conducted by using coils to improve the heat transfer mechanism by Nunhez and Mcgreavy [10]. By using sliding mesh computational Numerical Simulation, Lakghomi et al [11] have studied velocity of flow and heat transfer for both coil and jacketed agitated vessel in turbulent condition with Rushton Turbine . Recently, heat transfer studies were successfully attempted by Perarasu et al [12] in coil agitated vessel with disc turbine and propeller impellers at different heat inputs. The results show that the heat transfer coefficients were found to be higher for turbine impeller compared to propeller impeller.

II. Objectives

To design and fabricate the kanthal heating element embedded in knitted glass fabric type heating apparatus to evaluate heat transfer in immersion coil with different flow rates and two different coil length in the convective heat transfer mode.

To determine the viscosity by using rotating cylinder viscometer and to analyze the data so obtained with regression analysis.

To determine the overall heat transfer coefficient for coil and evaluate the individual heat transfer coefficients by using the theoretical empirical equations found in the literature.

III. Materials & Methods

2.1 Design Knathal Heating Element: Based on the published data [13,14,15], the design and fabrication of equipment used for this investigations has been carried out and details are given as under:

The heating element consists of 80% Nickel and 20% Chromium which has been long regarded as finest alloy of its type for better performance resistance heating.Itgives outstanding performance. Normally manufacturer test these alloys by Bash and Harwich life test. The wire is heated at fixed temperature for two minutes and allowed to cool for two minutes. The heating and cooling cycle is conformed to till the wire burns out. Nichrome 80/20 was selected for designing the heating element.

With 80/20 Ni Cr, the effects of repeated heating –cooling are far less compared to other alloys because the chromium rich oxide formed is more adherent than other oxides formed by iron containing alloys. After selection of suitable alloy, the diameter of wire is to be selected. On selection of diameter, to accommodate the length of the wire, they are made in spiral form at slow speed on suitable mandrel . The mandrel size should not exceed five times the wire diameter otherwise the element will not have mechanical strength to hold in the position. After making spiral, it is stretched to two half times length for uniform emitting of heat and to avoid heat losses.

The lead should have lower resistivity - at least three times the same wire is used to form a lead and twisted together to form connection. The wire emits its generated heat from its surface area and with higher surface area one can provide higher wattage .It is called surface loading. This factor determines life and temperature of the element, on the basis of the selection of insulation to be provided .The elevated temperature in the process vessel is either required to distill liquids or to produce chemical changes due to combination of temperature and chemical treatment. Here, we require to measure heat transfer through different liquids. As we need temperature requirement of 200/300°C, we have selected lower surface loading i.e Watts/cm^2 such that the heating element works on high temperature (550°C), hence fiber glass yarn has been selected as electrical insulating material.

Fiber glass is not only good electrical insulation but also good conductor of heat i.e heat generated will be transformed through surface area of the heater. The fiber glass yarn can withstand peak temperature of 550°C, normally limited to 450°C and suitable for liquid temperature of 350°C. The fiber glass yarn is knitted as fabric, so that the fabric is flexible, resistant and can be made to adopt to small difference in size of the vessel, perfectly. The knitted fabric is made to the shape of vessel used in the experiment and the elements are attached to it such that it gets embedded and forms part of the fiber glass fabrication.

The vessel is made of stainless steel and by taking into account approximate heat required, selection was made to have 1.5kW heater in three sections each of 500 Watts with selectable through individual toggle switches. This has been done purposely to select the heater as per quantity of material used in the experiment, to get better accuracy by avoiding high heating to prevent over shooting the temperature. This entire heating system is lagged with approximately 0.05m thickness of insulation of glass wool to avoid heat loss to surface and utilize entire heat energy.

2.2 Experimental Setup: A cylindrical vessel with flat bottom made of stainless steel with 2.4mm thickness, vessel diameter=190mm and height of the vessel 315 mm has been fabricated. The Copper tube with internal diameter=4.0mm, outer with two different lengths 2.362 m and 2. diameter of 6.4mm 82 m are shaped into a helical coil of three turns. Diameter of the helical coil being used is 156 mm for the study reported here. A 4-Flat Blade Paddle Impeller with diameter 63.3mm, 13mm wide and 3.0mm thickness made of SS is incorporated

with shaft diameter of 8.0mm and of 450mm in length. Impeller is fastened centrally to a erected shaft with a threaded nut at one end. The shaft is driven by a motor which is directly connected to the shaft. The speed of the impeller can be varied by speed reducing controller. Impeller height from the bottom of the vessel is made equal to the diameter of the impeller by design. Flow Meter Range of 135 cc/min-1950 cc/min has been used in the experiment setup. Four K-type thermocouples are inserted with kanthal heating element. A separate temperature indicator is provided to measure the temperature of the heating elements. Open type PT-100 sensor is used to measure the bulk temperature. Provision is made to note the inlet and outlet temperatures by using PT-100 sensors.

Hawke VT500 Viscometer [16] has been used to evaluate the viscosity of 0.05%CMC,0.1%CMC,0.15%CMC and 0.2%CMC test solutions. It has RS-232 interface with data interoperation system and preset adjustment for shear rate in the range 1 to 600 rpm. For our study the Ostwald model regression method is taken into consideration and the model equation is taken as $\tau = \mu . (\dot{y})^n$ where τ=shear stress, μ=viscosity factor, n= flow behavior index $\dot{y}$=shear rate. The ranges for different concentrations: Viscosity Range: 1000-1100 C.P. and Shear Rate Range: $1\text{-}200 \text{ s}^{-1}$ Temperature difference for each reading = 5^0 C .

2.3 Experimental Procedure: Initially, the vessel was filled with known volume of fluid solution upto a depth(Hd) equal to the diameter of the vessel(Dt), submerging the coil completely. The clearance between the impeller and vessel bottom was kept equal to the diameter of the impeller. Heating was achieved by heating the element. A 0.25kW rated electric pump was used to supply the test fluid through one end of the coil. Experimental observations like bulk temperature, inlet temperature and outlet temperature of the test fluid were measured by PT-100 thermocouples. Temperature readings were noted for every 2 min. beginning with turning on the power till a steady state was reached. Heating rates for each of the four concentration of 0.05%, 0.1% 0.15% and 0.2% CMC solutions, used separately in each experiment, were regulated at constant flow rate by maintaining constant speed of the motor during the experiment. The CMC powder of analytical grade was used. The air bubbles were allowed to escape after preserving the solution over night. The experiments were conducted by using four different flow rates at each concentration. Each experiment was repeated twice and the reproducibility was found to be excellent. All the experiments were carried by using two different lengths of the coil L=2.82m and L=2.362m with 1.0kW and 1.5kW heat inputs for all variables of concentrations and coil lengths.

IV.   Results and Discussions

3.1Over all Heat Transfer Coefficients:
The overall heat transfer coefficient for outer diameter of the coil pipe has been evaluated by using the heat balance equation[6]:
$$Q*\rho*C_p*(T_o - T_i)= U_o \ (A_o*(T_b - (T_{o+}T_i) /2) \qquad (1)$$
The properties of ρ_h and C_{hp} are taken into account at the average temperature of T_{ih} and maximum being T_{oh} for any experiment.

Time average overall heat transfer coefficient for outer coil pipe for heating was evaluated by using following relation[6]:
$$\bar{U}_o = \sum \ U_j t_j \ \Delta t_j / \sum t_j \ \Delta t_j \qquad (2)$$

Using C Program and Matlab7.0, time average overall heat transfer coefficients have been evaluated from the above two equations (1-2) for each test run. In our present study , the thermal properties like density(ρ),thermal conductivity (k) and specific heat (Cp) have been taken from the literature [17].

3.2Determination of Nusselt Number:
Newtonian Fluids: Newtonian fluids with Re:20-250, curvature ratio λ=0.0256 and Pr:150-800 Viscosity index:1.2-4.4 Rotational Speed N:40-120rpm were found to be in good agreement with the parameters used in obtaining the following relation as
$$Nuo=0.0366(Re)^{0.6127}(Pr)^{0.4478} (Viss)^{0.14} \qquad (3)$$
where Nu=ho do/k, Re=D_i^2 N ρ/μ, Pr=Cp μ/k and Viss=μ_m/μ_w

Varying density (ρ) and impeller rotational speed(N), Viscosity of the test solution ,the theoretical Nusselt Number (Nuo) for the helical coil of Newtonian fluids have been evaluated using equation (3) with thermal conductivity (k) and specific heat (Cp) of 0.05% and 0.1% CMC test solutions kept constant.

Fig 2 shows the comparison of experimental Nusselt Number for outer diameter of the helical coil with theoretical Nussult Number for 0.05% and 0.1% CMC test solutions showing Newtonian behavior and being

evaluated using equation (3). The correlation coefficient is found to be good agreement with test solutions as R^2 =0.804

Non-Newtonian Fluids: Dean Number :2.5-60, Rotational Speed N:60-200rpm
Theoretical Nusselt number (h_o) for the helical coil of non-Newtonian fluids have been evaluated using the following equation
$$Nu_o=C(De)^a \qquad (4)$$
Taking log on both sides for the above equation(4), we get
$$lnNu_o=lnC+alnDe_o \qquad (5)$$
Using Regression Method, the constants C and a in the equation(5) have been evaluated and substituted in the equation(6)
$$Nu_o=1.7(De)^{0.0955} \qquad (6)$$
where $Nu_o=h_o d_o/k$, $De=Re(d_o/D_c)^{0.5}$
Varying density (ρ), consistency index(K) and impeller rotational speed(N),the Nu_o have been evaluated using equations (4-6) with thermal conductivity (k),flow behavior index (n) and specific heat (Cp) of 0.15% and 0.2% CMC test solutions were kept constant.
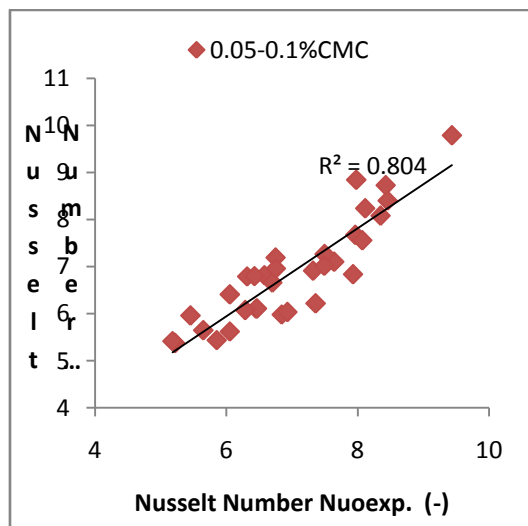
Fig 1 Nuexp Vs Nutho for Newtonian
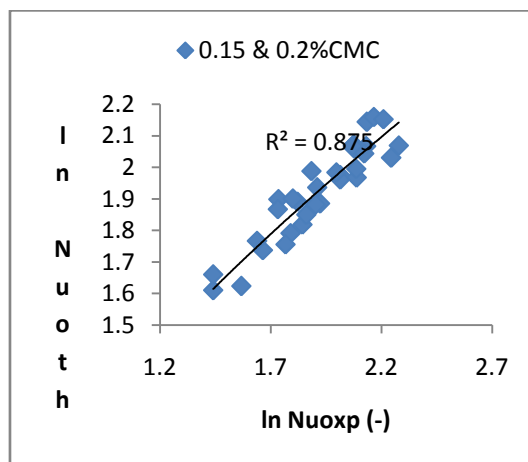
Fig 2 Nuexp Vs Nutho for Non-Newtonian Fluids
Re:15-300,Pr:1200-5200,K_m/K_w =2.2-5.4 Rotational Speed N=60-200rpm
$$Nu_o Pr^{0.4325}=8.16 Re^{0.3694} (K_m/K_w)^{0.14} \qquad (7)$$

It can be inferred from the Fig 3 that the trend line is parallel and increasing, when comparing the data for experimental Nusselt Number with theoretical Nusselt Number for non-Newtonian test solutions.
        The correlation coefficient is found to be good agreement with test solutions as R^2 =0.875 for the above equation (7).

V.   Conclusion

1. The rheological property that is the consistency index (K) equation s have developed for non-Newtonian fluids. The equations are as **K=1791*T$^{-2.18}$** (0.15%CMC) and **K=1033*T$^{-1.7}$** (0.2%CMC).The equations were evaluated using regression analysis . The consistency index(K) decreases as the temperature of the test solution increases .

2. The single parameter fit exponent 0.0366 , Reynolds Number exponent 0.6127 and Prandlt Number exponent 0.4478   in equation(3) for Newtonian fluids   is found to be in good agreement   with the range of parameters used in our present study and have been evaluated by Multi Regression Analysis.

3. CMC test solutions 0.05% and 0.1% shows Newtonian behavior of linear equation $Nu_{oth} =0.935(Nu_{oexp}) + 0.327$.

4. Non-Newtonian test solutions 0.15% and 0.2% have shown good agreement with power law equation $Nu_{oth} =1.347(Nu_{oexp})^{0.554}$.

5. The exponents in equation(7) have been evaluated using Multi Regression Method and found to be 0.4325 and 0.3694 respectively for non Newtonian test solutions. The equation(7) is more accurate than equation(6).

Acknowledgement

References

[1]   E N Sieder and G N Tate;   Heat Transfer and Pressure Drop of   Liquids in Tube Industrial Engineering Chemistry 28 (1936) p1429.
[2]   R M Krishnan and S B Pandya; Heat Transfer to Non-Newtonian Fluids in Agitated Vessels Indian Chemical Engineer (1966) T42-49.
[3]   R. K. Jha and M. Raja Rao; Heat Transfer through Coiled Tubes in Agitated Vessels. International Journal Heat & Mass Transfer 10 (1969) 395
[4]   K. K. Seth and E. P. Stahel; Heat Transfer from Helical Coils Immersed in Agitated Vessels Industrial & Engineering Chemistry 61 (1969) p39-48.
[5]   A. H. P. Skelland and G. R. Dimmick; Heat Transfer between Coils & Non-Newtonian Fluids with Propeller Agitation. Industrial Engineering & Chemistry Process Design Development 8 (1969) 267.
[6]   Y. P. Setty and N. S. Jayakumar; Heat Transfer Studies Using Half-Coil Jacket Indian Chemical Engineer. Section A 41 (1999) T27-T53.
[7]   M. T. Dhotre, Z. V. P. Murthy and N. S. Jayakumar; Modelling and Dynamic Studies of Heat Transfer Cooling of Liquid in Half-Coil Jackets Chemiocal Engineering Journal 118 (2006) 183.
[8]   S. M. C. P. Pedrosa & J. R. Nunhez; Improving Heat Transfer in Stirred Tanks Cooled by Helical Coils. Brazilian Journal of Chemical   Engineering 20 (2003) [links].
[9]   J. Y. Oldshue and A. T. Gretton; Helical Coil Heat Transfer in Mixing Vessels Chemical Engineering Progress 50 1954 p615-621.
[10]   J. R. Nunhez and C. Mcgreavy; A. Comparison of the Heat Transfer in Helical Coils and Jacketed Stirred Tank Reactors Brazilian Journal of Chemical Engineering 12 (1995) [links].
[11]   B. Lakghomi, E Kolahchian, A Jalai and F Farhadi; Coil and Jacket's Effects on Internal Flow Behavior & Heat Transfer in Stirred Tanks World Academy of Science Engg and Tech. 24 (2006) p147-151.
[12]   V. T. Perarasu, M. Arivazhagan P. Sivahanmugam Heat Transfer Studies in Coiled Agitated Vessel International Journal of Food Egineering 7 (2011) p1-13.
[13]   Kanthal; Handbook Wikipedia, Encyclopedia, Hallstahammer Sweden p106-115
[14]   Kanthal; Handbook Heating Alloys for Electric Household Appliances Design Factors p20-41
[15]   Kanthal;Handbook - Resistance Heating Alloys & Systems for Industrial Furnaces p1-28
[16]   Haake Information Haake Mess-Technik; GmbH Co Dieseistr Germany VT-500 Haake Visco tester p1-10
[17]   A M Mondal, J A Naser   A K M A Quader; Laminar Heat Transfer to Time-Independent Non-Newtonian Fluids in Tubes Indian Chemical Engineer Section A 39 1997 T27-T34.

OPEN ACCESS

Optimization of Multi Leaf Spring by using Design of Experiments & Simulated Annealing Algorithm

Narendra Yadav[1], Prof. S. A. K. Jilani[2]

[1](M E Scholar, RCET, Bhilai-India)
[2](Associate Professor, Department of Mechanical Engineering, RCET, Bhilai-India)

ABSTRACT: *This work carried out on a multi leaf spring of a tractor trolley with maximum load carrying capacity of 5 Tones. The CAD model of this MLS has been modeled in CATIA V5. After successfully preparing the CAD model, MLS is then tested in Static Structural Analysis workbench for stress and deflection computations. The finite element analysis of the leaf spring has been performed by converting the model into number of nodes and elements and then applying the relevant boundary conditions under the static loading conditions. After implementation of FEA it was observed that the red area close to shackle was undergoing maximum value of stress. This observation leads us to the workbench of Knowledge ware and this aided us in studying the response of crucial output parameters of MLS in the form of Stress and Deflection via Design of experiments. DOE paved the way for SAA where optimization was carried out in order to reach the minimal stress. The corresponding values of camber and leaf span were recorded for minimal stress.*

Keywords: *Computer Aided Design (CAD), Camber, Design of Experiments (DOE), Eye Distance, Finite Element Analysis (FEA), Multi Leaf Spring (MLS), (Simulated annealing algorithm (SAA).*

I. Introduction

A multi leaf spring is a curved shaped laminated plate with eye at both ends, generally used for the suspension in heavy vehicle. It is the oldest forms of springing techniques used. It's slender arc-shaped with uniform rectangular cross section throughout the length. The rear and front axle is mounted on the center of the arc, while the eye end is used for attaching to the chassis.

The basic problem which is encountered in MLS is the change in the dimensions of camber and leaf span due to frequent loading and continuous running of the tractor trolley. The basic observation carried out in this thesis is regarding the increase in the camber and decrease in the leaf span after a period of time. This acts as a limitation to spring action. Hence it becomes very essential to restore the spring action to the initial level. This is because the spring is always loaded and the load on it may be due to the trolley or due to its own weight. It is observed that due to the change in dimensions of camber and leaf span there is a decrease in the amount of comfort level both to the rider and the cargo loaded on it. The objective initially is to study the behavior of a MLS under static loading conditions by varying the camber and leaf span.

II. Multi Leaf Spring Dimension and Boundary Condition

The major difficulty in this work was that the rectangular cross section of the leaf spring was swept along the semi elliptical path. This tends to not assembled easily. So it needs to have proper attention and accuracy during the process of assembly. Hence in order to assemble in a proper manner it was very essential for us to use absolute dimensions of the each leave of MLS. The modeling and assembly of MLS has been carried out in CATIA V R20, the dimension of MLS has been maintain according to the manual measurement taken from the existing model of MLS.the dimension of MLS is as:

Leaf Span = 900 mm, Camber = 120, Thickness = 10 mm and width = 60 mm
There are two full length leaves, and seven graduated leaves used for the complete assembly of MLS.
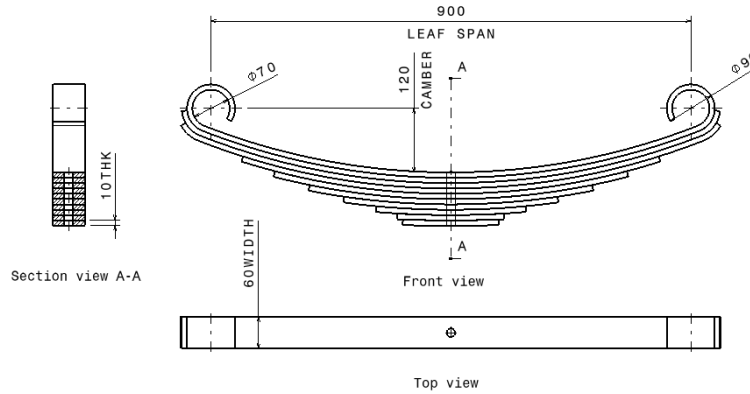
Fig. 1 Front Top & Sectional Side View of MLS

III.   Existing Material

Material properties:- The properties of the material 55Si2Mn90 being used in this analysis are shown in Table 1 Mechanical Properties of EN45.

Table 1: Mechanical Properties of EN45

PARAMETER	VALUE
Young's Modulus (E)	200GPa
Poisson's Ratio	0.3
Tensile Strength Ultimate	1962 MPa
Tensile Strength Yield	1800 MPa
Density	7850 kg/m^3
Thermal Expansion	11x10-6 / ^{o}C

IV.   Load and Boundary Conditions

One eye of the leaf spring is kept fixed (cylindrical support) and the other eye is given certain degree of rotation to allow the leaf spring to deflect by some amount along its length to meet the actual conditions which is shown in figure 4.14. After this load is applied of magnitude 12500 N in the upward direction at the centre of the MLS. This particular calculation of load to be applied has been done on the basis of GVW (Gross Vehicle Weight). This has been clearly shown the figure 2
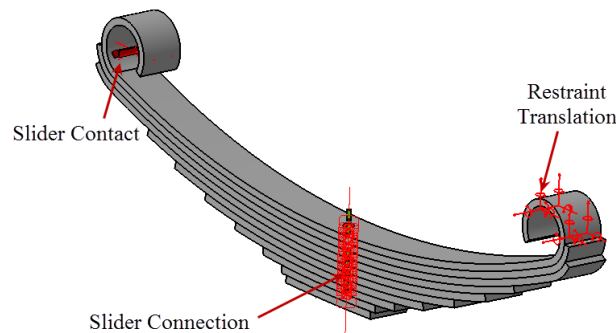

Fig. 2 Boundary condition of MLS

V.   Static Structural Analysis in CATIA V5 R20

After applying the boundary conditions the maximum von mises stress and maximum displacement is shown in Fig. 3 & 4
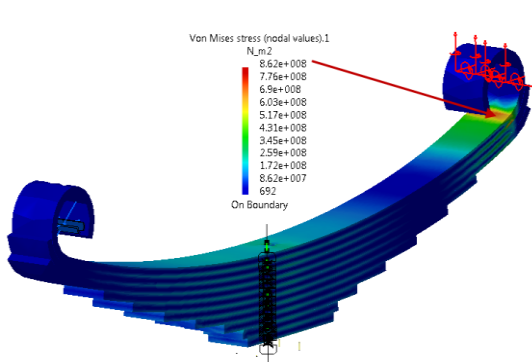
Fig. 3 Max. Stress at near eye end   Fig. 4 Max. Deflection
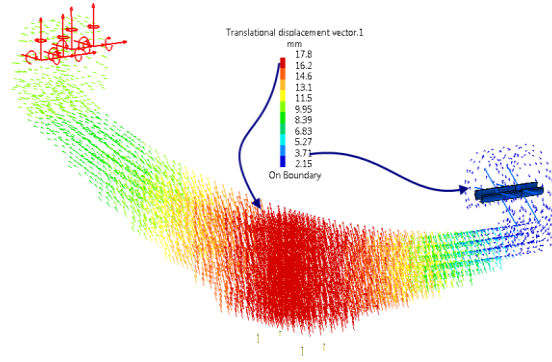
The values of stress and deflection obtained by FEA are shown in Table 4.3 below.

Table 2 Output parameters by FEA

S.N.	PARAMETER	VALUE
1	Max Von Mises Stress	8.621x108 N/m2
2	Max Deflection	17.756 mm
3	Energy	100.085 J
4	Mass	30.877 kg

VI.   Design of Experiments

After applying FEA, Design of experiments is performed for the same model where camber and leaf span were varied in a specific range that is camber between 110 mm to 130 mm & leaf span between 870 mm to 930 mm. It took approximately 300 minutes to compute the results based on 400 combinations of camber and leaf span. The optimum value for the stress is 587100000 N/m^2 and the camber is 123.68.
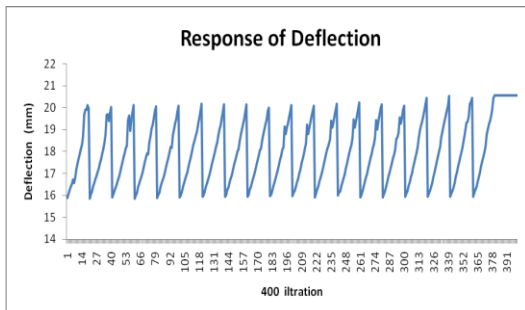

Fig. 5 Variation in deflection in MLS   Fig. 6 variation in Stresses in MLS
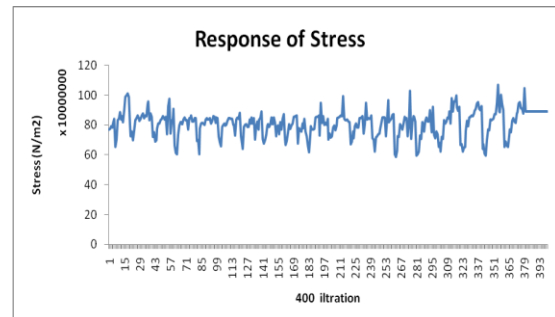
VII.   Optimization by SAA

In any optimization whether linear or non-linear there has to be an objective function which is supposed to be either maximized or minimized. In our case we will select Max Von Mises Stress as our objective function. We have to make sure that stress is reduced. As we know that stress directly depends on the dimensions of the existing MLS, hence in order to perform the optimization and compute various values of stress, the input parameters such as camber and leaf span will be varied. This is stochastic search process which will bounce itself from one local minimum to the other and ultimately it will reach a global minimum. In order to perform the optimization we need to open the optimization workbench in CATIA V5 and the initialize the parameters or factors affecting the outcome.

Table 3 Output parameter of SAA and DOE

S No.	Parameters	Stress via DOE (N/m^2)	Stress via SAA (N/m^2)
1	Existing stress	862100000	862100000
2	Optimized Stress	587100000	672923200
3	Percentage Reduction	32	22

SAA is basically a search algorithm and it starts the first iteration with maximum temperature and then gradually cools down to reach the most optimum configuration. As per the results obtained it was observed that in the 82nd iteration the stress value computed was minimum and has clearly shown in Figure 6.
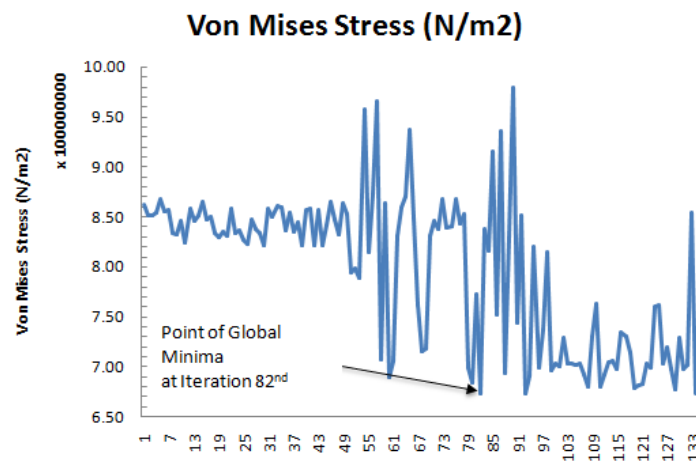

Fig. 7 Variation of Stress as per the iterations via SAA

VIII.   Results

- **Stress & Deflection computations from the existing dimensions by FEA**
        Stress and deflection are being calculated for the existing model. It is found that Max Von Mises stress is 862100000 N/m2 and corresponding deflection is 17.756 mm.

- **Stress & Deflection computations by DOE**
        With reference to the Table 3, it is clear that the optimum value for the stress is 587100000 N/m^2 and the camber is 123.68.which is 262th iteration in DOE table and the parameters corresponding to this stress are as follows: Camber = 123.68 mm & Leaf Span = 873.1 mm.

- **Stress & Deflection computations by SAA**
        With reference to the Table 3, the database obtained, it was observed that in the 82nd iteration von mises stress of magnitude 672923200N/m2 was minimum and the parameters corresponding to this stress are as follows: Camber = 123.8 mm & Leaf Span = 918.4 mm.

IX.   Conclusion

        The result obtained from FEA, SAA and DOE, it is observed that the most optimum setting of parameter was found in DOE. There was a considerable reduction in the magnitude of stress. We conclude that near about 32 percent of reduction in the stresses by DOE, while in SAA there was only 22 percentage of reduction in the stress. The new value of stress found by DOE is 587100000 N/m^2 for this magnitude, the corresponding parameter of camber is 123.6 and leaf span is 873.

REFERENCES

[1]   Narendra Yadav, Mr. Praveen Tandon Mr. S.A.K. Jilani , Material Optimization of Leaf Spring of Tractor Trolley by FEA, *International Journal of Modern Engineering Research, vol. 4 Issue 4 ,* 2014, 40-44.
[2]   Gulur Siddaramanna Shiva Shankar, Sambagam Vijayarangan, "Mono Composite Leaf Spring for Light Weight Vehicle Design, End Joint Analysis and Testing", *J. of Materials Science*, Vol. 12, pp. 220-225, Issue 3, 2006.
[3]   Sachin G. Wagle, Satish S. Oesai, S. B. Wadkar, "Optimized Design & Analysis of Parabolic Leaf Spring Considering Braking, Cornering & Bump loads", *National Conference of computational methods in Mechanical Engineering*, pp. 47–52 , September 2005.
[4]   Ahmet Kanbolat , Murathan Soner, Mustafa Karaagaç, Tolga Erdogus, "Parabolic Leaf Spring Optimization and Fatigue Strength Evaluation on The Base of Road Load Data, Endurance Rig Tests and Non Linear Finite Element Analysis", *SAE International*, 2011
[5]   Kumar Krishan and Aggarwal M.L. "A Finite Element Approach for Analysis of a Multi Leaf Spring using CAE Tools", *Research Journal of Recent Sciences*, Vol. 1, pp. 92-96, December 2012.
[6]   N.P.Dhoshi, N.K.Ingole, U.D.Gulhane, "Analysis and Modification of Leaf Spring of Tractor Trailer Using Analytical and Finite Element Method", *International Journal of Modern Engineering Research*, Vol. 1, pp. 719-722, Issue 2, December 2012.

[7]   Dakshraj Kothari, Rajendra Prasad Sahu and Rajesh Satankar, "Comparison of Performance of Two Leaf Spring Steels Used For Light Passenger Vehicle", *International Journal of Mechanical, Automobile & Production Engineering*, Vol. 2, pp. 9-16, Issue 1, 2012.

[8]   Kumar Krishan, Aggarwal M.L, "Computer Aided FEA Comparison of Mono Steel And Mono GRP Leaf Spring", *International Journal of Advanced Engineering Research and Studies*, Vol. 1, pp. 155-158, Issue 2, January-March, 2012.

[9]   C.K. Clarke and G.E. Borowski, "Evaluation of a Leaf Spring Failure", *Journal of Failure Analysis and Prevention*, Vol. 5, pp. 54-63, Issue 6, December 2005.

[10]   K.K. Jadhav and R.S. Dalu, "Experimental Investigation & Numerical Analysis of Composite Leaf Spring", *International Journal of Engineering Science and Technology*, Vol. 3, pp. 4759-4764, Issue 6, June 2012.

[11]   Vinkel Arora, Gian Bhushan and M.L. Aggarwal, "Eye Design Analysis of Single Leaf Spring In Automotive Vehicles Using CAE Tools", *International Journal of Applied Engineering and Technology*, Vol. 1, pp. 88-97, Issue 1, October-December, 2011.

[12]   M.Joemax Agu and V.C.Sathish Gandhi, "Finite Element Analysis of Leaf Spring Considering The Nature of the Material", *International Conference on Intelligent Science & Technology*, 2011.

[13]   M. M. Patunkar, D. R. Dolas, "Modelling and Analysis of Composite Leaf Spring under the Static Load Condition by using FEA", *International Journal of Mechanical & Industrial Engineering*, Vol. 1, pp. 1-4, Issue 1, 2011.

Economic Design of Water Tank of Different Shapes With Reference To IS: 3370 2009

M. Bhandari[1], Karan Deep Singh[2]

[1](*Department of Civil Engineering, Dr B R Ambedkar National Institute of Technology, Jalandhar, India*)
[2](*Graduate Civil Engineer, 94, Surya Vihar, Jalandhar, India*)

ABSTRACT: *The conventional method of designing water tanks which is working stress method outlined in the previous version of IS: 3370 1965 is irrational and leads to relatively thicker sections with a substantial amount of reinforcement. Limit state method which is widely used has been recently adopted in the new version of IS 3370-2009 concrete structures for storage of liquids – code of practice. For quick cost prediction of tanks, this study therefore examines the cost effectiveness in terms of amount of materials and formwork used for Circular, Square and Rectangular overhead water tanks each of three capacities of 100kl, 150kl, 200kl and draw reasonable inferences on tank's shape design effectiveness . Each water tank was designed by Limit State method and then the crack width was checked by limit state of serviceability IS 3370 (2009). The results have been presented in the form of graphs and tables and it has been observed that Circular-shaped tank consumed lesser of each material as compared to Square and Rectangular ones. The amount of formwork required for circular tank is also less than that for square and rectangular tanks thereby giving Circular-shaped tanks a more favorable selection over the rectangular and square shaped tanks.*

Keywords: *Working stress method, limit state method, Crack width, effective cost.*

I. Introduction

Safe drinking water is one of the basic elements for humans to sustain healthy life. Reinforced concrete overhead water tanks are widely used to provide the safe drinking water. Most water supply systems in developing countries, such as India, where urbanizing is increasing day by day rely on overhead storage tanks and hence there is need to construct more number of water tanks. Earlier design of water tanks was being done using the working stress method given in IS: 3370 1965. This method leads to thicker and heavily reinforced sections. The use of limit state method of design has been adopted in the revised code IS 3370: 2009 and provision for checking the crack width is also included in this code. This study is carried out to analyze the cost of overhead water tanks of varying capacities and having different shapes so as to determine the most economical shape of the tank.. This will help the designers in making the choice for their design.

II. Problem Formulation

In order to carry out the cost analysis, overhead water tanks of circular, rectangular and square shapes, which are commonly adopted by designers, were considered for the recent study. Water tank of each shape was designed for capacities of 100 kl, 150 kl, and 200 kl. Only the tank portion was considered in this study. The design of all water tanks was done by limit state method as per the the provisions of the IS: 3370 2009. Each element of water tank was also checked for crack width to ensure the proper strength and serviceability.

III. Analysis and Design

3.1 Circular Tank

The Overhead circular water tanks are built for direct distribution by gravity flow and are usually of smaller capacities. As the circular shape has least perimeter, circular tanks are widely used.

The main structural elements of overhead circular tank are shown in Fig. 3.1 and their design methodology is explained in the following sections.:
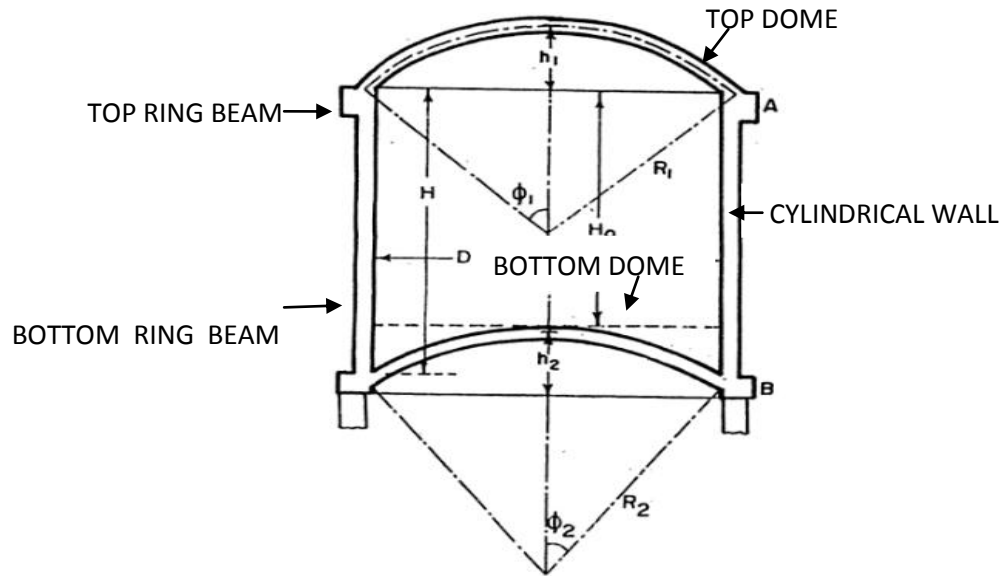
3.1.1 Top Dome: Top dome is designed for self weight and a service live load as per provisions of the relative Indian Standard Codes. . The top dome is supported on the cylindrical wall. Two types of forces that is the Meridional thrust (T) acting along the direction of meridian and the Hoop stress (H) – along the latitudes develop in the dome due to the applied loads. These are illustrated in Fig. 3.2 and 3.3 respectively.
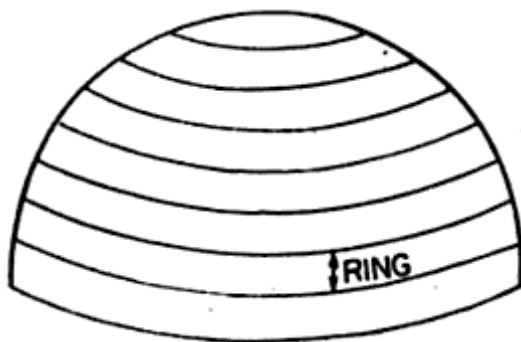

| Fig. 3.2 Frustum of spherical dome | Fig. 3.3 Vertical section of dome |
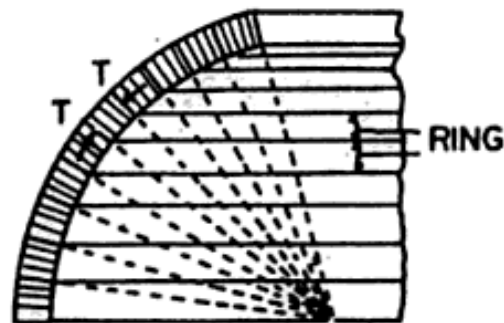
Top dome is designed and checked for these two forces. As the stresses developed are very small in magnitude, minimum reinforcement as specified in code is normally provided in the form of a mesh.

3.1.2 Top Ring Beam

Normally the domes are segmental and the meridional thrust developing at the base of the dome is at some inclination with the horizontal . The horizontal component of the meridional thrust produces hoop tension which is resisted by providing a ring beam at the base along the periphery of the dome. The ring beam is supported on the cylindrical wall of the tank and is designed for direct tension.

3.1.3. Cylindrical Vertical Wall

The tank wall is supported on the bottom ring beam the walls of tank are assumed to be free at top as well as bottom. . Due to this, the tank wall will be designed for hoop tension caused by the horizontal water pressure, without any bending moment. The maximum hoop tension will occur at the base. The tank walls are adequately reinforced with horizontal rings provided at both faces. In addition to this, vertical reinforcement is provided on the both faces in the form of distribution steel. The spacing of the vertical steel is halved at the bottom portion of the wall to cater for any bending moment.

3.1.4 Bottom Spherical Dome

The bottom dome is subjected to vertical loads consisting of self-weight and weight of water. The weight of water over the surface of dome is calculated as

Weight of water $= [\frac{\pi}{4}D^2 \times H - \frac{\pi}{3}h_2^2 (3 \times R_2 - h_2)] \times \gamma_w$

Where D = Inner diameter of tank
H = Height of cylindrical wall
h_2 = rise of bottom spherical dome
R_2 = Radius of bottom spherical dome
γ_w = unit weight of water

3.1.5. Bottom Ring Beam
Bottom Circular beam is supported usually on columns and is designed to support the tank and its contents. The girder should be designed for the bending moments, shear force and torsion. In addition to these forces, it is also subjected to hoop tension due to meridional thrust of bottom spherical dome.
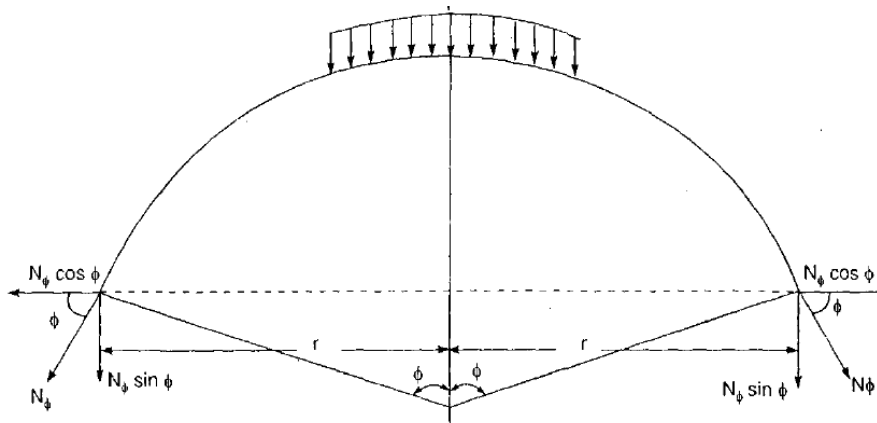
3.2 Over Head Square / Rectangular Water Tank
The main structural elements of a rectangular or square tank are the top slab, the side walls and the bottom slab.
1. Top slab/ Beam
2. Side walls
3. Bottom slab/ Beam

3.2.1. Top Slab:
The top slab is designed as one way continuous slab supported on beams. It is designed only for self-weight and service live load.

3.2.2. Cylindrical Side Walls:
The walls of a rectangular and square water tanks are subjected to bending moments both in the horizontal as well as in vertical direction. The analysis of the moment in the walls is difficult, since water pressure results in a triangular load on them. The magnitude of the moment will depend upon the several factors such as length, breadth and height of the tank and the conditions of support of the wall at top and bottom edges. If the length of the wall is more in comparison to its height the moments will be in the vertical direction i.e. Panel will bend as a cantilever. If, however, height is large in comparison to length, the moments will be in horizontal direction and panel will bend as thin slab supported on the edges. For the intermediate conditions bending will take place both in horizontal as well as in vertical direction. In addition to the moments, the walls are also subjected to direct pull exerted by water pressure on some portion of side walls. The wall of the tank will thus be subjected to both bending moment as well as direct tension. The design of the walls is done on the premise that no cracks are developed in it. Though, reinforcement is provided both for moments as well as direct tension.
There are two method of analysis that is the approximate method and the exact analysis. In this study exact analysis , which is based on the elastic theory, has been used. The resulting differential equations are very difficult to be solved directly. IS 3370 1965 (Part IV) gives the table for moments and shear forces in walls for certain edge conditions. Moment coefficients for individual panels considered fixed along vertical edges, but having different edge conditions at top and bottom are given in table in IS 3370 (Part IV). The coefficients for individual panels with fixed side edges apply without modification to continuous walls provided there is no rotation about the vertical edges.

3.2.3. Floor Slab:
The floor slab should be designed as two way slab supported on floor beams. Generally the thickness of base slab is kept equal to vertical walls.

Check for crack width: as per given in IS 3370 2009 part 2
To be effective in distributing cracking, the amount of reinforcement provided needs to be atleast as great as given below:

$$\rho_{crit} \geq \frac{fct}{fy}$$

where, ρ_{crit} = critical steel ratio, the minimum steel ratio, of steel area to the gross of the whole concrete section, required to distribute the cracking .

fct = Direct tensile strength of the immature concrete which is given in IS 3370 2009 part 2

f_y = characteristic strength of the reinforcement.

Maximum spacing of crack $S_{max} = \frac{fct}{fy} \times \frac{\emptyset}{2\rho}$

$\frac{fct}{fy}$ = ratio of the tensile strength of the concrete to the average bond strength between concrete and steel which can be taken as 2/3 for immature concrete.

$\emptyset$ = size of each reinforcing bar

Wmax = Width of fully developed crack,

$W_{max} = S_{max} \times \boldsymbol{\alpha} \times \frac{T1}{2}$

$\boldsymbol{\alpha}$ = (Coefficient of thermal expansion of concrete) , = 1×10^{-5} for concrete, T = 30^0 C

IV. Results and Discussions

The circular, rectangular and square water tanks of different capacities were designed following the provisions of IS 3370: 2009. The quantities of materials were calculated and have been tabulated and shown graphically in the following section.

Table1: Amount of Concrete in cubic meters.

Tank Capacity(kl)	Circular O.H.T	Square O.H.T	Rectangular O.H.T
100	22.834	23.04	24.375
150	28.274	36.86	39.765
200	35.689	52.83	55.275

Fig 1: Comparison of Concrete quantity for 100kl Capacity water tank with respect to shape of tank.
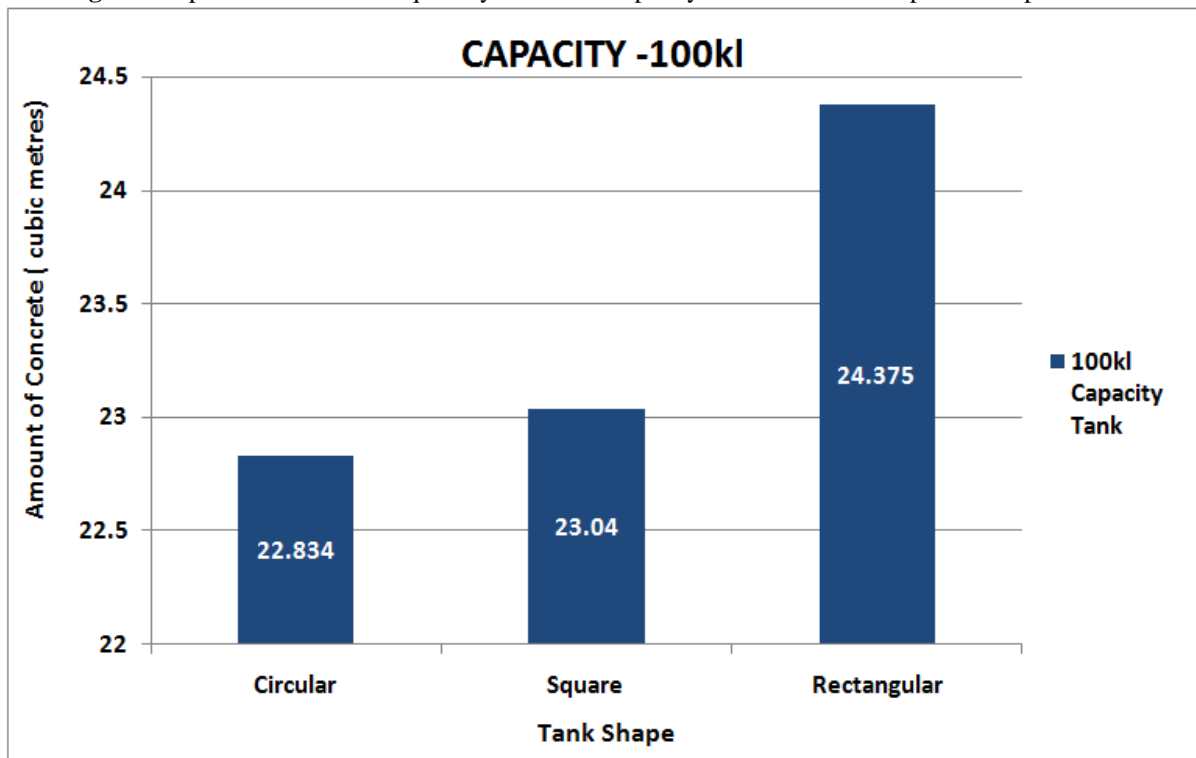
Fig 2: Comparison of Concrete quantity for 150kl Capacity water tank with respect to shape of tank.
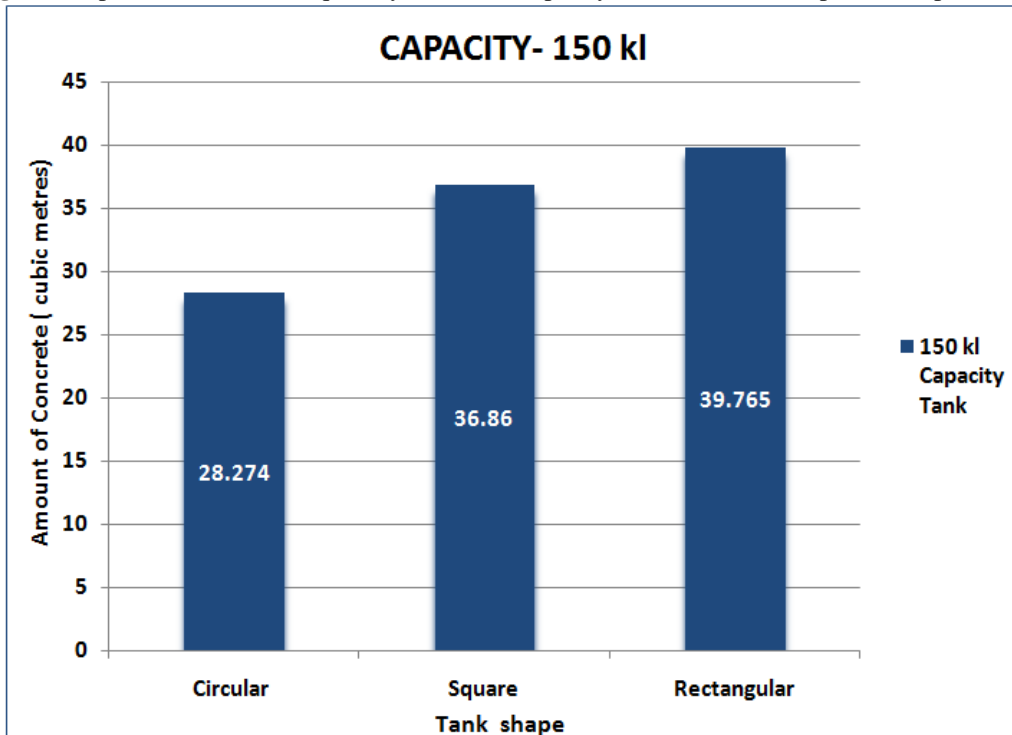

Fig 3: Comparison of concrete quantity for 200kl Capacity water tank with respect to shape of tank
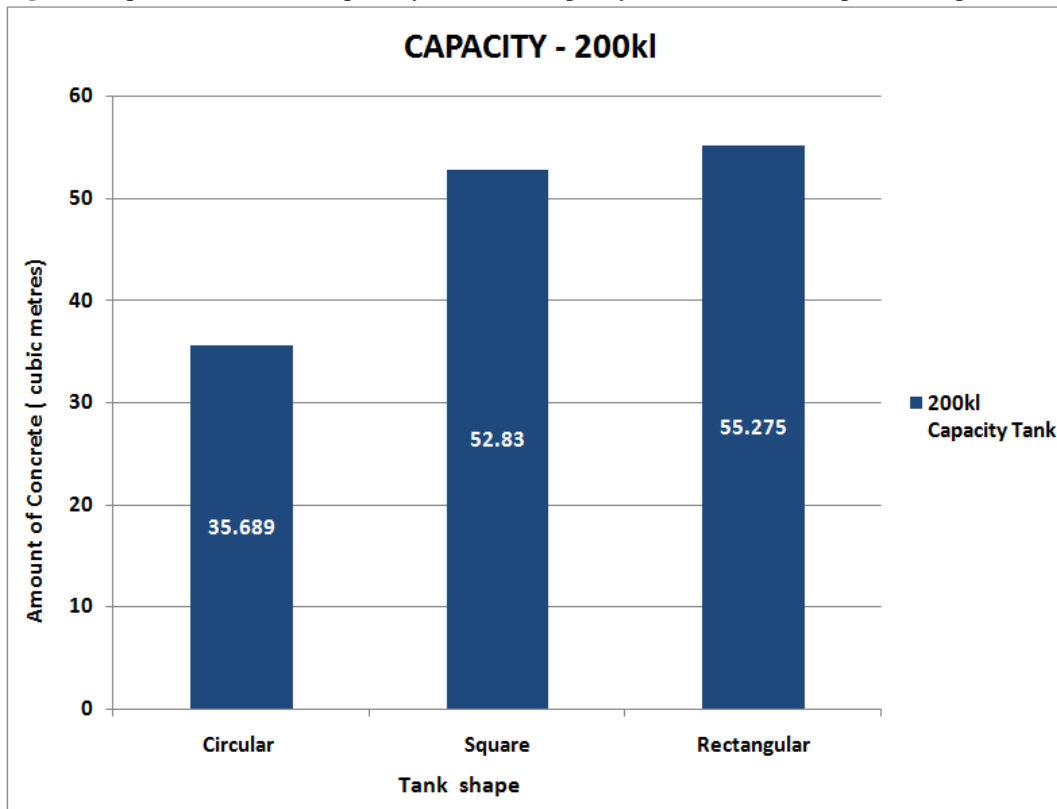
Fig 4: Amount of Concrete against Tank Capacity
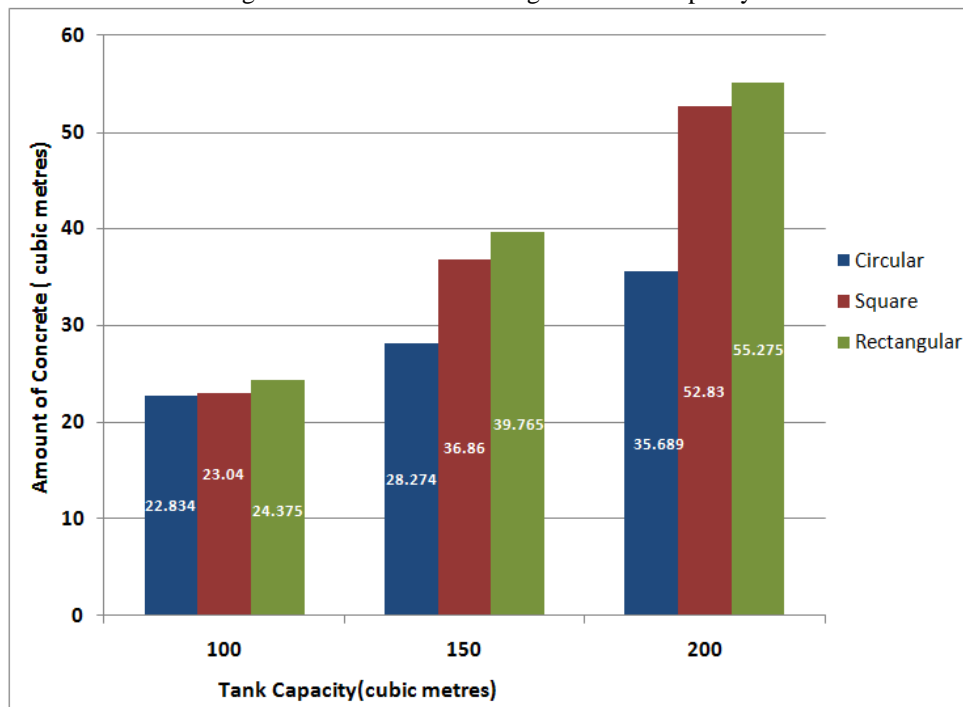
Table 2: Amount of Reinforcement in kilograms

Tank Capacity(kl)	Circular O.H.T	Square O.H.T	Rectangular O.H.T
100	1234.669	3566.7	4129.74
150	1816.71	5772.955	6038.77
200	2422	7696.549	8201.123

Fig 5. Comparison of Reinforcement quantity for 100kl Capacity water tank with respect to shape of tank
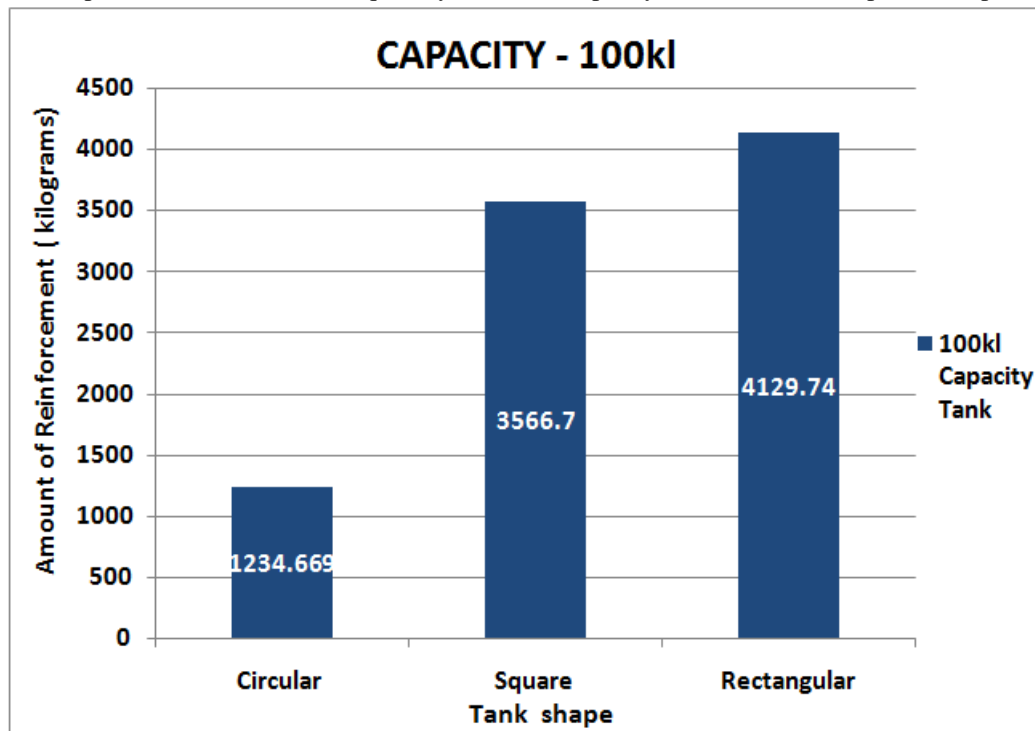
Fig 6. Comparison of Reinforcement quantity for 150kl Capacity water tank with respect to shape of tank
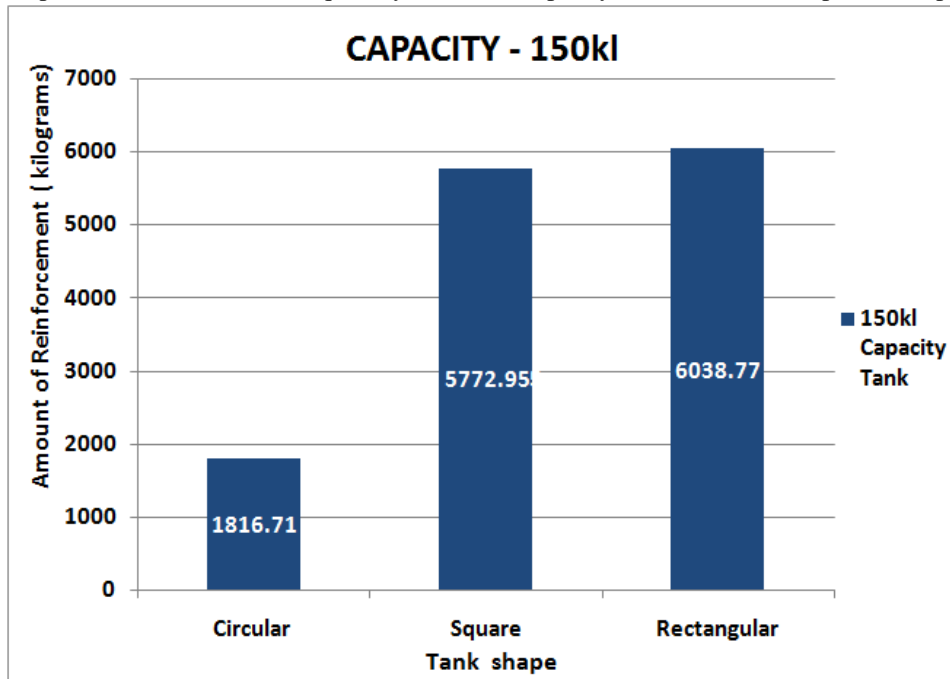

Fig 7. Comparison of Reinforcement quantity for 200kl Capacity water tank with respect to shape of tank
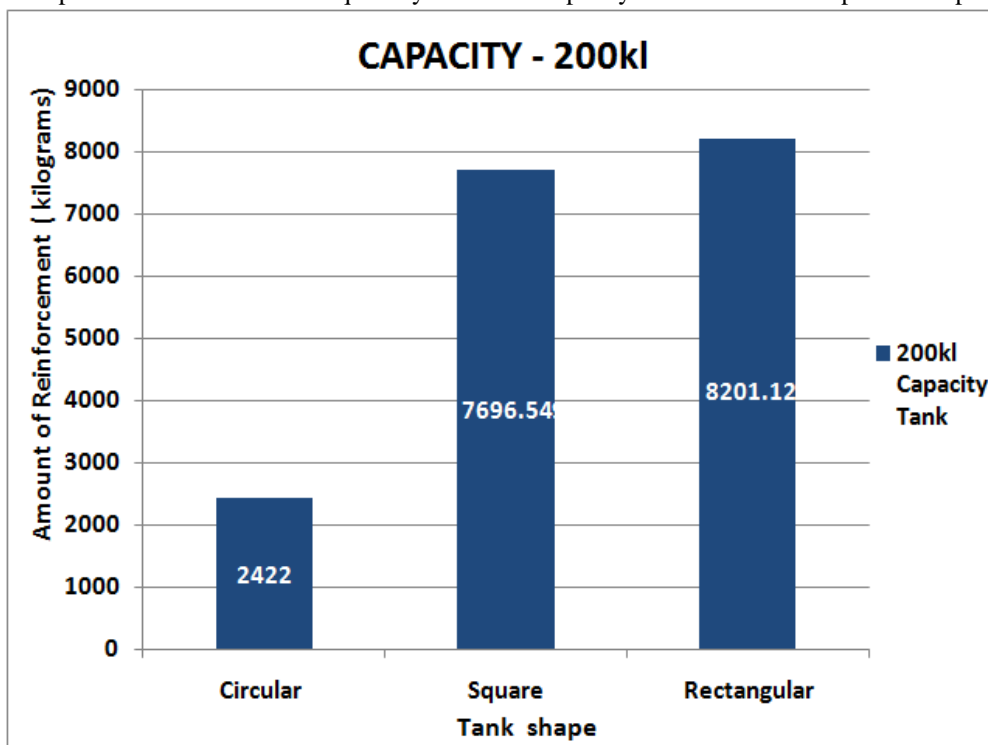
Fig 8:.Amount of Reinforcement against Tank Capacity
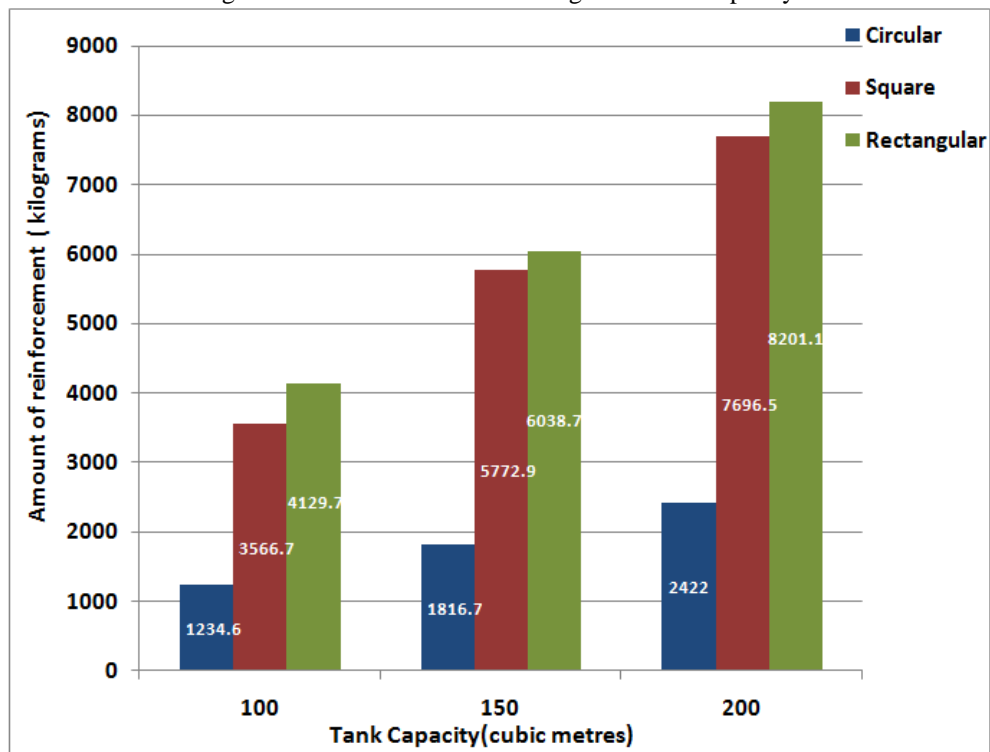
Table 3: Amount of Formwork in square meters

Tank Capacity(kl)	Circular O.H.T	Square O.H.T	Rectangular O.H.T
100	275.8	278.97	289.25
150	344	367.65	373.14
200	411.7	432.95	443.64

Fig 9: Amount of Formwork against Tank Capacity
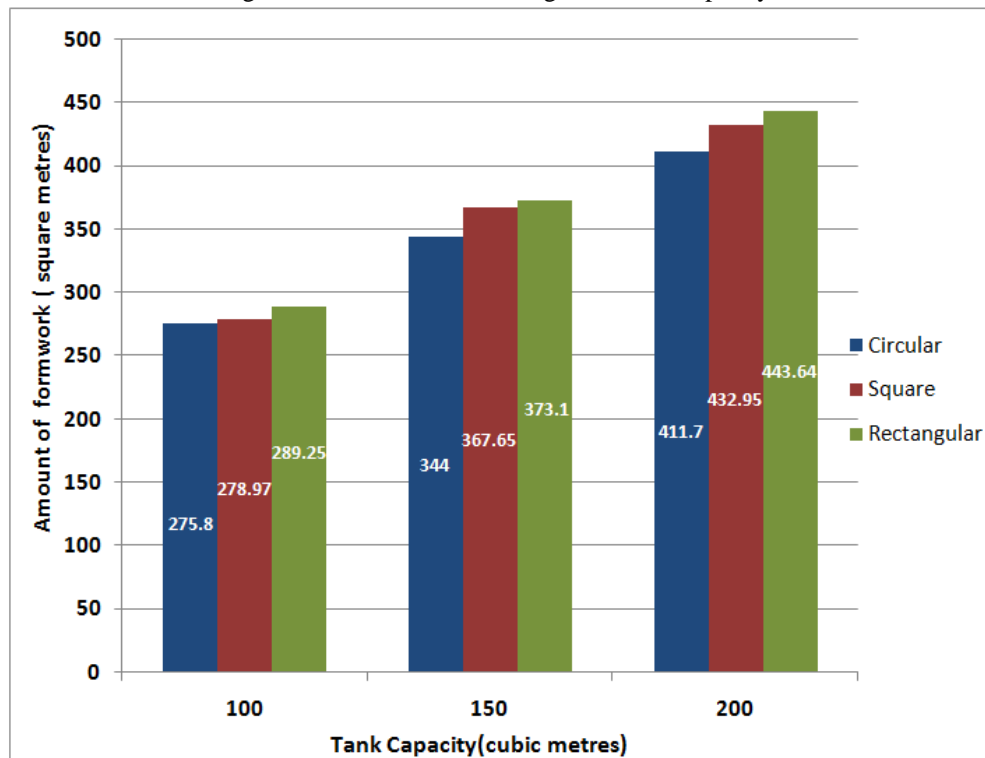
Assessing the relative reductions in the amounts of materials for the circular tanks when compared with those of square and rectangular tanks, it could be deduced that if the relative ease of putting up the shuttering; that is the formwork, would be significantly more challenged in the construction of the circular tanks, their presumed material-quantity advantage could be given up for a selection of rectangular tanks (though with potential increase in material-requirements).

V. Conclusions

➢ As the capacities increase, the amounts of materials for the structure also increases. But, a rather non-perfect proportionality resulted; that is, a proportional increase in the capacity would not, necessarily lead to a proportional increase in any of the materials required.

➢ The quantities of materials needed for the rectangular water tank were constantly more than those needed for square tank which is more than the quantity required for the circular water tank, at each varied capacity.

➢ It can be clearly seen from the results that the formwork required for the construction of water tank is minimum for circular shaped tank as compared to square shaped and rectangular shaped tanks.

➢ Generally, the construction material-outputs for all water tank capacities would be based on the choice of the design considerations and from the results obtained here points out that the circular shaped tank is the most economical among other two shapes considered for study as per IS3370 – 2009 adopting limit state method of design.

REFERENCES

[1]   W.O.Ajagbe, S I. Adedokun and W.B. Oyesile W.B, Comparative study on the design of elevated rectangular and circular concrete water tanks, *International Journal of Engineering Research and Development 1(1)*, 2012, 22-30.

[2]   R.V.R.K.Prasad, Akshaya B.Kamdi, Effect of revision of IS 3370 on water storage tank, *International Journal of Engineering Research and Applications 2(5)*, 2012, 664-666.

[3]   Tanetal, Minimum cost design of reinforced concrete cylindrical water tanks based on the British Code for   water tanks, using a direct search method, *European Journal of Scientific Research, 49*(4) 2011, 510-520.

[4]   Renmin Yuan, XupingWu, TaoLuo , HuizhiLiu , JianningSun, A review of water tank modeling of the convective atmospheric boundary layer, *Journal of Wind Engineering and Industrial Aerodynamics*.2012

[5]   D. L. Beneke; J. R. Thumkunta; and D. J. Koen, Optimal structural design of circular, rotationally molded, above-ground polyethylene water storage tanks" DOI*: 10.1061/(ASCE)SC .1943-5576.0000080. © 2011 American Society of Civil Engineers*, 2011.

[6]   IS : 456 – 2000, *Plain and Reinforced Concrete – Code of Practice*, 2000

[7]   IS : 3370 (Part I)*, Code of Practice for Concrete Structures for the Storage of Liquids,* 2009.

[8]   IS : 3370 (Part 2), *Concrete Structures for the Storage of Liquids – Code of Practice,* 2009.

[9]   IS : 1786, *Specification for High Strength Deformed Steel Bars and Wired for Concrete Reinforcement,* 1985.

[10]   Ashok K Jain, *Reinforced Concrete Limit State Design* (Roorkee: Nem Chand &Bros, Roorkee,2002)

[11]   Ramamrutham S, *Design of Reinforce Concrete Structures*, (New Delhi: Dhanpat Rai Publishing Company (P) Ltd. 2006)

[12]   I. C. *S*yal *,* A. K. Goel *Reinforced Concrete Structures,* (New Delhi: S.Chand & Co., 2004).

Application of PWM Control Strategy on Z-Source Isolated Dual active bridge DC-DC Converters

N. Mahathi[1], P. Pavan Kumar[2]

[1]*M. Tech (Power Electronics & Electric drives), Dept. of EEE, Anurag College of Engineering, Ghatkesar, Telangana, India[1]*
[2]*Assistant Professor, Dept. of EEE, Anurag College of Engineering, Ghatkesar, Telangana, India[2]*

Abstract: *This project presents a Z-source with bidirectional dc–dc converter. The switching count is reduced by adding a passive element. Thus, we are improving the output voltage level. The voltage regulation range of proposed converter is better than that of the traditional bidirectional dc–dc converter. The fully bridge symmetrical circuit configuration, is neither a high-voltage side nor a low-voltage side in the circuit structure, and the sources connected to the dc side of each H-bridge circuit with voltage sources and current sources. This method can reduce current stress and improves the system efficiency.*

In this paper we are presenting a dual active bridge (DAB) dc–dc converter is also known as Bidirectional DC-DC converter. Both simulation results are shown by using MATLAB software.

Index Terms: *Bidirectional dc–dc converter (BDC), coordinated control, double-closed loop, Z-source.*

I. Introduction

Bidirectional DC–DC converter (BDC) is a dual active bridge converter. It is a two quadrant operating dc–dc converter. Nowadays, the need for electric power is increased. Hence there is a need to implement bidirectional dc-dc converters.

Because of the features of saving in volume, weight, and cost, it has been widely used in applications such as dc motor driving systems, uninterruptible power supplies (UPSs), battery charging and discharging systems, and auxiliary power supplies for hybrid electrical vehicles where the function of bidirectional power flow is required. Generally, BDC is divided into two types: non insulated type and insulated type.

In addition, the isolated BDC (IBDC) is needed to provide absolute electrical isolation between the primary side and the secondary side for protecting the equipment and operators IBDC is usually based on the single phase and H-bridge topology with an isolation transformer.

Fig. 1 shows a typical configuration of Bidirectional DC-DC converter. From the aspect of circuit structure, it has the following points are: 1) The high-frequency transformer provides the required isolation and voltage matching between two voltage levels; 2) transformer voltage ratio is not one, and both sides of the circuit are defined as the high-voltage side compared to the low-voltage side, which makes the installation location of power sources for both sides not interchangeable; 3) the sources connected to the dc side of each H-bridge can only be voltage sources; and 4) the transformer's leakage inductance serves as the instantaneous energy storage device.
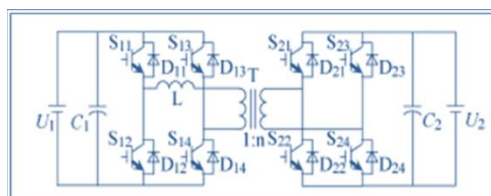
Fig.1 Schematic of the DAB dc–dc converter

This paper presented a Bidirectional DC-DC converter is also known as dual active bridge (DAB) dc–dc converter. We presented a Z-source with bidirectional dc–dc converter by reducing the switching count by adding an passive elements we are going to increases the output voltage level, Comparing with the traditional bidirectional dc–dc converter, the proposed converter has an wider regulation range of voltage and many application based converter for hybrid vehicles and for any hybrid application. The fully bridge symmetrical circuit configuration, is neither a high-voltage side nor an low-voltage side in the circuit structure, and the

sources connected to the dc side of each H-bridge circuit with voltage sources and current sources. This method can reduce current stress and improves the system efficiency.
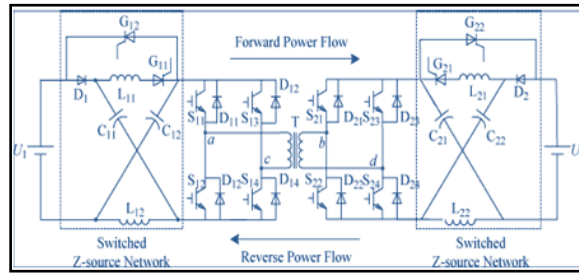

Fig.2 Schematic circuit of a Z- sources with bidirectional dc–dc converter

II. Theoretical Model of Dab Converter

A. Basic Principle of Operation

Fig. 1 consists of two full-bridge circuits connected through an isolation transformer and a coupling inductor *L*, which may be provided partly or entirely by the transformer leakage inductance. The full bridge on the left hand side of Fig. 1 is connected to the HV dc bus and the full bridge on the right hand side is connected to the low-voltage (LV) side. Each bridge is controlled to generate an HF square-wave voltage at its terminals. By incorporating an appropriate value of coupling inductance, the two square-waves can be suitably phase Shifted with respect to each other to control power flow from one dc source to another. Thus, bidirectional power flow is enabled through a small lightweight HF transformer and inductor combination, and power flows from the bridge generating the leading square-wave. Although various modes of operation of the DAB converter have been presented for high power applications the square-wave mode is supposedly the best Operating mode.

This is because imposing quasi-square-wave on the transformer primary and secondary voltages results in trapezoidal, triangular, and sinusoidal waveforms of inductor current in the bidirectional DC-DC converter. These modes are beneficial for extending the low-power operating range of the converter. Although these modes tend to reduce the switching losses, the voltage loss is significant due to zero voltage which reduces the effective power transfer at high-power levels. The key operating waveforms of the converter during buck mode, i.e., when power flows from the HV side to the LV side are shown. The voltages generated by the two full bridges, *VHV* on the HV side and *VLV* on the LV side, are represented as square-wave voltages with 50% duty cycle. But proposed circuit is with Z sources network i.e Switched Z-sources bidirectional DC-DC converter

B. Boost Model

According to the analysis, the upper and lower devices of each phase leg in both H-bridges can be gated on simultaneously, so its reliability is improved greatly. Furthermore, the shoot-through zero state brings the boost ability to the Z sources We also take the forward power flow as an example to analyze. Assuming that the inductors *L*11 and *L*12 and capacitors *C*11 and *C*12 have the same inductance and capacitance, respectively, the Z-source network becomes symmetrical. From the symmetry and the equivalent circuits, we have (3)

$$U_{C11} = U_{C12} = U_C \qquad (1)$$
$$u_{L11} = u_{L12} = u_L \qquad (2)$$

we have

$$u_L = U_1 - U_C \qquad (3)$$
$$u_d = U_1 \qquad (4)$$
$$u_i = U_C - u_L = 2U_C - U_1 \qquad (5)$$

Where, *ud* is the dc-link voltage of the switched Z-source network and *ui* is the dc-link voltage of the H-bridge we have

$$u_L = U_C$$
$$u_d = 2U_C \qquad (6)$$
$$u_i = 0$$

Given that a switching cycle T of SZIBDC consists of two sections, $T0$ for the shoot-through zero state and $T1$ for the normal switch state and the open zero state, respectively, the average voltage of the inductor over one switching cycle should be zero in steady state; thus, from (3) to (8), we have

$$U_L = \overline{u_L} = [T_0.U_C + T_1.(U_1 - U_C)]/T = 0$$

(7)

Where, T = T0 + T1, in which case (7) can then be expressed as

$$\frac{U_C}{U_1} = \frac{T_1}{T_1 - T_0}$$

(8)

In the normal switch state and the open zero state, by substituting (8) into (5), ui can be expressed as

$$u_i = \frac{T}{T_1 - T_0} U_1 = \frac{\pi}{\pi - 2\alpha} U_1$$

(9)

Therefore, we have

$$u_i = \begin{cases} 0, \\ \pi/(\pi - 2\alpha)U_1, \end{cases}$$

(10)

C. Voltage Regulation Model

In the traditional Z-source inverter, the regulation of voltage is achieved by the modulation index M and boost factor B which is unfit for the PWM in the SZIBDC.

Considering this, this paper presents a phase-shifting shoot through control method. Combining with the analysis of Section II, the main waveforms of SZIBDC in phase-shifting shoot-through control are shown in Fig. 6, where the transformer voltage ratio is one, $S0$ is the shoot-through pulse, $uD1$ is the voltage of the diode $D1$, $u$ac and $u$bd are the voltages of the primary and secondary sides of the transformer, respectively, and $iL11$, $iL12$, and $iL22$ are the currents flowing through the inductors $L11$, $L12$, and $L22$, respectively. In the traditional phase-shifting control of the H-bridge, the converter is in the open zero state for an interval ($t0$–$t2$, $t3$–$t5$). By regulating the width of the interval during a switching cycle, the average output voltage can be stepped down. Additionally, from (12), if the shoot-through pulse ($t1$–$t2$, $t4$–$t5$) in the open zero state is added, the average output voltage can be stepped up. Note that the shoot-through zero states are evenly allocated into each phase and it does not change the total zero-state time interval. That is, the active states are unchanged.

III. Simulation Analysis

This paper presented a Z-source with Bidirectional DC-DC converter. We presented a Z-source with bidirectional dc–dc converter by reducing the switching count by adding an passive elements to improve the system efficiency, we are going to increases level of output voltage, Comparing with the traditional bidirectional dc–dc converter, the proposed converter has an wider regulation range of voltage and many application based converter for hybrid vehicles and for any hybrid application. The fully bridge symmetrical circuit configuration, is neither a high-voltage side nor an low-voltage side in the circuit structure, and the sources connected to the dc side of each H-bridge circuit with voltage sources and current sources. This method can reduce current stress and improves the system efficiency.
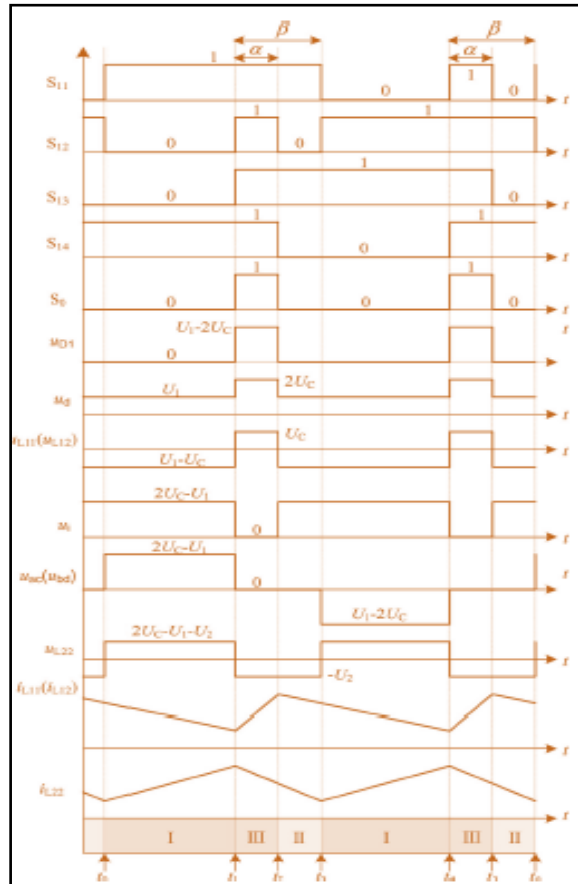
Fig.3 Main waveforms of SZIBDC in phase-shifting shoot-through control

A. Simulation circuit of an forward mode

Main Parameters of SZIBDC

In order to verify the correctness and validity of SZIBDC and its phase-shifting shoot-through bivariate coordinated control strategy, a simulation platform is established in electromagnetic transient simulation software Electro Magnetic Transients Including DC/Power System Computer Aided Design 4.2, and a laboratory prototype shown in Fig. 12 is constructed based on TMS320F2812 DSP. Furthermore, the main parameters of SZIBDC are as follows: inductors L11 = L12 = L21 = L22 = 0.1 mH, capacitors C11 = C12 = C21 = C22 = 220 μF, transformer voltage ratio n = 1, switching frequency f = 5 kHz, discretized values of a switching cycle N = 600, and input voltage U1 = 20 V.
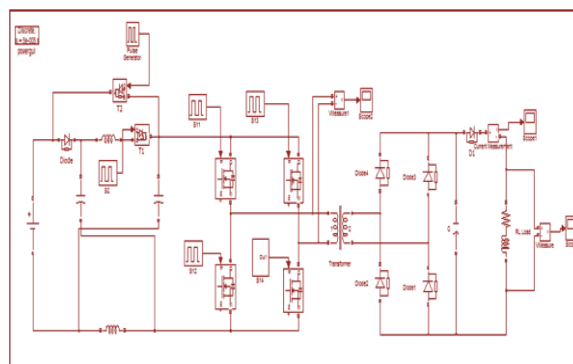
Fig 6.1 simulation arrangement for the proposed system in forward direction
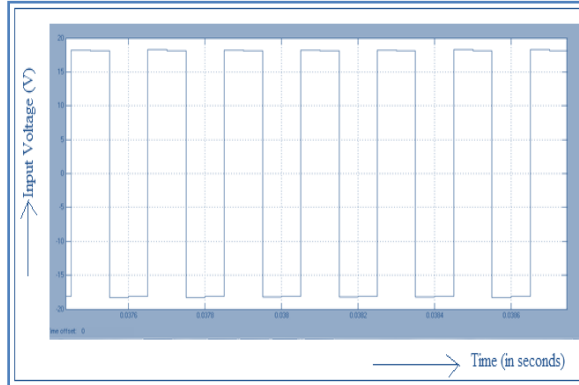
Fig 6.2 input side voltage of transformer in forward mode
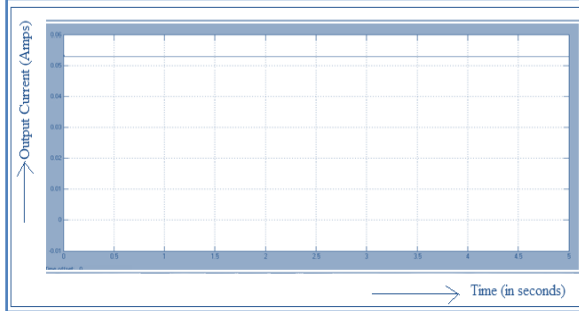
Fig 6.3 Output side current in forward direction mode

Fig 6.4 Output side voltage in forward direction mode
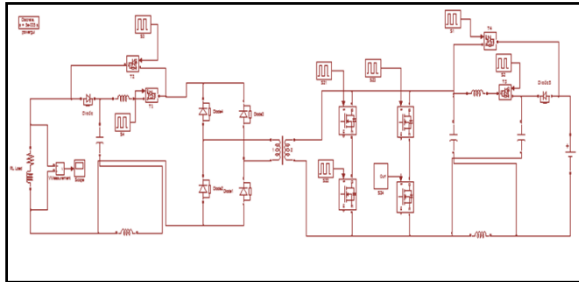
Fig 6.5 simulation arrangement for the proposed system in reverse direction
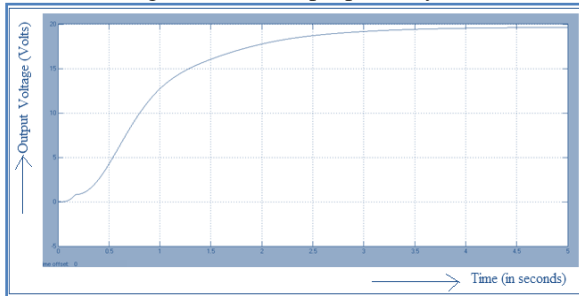
Fig 6.6 Output side voltage in reverse direction mode

B. Extinction of the work
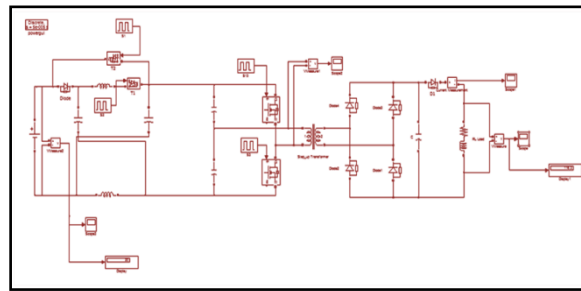
Fig 6.7 simulation arrangement for the proposed extinction of the system in forward direction
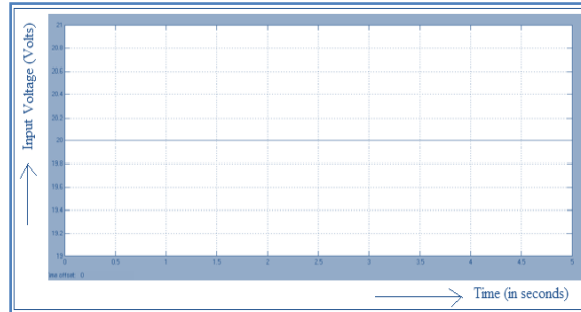
Fig 6.8 Input voltage waveform for the extinction of the system in forward direction mode
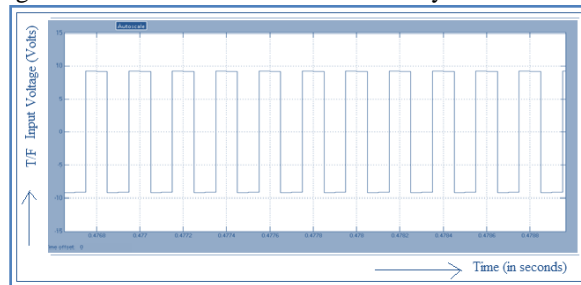
Fig 6.9 Transformer input voltage for the extinction of the system in forward direction mode
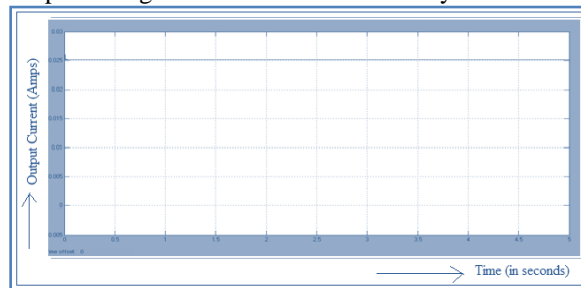
Fig 6.10 Output current waveform for the extinction of the work in forward direction mode

Fig 6.11 Output voltage waveform for the extinction of the system in forward direction mode
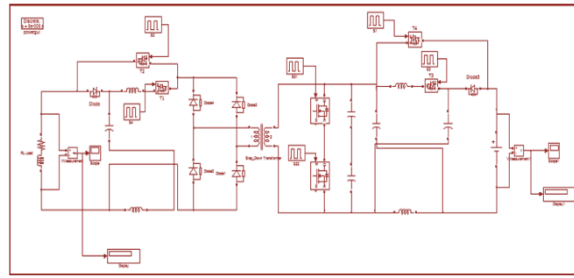
Fig 6.12 simulation arrangement for the proposed extinction of the system in reverse direction mode
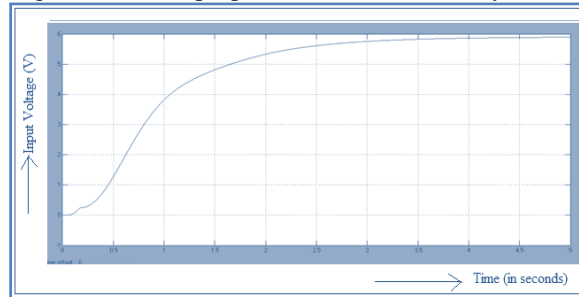
Fig 6.13 Input voltage for the extinction of the system in reverse direction mode
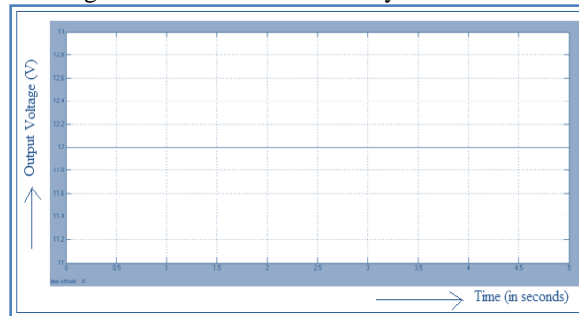
Fig 6.14 Output voltage waveform for the extinction of the system in reverse direction mode

C. Simulation Analysis

In simulation, SZIBDC is in open-loop control for an interval $t = 0$–0.5 s and in closed-loop control for an interval $t = 0.5$–2 s. The output voltage reference is given the values of 10, 40, and 10 V for three intervals $t = 0.5$–1 s, $t = 1$–1.5 s, and $t = 1.5$–2 s, respectively. Fig. 13 shows the simulation results for SZIBDC under different operating states. As can be seen from Fig. 13, in open-loop control ($t = 0$–0.5 s), $\alpha = \beta = 0$, and the output voltage is 19 V which approximately equals the input voltage. When $t = 0.5$ s, SZIBDC enters into bucking start-up closed-loop control ($t = 0.5$–1 s), and the output voltage reference is 10 V. Due to $\alpha = \beta = 0$ at this point, the control system works in control mode II, α remains zero and β increases, the output voltage decreases rapidly and stabilizes in 10 V after 0.04 s, and β stabilizes in 1.56 rad.

When $t = 1$ s, the output voltage reference jumps to 40 V, and SZIBDC jumps into boosting closed-loop control ($t = 1$–1.5 s). Due to $\beta > \alpha = 0$ at this point, the control system changes into control mode III, α remains zero and β decreases, and the output voltage increases. When $t = 1.003$ s, β decreased to be equal with α while the output voltage is lower than 40 V, the control system changes into control mode IV, α and β increase at the same speed, the output voltage increases rapidly and stabilizes in 40 V after 0.07 s, and α and β stabilize in 1.06 rad.

When $t = 1.5$ s, the output voltage reference jumps to 10 V again, and SZIBDC jumps into bucking closed-loop control ($t = 1.5$–2 s). Due to $\beta = \alpha > 0$ at this point, the control system changes into control mode I, α decreases and β remains constant, and the output voltage decreases. When $t = 1.535$ s, α decreases to zero while the output voltage is higher than 10 V, the control system changes into control mode II, β increases, the output voltage decreases rapidly and stabilizes in 10 V after 0.03 s, and β stabilizes in 1.56 rad. Note that the final state of the process is in line with the previous bucking start-up closed-loop control.

IV. Conclusion

In this project, by reducing the switching count and by adding a passive elements we improved the output voltage level of Z-sourced bidirectional dc–dc converter, Comparing with the traditional bidirectional dc–dc

converter, the proposed converter has an wider regulation range of voltage. This method can reduce current stress and improves the system efficiency. Both the simulation results are checked by using MATLAB software.

REFERENCES

[1] A. Shahin, M. Hinaje, J. P. Martin, S. Pierfederici, S. Rael, and B. Davat, "High voltage ratio dc-dc converter for fuel-cell applications," IEEE Trans. Ind. Electron., vol. 57, no. 12, pp. 3944–3955, Dec. 2010.

[2] R. P. T. Bascope, D. S. Oliveira, C. G. C. Branco, and F. L. M. Antunes, "A UPS with 110 V/220 V input voltage and high-frequency transformer isolation," IEEE Trans. Ind. Electron., vol. 55, no. 8, pp. 2984–2996, Aug. 2008.

[3] J. S. Bong, S. K. Jin, D. L. Jae, and S. K. Young, "The design of the PI compensator for the bidirectional dc-dc converter in the dc distributed power system," in Proc. IEEE Elect. Mach. Syst. Intell. Conf., 2010, pp. 372–376.

[4] P. Garcia, L. M. Fernandez, C. A. Garcia, and F. Jurado, "Energy management system of fuel-cell-battery hybrid tramway," IEEE Trans. Ind. Electron., vol. 57, no. 12, pp. 4013–4023, Dec. 2010.

[5] P. Das, B. Laan, S. A. Mousavi, and G. Moschopoulos, "A nonisolated bidirectional ZVS-PWM active clamped dc-dc converter," IEEE Trans. Power Electron., vol. 24, no. 2, pp. 553–558, Feb. 2009.

[6] L. S. Yang and T. J. Liang, "Analysis and implementation of a novel bidirectional dc-dc converter," IEEE Trans. Ind. Electron., vol. 59, no. 1, pp. 422–434, Jan. 2012.

[7] M. B. Camara, H. Gualous, and F. Gustin, "DC/DC converter design for supercapacitor and battery power management in hybrid vehicle applications-polynomial control strategy," IEEE Trans. Ind. Electron., vol. 57, no. 2, pp. 587–597, Feb. 2010.

[8] F. Z. Peng, H. Li, G. J. Su, and J. S. Lawler, "A new ZVS bidirectional dc-dc converters for fuel cell and battery application," IEEE Trans. Power Electron., vol. 19, no. 1, pp. 54–65, Jan. 2004.

[9] W. Chen, P. Rong, and Z. Y. Lu, "Snubberless bidirectional dc-dc converter with new CLLC resonant tank featuring minimized switching loss," IEEE Trans. Ind. Electron., vol. 57, no. 9, pp. 3075–3086, Sep. 2010.

[10] S. Jalbrzykowski, A. Bogdan, and T. Citko, "A dual full-bridge resonant class-E bidirectional dc-dc converter," IEEE Trans. Ind. Electron., vol. 58, no. 9, pp. 3879–3883, Mar. 2011.

[11] F. Krismer and J. W. Kolar, "Accurate power loss model derivation of a high-current dual active bridge converter for an automotive application," IEEE Trans. Ind. Electron., vol. 57, no. 3, pp. 881–891, Mar. 2010.

[12] M. N. Kheraluwala, R. W. Gascoigne, D. M. Divan, and E. D. Baumann, "Performance characterization of a high-power dual active bridge dc-todc converter," IEEE Trans. Ind. Appl., vol. 28, no. 6, pp. 1294–1301, Nov./Dec. 1992.

[13] B. Hua and M. Chris, "Eliminate reactive power and increase system efficiency of isolated bidirectional dual-active-bridge dc-dc converters using   novel dual-phase-shift control," IEEE Trans. Power Electron., vol. 23, no. 6, pp. 2905–2914, Nov. 2008.

[14] Y. H. Xie, J. Sun, and S. F. James, "Power flow characterization of a bidirectional galvanically isolated high-power dc/dc converter over a wide operating range," IEEE Trans. Power Electron., vol. 25, no. 1, pp. 54–65, Jan. 2010.

[15] C. Mi, H. Bai, C. Wang, and S. Gargies, "Operation, design and control of dual H-bridge-based isolated bidirectional dc-dc converter," IET Power Electron., vol. 1, no. 4, pp. 507–517, May 2008.

[16] D. Vinnikov and I. Roasto, "Quasi-Z-source-based isolated dc/dc converters for distributed power generation," IEEE Trans. Ind. Electron., vol. 58, no. 1, pp. 192–201, Jan. 2011.

[17] M. S. Shen, A. Joseph, J. Wang, F. Z. Peng, and D. J. Adams, "Comparison of traditional inverters and Z-source inverter for fuel cell vehicles," IEEE Trans. Power Electron., vol. 22, no. 4, pp. 1453–1463, Jul. 2007.

[18] K. R. Wang, F. C. Lee, and J. Lai, "Operation principles of bi-directional full-bridge dc-dc converter with unified soft-switching scheme and soft starting capability," in Proc. IEEE Appl. Power Electron. Conf., 2000, pp. 111–118.

BIOGRAPHY

N MAHATHI, received her B.Tech degree in Electrical and Electronics Engineering, in 2010 and pursuing M.Tech degree in Power Electronics and Electric Drives from Anurag College Of Engineering**,** Aushapur (V), Ghatkesar (M), R.R. (Dist.).
She is interested in Power Electronics, FACTS devices and their applications.

Mr. P. PAVAN KUMAR presently he is working as Assistant professor in Anurag College of Engineering, Aushapur (V), Ghatkesar (M), Ranga Reddy (Dist), Telangana, India. He did his B.Tech degree in Electrical & Electronics Engineering from Chaitanya College of Engineering, Vizag (Dist), Andhra Pradesh, India. And then completed his M.Tech in Electrical & Electronics Engineering as Power Electronics and Electric Drives is specialization at Vardhaman College of Engineering, Ranga Reddy (Dist), Telangana, India. He has a teaching experience of 3 years. His research area includes Power Electronics and Electric Drives and Control systems.

BER Estimation for Laser Based Underwater Communication

Preeti Kumari[1], Anjesh Kumar[2]

[1]*(Amity University, Gurgaon)*
[2]*(Scientist, DRDO, New Delhi)*

Abstract: Apart from land and air, sea has also become very important from defense strategic point of view and is required to be integrated with network centric communication. In future it may play a very important role in network centric warfare. Free space laser communications provide wide bandwidth and high security capabilities to unmanned aircraft systems in order to successfully accomplish intelligence, surveillance, target acquisition, and reconnaissance missions[l] Laser based communication is emerging as a most promising solution for underwater communication. Most of laser cannot penetrate through the sea due to be absorbed by the sea, but the blue-green laser (the wavelength is about $470 \sim 570nm$) has the minimum energy fading in the sea, whose fading rate is about 0.155~0.5dB/m, this feature of blue-green laser in the sea is said the window effect[2]. Long-range links use directed laser beams to transmit data, and can be used for building-to-building, ground-to-aircraft, or ground-to-satellite communication [3]. Laser communication throws quite different challenges in water in respect to air. Laser attenuation in water is key bottleneck for underwater communication as attenuation in water is roughly 1000 times as in air. This exponential variation plays a very important role in determining the type of laser (CW or Q switched laser) and place a restriction on the use of CW laser for longer distance because of impractical sizes. Turbulences and variation in salt concentration in different part of a sea and in different seas imposes a dynamic challenge for underwater laser communication. Issues at sea-air interface for aerial platform to underwater communication also plays crucial role for establishing an uninterrupted communication link. All these issues throttle the effective baud rate of transmission.

I. Introduction

Transmission of data at lower bit error rate (BER) is foremost characteristic of a communication system. It is a very important parameter to be considered while modeling a communication system and specially communication channel as sources of error at transmitting and receiving end can be modeled and optimized more deterministically. ON-OFF Key (OOK) is the most common and simple (Implementation point of view) modulation technique for CW laser beam. It is perfect solution for laser communication in air. In water, laser attenuation is roughly 1000 times with respect to air so power requirement for underwater communication is huge and vary exponentially . Size of CW laser imposes a practical constraint for higher power. Q switched pulse laser is a ideal solution for high peak power requirement but imposes a constraint on modulation technique.. Other possible modulation technique pulse width modulation (PWM) varies the energy of the Q switched pulses and hence the overall communication path length degrades. In this paper we have calculated the bit error rates for different sources of error in the water channel for both OOK and PPM.

BER calculation: Attenuation of laser beam in water degrades its intensity drastically and it degrades signal amplitude at the detector output. Decision device will occasionally make error and consider symbol 1 as symbol 0. To determine the average probability of error, we first consider the two possible kind of error separately. Assume that symbol 0 was transmitted, corresponding to a level of 0 volts. The output signal y(t) then consists of noise alone, as shown by

$$Y(t) = n(t), \qquad \text{symbol } 0 \text{ was sent}$$

When symbol 0 is transmitted, the random variable y_k is Gaussian-distributed with zero mean and variance σ^2 where y_k denote the sample value obtained by observing the sample function y(t) at time $t = t_k$ and Y_k denote the corresponding random variable Hence, the conditional probability density function of y_k given that symbol 0 was transmitted, equals

$$f_{Yk/0}(y_k/0) = \frac{1}{\sqrt{2\pi}\sigma} exp\left(-\frac{y_k^2}{2\sigma^2}\right)$$

Let P_{eo} denote the conditional probability of error, given that symbol 0 was transmitted. This probability is defined by the area under the $f_{Yk/0}(y_k/0)$ curve, from A/2 to ∞, which can be expressed as:

$$P_{eo} = \frac{1}{2} erfc\left(\frac{A}{2\sqrt{2}\sigma}\right)$$

The conditional probability density function of y_k given that symbol 1 was transmitted, can be expressed as

$$f_{Yk/1}(y_{k/1}) = \frac{1}{\sqrt{2\pi}\sigma} exp\left[-\frac{(y_k - A)^2}{2_{\sigma^2}}\right]$$

Let P_{e1} denote the conditional probability of error, given that symbol 1 was transmitted. This probability is defined by the area under the $f_{Yk/1}(y_{k/1})$ curve, from $-\infty$ to A/2. Assuming equally probable symbols and setting threshold midway between 0 and A, implies $P_{e1}=P_{eo}$. To determine the average probability of error in the receiver, we note that the two possible kinds of error considered above are mutually exclusive events in that if the receiver, at a particular sampling instant, chooses symbol I, then symbol 0 is excluded from appearing, and vice versa. Furthermore, P_{eo} and P_{e1} are conditional probabilities with P_{eo} assuming that a 0 was transmitted and P_{e1} assuming that a 1 was transmitted. Thus, assuming that the a priori probability of transmitting a 0 is P_o, and the a priori probability of transmitting a 1 is P_1, we find that the average probability of error P_e in the receiver is given by

$$P_e = P_o P_{eo} + P_1 P_{e1}$$

Since $P_{e1}=P_{eo}$ and we have assumed that $P_o=P_1$, we obtain

$$P_e = P_{e1} = P_{eo}$$

Which is given as:

$$P_e = \frac{1}{2} erfc\left(\frac{1}{2}\sqrt{\frac{\gamma}{2}}\right)$$

Where γ is the signal to noise ratio.

The above calculation is for the case of on-off keying. Now we analyze the probability of error for a Pulse Position Modulation (PPM) system. The PPM generally is applied to higher data rate in the underwater laser communication. The PPM adopts optical pulse as the carrier which is controlled by the modulated signal. The pulse position is varied with the modulated signal, and the message is transmitted via this position variation. The efficiency of Pulse position modulation is higher than others modulations, especially in the underwater laser communication system and it are most optimized. *k*-PPM decreases the average power requirement at the cost of large bandwidth[4]. In terms of power efficiency if the *k* is greater than 2, PPM modulation exhibits a higher efficiency than OOK does. An increase in *k* causes an increase in the bandwidth requirement. The average number of bit errors per *k*-bit symbol is:

$$P_b = \frac{2^{k-1}}{2^k - 1} \cdot P_m$$

Where P_b is the average number of bit errors per *k* bit symbol and P_m is the bit error rate for a PPM system.

II. Lab setup for BER analysis

Transmitter: 200mW frequency double ND-YAG green laser operating at 532nm
Water channel: Water tank of path length 10 m
Data transfer rate: 10 Kbps
Detector: Silicon PIN photodiode
Mode: Duplex(full/half)/Chat mode
File type: Text file and Binary file

To estimate the BER, four sources of error are considered in the above setup as follow:
1.   Effect of channel attenuation on BER
2.   Effect of channel turbulence on BER
3.   Effect of ambient noise on BER
4.   Effect of laser ON-OFF stabilization rate on BER
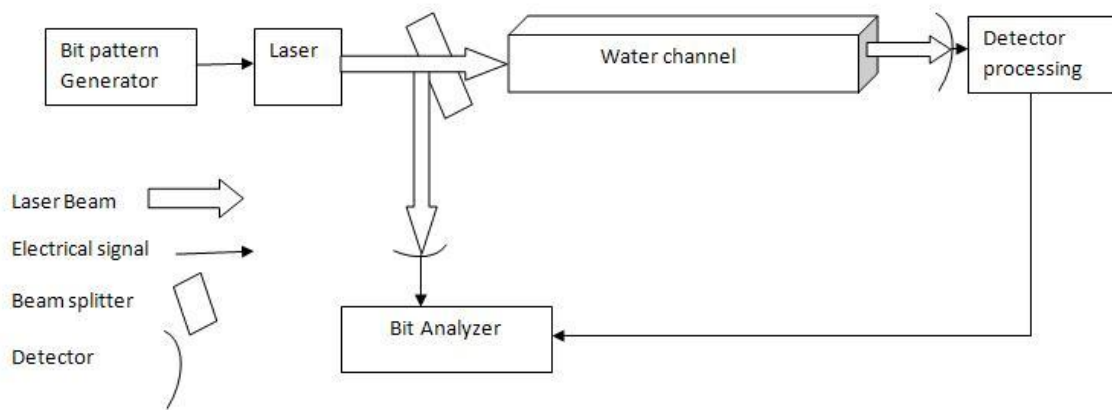
1. Effect of channel attenuation on BER: Channel attenuation plays very crucial role in determining the BER of a laser based communication system. Attenuation of laser beam propagation varies exponentially. Keeping other factors constant (K), Attenuation (α) is the only variable. Laser propagation equation can be expressed as

$$P_r = P_t.e^{-\alpha x}$$

Where P_r is received power, P_t is transmitted power and x is the path length. Attenuation is most important factor for deciding the power requirement of a communication channel. Attenuation factor α of water is 1000 times of the air implies huge laser power requirement for underwater communication. Unit of attenuation constant of beam of light is m^{-1} and used for finding laser attenuation underwater. It is not dependent on wavelength and is approximately equal to 0.02 m^{-1} in clear water [5]. To analyze the effect of α in the above setup, attenuation of water is varied by adding NaCl in various concentrations and keeping other sources of errors inactive. Transmitted laser power is kept constant and intensity modulated by a bit pattern generator. Received power and bit pattern generated at the detector are compared with transmitted laser beam to analyze the attenuation factor and BER. Results are present in the table below:

	OOK	PPM
Types of water	Av. BER(per 1Mb)	
RO water	< 1	<0.5
Tap water	< 1.5	<0.75
Salt water1	< 1.5-2.0	<1
Salt water2	< 2.5	<1.5

2. Effect of intrachannel turbulence on BER: Sea waves may contribute to BER. Disturbance at sea surface plays very crucial role in aerial platform to underwater communication. Waves at sea surface changes the incident angle of incoming aerial laser beam dynamically. This effect leads to the beam dancing at receiver. Maximum deviation of beam from normal may be 10.6°(paper reference). In present experiment only intra-water disturbances are simulated using water churning motor placed at interval of 1.5m.Without churning and with churning (RPM) average BER remains less 1 bit/Mb.

	OOK	PPM
Turbulence	Av. BER(per 1Mb)	
No churn	< 1	<0.5
With churn	< 1	<0.5

3. Effect of ambient light on BER: Ambient light at the detector may lead to the receiver decision error. Probability of discrimination between '1' and '0' decreases with increase in ambient light level. Ambient light effect may be diminished by using very sharp laser line filters but fabrication of very narrow laser line width (nm) filter is a great challenge worldwide Receiver should be very robust to handle the effect of ambient noise. In the above setup BER is calculated under different light condition and keeping other error sources inactive. Results are presented in the table below:

	OOK	PPM
Light intensity	Av. BER(per 1Mb)	
No light	< 1	<0.5
100W bulb	1-2	0.5-1

4. Effect of laser ON-OFF stabilization rate on BER: Here we have used Nd-Yag laser rated 30 KHz TTL modulation. it was observed that up to 10 KHz the laser works smoothly but after 10 KHz it starts missing pulses. Due to these missed pulses there is an increase in the bit error rate.

	OOK	PPM
frequency	Av. BER(per 1Mb)	
10 KHz<	< 1	<0.5
10KHz to 15 KHz	< 2.5	<1
>15 KHz	< 3.0-4.0	<1.5-2

III.   Conclusion

As the salt content of water increases the bit error rate increases. Churning of water has no considerable effect on the bit error rate. As the frequency of the laser is increased beyond 10 kHz the bit error rate increases significantly. When the source of ambient light is brought very near to the receiver the BER increases drastically and all the information content is lost. PPM modulation technique offers less BER as compared to OOK and provides an improved overall performance.

REFERENCES

[1]   S. Luryi, M. Gouzman, "Feasibility of an optical frequency modulation system for free-space optical communications". International Journal of High Speed Electronic System, Volume 16, Issue 2, pp 559–566. 2006.
[2]   Ziad T. Al Dahan , Samar Y. Al Dabagh and Asmahan Assad. "Design and Implementation of Under Water Optical Communication System", International Journal of Application or Innovation in Engineering & Management (IJAIEM), Volume 2, Issue 6, June 2013.
[3]   X. Zhu, and J. M. Kahn, "Free-space optical communication through atmospheric turbulence channels," IEEE Trans. on Commun. 50, pp1293-1300. 2002.
[4]   Viorel Manea, Radu Dragomir, Sorin Puscoci. "OOK and PPM modulations effects on bit error rate in terrestrial laser transmissions", Institutul Național de Studii și Cercetări pentru Comunicații – I.N.S.C.C, Telecomunicații Anul LIV volume 2, pp 56-58, 2011.
[5]   Yagimli "Design of Laser Based Underwater Communication System". Journal of Naval Science and Engineering, Volume 7, Issue 2, pp 1-10. 2011.

International Journal of Modern Engineering Research (IJMER)

Contents :

Effect of Co doping on the structural and physical properties of $SrC_4H_4O_6.3H_2O$ and $SrC_4H_4O_6.4H_2O$ crystals

T. Vijayakumari[1], C. M. Padma[2], C. K. Mahadevan[3]

[1,2]*Physics Research Centre, Women's Christian College, Nagercoil-629001, Tamilnadu, India*
[3]*Centre for Scientific and Applied Research, PSN College of Engineering and Technology, Tirunelveli-627152, Tamilnadu, India*

ABSTRACT: *Single crystals of strontium tartrate and cobalt doped strontium tartrate crystals were grown by the single diffusion gel growth technique. The growth conditions were optimized by varying the parameters such as pH, concentration of the gel, gel setting time and concentration of the reactants. Silica gel was used as the growth medium with test tubes as crystallization vessels. Crystals having different morphologies were obtained (transparent and few opaque). The grown crystals were characterized by carrying out PXRD, SXRD, FTIR spectral, UV-Vis-NIR spectral, SHG, PL spectral, AAS, microhardness and TG/DTA measurements. The tri hydrate crystals belong to the monoclinic crystal system and the tetra hydrate crystals belong to orthorhombic crystal system and are optically transparent, NLO active, mechanically soft and thermally stable up to 100 °C. AAS measurement revealed the presence of Co atoms in the doped crystals. Results indicate that Co-doping significantly increases SHG efficiency. Details are presented.*

Keywords: *Gel technique, mechanical properties, optical properties, PXRD, SXRD.*

I. Introduction

Single crystals and polycrystalline form of materials are of great interest, from both solid state sciences aswell as technological point of view.A series of pure and mixed crystals have been grown by several researchers with the aim of identifying new materials for practical and industrial purposes[1]. A systematic study of crystallization in gels began with Liesegang's famous discovery of periodic crystallization in gels [2,3]. The gel technique is an alternative technique to solution growth with controlled diffusion and is free from convection. Gel media prevent turbulence and help in the formation of crystals by providing a framework of nucleation sites[1].

Tartaric acid may serve as a base for the development of new class of materials. Mainly tartrate crystals possess application as dielectric, ferroelectric and piezoelectric materials along with non-linear optical properties [4]. Because of these characteristics, the tartrate crystals are utilised in transducers, linear and non-linear mechanical devices, crystal oscillators and resonators and controlled laser emission [5,6]. Strontium tartrate is used in ammunition units.Some tartrate compounds are used in military applications. The non-linear nature of ferroelectric materials can be used to make capacitors with tunable capacitance. Nowadays great attention has been devoted to the growth and characterization of pure and doped tartrate crystals with the aim of identifying new materials for application purposes [7]. Strontium tartrate tetrahydrate crystal is reported to be orthorhombic[8]. Strontium tartrate trihydrate is reported to be monoclinic[9]. The effects of dopants on various properties of single crystals are of great interest for both solid state science as well as technological point of view [7]. Cobalt tartrate crystals have several applications in semiconductors, medicine, optics, gold industries, veterinary drugs, etc[1].

In the present study, single crystals of pure and cobalt doped strontium tartrate tri and tetrahydrate crystals were grown by the gel technique. Optimum growth conditions were determined by varying gel concentration, pH, gel setting time and concentration of reactants. The grown crystals were characterized by carrying out powder X-ray diffraction (PXRD), single crystal X-ray diffraction (SXRD), FTIR spectral, UV-Vis-NIR transmittance spectral, photoluminescence (PL) spectral and atomic absorption spectroscopic (AAS), second harmonic generation (SHG), microhardness and thermogravimetric (TG/DTA) measurements. The results obtained are reported and discussed herein.

II.   Growth Of Single Crystals

Good quality single crystals can be grown in gels in a variety of ways; the test tube diffusion method was employed to grow pure and cobalt doped strontium tartrate tri and tetrahydrate crystals. The apparatus used for crystallization consists of borosilicate glass tubes. Silica gel was prepared by adding a solution of sodium meta silicate and tartaric acid by stirring slowly [3]. A fixed amount of gel solution with 1.03g/cm^3 specific gravity and pH was set at 4.0 by adding 0.5M tartaric acid and transferred to several test tubes. The test tubes were sealed. The setting of gel is strongly dependent on pH. High pH value gel takes lower time to set than the low pH value[10].After gel setting, the supernatant solution, strontium chloride of 0.5M was poured over the gel slowly. The test tube was kept undisturbed at room temperature. The supernatant solution diffuses in to the gel column and reacts with the inner reactant, giving rise to the formation of strontium tartrate crystals [6]. We obtain pale yellowish crystals at the bottom of tubes along with transparent and faceted crystals near the gel surface [11]. The chemical reaction is [12,13,14]:

$SrCl_2 + C_4H_6O_6 \longrightarrow SrC_4H_4O_6 + 2HCl$
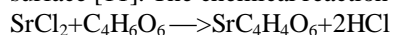
The yellowish crystals were strontium tartrate tetrahydrate(ST4) and the transparent well faceted crystals were strontium tartrate trihydrate(ST3) [11]. For the growth of cobalt doped strontium tartrate crystals, the supernatant solution was a mixture of 0.5M strontium chloride and 0.0025/0.005M cobalt chloride. Slow diffusion of the upper reactant ions through the narrow pores of the silica gel leads to the formation of crystals[14].

Two types of crystals were got in a same test tube due to the change in pH. After the supernatant solution was added, it diffuses in to the gel media and the pH value in the gel surface decreases to 2.6. The bottom layer of the gel remains in the pH value 3.8. It was found that when the pH value is raised from 4.5 to 5, more number of tetrahydrate crystals were obtained. If the pH is lowered to 3, more number of trihydrate crystals can be obtained. The growth of these crystals depends strongly on pH and the specific gravity of the gel. In the discussion hereafter the doped crystals are named as CST31, CST41, CST32 and CST42 (3 for tri and 4 for tetra).

The optimum conditions obtained for the growth of pure and cobalt doped strontium tartrate tetrahydrate crystals are given in Table 1. The crystallographic parameters obtained are provided in Table 2. Figs. 1-3 show the grown crystals of pure and cobalt doped strontium tartrate crystals (ST3,ST4,CST31,CST41, CST32 and CST42).

Table1: Optimum conditions obtained for the growth of pure and cobalt doped strontium tartrate crystals

Parameters	ST3/ST4	CST31/CST41	CST32/CST42
Density of sodium meta silicate (g/cm^3)	1.03	1.03	1.03
Concentration of tartaric acid (M)	0.5	0.5	0.5
pH	4	4	4
Temperature (^{0}C)	30	30	30
Concentration of strontium chloride (M)	0.5	0.5	0.5
Concentration of cobalt chloride (M)	---	0.0025	0.005
Gel setting time (week)	1	1	1
Crystal growth time (days)	25	25	25

(a)   (b)   (c)
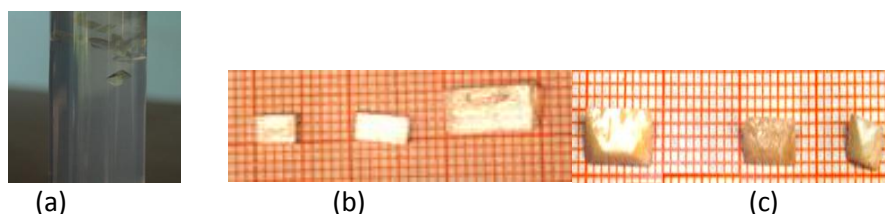
Fig.1: Photographs showing the (a)growing ST3 and ST4 crystals, (b)grown ST3crystals and (c)grown ST4 crystals
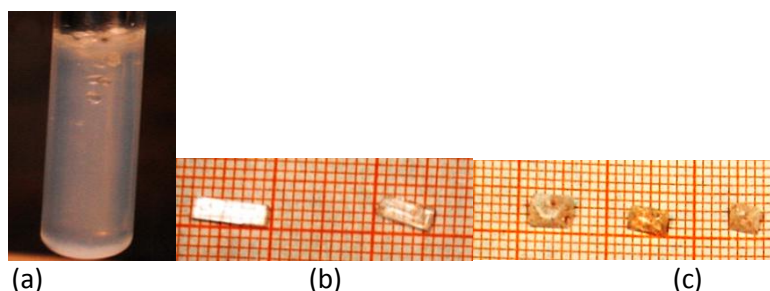
Fig.2: Photographs showing the (a)growing CST31 and CST41 crystals, (b)grown CST31 crystals and (c)grown CST41 crystals
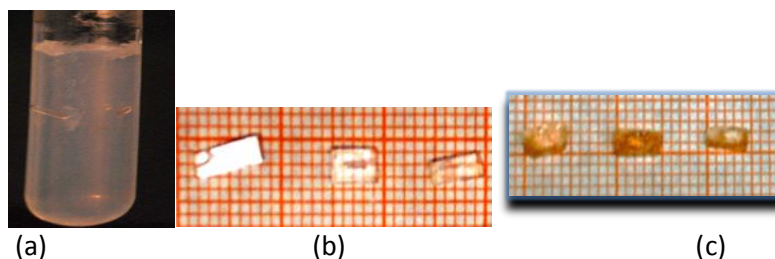
Fig.3: Photographs showing the (a)growing CST32 and CST42 crystals, (b)grown CST32 crystals and (c)grown CST42 crystals

III. PXRD and SXRD Analysis

The PXRD patterns were recorded using an automated X-ray powder diffractometer with Cu Kα (λ=1.54056 Å) radiation. The indexed (using a software) PXRD patterns are shown in Fig.4.The crystallinity of the crystals are quite clear from the occurance of sharp peaks at specific Bragg angles. SXRD data were collected using an EnrafNonius CAD4-F diffractometer. Lattice parameters were determined and the crystal system was identified. The SXRD analysis indicates that the cell parameters obtained for the pure crystals are closely matching with the values already reported [8,9]. No significant variation of lattice parameters due to doping is observed which indicates that cobalt doping does not lead to any serious lattice distortion. However, the small increase in lattice volume observed due to doping indicates that the cobalt atoms have entered into the strontium tartrate crystal matrix.
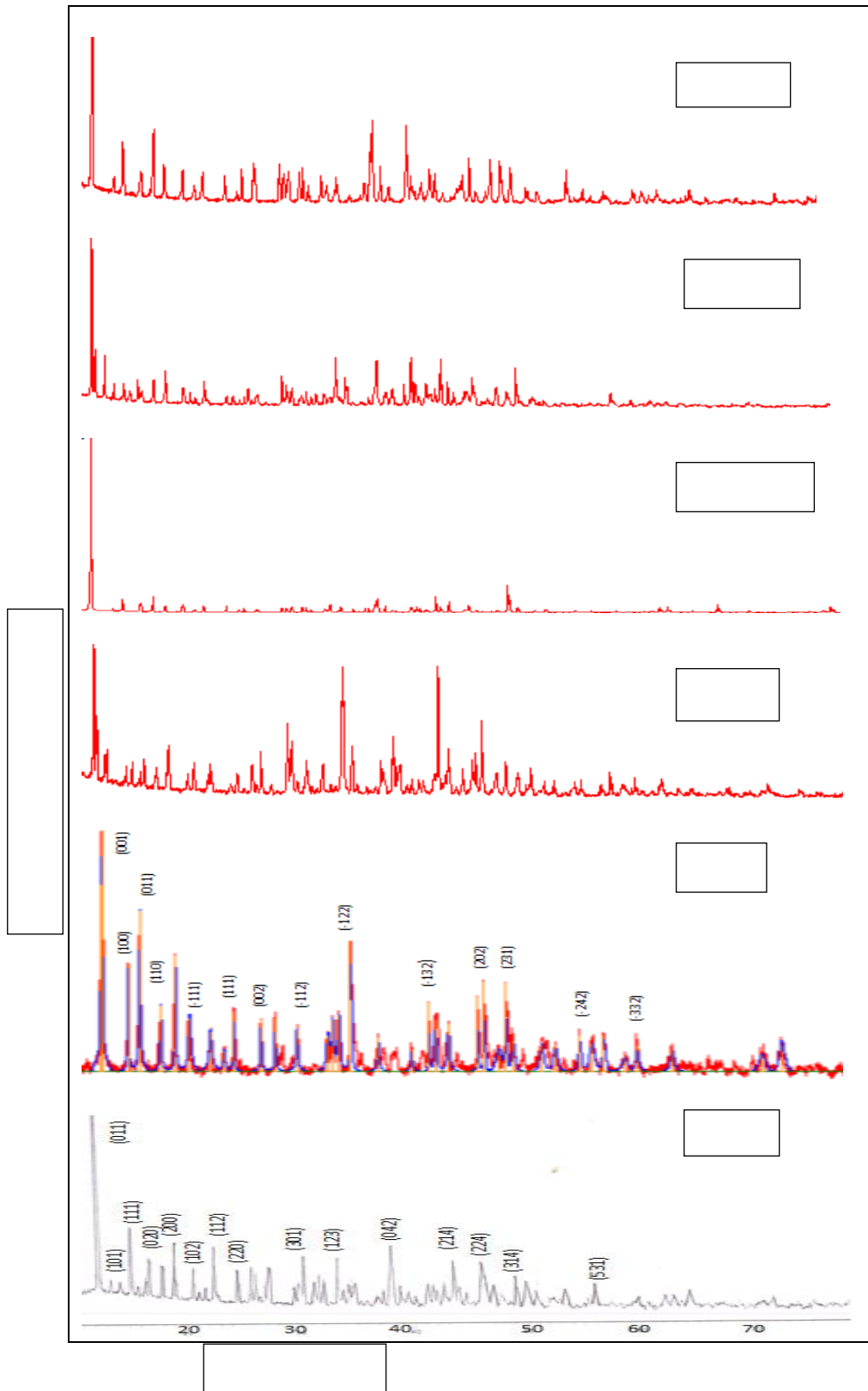
Fig.4: The PXRD patterns observed

Table2: Crystallographic parameters for pure and cobalt doped strontium tartrate crystals

Parameters	Pure(ST 3)		Pure(ST4)		CST31	CST41	CST32	CST42
	Reported [9,11]	Present work	Reported[8]	Present Work				
a(Å)	7.55	7.47	9.48	9.47	7.48	9.44	7.48	9.47
b(Å)	10.06	10.03	10.96	10.92	10.03	10.91	10.04	10.92
c(Å)	6.47	6.44	9.46	9.39	6.47	9.49	6.50	9.50
Crystal system	monoclinic	monoclinic	orthorhombic	orthorhombic	monoclinic	Orthorhombic	monoclinic	orthorhombic
Space group	P2$_1$	P2$_1$	P2$_1$2$_1$2$_1$	P2$_1$2$_1$2$_1$	P2$_1$	P2$_1$2$_1$2$_1$	P2$_1$	P2$_1$2$_1$2$_1$
Volume(Å^3)	491.42	482.51	984.98	971.04	485.41	977.38	488.14	982.42

IV.   FTIR Spectral and AAS Analysis

The FTIR spectra were recorded by employing a SHIMADZU spectrometer in the wave number range 400-4000cm^{-1}for the grown crystals are shown in Fig. 5. Due to the small dopant concentration, there is no significant difference observed for the doped crystals.

The O-H stretching frequency of the sample appears at 3400 cm^{-1}[1]. The bands at 3200 cm^{-1} are assigned to C-H stretching vibrations [10,14,15]. This indicates the presence of water and it belongs to free water symmetry stretch. The strong C-O stretch has been found around 1399cm^{-1} [6]. C-O-C asymmetric strong stretching has been observed in the range 1300-1270cm^{-1}[6]. The band at 1591cm^{-1}is attributed to the C-O stretch of carbonyl group [6,16].

The AAS analysis carried out by using a Perkin Elmer spectrophotometer indicates the presence of cobalt in the doped crystals. The Co content present in the crystal is nearly proportional to the concentration considered in the solution used for the growth of single crystals. It is found that the tetrahydrate crystals are having high cobalt content than the trihydrate crystals (see Table 3).
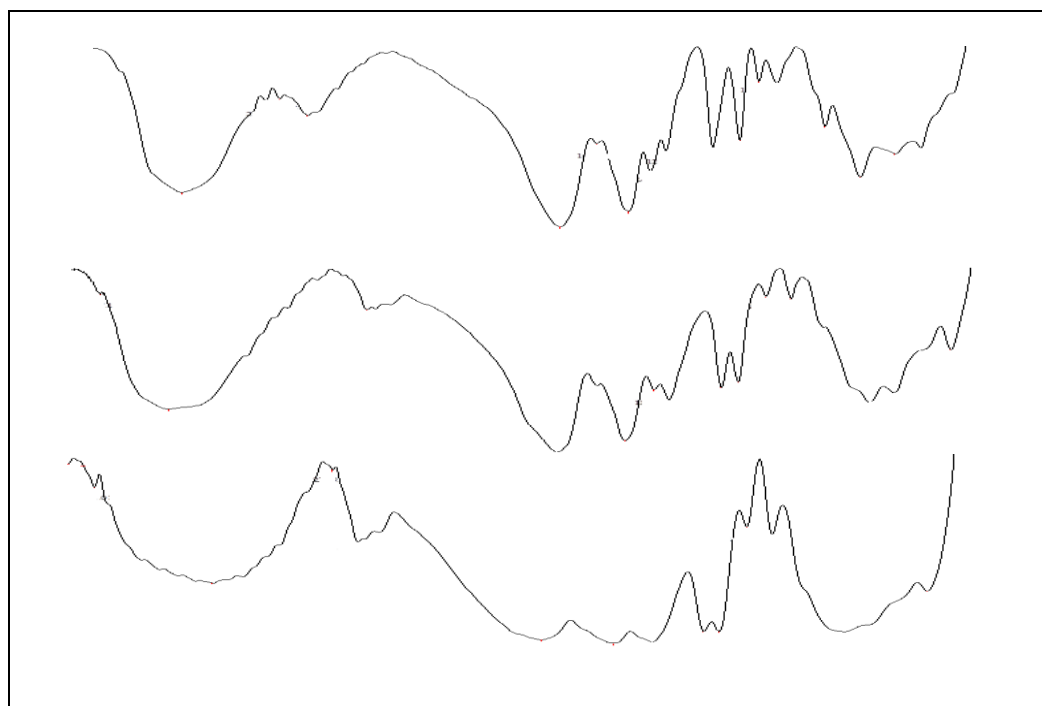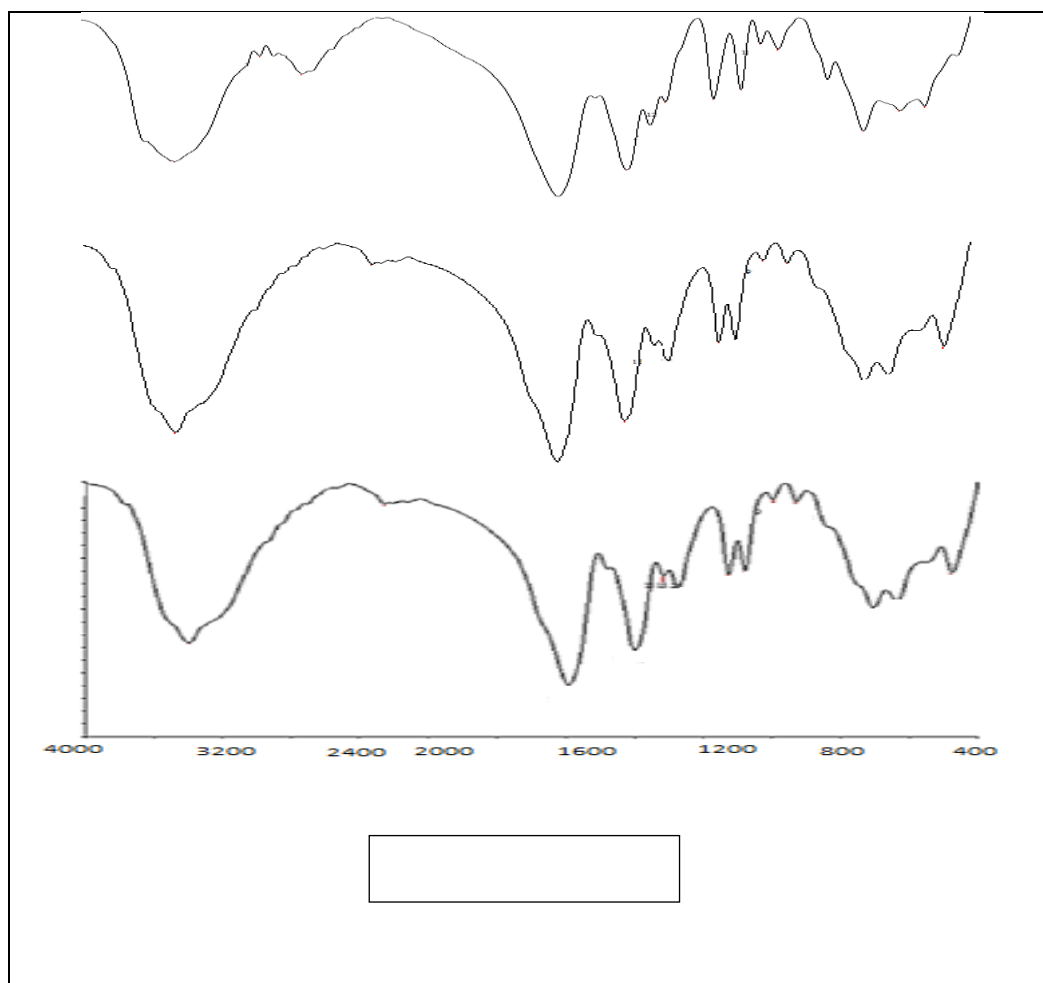
Fig.5 : The FTIR spectra(From top CST31, CST41, CST32, CST42, ST3 and ST4)

V. Optical Properties

Single crystal is mainly used in opto-electronic applications. So, the optical transmission range and transparency cut-off wavelength are essential [17]. UV-Vis-NIR transmittance spectra (shown in Fig. 6) of pure and cobalt doped strontium tartrate crystals dissolved in water were recorded using a SHIMADZU UV-2450 UV-Visible Spectrophotometer in the wavelength range 200-1100nm. From the spectra it can be seen that these crystals have sufficient transmission in the entire visible and most of the UV regions. There is a transparency around 250nm which shows that thesecrystals are suitable for second harmonic generations[18].Efficient nonlinear optical crystals have an optical transparency lower cut off wavelengths between 200 and 400nm. From this, it can be understood that these crystals can be considered as promising nonlinear optical (NLO) crystals.
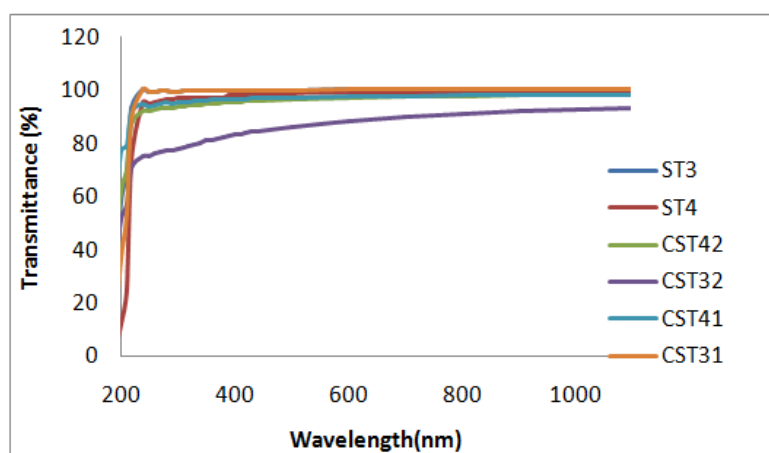
Fig.6: The observed UV-Vis-NIR spectra

The second harmonic generation property was tested for the grown crystals by passing the output of Nd-YAG Quanta ray laser through the crystalline powder sample. The SHG efficiencies observed for the grown crystals are given in Table 3. All the grown crystals are observed to be NLO active.The SHG efficiency increases very significantly due to doping.

Photoluminescence spectra (shown in Fig. 7) were recorded using a Perkin Elmer LS55 fluorescent spectrophotometer at room temperature. The spectra show three peaks at 390, 520 and 770nm. Most intense peak is at 390nm which is the violet emission. Peak at 520 nm, the green emission is less intense and there is red emission at 780nm having sharp peak [4]. It can be seen that the grown crystals are having the fluorescent property. The maximum PL yield is observed for the ST4 crystal.
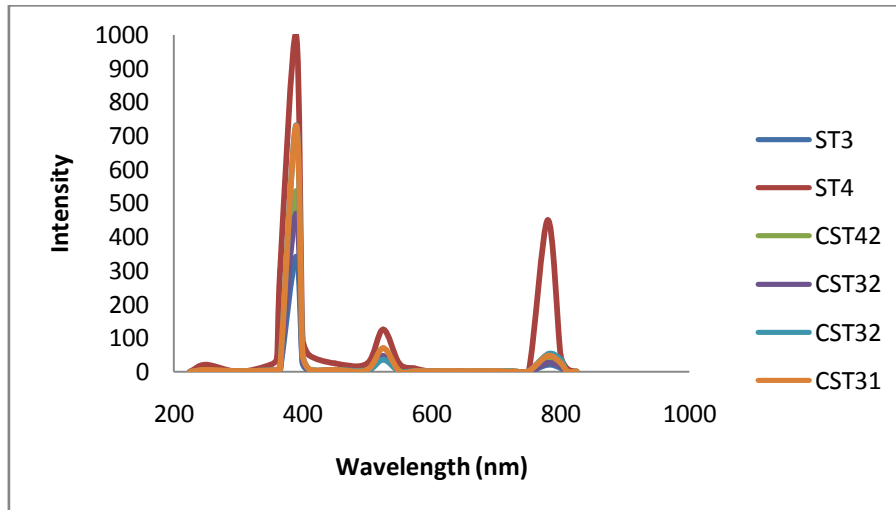
Fig.7: The observed emission (PL) spectra

VI.   Mechanical Properties

The Vicker's hardness number (H_v) is defined as

$H_v = 1.8544 \, P/d^2$ kg/mm^2 [19,20]

Here P is the load applied and d is the diagonal length of the indentation made on the crystal surface.

The Vicker's hardness numbers(H_v) observed (by carrying out the microhardness measurements using a Shimadzu HMV-2 microhardness tester) for various loads(P) in the present study for all the 6 crystals grown are shown in Fig. 8. It is found that the hardness number increases with the increasing load. Also, the hardness numberis found to be more for the trihydrate crystals than for the tetrahydrate crystals.

The work hardening coefficients(n), were determined from the slopes of log P vs log d Plots(not shown here) .The values of n are found to be >2 (see Table 3). According to Onitsch and Hanneman 'n' should lie between 1.0 and 1.6 for hard materials and above 1.6 for soft ones [19].The 'n' values observed in the present study indicate that all the crystals grown belong to soft materials category.
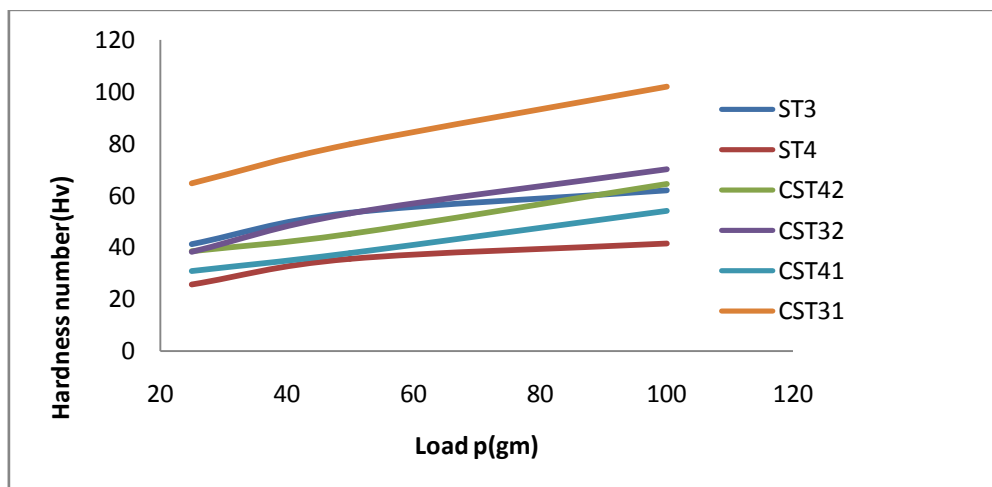
Fig.8: The hardness behaviour

Table 3: The observed SHG efficiencies, work hardening coefficients (n) and Co atom contents (from AAS analysis)

Name of the crystal	SHG efficiency (KDP unit)	n	Co atom content (ppm)
ST3	0.58	2.7	-----
ST4	0.55	3.1	-----
CST31	0.98	3.1	7.98
CST41	1.23	3.2	73.58
CST32	0.93	3.5	10.36
CST42	1.18	3.1	190.13

VII. Thermal (TG/DTA) Analysis

The TGA and DTA patterns recordedby using a thermal analyser (model SDT-Q600)for the pure and doped crystals in the temperature range 50 to 800°C are shown in Fig. 9. It is found that the material is stable up to 100°C. The decomposition process starts at 100°C and this continues up to 220°C. This is due to the removal of entrapped lattice water[5]. Then it remains stable up to 250°C. After that the second decomposition starts and extends up to 340° C resulting in the formation of strontium oxalate (SrC_2O_4). The third decomposition starts at 380° C and ends at 450°C resulting in the formation of strontium carbonate($SrCO_3$)[8]. The water molecules ejected during the first decomposition stage and are in confirmity with the IR spectral studies.

DTA curve shows an endothermic peak (around 170°C for ST4 and ST3 crystals and 140°C for CST42 and CST32 crystals) corresponding to the elimination of the water molecules. Thermal decomposition reactions are usually endothermic. Exothermic peak (around 440°C for ST4 and ST3 crystals and 410°C for CST42 and CST32 crystals) is due to the oxidation reaction taking place along with decomposition.
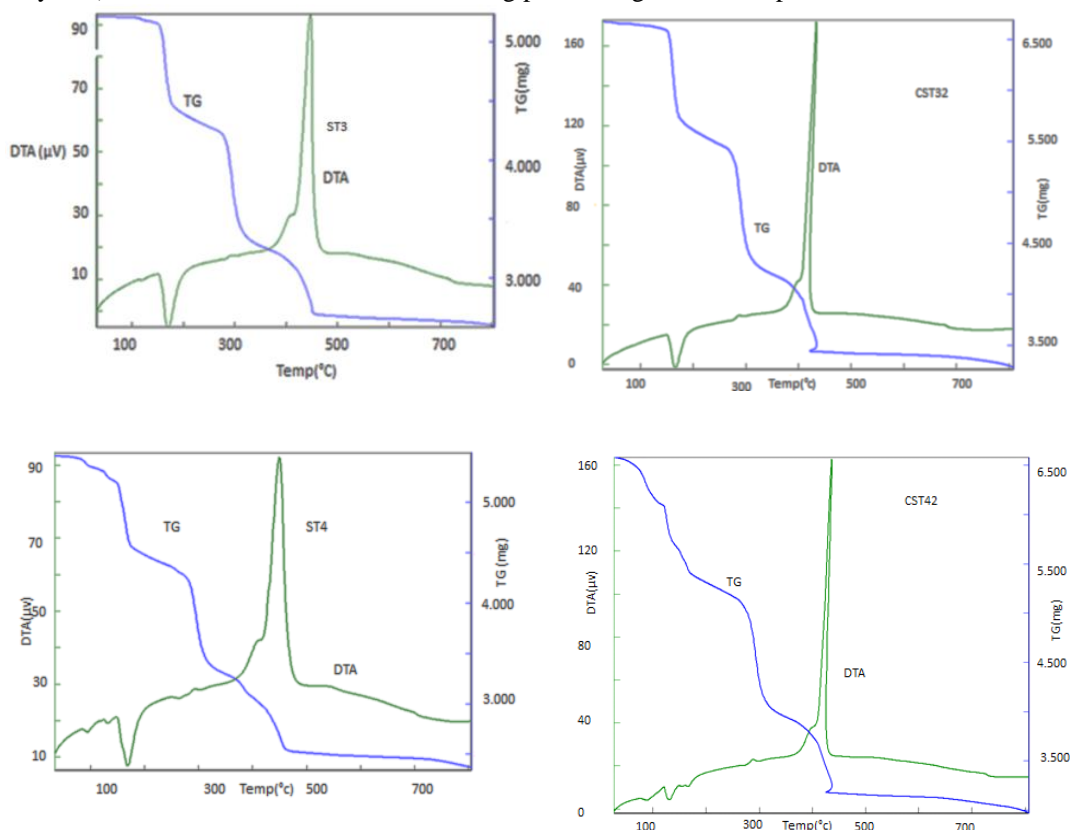
Fig.9: The TG/DTA patterns observed

VIII. Conclusions

Pure and cobalt doped strontium tartrate crystals have been grown successfully by the single diffusion gel growth technique. It was found that the number of tetrahydrate crystals decreases during doping process.Tri and tetrahydrate crystals were obtained due to the change in pH in the test tube during the diffusion of the supernatant solution. The pure and cobalt doped strontium tartrate tetrahydrate crystals are found to be pale

yellow and the trihydrate crystals are transparent in nature and are of good quality crystals. PXRD confirms the crystallinity of the grown crystals. SXRD confirms the orthorhombic crystal system for the growntetrahydrate and monoclinic for the trihydrate crystals. Unit cell parameters of the undoped (pure) crystals match well with the reported SXRD standard values. AAS confirms the presence of cobalt in the doped crystals. It is found that the doped tetrahydrate crystals are having high cobalt concentration. The grown crystals show a wide optical transparency above 250 nm and are found to be useful for the second harmonic generation. Cobalt doping is found to increase the SHG efficiency very significantly. Photoluminescence spectra show that the grown crystals are having the luminescent nature. Microhardness test reveals that the grown crystals belong to soft materials category. The grown crystals are found to be thermally stable at least up to 100 °C. The present study indicates that the optical and mechanical properties of strontium tartrate (both trihydrate and tetrahydrate) single crystals can be tuned significantly by cobalt doping.

REFERENCES

[1]   Mathivanan.V, Haris.M, Prasanyaa.T and Amgalan.M (2014) Synthesis and characterization of gel-grown cobalt tartrate crystals. *Pramana- journal of physics, V-82, No.3,*pp(537-548).
[2]   Heinz K Henisch (1988) *Crystals in Gels and Liesegang Rings* (Cambridge University Press, Cambridge).pp(2).
[3]   Suresh KedaBachhav, PadmakarArjunDavale and Suresh TrimbakPawar (2010) Growth and study of BaTr single crystals by gel technique. *Advances in Applied Science Research*, 1(1), pp(26-33).
[4]   Sawant.D.K, Patil.H.M, Bhavsar.DD, Patil.J.H and Girase.K.D (2011). SEM, PL and UV properties of mixed crystals of Ca-Ba tartrate in Silica gel. *Der ChemicaSinica2(3):63-69*
[5]   Firdous A, Quasim I, Ahmad M M and Kotru P N (2010) Dielectric and thermal studies on gel grown strontium tartrate pentahydrate crystals. *Bull.Mater.Sci*, 33(4), pp(377-382).
[6]   Mary Freeda M, Krishna Priya R, Freeda T H and Mary Delphine S (2012) Crystallization and characterization of mixed crystals of strontium calcium barium tartrate. *Archives of Applied Science Research,* 4(1), pp(128-136).
[7]   Suresh Kumar B, Rahim Kutty M H, Sudarsana Kumar M R and RajendraBabuK (2007) Growth and characterization of pure and lithium doped strontium tartrate tetrahydrate crystals by solution-gel technique. *Bull. Mater. Sci*., 30(4), pp(349-355).
[8]   Rahim Kutty M H, RajendraBabu K, SreedharanPillai K, Sudarsana Kumar M R, and Nair C M K (2001) Thermal behaviour of strontium tartrate single crystals grown in gel. *Bull. Mater. Sci.*, 24(2), pp (249-252).
[9]   Ambady G K (1968) The crystal and molecular structures of strontium tartrate trihydrate and calcium tartrate tetrahydrate.*ActaCryst.,*B24, pp(1548).
[10]   Mathivanan V, HarisM(2013) Investigation of sodium potassium bitartrate crystals grown in silica gel and its characterization. Optic-*Int. J. Light Electron Opt.(2013)*
[11]   Arora S K, Vipul Patel, Brijesh Amin and Anjana Kothari (2004) Dielectric behaviour of strontium tartrate single crystals. *Bull. Mater. Sci.,* 27(2), pp(141-147).
[12]   Angel Mary Greena J, SahayaShajan X and Alex Devadoss H (2010) Electrical conductivity studies on pure and barium added strontium tartrate trihydrate crystals. *Indian Journal of Science and Technology*, 3(3), pp(250-252).
[13]   VijayaKumari.T, Padma.C.M and Mahadevan.C.K (2014) Optical and mechanical properties of pure and manganese doped strontium tartrate tetrahydrate single crystals. *Int. Journal of Engineering Research and Applications, V-4, Issue-2(Version 4), pp(47-52).*
[14]   Sachin J.Nandre, ShardaJ.Shitole and RajendraR.Ahire(2013) Structure, surface morphology and thermal study of strontium tartrate crystals grown in silica gel by single diffusion method. *Adv. In Applied Science Research, 4(5) 00(223-231).*
[15]   Joshi S J, Parekh B B, Vohra K D and Joshi M J(2006), Growth and characterization of gel grown pure and mixed iron-manganese levo-tartrate crystals. *Bull. Mater. Sci.* V-29, N0-3, pp(307-312).
[16]   SahayaShajan X and Mahadevan C (2004) On the growth of calcium tartrate tetrahydrate single crystals. *Bull. Mater.Sci.,*27(4), pp(327-331).
[17]   Cynthia. S and Milton Boaz. B(2013) Synthesis growth and Characterization of a Novel Non-Linear Optical Crystal: Cadmium Mercury ThiocyanateDimethylsulphoxide. *Journal of Applied Physics V-3, Issue 6, pp(06-11).*
[18]   Sawant D K and Bhavsar K S (2012) Photo-luminescence and band gap energy of Ca-Sr tartrate. *Archives of Physics Research*, 3(1), pp(29-35).
[19]   Kavitha J M and Mahadevan C K (2013) Growth and characterization of pure and glycine added morenosite single crystals. *Int. J. Eng. Res. Appl.(IJERA),* 3(5), pp(1931-1940).
[20]   Anitha Hudson J, Mahadevan C K and Padma C M (2013) Effect of ZnS as an impurity on the physical properties of (NH₄)H₂PO₄ single crystals.*Int. Journal of Research in Engineering and Technology V-02, Issue-12, pp(674-683).*

Black Hole Detection in AODV Using Hexagonal Encryption in Manet's

Mr. S. Balamurugan[1], V. Kanmani[2] (MCA), S. Radhika[3] (MCA),
[1]Assistant Professor, MCA Deptt.
Sir Manakula Vinayagar Engineering College Madagadipet Pondicherry

ABSTRACT: *In MANETs (mobile ad hoc network), security is common problem and lack of issues in MANET network. When comparing to wired network, MANETs are harmed to security attacks due to the scarcity of a trusted centralized enforce authority and limited resources. This paper proposed a technique to avoid Blackhole node behaviour in AODV (Ad Hoc On-Demand Distance Vector) using Hexagonal Encryption inNS2. Hexagonal Encryption has been chosen for low cost and high computation speed up. Compared to existing blackhole detection technique, this proposed technique obtains better result by stimulating in NS2.*

Keywords: *AODV, Blackhole node behavior, Hexagonal Encryption, MANET's, Security attackss.*

I. Introduction

A **mobile ad hoc network** (**MANET**) is a continuously self-configuring, infrastructure-less network of mobile devices connected without wires. Each device in a MANET is free to move independently in any direction, and will therefore change its links to other devices frequently. Each must forward traffic unrelated to its own use, and therefore be a router. The primary challenge in building a MANET is equipping each device to continuously maintain the information required to properly route traffic. Such networks may operate by themselves or may be connected to the larger Internet. They may contain one or multiple and different transceivers between nodes. This results in a highly dynamic, autonomous topology. In a MANET, nodes within each other's wireless transmission ranges can communicate directly; however, nodes outside each other's range have to rely on some other nodes to relay messages. Any routing protocol must encapsulate an essential set of security mechanism. These mechanisms are used to prevent, detect and respond to security attacks.

The advantage of wireless networks as opposed to wiredor fixed wireless networks is that they are truly wireless. Most traditional "wireless" access points still need to be wired to the Internet to broadcast their signal. For large wireless networks, Ethernet cables need to be buried in ceilings and walls and throughout public areas. For this mechanism, we are using AODV protocol. This algorithm enables dynamic, self-starting, multihop routing between participating mobile nodes wishing to establish and maintain an ad hoc network.

AODV allows mobile nodes to respond to link breakages and changes in network topology in a timely manner. The operation of AODV is loop-free, and by avoiding the" counting to infinity" problem offers quick convergence when the ad hoc network topology changes (typically, when a node moves in the network). When links break, AODV causes the affected set of nodes to be notified so that they are able to invalidate the routes using the lost link.

II. Black Hole Attack

In a black hole attack, a malicious node can impersonate a destination node by sending a spoofed route packet to a source node that initiates a route discovery. A blackhole has two properties:

1. The node exploits the ad hoc routing protocol to advertise itself as having a valid route to a destination, even though the route is spurious, with the intention of intercepting packets.
2. The node consumes the intercepted packets. In an ad hoc network that uses the AODV protocol, a black hole node absorbs the network traffic and drops all packets. To explain the black hole attack we add a malicious node that exhibits black hole behavior.
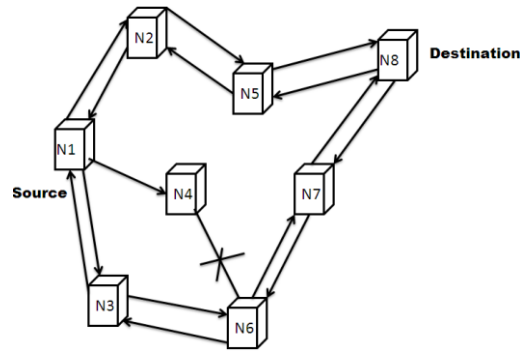
Fig. 1: Black hole attack in AODV

An attacker suppresses or modifies packets originating from some nodes, while leaving the data from the other nodes unaffected, which limits the suspicion of its wrong doing.

NS is a discrete event simulator targeted at networking research. Ns provides substantial support for simulation of TCP, routing, and multicast protocols over wired and wireless (local and satellite) networks.

- It should be aligned with the simulation needs of modern networking research.
- It should encourage community contribution, peer review, and validation of the software.

Since the process of creation of a network simulator that contains a sufficient number of high-quality validated, tested and actively maintained models requires a lot of work, ns-2 project spreads this workload over a large community of users and developers

Ns2 is built using C++ and Python with scripting capability. The ns-2 library is wrapped to python thanks to the pybindgen library which delegates the parsing of the ns-2 C++ headers to gccxml and pygccxml to generate automatically the corresponding C++ binding glue. These automatically-generated C++ files are finally compiled into the ns-3 python module to allow users to interact with the C++ ns-2 models and core through python scripts. The ns-2 simulator features an integrated attribute-based system to manage default and per-instance values for simulation parameters. All of the configurable default values for parameters are managed by this system, integrated with command-line argument processing, Doxygen documentation, and an XML-based and optional GTK-based configuration subsystem.

Tcl (Tool Command Language): Tcl gained acceptance on its own. It is commonly used for rapid prototyping, scripted applications, GUIs and testing. Tcl is used on embedded systems platforms, both in its full form and in several other small-footprint versions.

The interpreted class hierarchy is automatically established through methods defined in the class TclClass. user instantiated objects are mirrored through methods defined in the class TclObject. There are other hierarchies in the C++ code and OTcl scripts; these other hierarchies are not mirrored in the manner of TclObject.

III. AODV Protocol

AODV is a reactive routing protocol that does not require maintenance of routes to destination nodes that are not in active communication. Instead, it allows mobile nodes to quickly obtain routes to new destination nodes. Every mobile node maintains a routing table that stores the next hop node information for a route to the destination node. When a source node wishes to route a packet to a destination node, it uses the specified route if a fresh enough route to the destination node is available in its routing table. If such a route is not available in its cache, the node initiates a route discovery process by broadcasting a Route Request (RREQ) message to its neighbors. On receiving a RREQ message, the intermediate nodes update their routing tables for a reverse route to the source node. All the receiving nodes that do not have a route to the destination node broadcast the RREQ packet to their neighbors. Intermediate nodes increment the hop count before forwarding the RREQ.

A Route Reply (RREP) message is sent back to the source node when the RREQ query reaches either the destination node itself or any other intermediate node that has a current route to the destination. As the RREP propagates to the source node, the forward route to the destination is updated by the intermediate nodes receiving a RREP. The RREP message is a unicast message to the source node. AODV uses sequence numbers to determine the freshness of routing information and to guarantee loop-free routes. In case of multiple routes, a node selects the route with the highest sequence number. If multiple routes have the same sequence number, then the node chooses the route with the shortest hop count. Timers are used to keep the route entries fresh.

3.1 Tradeoff between Delay and Capacity

Increasing transmission power has the side effect of reducing the maximum achievable throughput in a WSN due to increased channel contention and interference. Our focus is on real-time applications in which

meeting the deadlines of critical data is more important than the total throughput. For example, in a surveillance application, timely delivery of the location of an intruder is more important to the user than delivering a large amount of non-critical data. It is also important to note that the reduced capacity is a problem only when the workload approaches the network capacity. Recent advances in real-time capacity theory show that the performance degradation may be avoided as long as the amount of high-priority data transmitted in the network is small enough not to trigger capacity bottlenecks.

AODV achieves the desired tradeoff among communication delay, energy consumption, and network capacity by adapting the transmission power based on required communication delays. When deadlines are tight, AODV trades capacity and energy for shorter communication delay by increasing the transmission power. Conversely, when the deadlines are loose, AODV lowers the transmission power to increase throughput and reduce energy consumption. This adaptive approach is a key feature of AODV.

AODV assumes that each packet is assigned a soft deadline by the application, which specifies the desired bound on the end-to-end delay of a packet. The primary goal of AODV is to increase the number of packets that meet their deadlines while minimizing the energy consumed for transmitting packets under their deadline constraints. AODV focuses on minimizing the energy consumed in packet transmissions. In addition, AODV is designed based on the following principles:

MANETs applications have varied communication requirements resulting in workloads with diverse deadlines. A real-time power-aware routing protocol should dynamically adapt its transmission power and routing decisions based on workload and packet deadlines.

The design of AODV should account for the realistic characteristics of MANETs including loss links and extreme resource constraints in terms of memory, bandwidth and energy. AODV should be localized protocol that makes decisions based solely on onehop neighborhood information.

IV. Blackhole Detection Methods

Black hole is nothing but the malicisious node. This node accepts the data from source but does not forward it to the destination. This node used for hacking purpose. There are two detection techniques are involved in the detection of black hole:

- Depending upon how many times that path is used for transmission.
- By updating the routing table and comparing unique sequence number at each time.

Method 1

In this method, the sender node needs to verify the authenticity of the node that initiates the RREP packet by utilizing the network redundancy. Since any packet can be arrived to the destination through many redundant paths, the idea of this solution is to wait for the RREP packet to arrive from more than two nodes. During this time the sender node will buffer its packets until a safe route is identified. Once a safe route has identified, these buffered packets will be transmitted. When a RREP arrives to the source, it will extract the full paths to the destinations and wait for another RREP. Two or more of these nodes must have some shared hops (in ad hoc networks, the redundant paths in most of the time have some shared hops or nodes). From these shared hops the source node can recognize the safe route to the destination. If no shared nodes appear to be in these redundant routes, the sender will wait for another RREP until a route with shared nodes identified or routing timer expired. This helps for find secure type of communication between the source and destination. But the major disadvantage of the this method is its time consuming. Because here secure intermediate node is find out on the basis how many times that node is used for the data transfer. Now if that node is busy when source wants to transmit data then source have to wait for it. It might be possible that another node which is available for transmissions not black hole. This increase unnecessary delay for transmission of data.

Method 2

Every packet in MANETs has a unique sequence number. This number is an increasing value, i.e., the next packet must have higher value that the current packet sequence number. The node in regular routing protocols keeps the last packet sequence number that it has received and uses it to check if the received packet was received before from the same originating source or not. Packet-sequence-numbers for the last packet received from every node. These tables are updated when any packet arrived or transmitted. The sender broadcasts the RREQ packet to its neighbors. Once this RREQ reach the destination, it will initiate a RREP to the source, and this RREP will contain the last packet-sequence-numbers received from this source. When an intermediate node has a route to the destination and receives this RREQ, it will reply to the sender with a RREP contains the last packetsequence- numbers received from the source by this intermediate node. This method provides secure type of data transmission and fast transmission of data as compared to the previous method.

V. Black Hole Prevention

Real Time Monitoring

This method first identifies the neighbor of the RREP node creator i.e. suspected node. Neighbor node is instructed to listens the packets send by suspected node. Fcount and rcount are the two counters maintained by neighbor node. When a neighbor node forwards any packet to suspected node it will increase the fcount counter by 1. If suspected node forward a packet it will be overheard by the neighbor node and rcount is increased by 1. After source node receives RREP it sends packets to path to check the node is malicious node or not. Neighbor node forwards packets to suspect node until fcount reaches a threshold; thereafter if rcount is 0. RREP creator will identify as malicious node and blocked.

Overcome Blackhole attack

By modifying an original AODV. To participate in Communication RREP originator must exhibit its honesty. If the node is the first receiver of the RREP packet, it will forward it to Source andcheck forthe honesty of node based on the opinion of the neighbors of RREP originator Node. Neighbors are requested to send an opinion about the RREP originator node. After receiving reply from all neighbor nodes. It checked if RREP originator node has delivered many packets to destination it a an honest node, if RREP originator node as received many packets but do not forward packets further or it has send many RREP packets, it is a misbehaving node. Such nodes are added to the quarantine list and blocked.

Comparing Destination Sequence Number

To prevent Blackhole attack in AODV. In the method source node collects all the RREP from different intermediate node. The first entry received by source is marked first entry in Route reply table (RRT). The destination sequence number (DSN) of first entry is compared with sequence number of source node. If the DSN of first entry is very large as compared to source sequence number, the node is considered as malicious node and removed from the RRT. Path is selected based on the remaining entries in RRT which is arranged according to DSN. The node with highest DSN is selected for path.

VI. Hexagonal Encryption Algorithm

```
1. The sender sends a RREQ packet which contains a plain text.
2. When a node recieves the RREQ packet
if(not(Reciever)) then
if((has better route to reciever) ||
(has shorter route to reciever) then
Save the reverse route
Forward the packet
fi
else
Encrypt the plaintext in the packet with
the partition and key preagreed upon
Send a RREP towards the sender with the cipher text
fi
3. When a node node recieves a RREP packet
if(not(Sender)) then //By Sender we mean the
// original source of the RREQ packet
Forward the packet towards sender
else
if(RREP packet contains the required cipher) then
        Forward data packets to the last forwarder
of the RREP packet
else
Drop the RREP packet
fi
fi
```

Fig 2: Algorithm for hexagonal encryption

VII. Experimental Result

The simulation was done with 20,25,30,35,40 nodes. The simulation was done in TCl. With simulations for each in both AODV Black hole Aodv environments, the scenarios for which were created using the stedest command.

In each case the number of packets sent, received, dropped and percentage of packets recieved were recorded by analyzing the trace file. If the nodes are attacked by black hole attack. The hexagonal encryption technique detect the black hole attack node in network and its changes the route path to some other route without any data(packet) drops. From this simulation we are increasing packet delivery ratios and reducing packet end-to-end delay and average packet lengths.The results are shown in the graphs respectively.

Graph 1
It shows the efficient increasing packet delivery ratio when compared to existing one.
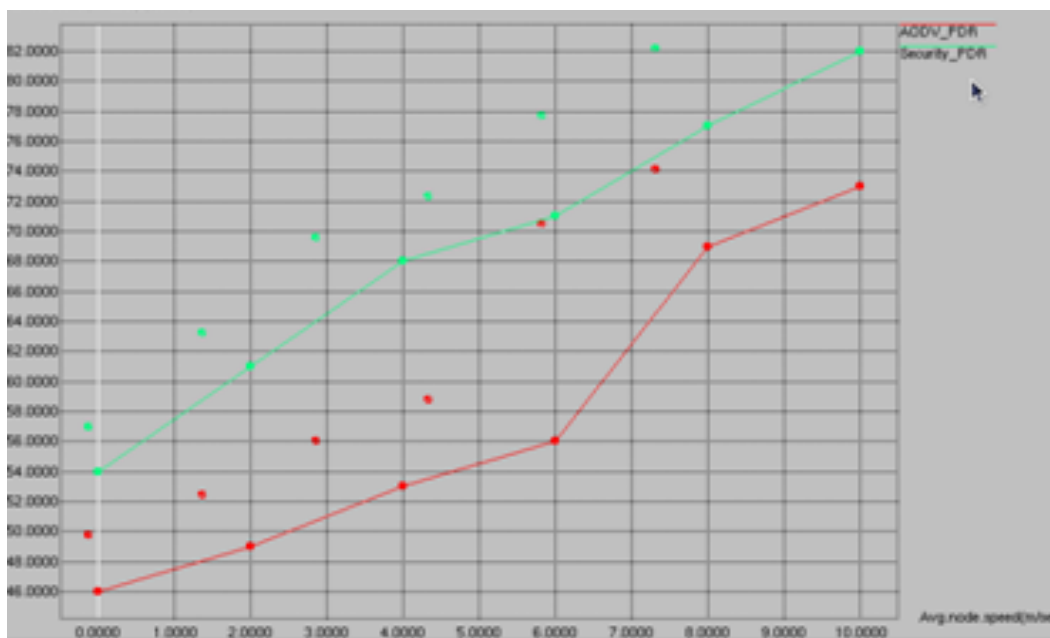
Fig 3: Increasing packet delivery ratio using hexagonal encryption

Graph 2
It shows the decreased average packet length when compared to existing one.
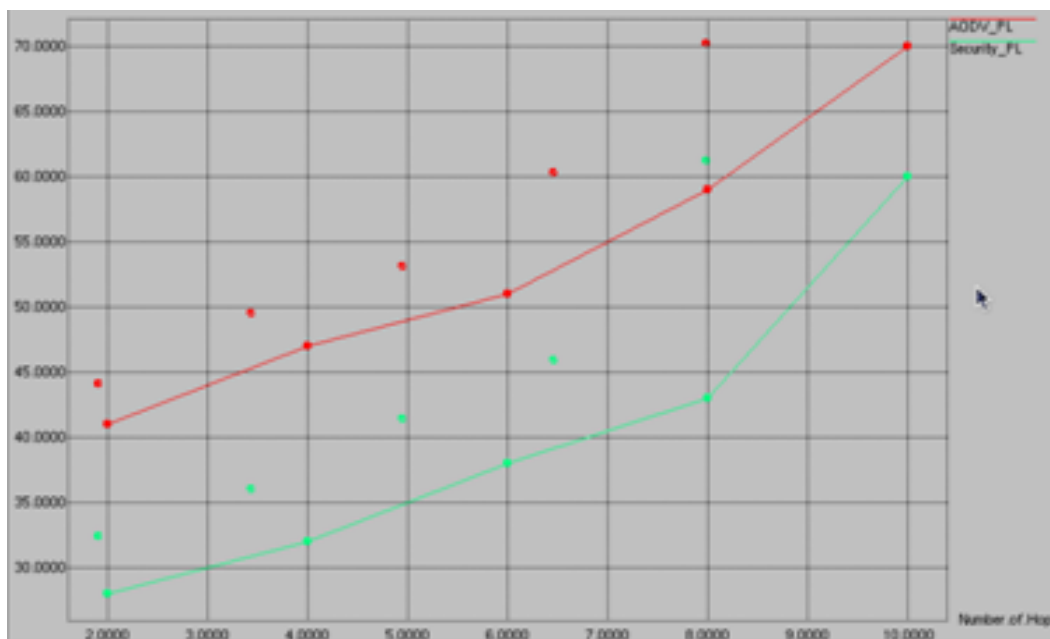
Fig 4: Average packet length

Graph 3
It shows the decreased End-to-End delay when compared to existing one.
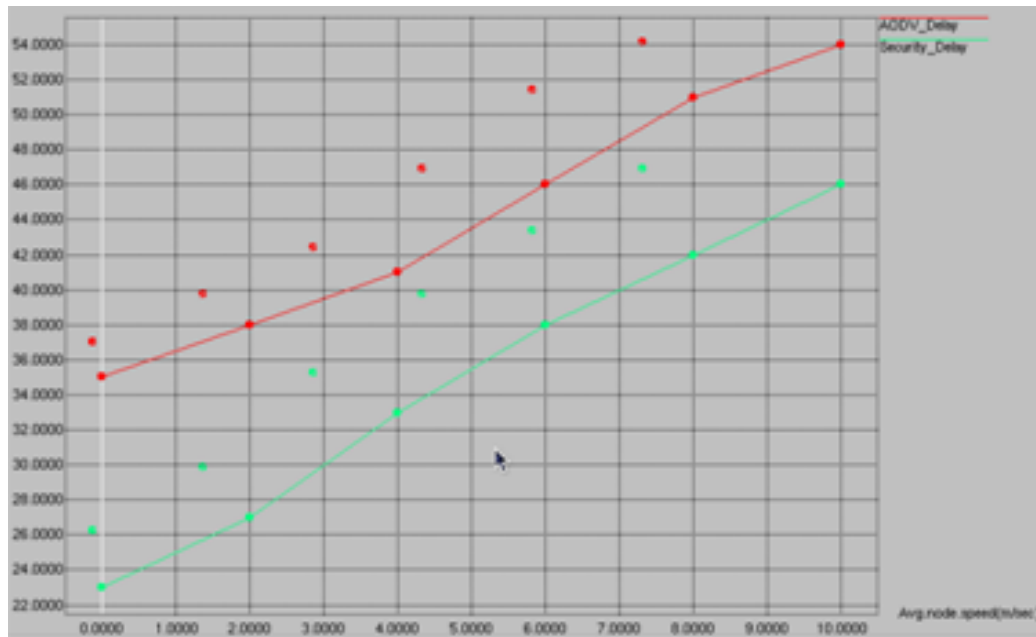
Fig 5: End-to-end delay

VIII. Conclusion

The proposed technique to avoid Blackhole node behaviour in AODV(Ad Hoc On-Demand Distance Vector) using Hexagonal Encryption in NS2. Hexagonal Encryption has been chosen for low cost and high computation speed up. Compared to existing blackhole detection technique, this proposed technique obtain better result by stimulating in NS2.

REFERENCES

[1]   L. Raja1, Dr. S. Santhosh Baboo, Dept. of Computer Applications, Pachaiyappa's College, Chennai"Analysis *of Blackhole attacks on AODV Routing Protocol in MANET*" December 2012 | Vol 2, Issue 12, 1522-1526

[2]   Shraddha Raut & Sd Chede **"***detection and removal of black hole in mobile Ad-hoc network (manet)"* Electronics & Telecommunication Department.

[3]   Mohammad Al-Shurman and Seong-Moo Yoo, Seungjin Park," *Black Hole Attack in Mobile Ad Hoc Networks*"

[4]   Vishnu K, Amos J Paul," *Detection and Removal of Cooperative Black/Gray hole attack in Mobile ADHOC Networks*"

[5]   AWANDHIYA, P.M., GHONGE, M.M., M.S.ALI, D., DESHPANDE, P.J.. *A Survey of Mobile Ad Hoc Network Attacks. International Journal of Engineering Science and Technology 2010;*.

[6]   Perkins, C., Belding-Royer, E., Das, S.. *Ad hoc On-Demand Distance Vector (AODV) Routing. Tech. Rep. RFC 3561; IETF; 2003. URL:https://tools.ietf.org/html/rfc3561*.

[7]   Dutta, S.. *An approach towards development of effecient encryption techniques*. Ph.D. thesis; The University of North Bengal; 2004.

[8]   The ns Manual (formerly ns Notes and Documentation). UC Berkeley, LBL, USC//ISI, and Xerox PARC; 2011.

[9]   Greis, M.. *Tutorial for the Network Simulator "ns". 2004*.

[10]   Dokurer, S.. *SIMULATION OF BLACK HOLE ATTACK IN WIRELESS AD-HOC NETWORKS. Master's thesis; Atılım University; 2006*.

[11]   Sun, B., et al. *Detecting Black-hole Attack in Mobile Ad Hoc Networks. Personal Mobile Communications Conference, 5th European* 2003;(492).

[12]   Berkeley, U., LBL, , USC/ISI, , PARC, X.. *The ns Manual; 2011*.

[13]   Ross, F.J., Ruiz, P.M.. *Implementing a New Manet Unicast Routing Protocol in NS2. Tech. Rep.; Dept. of Information and Communications Engineering University of Murcia; 2004*.

[14]   Sukla Banerjee, *"Detection/Removal of Cooperative Black and Gray Hole Attack in Mobile Ad-Hoc Networks"*, Proceedings of the World Congress on Engineering and Computer Science 2008

[15]   Bing Wu, Jianmin Chen, Jie Wu, Mihaela Cardei , *"A Survey on Attacks and Counterme asures in Mobile Ad Hoc Network,"* Wireless/Mobile Network Security, Y. Xiao, X. Shen, and D.-Z. Du (Eds.) pp, @ 2006 Springer.

[16]   Nishu Garg and R.P.Mahapatra, *"MANET Security Issues ,"* IJCSNS International Journal of Computer Science and Network Security, VOL.9 No.8, August 2009.

[17]   N.Shanthi, Dr.Lganesan and Dr.K.Ramar, *"Study of Different Attacks on Multicast Mobile Ad hoc Network,"* Journal of Theoretical and Applied Information Technology.

Retrofitting and Strengthening of Damaged Reinforced Concrete Columns Using Steel Angels Wrapped with Steel Wire Mesh

Abd-ELhamed, M. K.[1], Ezz-Eldeen, H. A.[2]

1and 2 Faculty of Engineering, Al – Azhar University, Cairo, Egypt

ABSTRACT: *Six reinforced concrete rectangular columns with a cross section 120x160 mm and 800 mm length were casted and tested until failure. Two control columns were tested under axial load and four columns were tested under different eccentricities e/t= (6.30%, 12.5%, 18.75% and 25%). All specimens were retrofitted by replacing the loose concrete part by grout mortar. Strengthening was carried out using four vertical steel angles, two angles 30x30x3mm in eccentricity direction and two angles 15x15x3 mm in the reverse direction all wrapped with expanded three plies steel wire mesh. However, the steel wire mesh jacket was injected by cement mortar. The test results showed that columns strengthened with four vertical steel angles wrapped with three plies steel wire mesh tested under different eccentricity recorded a higher failure load than that wrapped with three plies steel wire mesh only. The increase in column carrying capacity ranged from 102.5% to 112%.*
Keywords: *Column; Eccentricity; Retrofitting; Strengthened; Jacket; Wire mesh;*

I. Introduction

A large number of reinforced concrete columns have been damaged by earthquakes or as a result of deficiencies in the design. The demand for retrofitting and strengthening of columns has stimulated the development of many different systems for external confinement. The selection of a specific retrofitting and strengthening system depends on the structural performance and economic importance factors for structural. Retrofitting RC columns may be defined as an attempt to restore the original strength and stiffness of damaged as well as deteriorated RC columns. Josh L. Ramirez (1996) performed ten repair methods for RC columns to identify the advantages and limitations of the various strengthening methods. The methods presented were divided into two groups. The first deals with the strengthening of the entire column height, while the second focuses on the problem of damage and loss of strength on a localized section. The comparison showed that the first six methods that extend along the entire column height, in terms of efficiency and cost, appear to be the simple concrete jacket and the steel angle method. The simple concrete jacket is easy to construct and transmission of load is direct. Ghobarah A. and et al (1997) conducted an experimental investigation to study the failure mode of existing reinforced concrete columns designed during the 1960s. Three large-scale columns were strengthened with corrugated steel jacket and tested under cyclic loading. The variable in the test specimens include the amount of column transverse reinforcement and jacketing of the column. The corrugated jacket was found to be effective in the rehabilitation of the selected existing structure. Julio E. S. and et al (2003) evaluated the retrofitting techniques of reinforced concrete columns according that different characteristics. Julio E. S. and et al conducted that the reinforced concrete jacketing strengthening method, unlike other techniques, leads to a uniformly distributed increase in strength and stiffness of columns. Ozcan O. and et al (2007) investigated the structural behavior of undamaged and moderately damaged columns, which were retrofitted with carbon fiber reinforced polymers (CFRP). The experimental program consists of four specimens having inadequate tie spacing 90 degree hooks and plain reinforcing bars that were tested under lateral cyclic displacement excursions under a constant axial load of approximately 27% of the axial load carrying capacity. One control specimen without any strengthening and another specimen with strengthening but without any pre-damage were tested. In one of the pre-damaged columns the repairing process was performed in the presence of constant axial load. The main parameters investigated in this study were the presence of axial load on the column during repairing, the effect of pre-damage on ultimate displacements and the effect of CFRP wrapping on strengthened and repaired columns. LIU Tao and et al (2008) presented a new retrofit method, which utilized fiber-reinforced plastics (FRP) confinement mechanism and anchorage of embedded bars. Carbon FRP (CFRP) sheets and glass FRP (GFRP) bars were used in this test. Five scaled RC columns were tested to examine the function of this new method for improving the ductility of columns. Responses of columns were examined before and after being retrofitted. The test results showed indicate that this new composite method can be effective to improve the anti-seismic behavior of non-ductile RC columns compared with normal CFRP sheets retrofitted column.

Adnan S. AL-Kuaity (2010) tested three groups of reinforced concrete squared tied columns reinforced with 2% longitudinal steel reinforcement ratio. Adnan measured the behavior of repaired by strain on the concrete surface under axial load up to cracking load. The test results showed that the strength of the failed column can be restored by replacing the cracked shell with new shell having high compressive strength. The strength of columns repaired by these materials can reach up to 136% of their original strength depending on both the compressive strength and the condition of pre loading. Ruili H. and et al (2013) used experimental five large-scale severely damaged square RC columns with the same geometry and material properties but with different damage conditions. Each column was repaired and retested under the same loading combination as the corresponding original column. Quickset repair mortar was used to replace the removed loose concrete. Without any treatment to damaged reinforcing bars, longitudinal and transverse CFRP sheets were externally bonded to the prepared surface to restore the column strength. Measured data were analyzed to investigate the performance of the repaired columns compared to the corresponding original column responses. It was concluded that the technique could be successful for severely damaged columns with damage to the concrete and transverse reinforcement. Ruili H. and et al (2014) evaluated a method for repairing severely damaged RC columns subjected to torsional moment using externally bonded carbon fiber-reinforced polymer (CFRP) composites. A half-scale RC column that was previously tested to failure under constant axial load and cyclic torsional moment was repaired with externally bonded CFRP. The results showed that this method can be used to restore the torsional performance of severely damaged RC columns. Contributions of the transverse and longitudinal CFRP sheets to the torsional resistance are evaluated, and repair design for torsional moment using this method is discussed. Elsamny, M.K. and et al (2014) presented a thirty seven specimens tested under different eccentricities from e/t= 0% up to 25% divided it into three groups. Group one consisted of five specimens tested under different eccentricity as control columns. Group two consisted of sixteen specimens were strengthened with different numbers of steel wire mesh plies (2, 3, 4 and 6). Group three consisted of sixteen specimens were strengthened with a sandwich made of different numbers of steel wire mesh plies (2,3,4,6) and external vertical steel bars 3Ø8 in compression side. The test results showed that using wire mesh jacketing technique gives an increase in the load carrying capacity up to 23%. However, using sandwich wrapping system technique which made of steel wire mesh and external vertical steel bars in compression side gives an increase in the load carrying capacity up to 54%. However, the majority of strengthening techniques used GFRP and CFRP are very expensive. Thus, there is an urgent need for the development of improved, lower cost and less disruptive techniques which will make necessary interventions in many structures economically viable.

II. Proposed The Techniques Of Retrofitting And Strengthening

In this investigation the proposed techniques was replacing the loose concrete part by using grout mortar to retrofitting the damage of columns. In additions, two different techniques were used to strengthen the columns as follows:

- Wrapped columns with only three plies expanded steel wire mesh wrapped with two steel straps 30x3 mm at the column top and bottom.
- Four vertical steel angles were used at the corners of column wrapped with three plies expanded steel wire mesh. Two angles 30x30x3 mm were placed in eccentricity direction and two angles 15x15x3mm were placed in the reverse direction as shown in figure 1.

III. Experimental Program And Testing Procedure

Six reinforced concrete columns having a cross section of (120x160) mm and a length of (800) mm were tested until failure as shown in table 1. All specimens contain four longitudinal reinforcement bars 8mm diameter and stirrups 6mm diameter bars at spacing of 150mm. Strain gauges were mounted on the vertical steel bars as well as the external vertical steel angles on the compression side as shown in figures 1, 2. Two specimens were tested until failure under centric loads e/t= 0 and the other four specimens were tested until failure under different eccentricity e/t= 6.3, 12.6, 18.8 and 25 %. Figure 3 shows all specimens after casting and tested until failure before retrofitting. Total removed of damaged parts were replaced by grout mortar.
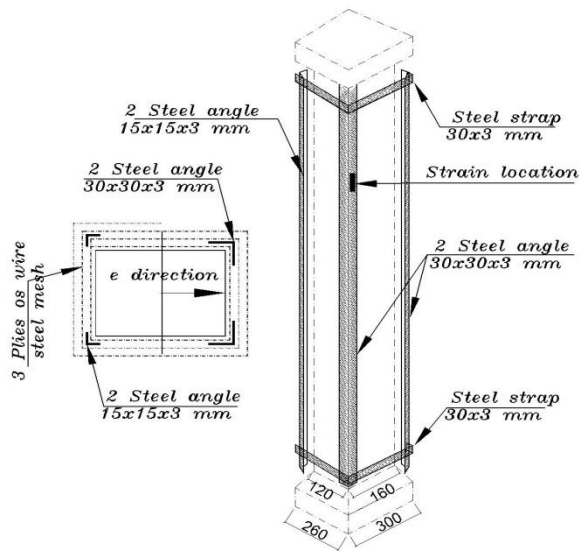
Figure 1 specimens and strengthened details
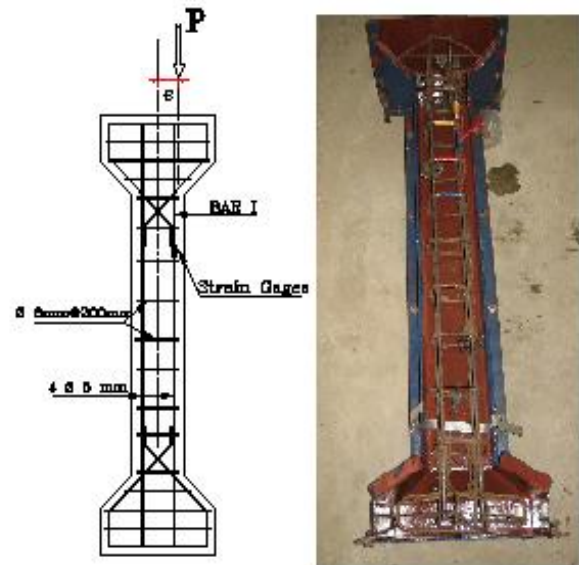
Figure 2 Reinforcement details and strain gages location

Figure 3 Specimens after testing before retrofitting.
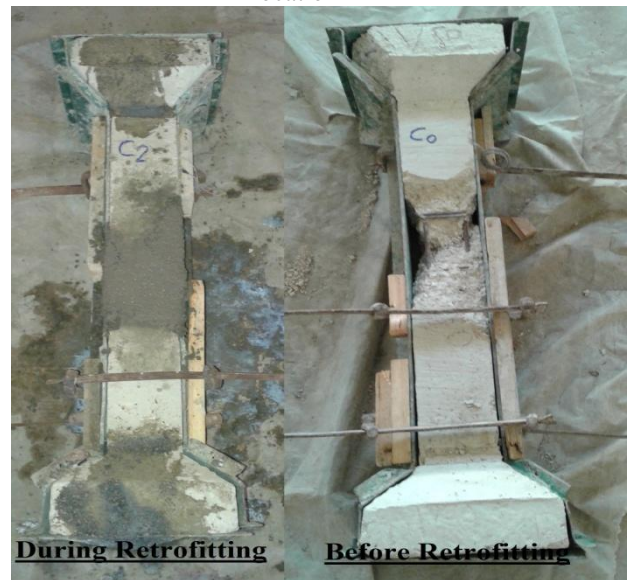
Figure 4 Details of retrofitting columns with Grout mortar.

The Cetorex grout mortar with high-strength, low or non-shrink is used for replacing the damaged concrete part and restore specimens dimension as shown in figure 4. Special attention was made to achieving a good bond between the new and the existing concrete. The specimens were cured with wet sackcloth for seven days. One of the specimen was strengthened with three plies steel wire mesh only and tested under eccentricity e/t= 0. In addition, one specimen was strengthened with four vertical steel angles 30x30x3mm at each column corners after the column wrapped with one plie steel wire mesh and then wrapped with two plies steel wire mesh as shown in figure 5 and then tested under eccentricity e/t= 0.The other four specimens were wrapped with one plie steel wire mesh then placing the vertical steel angles in each column corners and then wrapped with two plies of steel wire mesh. Two angles 30x30x3mm were placed in the eccentricity direction and other two angles 15x15x3mm were placed in the reverse direction. All specimens were wrapped with two steel straps 30x3 mm at the column top and bottom. The Strain Gauges were mounted on the vertical steel angle in the compression side. Thereafter, all the specimens were plastered with rich mix mortar cement sand ratio of 1:2.5 with water-cement ratio = 0.55 as shown in figure 6. In order to improve workability, super plasticizer was used. All columns were cured for 28 days from the date of casting of jacketing. All casted specimens were kept in a dry place for a few hours for attaining surface dry condition. Thereafter, all columns were tested using hydraulic compression testing machine of capacity 2000 KN at the Material laboratory of Al-Azhar University as shown in figure 7. The different eccentricities were controlled by column head steel plates as shown in figure 8.

IV. Used Materials

- The concrete mix was designed according to the Egyptian code of practice to obtain target strength of 25 N/mm2 at the age of 28 days.
- The used steel reinforcement was normal mild steel St24/37-smooth rebar of 6 and 8 mm diameter. Tension tests were performed on the steel specimens using Shimadzu 500-KN universal testing machine according to the Egyptian Standard Specifications ESS 262-1999.
- .Using cetorex grout mortar which is a cementations mix requiring only the addition of water to produce high strength non-shrink mortar.
- The used galvanized welded steel wire mesh has a specification 12.7x12.7 mm panel size and 1.6 mm wire diameter.
- The used steel angles have a yield stress of 325 N/mm2 and tensile strength of 420 N/mm2 with an elongation percentage of 30%.
- The used strain   gauges were manufactured   by KYOWA electronic instrument co, ltd. the type used was kfg-5-120-c7-11 11m2r, which has a resistance of 119.6 ± 0.4% ohms at 24°c, and a gage factor of 2.1 ± 1.0%.

Figure 5 Details of strengthened column with 4 angles and 3 plies wire mesh

Figure 6 Form shape used for cement mortar

Figure 7 Test machine and test setup

Figure 8 Column head was used to applied eccentricity

V.   Experimental Test Results

The obtained results are discussed as follows:

1. Test Results of Control Columns (non-Strengthened Columns)

- Table 1 shows the maximum failure load of columns (control columns) and the percentage decrease in ultimate column capacity due to different eccentricities e/t= (0% to 25%). The increase in eccentricity from e/t= 0% to 25% decreases the ultimate load carrying capacity by 93% to 71% from column carrying capacity e/t=0.

  Figure 9 shows the relationship between the load and longitudinal strain. For the internal vertical steel bar in the eccentricity direction BAR I (no retrofitting and no strengthened) Due to increasing eccentricity, the strain in BAR I increases from 820micro strain to 1500 micro strain while the load decreased from 541 KN to 385 KN.

2. Test Results of Strengthened Columns

- Table 2 shows the maximum failure load of columns (Strengthened Columns)and the percentage decrease in ultimate column capacity due to different eccentricities e/t= (0% to 25%). The increase in eccentricity from e/t= 0% to 25% decreases the ultimate load carrying capacity by 112% to 102.5% from column carrying capacity e/t=0.

- Figure 10 shows the relationship between the load and longitudinal strain. For the internal vertical steel bar in the eccentricity direction BAR I (after retrofitting and strengthened with 4angles&3 plies wire mesh) Due to increasing eccentricity, the strain in BAR I increases from 1100micro strain to 2100 micro strain while the load decreased from 608 KN to 555 KN.

- Figure 11 shows the load-strain relationship between the load and longitudinal strain.   For the external vertical steel angles in the eccentricity direction (after retrofitting and strengthened with 4angles&3 plies wire mesh Due to eccentricity, the strain in the external angles increases from 400micro strain to 1500 micro strain while the load decreased from 608 KN to 555 KN.

Table 1 Failure loads of control columns

Specimen name	e/t %	Specimen description	Failure loads KN	% of Column carrying capacity from e/t=0
C_0	0	Control column	545	--
C_1	0	Control column	541	100%
C_2	6.3	Control column	505	93%
C_3	12.6	Control column	487	90%
C_4	18.8	Control column	423	78%
C_5	25	Control column	385	71%
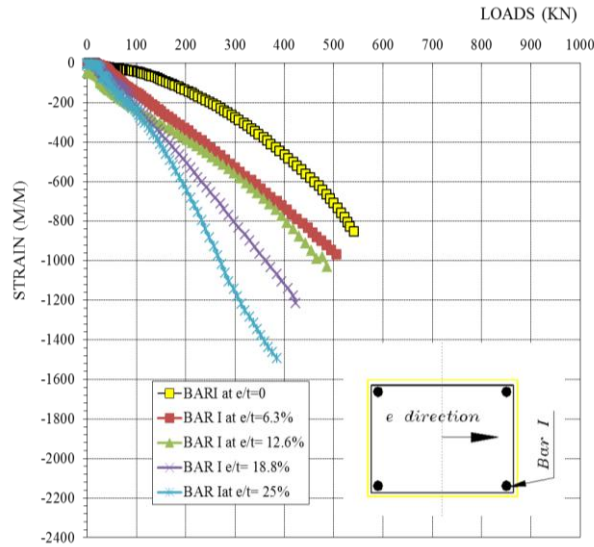
Figure 9: The relationship between load and longitudinal strain for Bar I at e/t= 0% to 25%
(Control Column-non strengthened)

Table 2 Failure loads of strengthened columns

Specimen name	e/t %	Specimen description	Failure loads KN	% of Column carrying capacity from e/t=0
C0$_R$	0	Strengthened with 3 plies wire mesh	490	89%
C1$_R$	0	Strengthened with 4angles&3 plies wire mesh	608	112%
C2$_R$	6.3	Strengthened with 4angles&3 plies wire mesh	587	108.5%
C3$_R$	12.6	Strengthened with 4angles&3 plies wire mesh	571	105.5%
C4$_R$	18.8	Strengthened with 4angles&3 plies wire mesh	567	104.8%
C5$_R$	25	Strengthened with 4angles&3 plies wire mesh	555	102.5%
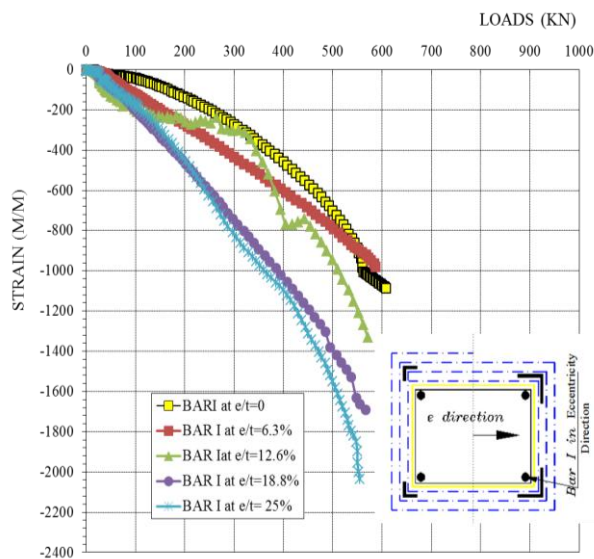
Figure 10: The relationship between load and longitudinal strain for Bar I at e/t= 0% to 25%
(4angles&3 plies wire mesh)

- Table 3 shows the values of the forces in the vertical steel bars in the eccentricity direction BAR I as well as the vertical steel angles. The shown values were obtained by converting the strain values to the forces taken the modulus of elasticity of steel bars equal 210 KN/m2 and cross-sectional area of longitudinal reinforcement bars is 50.29 mm2 per one 8mm diameter bar. Also, the cross-sectional area of vertical steel angles 174mm2 per one angle 30x30x3.

- Figure 12 shows the relationship between the forces in a vertical steel BAR I (before and after strengthened) as well as steel angles with respect to control column at failure loads and increasing eccentricity from e/t= (0% to 25%). The percentage of forces in the steel bars at the eccentricity direction increased from 4% to 8.2 % of the failure load with eccentricity increased from e/t= 0% to 25% in case of control columns. However, the percentage of forces on the bar at eccentricity direction increased from 3.8% to 7.8 % of the failure load with eccentricity increased from e/t= 0% to 25% in case of strengthened columns. The percentage of forces in the vertical steel angles used in the strengthening techniques found to be in the range of 5.2% to 20 % of the failure load.

- Figure 13 shows the relationship between percentage column load carrying capacity control (e/t=0) and percentage of eccentricity for (control and strengthened columns). The column strengthened with three plies steel wire mesh only could not reach the ultimate loads of control column. The ultimate load of column was found to be 89% of the original ultimate load. The columns strengthened with four steel angles and wrapped with three plies steel wire mesh gives an increase in the load carrying capacity from 102.5% up to 112%.

- Figure 14 shows the failure mode of columns under different eccentricities. The failure mode of the control reinforced concrete columns was brittle failure while strengthening with steel wire mesh jacket changed failure mode to be ductile.

Table 3: Forces in a vertical steel bar I and steel angle with respect to control column at failure loads due to increasing eccentricity

Specimen name	e/t%	Failure loads KN	%force in BAR I / failure load KN	% Force in angle / failure load KN
C1	0	541	3.32%	
C2	6.3	505	4.06%	
C3	12.6	487	4.47%	
C4	18.8	423	6.07%	
C5	25	385	8.20%	
C1R	0	608	3.78%	5.14%
C2R	6.3	587	3.52%	13.57%
C3R	12.6	571	4.93%	17.84%
C4R	18.8	567	6.30%	17.41%
C5R	25	555	7.74%	19.89%
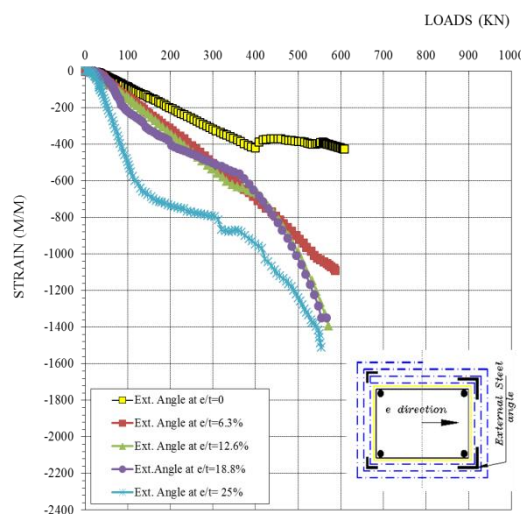
Figure 11: The relationship between load and longitudinal strain for angle at e/t= 0% to 25% (4angles&3 plies wire mesh)
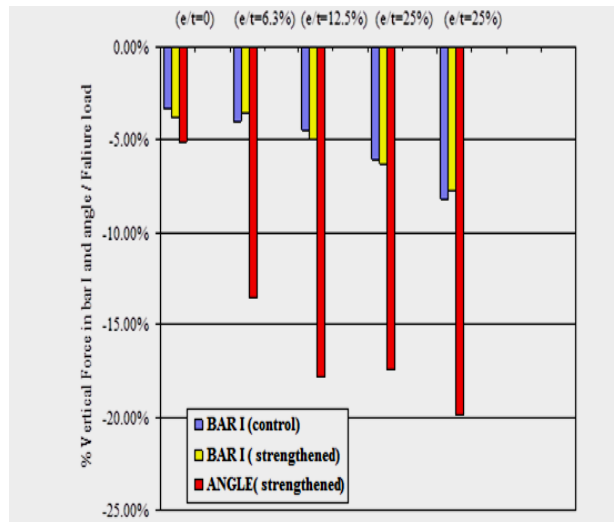
Figure 12: The relationship between forces in a vertical steel bar I and steel angle with respect to control column at failure loads
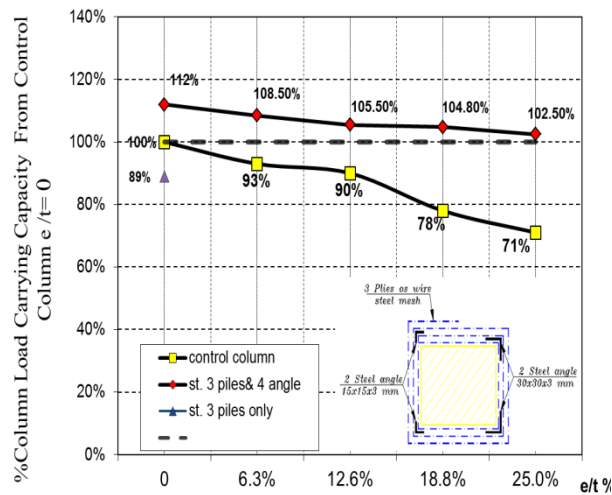
Figure 13: The relationship between % column load carrying capacity of control (e=0) and percentage of eccentricity for (control and strengthened column)

Figure 14: Failure Modes of Strengthened Columns

VI. Conclusions

The used retrofitting and strengthening technique is successful for damaged columns to improve the load carrying capacity under to eccentric loads. From the experimental results the followings are concluded:

- The increase in eccentricity from e/t= 0% to 25% decreases the ultimate load carrying capacity of columns by 93% to 71% from column carrying capacity e/t=0.
- The percentage of forces on the internal vertical steel bars at eccentricity direction decreases about 5% while the strain increases about 25%.
- The columns strengthened with four vertical steel angles at the corners wrapped with three plies steel wire mesh recorded a higher failure load than that strengthened with three plies steel wire mesh only.
- The columns strengthened with four steel angles and wrapped with three plies steel wire mesh give an increase in the load carrying capacity from 102.5% up to 112%.
- Columns retrofitted with grout mortar and strengthened with four steel angles wrapped with three plies steel wire mesh were found to be very effective for to improving the ultimate capacity as well as the ductility of columns.
- The number of plies is the recommended to be not less than three plies. In additions, the area of the vertical steel angles in the reverse direction is recommended to be not less than 50% of the area of vertical steel angel in eccentricity direction.

ACKNOWLEDGEMENT

REFERENCES

[1] Adnan S. AL-Kuaity (2010);"Rehabilitation of Damage Reinforced Concrete Columns" Al-Qadisiya Journal For Engineering Sciences Vol.3, No.1, Year 2010.
[2] Elsamny, M.K., Abd-Elhamed, M.K, Ezz-Eldeen, H.A. and Elmokrany,A.A. (2014), "Strengthening of Eccentrically Loaded Rectangular Reinforced Concrete Columns Using Steel wire Mesh" Civil Engineering Research Magazine (CERM) Civil Engineering Department, Faculty Of Engineering, Al-Azhar University, accepted for publication.
[3] Ghobarah A., Biddah A. and mahgoub M. (1997)" Rehabilitation of Reinforced Concrete Columns Using Corrugated Steel Jacketing" Journal of Earthquake Engineering Volume 1, Issue 4, pages 651-673, year1997
[4] Julio E. S., Branco F. and Silva V. D. (2003)"Structural Rehabilitation of Columns with Reinforced Concrete Jacketing" Prog. Struct. Engng Mater. Vol. 5, pp.29–37, (year 2003).
[5] LIU Tao, FENGWei, ZHANG Zhi-mei and OUYANG Yu(2008) " Experimental Study on Ductility Improvement of Reinforced Concrete Rectangular Columns Retrofitted with a New Fiber Reinforced Plastics Method" J Shanghai University (Engl Ed) vol.12(1), pp. 7–14, (year 2008).
[6] Ozcan O., Binici B. and Ozcebe G. (2007);" Seismic retrofitting of Reinforced Concrete Columns Using Carbon Fiber Reinforced Polymer (CFRP)" Asia-Pacific Conference on FRP in Structures (APFIS 2007).
[7] Ramirez Josh L. (1996)"Ten Concrete Column Repair Methods" Construction and Building Materials, Vol. 10, No. 3, pp. 195-202, year 1996.
[8] Ruili H., Lesley H. S., and Abdeldjelil B. (2014)" Torsional Repair of Severely Damaged Column Using Carbon Fiber-Reinforced Polymer" ACI Structural Journal, Vol. 111, No. 3, May-June 2014.
[9] Ruili He., Lesley H. Sneed, and A. Belarbi (2013); "Rapid Repair of Severely Damaged RC Columns with Different Damage Conditions: An Experimental Study" International Journal of Concrete Structures and MaterialsVol.7, No.1, pp.35–50, March 2013.

An Experimental Investigation on Mode-II Fracture of Light Weight Pumice Aggregate Concrete

Dr. V. Bhaskar Desai[1], K. Mallik Arjunappa[2], A. Sathyam[3]

[1] *Professor, Dept. of Civil Engineering, JNTUA College of Engineering, Anantapur – 515002, A.P.*
[2] *Dy. Executive Engineer, Dharmavaram Municipality, Dharmavaram – 515671, & Research Scholar, JNTUA College of Engineering, Anantapur – 515002, A.P.*
[3] *Conservation Assistant Gr-I, Archaeological Survey of India, Anantapur Sub Circle, Anantapur & Research Scholar, JNTUA College of Engineering, Anantapur – 515002, A.P.*

ABSTRACT: *Shear strength is a property of major significance for wide range of civil engineering materials and structures. Shear and punching shear failures particularly in deep beams in corbels and in concrete flat slabs are considered to be more critical and catastrophic than other types of failures. To study such failures the past literature suggests best suited geometry as Double Centered Notched (DCN) specimen geometry proposed by Sri Prakash Desai and Sri Bhaskar Desai. In the present scenario light weight aggregate has been the subject of extensive research which affects the strength properties of cement concrete. Light weight aggregate concrete has become more popular in recent advancements owing to the tremendous advantages it offers over the conventional concrete but at the same time light in weight and strong enough to be used for structural purposes. In this present experimental investigation an attempt is made to study the Mode-II fracture properties of natural light weight aggregate concrete, such as pumice aggregate (which is volcanic based and imported from Turkey) concrete. By varying the percentage of light weight pumice aggregate in concrete replacing the conventional granite aggregate in percentages like 0%, 25%, 50%, 75% and 100% by volume of concrete, the mode-II fracture property such as in plane shear strength is studied. Finally an analysis is carried out regarding Mode-II fracture properties of pumice concrete and it is concluded that shear strength is decreased continuously with increase in percentage of pumice.*

Key words: Pelletization, light weight aggregate, cold bond.

I. Introduction

Due to poor design and the material deficiencies in the form of pre-existing flaws initiating the cracks and fractures which are responsible for the failure of structures. With the advancement in the new construction materials with high strength and stress analysis methods were developed which enable a more reliable determination of local stresses, which permits the safety factors to be reduced resulting in weight savings.

Consequently, structures designed with high strength materials have low margins of safety. But the service stresses with aggressive environment may be high enough to induce cracks, particularly if pre-existing flaws or high stress concentrations are present. The high strength materials have a low crack resistance (fracture toughness). The residual strength under the presence of cracks is low. When small cracks exist, structures designed with high strength materials may fail at stresses below the highest service stress that they are designed.

The occurrence of low stress fractures in high strength materials induced the development of fracture mechanics. Fracture mechanics is a method of characterizing the fracture behavior in terms of structural parameters that can be easily understood by the engineer i.e. Stresses, crack size etc.

Fracture mechanics can deliver the methodology to compensate the inadequacies of conventional design concepts. The conventional design criteria are adequate for many engineering structures, but they are insufficient when there is the likelihood of cracks. Now the fracture mechanics has become a useful tool in the design with high strength materials.

II. Modes of Cracking

A crack in a structural component can be stressed in three different modes, which are as shown in Fig 1.

Mode I: Opening Mode   **Mode II: In-plane shear Mode**   **III: Out of plane Shear**
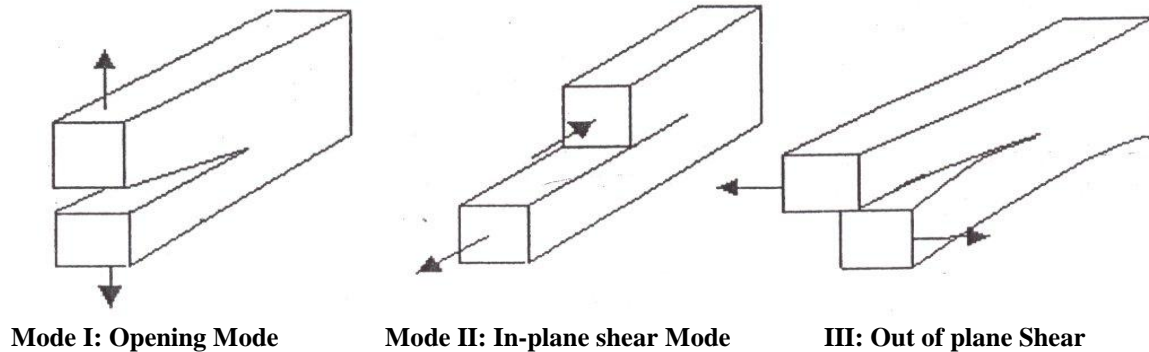
Fig 1. Different modes of cracking

Normal stresses give rise to the "Opening mode" denoted as Mode-I in which the displacements of the crack surfaces are perpendicular to the plane of the crack. In-plane shear results in Mode-II or "Sliding mode", in which the displacement of the crack surfaces is in the plane of the crack and perpendicular to the leading edge of the crack (crack front). The "Tearing mode" or Mode-III is caused by out-of-plane shear, in which the crack surface displacements are in the plane of the crack and parallel to the leading edge of the crack.

III. Light Weight Aggregate

Structural lightweight aggregate concretes are considered as alternatives to concretes made with dense natural aggregates because of the relatively high strength to unit weight ratio that can be achieved. One of the disadvantage of conventional concrete is the high self weight of concrete. Density of the normal concrete is in the order of 2200 to 2600Kg/m³. This heavy self weight will make it to some extent an uneconomical structural material. Attempts have been made and lightweight aggregate concrete have been introduced whose density varies from 300 to 1850Kg/m³.

PUMICE: Increasing utilization of lightweight materials in structural applications making use of pumice stone, has gained importance. Therefore, the need arises to analyze the materials to be used in construction experimentally in detail. Pumice stone has been used since centuries in the world. Pumice aggregate can be found in many places around the world where volcanoes are present. Pumice is a natural sponge-like material of volcanic origin composed of molten lava rapidly cooling and trapping millions of tiny air bubbles.

Review of Literature: In this paper brief reviews of the available studies related to the present Mode-II fracture of cementitious materials are presented. The review covers the study on mode-II fracture parameters analytically and experimentally, light weight aggregate concrete properties etc.

Aggarwal and Giare (1) investigated that critical strain energy release rate in Mode-II is less than half of that in Mode-I or Mode-III indicating that in the case of fibrous composites, the fracture toughness tests in Mode-II may be more important than the tests in mode-I and Mode-III.

Symmetrically notched "Four point shear test specimen was used by Bazant and Pfeiffer (2,3) to study the shear strength of concrete and mortar beams and they concluded that the ratio of fracture energy for Mode II to Mode I is about 24 times for concrete and 25 times for mortar.

Punch Through Shear Specimen Geometries: Prakash Desayi, Raghu Prasad B.K, and Bhaskar Desai.V, (4, 5, 6, 7, 8, 9 and 10) arrived at Double Central Notched specimen geometry which fails in predominant Mode-II failure; They also made finite element analysis to arrive at stress intensity factor. Using this DCN geometry lot of experimental investigation using cement paste, mortar, plain concrete was carried out.

V. Bhaskar Desai, D. Jagan Mohan, V. Vijay kumar (11) studied the mechanical properties like compressive, split tensile strength, modulus of elasticity and flexural behavior of partial replacement of normal coarse aggregate by Hematite aggregate.

Bhaskar Desai. V, Balaji Rao . K, Jagan Mohan . D (12,13) studied the properties like compressive strength, split tensile strength, mode-II fracture properties by using DCN specimen and the fracture toughness values in Mode-II (K_{IIc}) are calculated from the theoritical equations suggested by the earlier researchers and are compared with those obtained from load verses deflection (p-δ) diagrams.

K. Balaji Rao, V. Baskar Desai, D. Jagan Mohan, (14) made probabilistic analysis of Mode-II fracture energy of concrete. The experimentally observed values of mean, minimum and maximum G_{IIF} are compared with their respective values obtained from probabilistic analysis, which are found to be in good agreement. The results of K-S tests performed for different (a/w) ratios and different percentage replacements, an equation is proposed for estimation of characteristic Mode-II Fracture energy.

Light Weight Aggregate Concrete: Owens, P.L. (15) has stated that Light weight aggregate concrete has been used for structural purposes since the 20ᵗʰ century. The Light weight aggregate concrete is a material with low unit weight and often made with spherical aggregates. The density of structural Light weight aggregate concrete typically ranges from 1400 to 2000 kg/m³ compared with that of about 2400 kg/m³ for normal weight aggregate concrete.

Pumice Aggregate: L. Calaveri et.al (16) discussed the properties of lightweight pumice stone concrete (LWPSC) and suggested that pumice can really be considered an alternative to common artificial light weight aggregate, taking into account the performance pointed out by loading tests carried out on structural systems made of LWPSC.

From the brief literature survey conducted in this investigation it is observed that even though primary properties are studied on pumice aggregate concrete, little work is reported on Mode-II fracture properties of pumice aggregate concrete. Hence the present study has been under taken.

IV. Experimental Investigation

An experimental study has been conducted on concrete with partial replacement of conventional coarse aggregate i.e., granite by light weight aggregate i.e., Pumice in Mode-II fracture with few different volumetric fractional additions ranging from 0% to 100%. Concrete of basic M_{20} design mix is used in the present investigation. The test programme consists of carrying out shear strength tests on notched specimens having different a/w ratios. Analysis of the results has been done to investigate the strength variation and shear strength variation in Mode-II fracture with addition of different percentages of Pumice. Variations of various combinations have been studied.

Properties of Constituent Materials: The constituents used in the present investigation are presented in table 1 and constituent materials are shown in plate 1.

Table 1: Properties of Constituent Materials in M_{20} Grade of Concrete

Sl.No	Name of the material	Properties of material	
1	OPC – 53 Grade	Specific Gravity	3.07
		Initial setting time	33 min
		Final Setting time	489 min
		Fineness	4 %
		Normal consistency	33.50 %
2	Fine Aggregate passing 4.75mm sieve	Specific Gravity	2.60
		Fineness modulus	4.10
3	Coarse Aggregate passing 20 – 10 mm	Specific Gravity	2.68
		Fineness modulus	3.37
		Bulk density compacted	1620 Kg/m³
4	Pumice Aggregate passing 20-10mm	Specific Gravity	1.14
		Fineness modulus	5.85
		Bulk density compacted	570 Kg/m³
		Water absorption	21.50 %

Mix Design of Concrete: The concrete mix has been designed for M_{20} grade concrete using ISI method. The mix proportion obtained is 1:1.55:3.04 with constant water cement ratio 0.50.

Test Programme: In this present investigation it is aimed to study the shear strength variations in Mode-II fracture of concrete by modifying the conventional concrete with Pumice in percentages of 0%, 25%, 50%, 75% & 100%, by volume of concrete and designated as mixes P-0, P-25, P-50, P-75 & P-100 respectively as shown in table 2.

Table: 2 Details of Mix Designation

Name of the Mix	Percentage replacement of Pumice aggregate		No of specimens cast	
	Natural Aggregate	Pumice Aggregate	DCN Specimens	Plain Specimens
P-0	100	0	12	3
P-25	75	25	12	3
P-50	50	50	12	3
P-75	25	75	12	3
P-100	0	100	12	3
		Total	60	15

To proceed with the experimental programme initially steel moulds of size 150x150x150 mm with different a/w ratios of 0.3, 0.4 ,0.5, and 0.6 were taken and these moulds were cleaned without dust particles and were brushed with machine oil on all inner faces to facilitate easy removal of specimens afterwards. These moulds are presented in plate 2. To start with, all the materials were weighed in the ratio 1:1.55:3.04. Keeping the volume of concrete constant with saturated and surface dry pumice aggregate was added to concrete in 5 different volumetric fractions to prepare five different mixes which are designated as shown in table 2. First fine aggregate and cement were added and mixed thoroughly and then coarse aggregate with granite and partially replaced Pumice was mixed with them. All of these were mixed thoroughly by hand mixing.

Each time 12 cube specimens with a/w ratios 0.3, 0.4, 0.5, and 0.6 along with 3 plain cubes were cast. Plate 2 shows the arrangement of different notches to suit a/w ratios 0.3, 0.4, 0.5, and 0.6. For all test specimens, moulds were kept on the vibrating table and the concrete was poured into the moulds in three layers, each layer being compacted thoroughly with tamping rod to avoid honey combing. Finally all specimens were vibrated on the table vibrator after filling up the moulds up to the brim. The vibration was effected for 7 seconds and it was maintained constant for all specimens and all other castings. The steel plates forming notches are removed after 3 hour of casting carefully and neatly finished.

However the specimens were demoulded after 24 hours of casting and were kept immersed in a clean water tank for curing. After 28 days of curing the specimens were taken out of water and were allowed to dry under shade for few hours.

V. Testing Of Plain and DCN Specimens

The compression test on the Plain cubes & DCN cubes was conducted on 2000KN digital compression testing machines. The rate of load being applied at 0.1KN/sec.

The specimens after being removed from water were allowed to dry under shade for 24 hours and white washed for easy identification of minute cracks, while testing.

The plain cube specimens were placed on the plate of the hydraulic ram of the compression testing machine such that load was applied centrally. The top plate of the testing machine was brought into contact with the surface of the plain cube specimen to enable loading.

For testing double centered notched (DCN) specimen of size 150x150x150mm, notched were introduced at one third portion centrally as shown in fig 2.

The notch depths provided were 45,60,75 and 90mm running throughout the width of the specimen. Thus the values of a/w ratio were 0.3, 0.4, 0.5, and 0.6 where 'a' is the notch depth and 'w' is the specimen depth 150mm. The distance between the notches is kept constant at 50mm and width of the notch was 2mm.
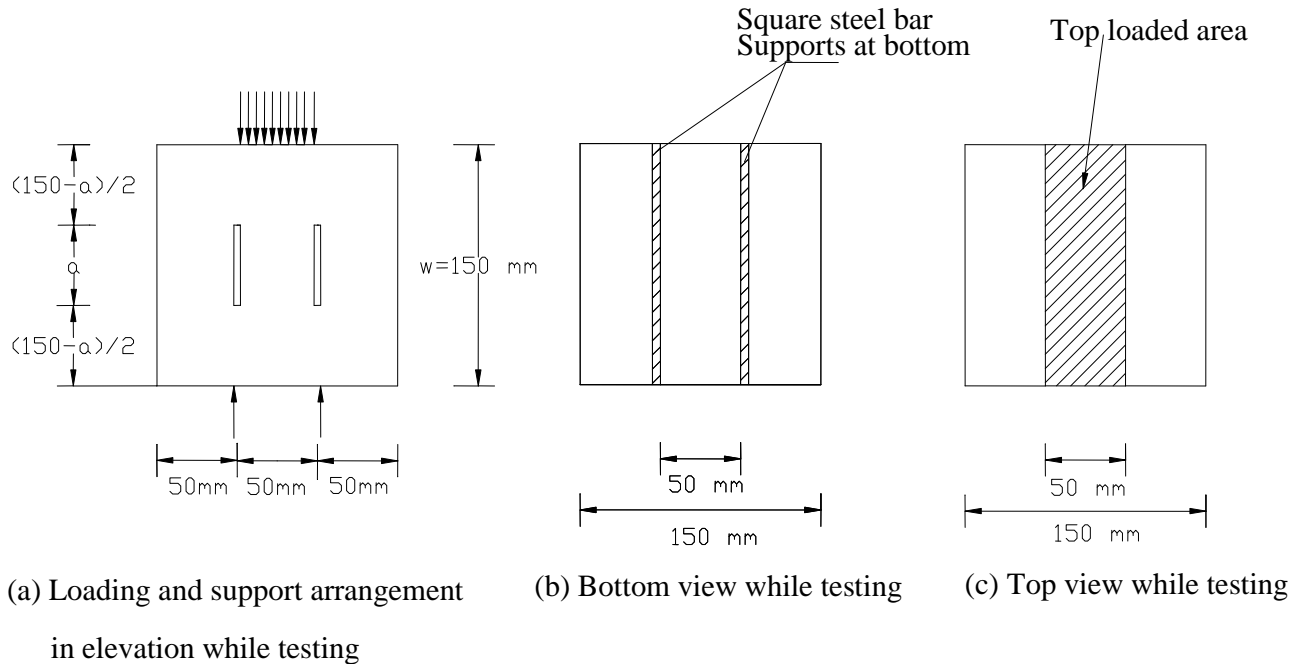
Fig 2. Details of DCN test specimen geometry

(a) Loading and support arrangement in elevation while testing

(b) Bottom view while testing

(c) Top view while testing

VI. Discussion of Crack Patterns

In case of cubes under compression initial cracks are developed at top and propagated to bottom with increase in load and the cracks are widened at failure. The crack patterns obtained for DCN specimen geometry for the four notch depths and cement concrete mixes are presented in plates 5 to 9. During testing, for most of the specimens with a/w= 0.3 initial hair line cracks started at the top of one or both the notches, and as the load was increased further, the cracks widened and propagated at an inclination and sometimes to the middle of the top loaded zone. Simultaneously the cracks formed at the bottom of one or both the notches and propagated downwards visible inclination. In some cases cracks branched into two either at the two edges of the supporting square bar at bottom or at the edge of the loaded length at top or at both places.

In a few cases, initial cracks started at the bottom of the one or both notches. As the load was increased propagation of theses cracks at an inclination was observed along with the formation of cracks at top of the notches. These cracks finally propagated toward the middle of the top loaded zone leading to failure of the specimen. Hence failure of the specimens with a/w = 0.3, could be attributed to the flexure cum shear type of failure.

For most of the specimens with a/w = 0.4, 0.5, 0.6, as the load was applied formation of initial hair line cracks at the top of one or both the notches was observed. With the increase of load propagation of these cracks in more or less vertical direction along with the formation of new cracks at the bottom of one or both the notches was observed. Finally the specimens failed by shearing along the notches. In most of the cases the cracks branched into two to join either the two edges of the supporting square bars at bottom or at the edge of the loaded length at top or at both places. In this case also, in a few specimens, initial cracks started at the bottom of one or both the notches. As the load was increased propagation of these cracks in more or less vertical direction along with formation of new cracks at top of the one or both the notches was observed leading to final collapse of the specimens along the notches.

Thus except for some of the specimens of lower notch-depth ratio i.e., 0.3, the specimens of other higher a/w ratios of cement concrete failed all along the notches in more or less vertical fashion.

VII. Discussion of Test Results

Influence of Pumice on Cube Compressive Strength: In the present study the influence of pumice has been studied by replacing it with the natural coarse aggregate in volumetric percentages of 0%, 25%, 50%, 75% and 100%. The variation between cube compressive strength and percentage of pumice replacing the natural

aggregate results is as shown in table 3 and the graphical representation of superimposed variation is as shown in fig 3 for 28 days of curing. By observing the table of results as well as graphical representation, with the percentage increase of pumice the cube compressive strength decreases continuously from 0 to 100%. The test set up is presented in plate 3.

Discussion on the Effect of Pumice on DCN Specimens: All the DCN specimens with different a/w ratios i.e., 0.3, 0.4, 0.5, and 0.6 and with different percentage of Pumice i.e., 0%, 25%, 50%, 75%, 100%, were tested in Mode-II arrangement (in-plane shear) as shown in fig 2. The corresponding first crack loads, ultimate loads and the percentage of increase or decrease are presented in table 4 to 7. The In-plane shear stress was calculated by the standard formula.

In-plane shear stress $= \dfrac{P}{A}$

Where, P = Ultimate or First crack Load in 'N'
  A = Shear area in 'mm^2' which is = 2B (w-a).
  B = Width or breadth of the specimen = 150 mm
  w = Depth of the specimen = 150 mm
  a = Notch depth varies i.e 45, 60, 75 and 90mm

The variations of the above parameters versus percentage of pumice are graphically presented in fig 4 to 7. The first crack load and ultimate load in In-plane shear stress is decreased with increase in replacement of percentage of pumice for all A/W ratios from 0.30 to 0.60. The test set up of DCN specimen is presented in plate 4.

Calculation of Stress Intensity Factor (K_{IIC}): The stress intensity factors for cement concrete mixes have been determined using two approaches viz.,(i) Fracture energy approach, (ii) Finite element analysis approach, that is making use of the formulae arrived at through the finite element analysis proposed by Prakash Desayi et al (17).

Fracture-Energy Approach: In this approach, P (load)-δ (displacement) diagrams were plotted to a suitable scale separately for each a/w ratio and for each percentage of Pumice. A sample P-δ diagram is presented in fig 8. In these diagrams the points shown by arrows indicate the loads at first crack and ultimate load. From the P-δ diagrams, the areas included between the X-axis and the P-δ curves were calculated using simpson's 1/3 rule. The areas so obtained are presented in the table 8.

Then the fracture energy (G) was determined as the area under P-δ diagram per unit shear area. The shear area (A) = 2B (W-a)
  Where B= width or breadth of the specimen = 150 mm
    W= depth of the specimen = 150 mm
    a = notch-depth.
From the fracture energy values so obtained, the critical stress intensity factors for Mode-II, K_{IIC} were calculated using the standard relation i.e. $G = K^2_{IIc} (1-\upsilon^2)/E$
  Where υ = poison's ratio
    E = modulus of elasticity in N/mm^2 = $5000\sqrt{f_{ck}}$
    f_{ck} = 28 days cube compressive strength in N/mm².

Finite Element Analysis Approach: In this approach, the expression for K_{IIC} in terms of a/w using the least square curve fitting method done by Prakash Desayi et al (17) was considered as
$K_{IIC}/(P\sqrt{(\pi a)}/2) = 6.881-11.355(a/w)+15.599(a/w)^2-6.33(a/w)^3$
Where P =total load/ loaded area
  a =depth of notch
  w = depth of DCN specimen = 150mm
Comparing the K_{IIC} values calculated from the two approaches it may be observed that the K_{IIC} values obtained from fracture energy approach are found to be lesser.

VIII. Conclusions

From the limited experimental study the following conclusions are seem to be valid:

1. From the study it is observed that the cube compressive strength is decreased continuously with the increase in percentage of Pumice i.e., from 0% to 100% replacing of conventional aggregate by Pumice aggregate.
2. It is observed that the first crack load as well as ultimate load in mode-II is decreased with the increase in percentage of pumice from 0% to 100%.
3. It is also observed that the first crack load as well as ultimate load in Mode-II is decreased with increased a/w ratios.
4. It is observed that In-plane shear stress at first crack load as well as ultimate load is decreased with increasing percentage of pumice.
5. It is also found that the In-Plane shear stress at first crack load and Ultimate load in Mode-II are decreased with increased a/w ratios.
6. The K_{IIC} values calculated from the fracture energy approach are found to be lesser than those values arrived from Finite element analysis.
7. In both the approaches the K_{IIC} values are found to decrease continuously with the percentage increase in Pumice aggregate content.

Table 3: Cube Compressive Strength Results

S. No	Name of the mix	Percentage replacement of coarse aggregate		Compressive strength (N/mm^2)	Percentage increase or decrease in Cube compressive strength w.r.t. P-0
		Natural coarse aggregate	Pumice aggregate		
1.	P-0	100	0	41.08	0.00
2.	P-25	75	25	34.18	-16.80
3.	P-50	50	50	22.28	-45.76
4.	P-75	25	75	16.12	-60.76
5.	P-100	0	100	12.87	-68.67

Table 4: First Crack Load and Percentage Increase or Decrease in First Crack Load in Mode-Ii of DCN Specimens with A/W Ratio = 0.30, 0.40, 0.50, 0.60.

Sl. No	Name of the Mix	Percentage replacement of coarse aggregate		a/w = 0.30		a/w = 0.40		a/w = 0.50		a/w = 0.60	
		Conventional aggregate	Pumice aggregate	First crack load in KN	Percentage increase or decrease in First crack load w.r.t. P-0	First crack load in KN	Percentage increase or decrease in First crack load w.r.t. P-0	First crack load in KN	Percentage increase or decrease in First crack load w.r.t. P-0	First crack load in KN	Percentage increase or decrease in First crack load w.r.t. P-0
1.	P-0	100	0	110.00	0.0	93.00	0.0	76.00	0.0	57.00	0.0
2.	P-25	75	25	77.67	-29.39	58.33	-37.28	47.67	-37.28	35.33	-38.02
3.	P-50	50	50	64.67	-41.21	51.67	-44.44	42.00	-44.74	32.67	-42.68
4.	P-75	25	75	47.33	-56.97	39.33	-57.71	30.33	-60.09	23.00	-59.65
5.	P-100	0	100	32.00	-70.91	26.00	-72.04	21.00	-72.37	9.00	-84.21

Table 5: Ultimate Load and Percentage Increase or Decrease in Ultimate Load in Mode-II of DCN Specimens with A/W Ratio = 0.30, 0.40, 0.50, 0.60

Sl. No	Name of the Mix	Percentage replacement of coarse aggregate		a/w = 0.30		a/w = 0.40		a/w = 0.50		a/w = 0.60	
		Conventional aggregate	Pumice aggregate	Ultimate load in KN	Percentage increase or decrease in Ultimate load w.r.t. P-0	Ultimate load in KN	Percentage increase or decrease in Ultimate load w.r.t. P-0	Ultimate load in KN	Percentage increase or decrease in Ultimate load w.r.t. P-0	Ultimate load in KN	Percentage increase or decrease in Ultimate load w.r.t. P-0
1.	P-0	100	0	144.00	0.0	105.00	0.0	83.00	0.0	62.00	0.0
2.	P-25	75	25	98.00	-31.94	82.33	-21.59	62.67	-24.49	41.67	-32.79
3.	P-50	50	50	91.33	-36.58	72.33	-31.11	58.00	-30.12	40.33	-34.95
4.	P-75	25	75	71.67	-50.23	56.67	-46.03	43.33	-47.80	34.00	-45.16
5.	P-100	0	100	40.00	-72.22	33.00	-68.57	25.00	-69.88	19.00	-69.35

Table 6: In-Plane Shear Stress and Percentage Increase Of Decrease in In-Plane Shear Stress at First Crack Load in Mode-II of DCN Specimens with A/W Ratio = 0.30, 0.40, 0.50, 0.60

Sl. No	Name of the Mix	Percentage replacement of coarse aggregate		a/w = 0.30		a/w = 0.40		a/w = 0.50		a/w = 0.60	
		Conventional aggregate	Pumice aggregate	In-Plane shear stress in N/mm²	Percentage increase or decrease w.r.t. P-0	In-Plane shear stress in N/mm²	Percentage increase or decrease w.r.t. P-0	In-Plane shear stress in N/mm²	Percentage increase or decrease w.r.t. P-0	In-Plane shear stress in N/mm²	Percentage increase or decrease w.r.t. P-0
1.	P-0	100	0	3.49	0	3.45	0	3.38	0	3.17	0
2.	P-25	75	25	2.47	-29.23	2.16	-37.39	2.12	-37.28	1.96	-38.17
3.	P-50	50	50	2.05	-41.26	1.91	-44.64	1.87	-44.67	1.82	-42.59
4.	P-75	25	75	1.5	-57.02	1.46	-57.68	1.35	-60.06	1.28	-59.62
5.	P-100	0	100	1.02	-70.77	0.97	-71.88	0.94	-72.19	0.5	-84.23

Table 7: In-Plane Shear Stress and Percentage Increase Of Decrease in In-Plane Shear Stress at Ultimate Load in Mode-II of DCN Specimens with A/W Ratio = 0.30, 0.40, 0.50, 0.60.

Sl. No	Name of the Mix	Percentage replacement of coarse aggregate		a/w = 0.30		a/w = 0.40		a/w = 0.50		a/w = 0.60	
		Conventional aggregate	Pumice aggregate	In-Plane shear stress in N/mm²	Percentage increase or decrease w.r.t. P-0	In-Plane shear stress in N/mm²	Percentage increase or decrease w.r.t. P-0	In-Plane shear stress in N/mm²	Percentage increase or decrease w.r.t. P-0	In-Plane shear stress in N/mm²	Percentage increase or decrease w.r.t. P-0
1.	P-0	100	0	4.57	0	3.89	0	3.69	0	3.45	0
2.	P-25	75	25	3.11	-31.95	3.05	-21.59	2.79	-24.39	2.32	-32.75
3.	P-50	50	50	2.9	-36.54	2.68	-31.11	2.58	-30.08	2.24	-35.07
4.	P-75	25	75	2.28	-50.11	2.1	-46.02	1.93	-47.70	1.89	-45.22
5.	P-100	0	100	1.27	-72.21	1.22	-68.64	1.11	-69.92	1.06	-69.28

Table 8: Variation between K_{IIC} Verses a/w Ratio Using Formula Obtained From Fracture Energy Approach and Finite Element Analysis

S. No	Name of the mix	Percentage by volume replacement of coarse aggregate		f_{ck} N/mm²	a/w ratio	Area under p-δ diagram KN-mm	Stress Intensity factor (K_{IIC}) MN/m$^{3/2}$	
		Natural Coarse aggregate	Percentage of Pumice				From Fracture energy	From finite element analysis
1.	P-0	100	0	41.08	0.3	97.980	10.06	24.02
					0.4	57.920	8.36	19.03
					0.5	33.990	7.01	16.37
					0.6	28.105	7.13	13.41
2.	P-25	75	25	34.18	0.3	54.858	7.19	16.35
					0.4	40.238	6.65	14.93
					0.5	30.459	6.34	12.37
					0.6	23.930	6.28	9.02
3.	P-50	50	50	22.28	0.3	42.043	5.66	15.24
					0.4	40.417	5.99	13.12
					0.5	26.785	5.95	11.44
					0.6	20.375	5.21	8.73
4.	P-75	25	75	16.12	0.3	41.978	5.21	11.96
					0.4	38.405	5.38	10.28
					0.5	22.903	4.55	8.55
					0.6	19.850	4.74	7.36
5.	P-100	0	100	12.87	0.3	29.800	4.15	6.67
					0.4	22.610	3.90	5.98
					0.5	9.315	2.75	4.93
					0.6	8.030	2.85	4.11

REFERENCES

[1] Agarwal, B.D. and Giare, G.S., "Fracture toughness of short-fiber composites in Modes-I and II", Engineering Fracture Mechanics, Vol. 15, No. 1, 1981, pp.219-230.

[2] Bazant , Z.,p, and Pfeiffer, P.A., "Shear fracture tests of concrete", materials and structures (RKLEM) , 1984, vol. 19, pp.111-121.

[3] Bazant , Z.,p, and Pfeiffer, P.A., "Tests on shear fracture and strain softening in concrete", proceedings of second symposium on interaction of Non-nuclear Munition with structures Florida, USA, April 1985, pp. 254-264.

[4] Bhaskar Desai . V, "Some studies on Mode - II fracture and stress – strain behavior in shear of cementitious materials", Ph.D thesis, Indian Institute of Science, Banglore".

[5] Prakash Desayi, Raghu Prasad .B.K, and Bhaskar Desai . V, "Experimental determination of K_{IIc} from compliance and fracture energy", proceedings national seminar on Aerostructures, organized by IIT, Kanpur, India, 29-30, Dec, 1993, pp. 33-34.

[6] Prakash desayi, B.K.Raghu Prasad and V.Bhaskar Desai, "Mode – II fracture of cementitious materials- part – I : Studies on specimens of some new geometries", Journal of Structural Engineering, Vol.26, No.1, April 1999, pp.11-18.

[7] Prakash desayi, B.K.Raghu Prasad and V.Bhaskar Desai, "Mode – II fracture of cementitious materials- part – II: Fracture toughness of cement paste, mortar, concrete and no-fines concrete. Journal of structural engg Vol. 26, No. 1, April 1999, pp. 19-27.

[8] Prakash desayi, B.K.Raghu Prasad and V.Bhaskar Desai, "Mode – II fracture of cementtiotus materials- part – III: Studies on shear strength and slip of cement paste, mortar, concrete and no-fines concrete. Journal of structural engg Vol. 26, No.2, July 1999, pp. 91-97.

[9] Prakash desayi, B.K.Raghu Prasad and V.Bhaskar Desai, conducted Mode-II fracture of cementitious materials- part-IV: Fracture toughness, shear strength and slip of fibre reinforced cement mortar and concrete. Journal of structural engg. Vol. 26, No. 4, Jan 2000, pp. 267-273.

[10] Prakash desayi, B.K.Raghu Prasad and V.Bhaskar Desai, conducted Mode-II fracture of cementitious materials- part-V: Size effect on fracture toughness shear strength and slip of cement mortar and concrete reinforced with and without fibers. Journal of structural engg, Vol, 27, No. 2, July 2000, pp.99-104.

[11] V. Bhaskar Desai, D. Jagan Mohan, V. Vijay kumar, " Some studies on strength properties of Metallic aggregates", Proceedings of the International conference on advance in concrete composites and structures, January 2005, pp. 235-246.

[12] V. Bhaskar Desai, K. Balaji Rao, D. Jagan Mohan, "Some studies on Mode-II fracture of heavy weight Metallic aggregate cement concrete", An International Research of Engineering sciences and technologies, Vol. 1, No. 2, October 2008, pp. 41-47.

[13] V. Bhaskar Desai, K. Balaji Rao, D. Jagan Mohan, "experimental investigations on Mode-II fracture of concrete with crushed granite stone fine aggregate replacing sand", Materials research, received March 2011.

[14] K. Balaji Rao, V. Bhaskar Desai, D. Jagan Mohan, "Probabilistic analysis of Mode-II Fracture of Concrete with crushed granite stone fine aggregate replacing sand", Construction and building Materials, Vol. 27, No, 1, Febrauary 2012, pp. 319-330.

[15] Owens, P.L. (1993). "Light weight aggregates for structural concrete," Structural Light weight Aggregate Concrete, Chapman & Hall, London, pp.1-18.

[16] L. Cavaleri , N. Miraglia and M. Papia, "Pumice Concrete for structural wall panels", Engineering structures, Vol. 25, No. 1,Jan 2003, pp. 115-125.

[17] Bhaskar Desai. V, "Some studies on Mode - II fracture and stress – strain behavior in shear of cementitious materials", Ph.D thesis, Indian Institute of Science, Bangalore".
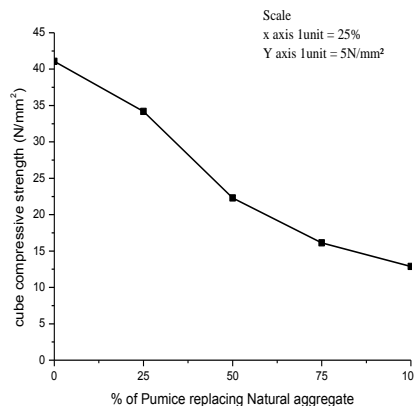
Fig 3: Variation between Cube compressive strength and percentage of Pumice replacing Natural aggregate
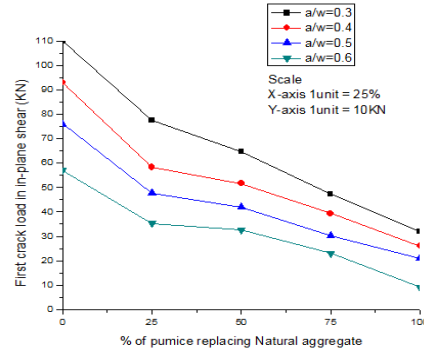
Fig 4: Variation between first crack load in in-Plane shear and Percentage of Pumice replacing Natural aggregate with a/w=0.3,0.4,0.5,0.6
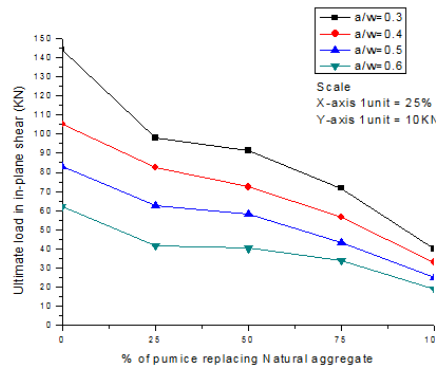
Fig 5: Variation between ultimate load in in-Plane shear and percentage of Pumice replacing Natural aggregate with a/w=0.3,0.4,0.5,0.6
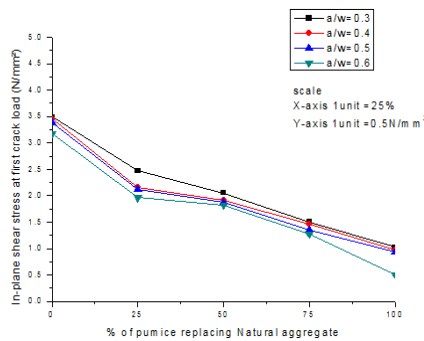
Fig 6: Super imposed variation between in-Plane shear stress at first crack load and percentage of Pumice replacing Natural aggregate with a/w=0.3,0.4,0.5,0.6
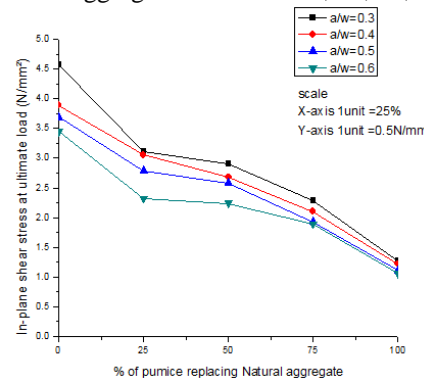
Fig 7: Super imposed variation between in-Plane shear stress at ultimate load and Percentage of Pumice replacing Natural aggregate with a/w=0.3,0.4,0.5,0.6
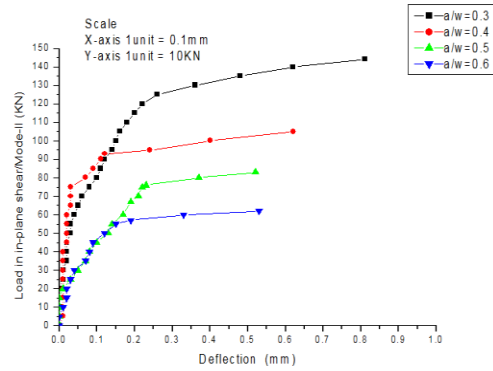
Fig 8: Super imposed variation between In-plane shear load and deflection for 0 % Pumice replacing natural aggregate with a/w=0.3,0.4,0.5,0.6

Plate 1. Ingredients of concrete

Plate. 2 View of the moulds with double centered notches
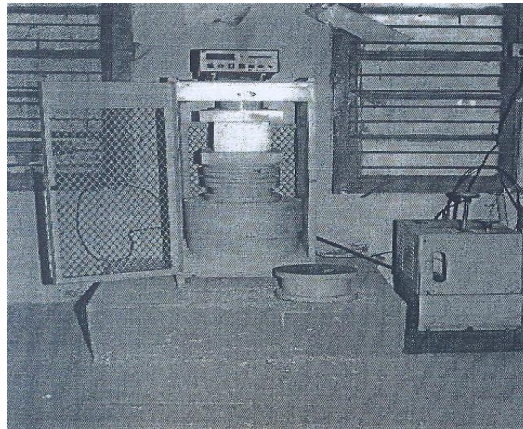
Plate 3. Test setup for cube compressive strength test

Plate 4. Test setup for DCN specimen
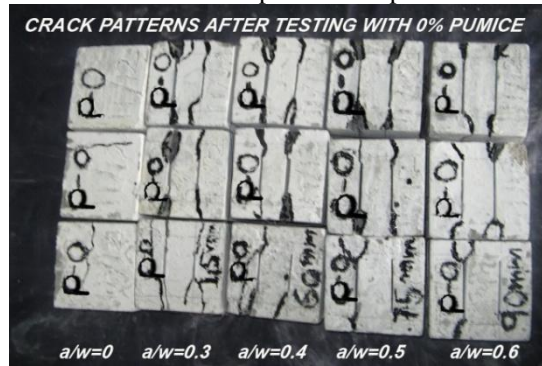
Plate 5. Crack pattern of the specimens after testing with 0% of pumice
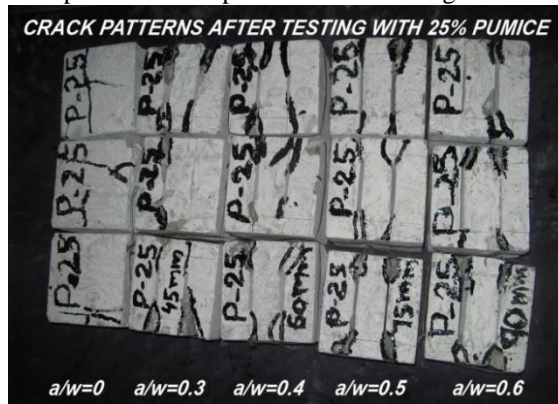
Plate 6. Crack pattern of the specimens after testing with 25% of pumice
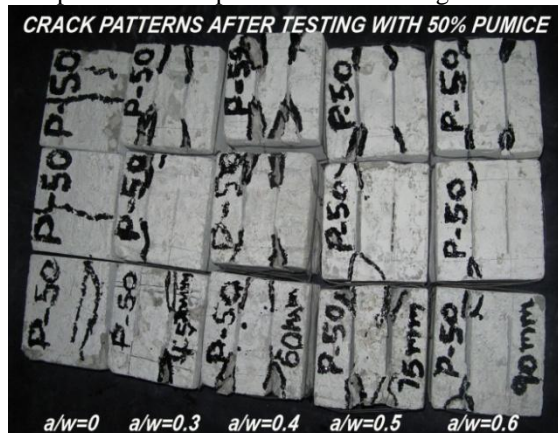
Plate 7. Crack pattern of the specimens after testing with 50% of pumice
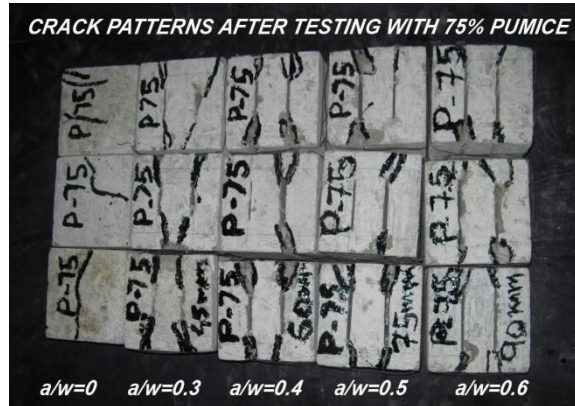
Plate 8. Crack pattern of the specimens after testing with 75% of pumice
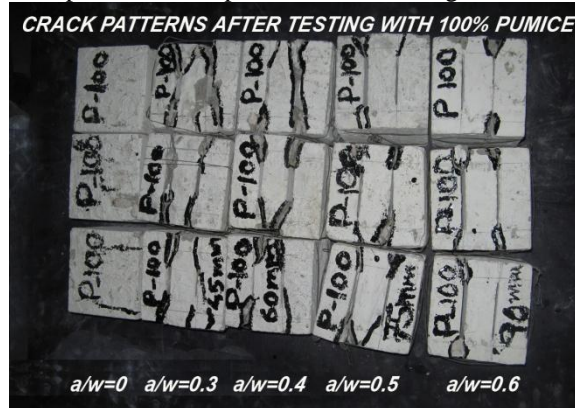
Plate 9. Crack pattern of the specimens after testing with 100% of pumice

A Comparative Study on Linear Friction Welding for Dissimilar Metals

Syed Hameeduddin Ahmed[1], Syed Khaja Imtiyazuddin Ahmed[2],
Mohammed Ehaabuddin Farooqui[3], Mohammed Ibrahim Abdul Aleem[4],
Faraz Hussain Hashmi[5], M A Salman[6], Md. Mohiuddin[7]

[1]*Industrial Production Engineering Department, Student at Muffakham Jah College of Engineering & Technology*
[2]*Mechanical Engineering Department, Student at Green Fort College of Engineering & Technology*
[3]*Industrial Production Engineering Department, Student at Muffakham Jah College of Engineering & Technology*
[4]*Industrial Production Engineering Department, Student at Muffakham Jah College of Engineering & Technology*
[5]*Industrial Production Engineering Department, Student at Muffakham Jah College of Engineering & Technology*
[6]*Industrial Production Engineering Department, Student at Muffakham Jah College of Engineering & Technology*
[7]*Mechanical Engineering Department, Student at Moghal College of Engineering & Technology*

ABSTRACT: *Linear Friction welding (LFW) is a solid state joining process in which a joint between two metals can be formed through the intimate contact of a plasticised layer at the interface of the adjoining specimens. When a stationary workpiece is pushed against another workpiece which is moving in a linear reciprocating manner, the plasticised layer is created through a combination of frictional heating between these two metals. This paper will cover the basics of the process and the fundamental aspects of operating a LFW machine using dissimilar metals.*

Keywords: *Linear friction welding, titanium, 304L stainless steel, nickel layer, microhardness structure.*

I. Introduction

Linear friction welding was first patented in 1929. However, the description of the process was vague. Some discussion of the concept was then recorded in the 1960s, but it was described as 'very doubtful' because of the difficulty in generating linear reciprocation. The Caterpillar Tractor Company was the next to mention the process in a patent. However, the patent primarily focused on the machine that generates the linear reciprocation and not the actual welding process. Indeed a patent search has shown that no currently valid patents exist that protect the fundamentals of the LFW process. However many patents protect certain aspects of LFW, such as particular applications, welding methods or tooling concepts.

It is actually a solid-state joining process that is a combination of extruding and forging and is not a true welding process. In this process a stationary part is forced against a part that is reciprocating in a linear manner in order to generate frictional heat as shown in (*Fig.1,2 & 3*). The heat, along with the force applied perpendicular to the weld interface, causes material at the interface to deform and plasticise. Much of this plasticised material is removed from the weld, as flash, because of the combined action of the applied force and part movement. Surface-oxides and other impurities are removed, along with the plasticised material, and this allows metal-to-metal contact between parts and allows a joint to form. Although the LFW of dissimilar materials has been almost totally unexplored, there has been a large amount of work on the RFW of dissimilar materials, with some good results produced. As the two processes are fundamentally similar (*i.e.* in both processes heat is generated by contact and relative movement between parts, and plasticised material is ejected by a combination of part movement and applied force), this provides hope that dissimilar welds can also be produced with the LFW process.
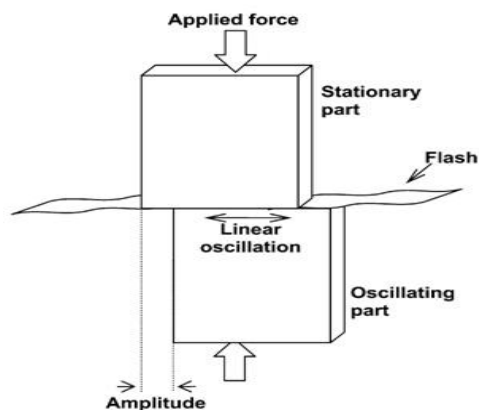
Fig.1
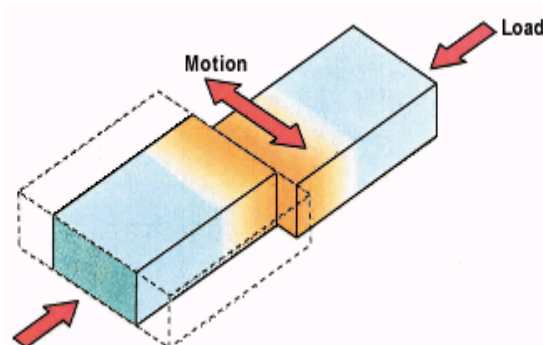
Fig.2
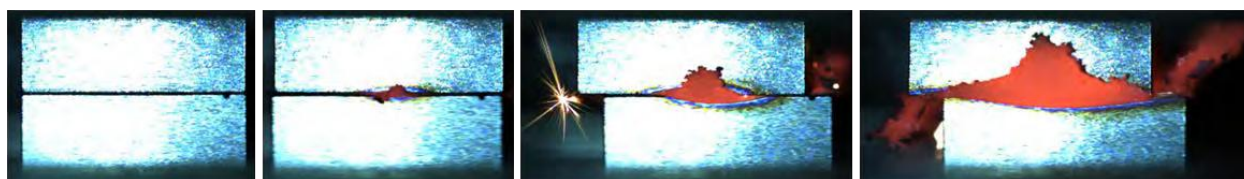
Fig.3 *1 Images taken during welding showing the different process phases*

The process can be divided into six phases: *contact* - initial advancement of actuators seating the blade onto the disc stub and applying a seating force, *ramp up* - blade oscillations start to occur, *conditioning* – maintaining the oscillations to enable frictional heat to build up, *burn-off* – material deforming plastically under compression, *ramp down* – blade decelerated to a static position, and *forging* – allowing the weld to complete under a constant pressure.

II. Linear Friction Welding Machine Operation

The machine operation of the LFW process can be broken down into six separate stages. These are:

Part clamping: The parts are held using tooling designed to withstand the forces experienced during the process. Specimen and tooling preparation is critical to the process, with accurate sides and edges needed on the specimen, and a tight-fit needed between the specimen and the tooling. This generally means that the tooling is custom built to fit particular specimen geometries.

Datum and retract: The clamped parts are brought together under a small compressive force in order to determine the location of the parts and set the machine datum to zero. The parts are then retracted to leave a small separation distance between the work pieces.

Conditioning phase: Oscillation of one of the parts is increased and stabilized over a set period (usually very quickly) and the parts are brought together under a small force for a predetermined time (*Fig.4*).

Frictional phase: The compressive force (friction force) is increased to a set level and heat is generated at the interface. The material at the interface becomes plastic and flows out of the weld, as flash, because of the shearing motion between the two parts and the applied force. This loss of material from the weld causes the parts to shorten (or burn-off). This phase usually ends, and the next is triggered, when a predetermined loss of length, or burn-off distance, is reached. However, the next phase can also be triggered after the frictional phase has continued for a predetermined time (burn-off time) or number of oscillation cycles (burn-off cycles). The LFW process is always carried out under load control, but other parameters also play a role in controlling the welding process. For example when using a burn-off distance the load is controlled throughout the welding process, however the burn-off is also monitored (although not controlled) and at a set burn-off distance the next phase (forge phase) is triggered. Similarly with burn-off time or cycles the load is controlled throughout welding and the amount of time or cycles determines the transition to the next phase.

Forge phase: The amplitude is decayed to zero over a predetermined time to ensure good alignment (usually very quickly), and a forge force is rapidly applied and held for a set time to consolidate the joint. The forge force can either be the same as or higher than (more common) the friction force.

Release phase: The welded parts are released from the clamps and removed from the machine.
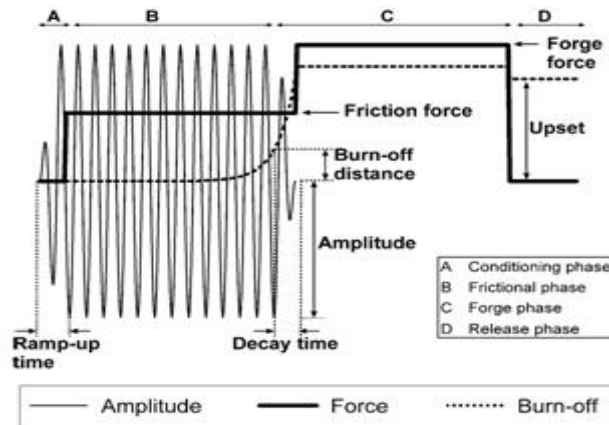
Fig.4. *Schematic diagram of the parameter traces that are obtained during the linear friction welding process A number of input variables are defined in the diagram. Burn-off is defined as the loss of length occurring as the process continues, whilst upset is the total loss of length measured after the weld has been produced*.

III. Linear Friction Welding Of Titanium-Stainless Steel Joints with a Nickel Interlayer Nickel Alloys

Linear Friction Welding is particularly suited to joining materials that have good high temperature properties, especially compressive yield and shear strength, and a low thermal conductivity. The good high temperature mechanical properties allow a high level of frictional heat generation, whilst the low thermal conductivity helps confine heat to the interface. This makes titanium and nickel alloys, with their good high temperature mechanical properties and low thermal conductivities, particularly suitable for the process.

The joining of titanium to steel by using conventional fusion welding techniques is resulted in major metallurgical problems. He et al. (1999). Sun et al. (1996) studied on dissimilar metal joint by convectional arc welding processes reported that the joints between Ti and Steels unsuccessful due to involve in melting of base materials.

Titanium:

Titanium possesses high strength when alloyed with additional metals and elements. It is highly resistant to most types of corrosion. Most metals will corrode in the presence of salt water, acids, and other chemical solutions, however titanium shows surprising resilience to these. Titanium is also very resistant to stress corrosion cracking unlike stainless steel.
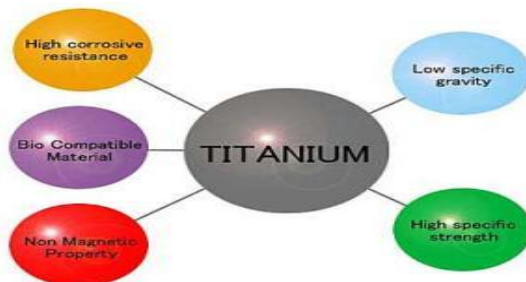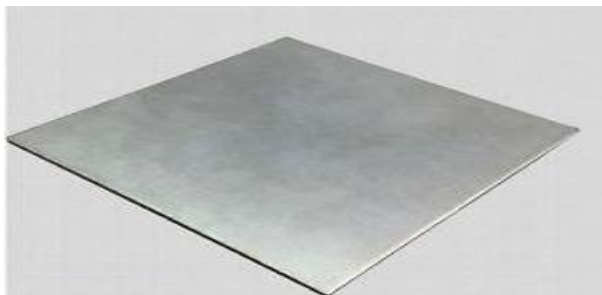
Stainless Steel (304L): 304L is a low carbon version of type 304 stainless. 304L is used almost interchangeably with 304 but is preferred for welding operations. It offers a good combination of strength, corrosion resistance and fabric ability.

Nickel:

Nickel metal has been used for many purposes and applications because of its high melting point, its resistance to corrosion, and its catalytic properties. It is face centered cubic and undergoes no phase changes as it cools from melting point to room temperature; similar to a stainless steel. All the conventional welding processes can be used to weld nickel and its alloys and matching welding consumables are available.
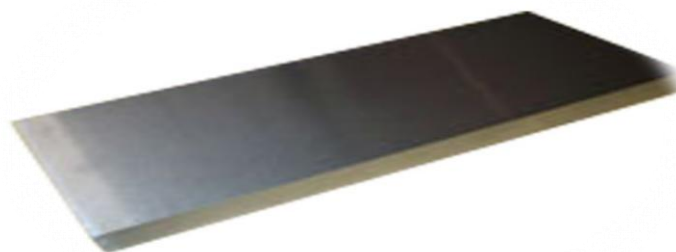
IV. Experimental procedure

The materials used in the present experiment were titanium and 304L austenitic stainless steel metal which are machined respectively. The contact surfaces of titanium and stainless steel specimen were polished by using a range of emery papers and alumina cloth polishing to maintain an equal surface roughness. The interlayer material such as Nickel was deposited by electro plating on the stainless substrates. The substrates were cleaned with acetone to remove the grease and enduring contaminants before performing friction welding. The welds which were made between and 304L stainless steel with nickel interlayer by linear friction welding process, each deform resistance differs greatly, in that the titanium base metal deforms by plastic deformation during joining. The titanium metal maintained as a oscillating member and stainless steel positioned in a stationary side. The produced friction weld were resulted in the physical appearance of titanium linear flash is greater than the stainless metal.
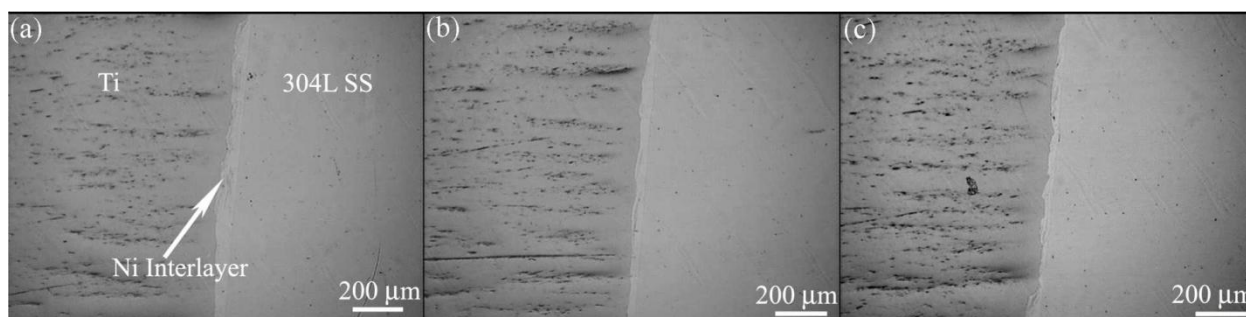
Fig.5. Different interlayer thickness of joints

The evaluation of joint strengths was conducted after making joints immediately performed a drop test for all the welds at various welding parameters. After completion of welding the resulted weld are taken out from the machine and tensile specimen was prepared as per ASTM-E8 standard. Ti was experienced to plastic deformation at higher temperature; hence the existed dynamic recrystallization had resulted in fine equi-axed grains closed to the weld interface. The thermal conductivity of stainless steel is larger than that of titanium substrate. Thus the formation of heat at interface by frictional effect is mainly produced on titanium side because of its low thermal conductivity temperature. However there is no noticeable change of recrystallization effect at the stainless side. The weld interface between titanium nickel interlayer is characterized by thin transition layer revealed at the interface region. The transition layer thickness increases with increasing friction time. The linear depends of the transition layer thickness on the square root of the friction time implies that the growth of interface caused by the diffusion.
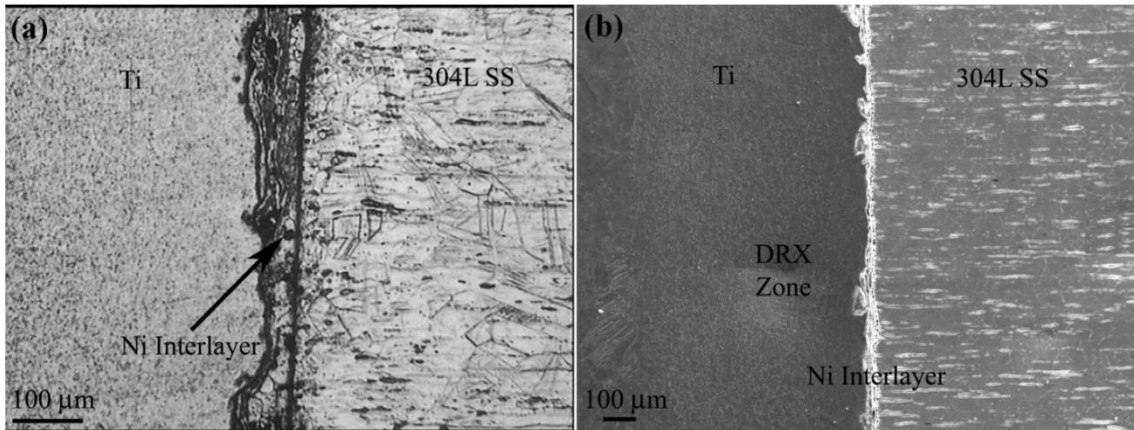
Fig.6. linear friction welded piece of titanium-stainless steel joints with a nickel interlayer.

4.1 Micro hardness distribution

The micro hardness measurement were made across the welds to identify the microstructural strength on heat affected zone, base metals, interlayer materials and both interfaces are shown in Fig. 7. The hardness profile gradually increasing from the substrates to the respective weld interface. Virtually the similar tendency of hardness distribution is identified for the two welded material are considerably increases in the dynamic crystallization zone and the highest hardness value is attained near the weld interfaces. This is due to the grain size in dynamic crystallization zone is finer than that of heat affected zone, so the dynamic crystallization zone has a higher hardness value rendering to the Hall-Petch relationship, Sato et al., (2003) . It is observed that the hardness profile in Fig.7 showing a steep increase in hardness in titanium side near the weld interface is directly related to the microstructure formed in the welds as a result of strain hardening effect during the friction welding process. The increase in hardness at stainless steel side is very less compare to titanium side, it is indicating the strain hardening effect is less and extent of deformation is limited in stainless steel compare to titanium. Based on the distribution of hardness profile it can be declared that the hardness values of the combination of intermetallic compounds were newly generated in the welds has higher value than that of substrates. The highest recorded at titanium-nickel interface can be attributed to the formation of intermetallics of titanium and nickel. All the above discussed factor can together impact and result in the hardness profile may directed that the weld interfaces is the weakest region when experienced to load. The formation Ni/Ti intermetallics at weld interface are came to the degradation of weld strength of the joints.
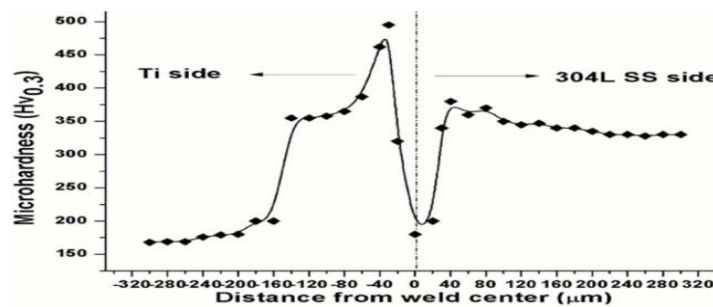
Fig. 7: Micro hardness distribution across the joints

V. Weld Ability

Most of the publicly available work on weld ability and welding parameters has been conducted on Ti-64, however similar concepts should be equally applicable to other materials. Vairis and Frost showed that for sound linear friction welds to be formed in Ti-64, a specific power input parameter must be exceeded. It was shown that frequency; amplitude and pressure have an effect on this parameter, which was defined as:

$$w = \frac{\alpha f P}{2\pi A}$$

with α being the amplitude, f the frequency, P the pressure and A the weld area. From this equation it can be seen that the power input can be increased by increasing the frequency, amplitude or pressure. A similar critical power input has also been suggested to exist for linear friction welds in 304L stainless steel.

Wanjara and Jahazi showed that another parameter, the upset, was also important in forming sound welds and demonstrated that a minimum level of upset was necessary to consolidate the weld. Therefore the power input parameter devised by Vairis and Frost cannot be used as an exclusive criterion for obtaining sound welds.

VI.   Effects of Welding Parameters

The influences of various welding parameters on the size of recrystallised β grains in the near weld line region of Ti-64 welds have been reported. This work gives a good insight as to how the interface temperature varies as welding parameters are changed, as the β grain growth will be dependent on it. It was shown that an increase in frequency or pressure increases the size of the prior β grains (Fig .8). This is thought to be because an increase in power input, associated with an increase in frequency or pressure, causes the temperature at the interface to be greater. However, the increased prior β grain size could also be related to slow cooling rates when high parameters were used.
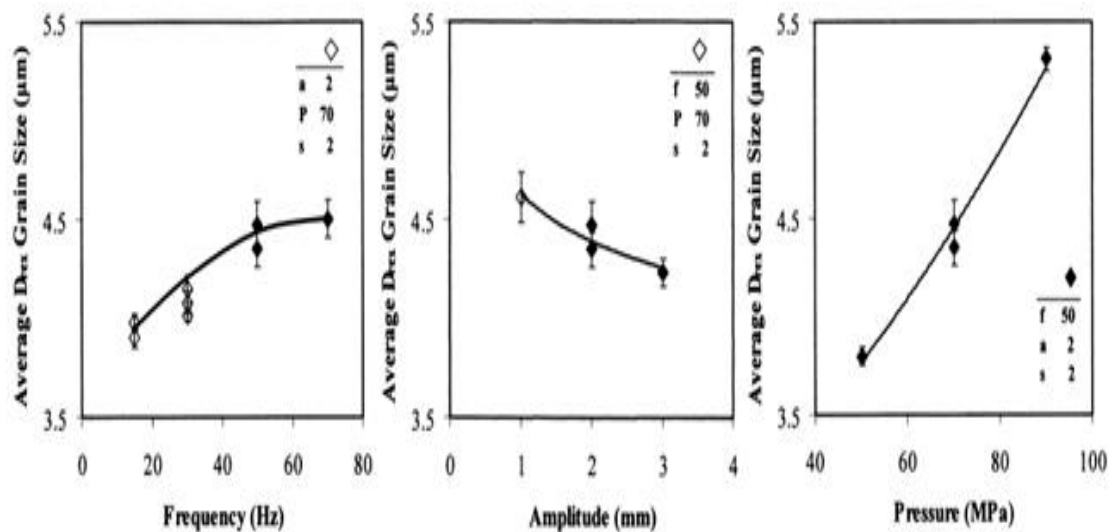
Fig.8 *Effects of frequency, amplitude and pressure on average prior β grain size in the weld zone of Ti-64 linear friction welds. a: amplitude, P: pressure, f: frequency, s: burn-off distance. Open markers indicate poor welds.*

More recent work, however, has shown that the prior β grain size actually decreases at high pressures, which has been interpreted as a reduction in the peak welding temperature, although changes in the overall weld thermal cycle may also have contributed to producing these effects. This proposed decrease in temperature was attributed to a large amount of flash expulsion at high pressures, which caused large heat rejection, and short welding times.

VII.   Equations of Power Input And Modeling of Linear Friction Welding

The heat input power per unit area in this model was defined as:

$$q_A = \tau * \upsilon = \frac{F_S}{A} * \upsilon = \frac{\mu F_N}{A} * \upsilon$$

$$= \frac{\mu F_N}{D(W - \alpha \sin(\alpha t))} * \alpha \omega \cos(\alpha t)$$

Equation.1

where T is the shear stress, ν is the sliding velocity, F_S is the shear force, μ is the co-efficient of friction, FN the force normal to the interface, α is the amplitude, Ω is the angular frequency (2Π*oscillation frequency), t is the time, D is the thickness, and W is the width of the specimen (weld area = DW). A is the contact area, which is not constant and will change during the oscillatory cycle.

Although the equation of power input into the weld (equation (1)) is likely to be sufficient for a retrospective analysis of heat input, it may not satisfy requirements for a forward, predictive, analysis from a given set of initial welding parameters (*i.e.* pressure, force, frequency, amplitude and burn-off distance). This is

largely because of the difficulty in predicting the shear force (force in the reciprocating direction) that results from the initial parameters. The shear force will be dependent on both sliding velocity and the real (or true) contact area (area of contact of microscopic asperities), and this is not brought out in equation (1). Although equation (1) does have a shear stress that is contact area dependent, this is solely a result of dividing a constant shear force by an area that is changing due to the oscillation. Therefore, the model is not an accurate depiction of the welding process as the shear force also oscillates with both contact area and velocity14. This unsatisfactory representation of the shear force may also mean that there is an inadequate representation of the power generation, and better models may be needed to accurately describe the power generation and temperature profiles produced by the LFW process.

Despite the criticism of the LFW process models currently available in the open literature, it is important to remember that the development of any reliable process model is difficult. It will largely depend on the accurate knowledge of friction coefficients and forces, and will rely on an accurate material data base over a wide temperature range and for exceptionally high strain rates.

VIII. Conclusion

In the present study, titanium-stainless steel joints with a nickel interlayer were welded successfully. With the wider application of titanium and stainless steel, the dissimilar welding technique for joining titanium to stainless steel will become more and more important. The sustainabilty properties of dissimilar metals capable of resisting high temperatures and low thermal conductivity has its applications in various manufacturing industries. The process is currently established as a niche technology for the fabrication of titanium alloy bladed disk (blisk) assemblies in aero-engines, and is being developed for nickel based superalloy assemblies.

Due to the complexity of Linear Fricrtion Welding, it is clear that it could help to significantly improve our understanding of the process, and in this way provide strategies to further improve welding parameters for LFW.

REFERENCES

[1]   P.L. Threadgill, M.J. Russell, & R. Andrews: Introduction to linear friction welding, TWI Ltd, unpublished work, 2007.
[2]   C. Mary and M. Jahazi: 'Linear friction welding of IN-718: process optimization and microstructure evolution', Advanced Materials Research, 2007.
[3]   S. Kallee: 'Development of low-cost linear friction machine', *Assembly Automation*, 2001, 21(2).
[4]   M. Maalekian: 'Friction welding - critical assessment of literature', *Sci. Technol. Weld. Join.*, 2007,12(8), 738-759.
[5]   M. E. Nunn: 'Aero engine improvements through linear friction welding', Proc. 1st Int. Conf. on 'Innovation and Integration in Aerospace Sciences', Paper no 2005-0040, Queen's University Belfast, 4-5 August 2005, 2005, CEIAT, Queen's University Belfast.
[6]   W. Richter: 'Herbeifuehrung einer haftverbindung zwischen plaettchen aus werkzeugstahl und deren traegern nach art einer schweissung oder loetung', Patent: DE477084, 1929.
[7]   R. Maurya and J. Kauzlarich: 'Bonding apparatus - friction welding by reciprocal motion', Patent: Caterpillar Tractor Co, US3420428-A; DE1552871-A; CA844858-A, 1969.
[8]   K. T. Slattery: 'Structural assembly's e.g. wing, preform for e.g. aircraft, has set of structural members connected by linear friction weld joint to base member, where each structural member defines connection surfaces', Patent: Boeing Co, US2007186507-A1, 2007.
[9]   R. D. Trask, S. H. Goetschius, and S. A. Hilton: 'Process for linear friction welding - comprises providing two members to be joined to one another at an interface by linear friction welding, where one of the two members is stub, etc', Patent: United Technologies Corp, EP850718-A; EP850718-A1; JP10193141-A; US5865364-A; EP850718-B1; DE69734232-E; DE69734232-T2, 1998.
[10]   K. T. Slattery: 'Preform forming method for structural assembly, involves moving pair of structural units relative to two base units to form plasticized region of material, and urging structural units against surface of base units', Patent: Boeing Co, US2005127140-A1, US7225967-B2, 2005.
[11]   A. Vairis and M. Frost: 'High frequency linear friction welding of a titanium alloy', Wear, 1998,217(1), 117-131.
[12]   M. Karadge, M. Preuss, P. J. Withers, and S. Bray: 'Importance of crystal orientation in linear friction joining of single crystal to polycrystalline nickel-based superalloys', *Mater. Sci. Eng., A*, 2008, 491(1-2), 446-453.
[13]   C. Mary and M. Jahazi: 'Linear friction welding of IN-718: process optimization and microstructure evolution', *Advanced Materials Research*, 2007, 15-17, 357-362.
[14]   A. Vairis and M. Frost: 'On the extrusion stage of linear friction welding of Ti6Al4V', *Mater. Sci. Eng. A-Struct. Mater. Prop. Microstruct. Process.*, 1999, 271(1-2), 477-484.
[15]   'BS EN 15620:2000: Welding - Friction welding of metallic materials', British Standards Institution, 2000.
[16]   H. H. Koo and W. A. Baeslack: 'Structure, properties, and fracture of linear friction welded Al-Fe-V-Si alloy 8009', *Materials Characterisation*, 1992, 28(2), 157-164.
[17]   R. J. Harvey, M. Strangwood, and M. B. D. Ellis: 'Bond-line structures in friction welded Al2O3 particle reinforced aluminium alloy metal matrix composites (MMC's) ', Proc. 4th Int. Conf. on 'Trends in Welding Research' (ed: H. B. Smartt, J. A. Johnson, and S. A. David), Gatlingburg, Tennessee, 5-8 June 1995, 1995, ASM, 803-808.

[18]   T. S. Jun, F. Rotundo, L. Ceschini, and A. M. Korsunsky: 'A study of residual stresses in Al/SiCp linear friction weldment by energy-dispersive neutron diffraction', *Advances in Fracture and Damage Mechanics Vii*, 2008, 385-387, 517-520.

[19]   G. T. Murray: 'Introduction to engineering materials: behavior, properties and selection;1993, New York, CRC Press.

[20]   B. J. Ginn and T. G. Gooch: 'Toughness of 12%Cr ferritic/martensitic steel welds produced by non-arc welding processes', *Welding Journal*, 1998, 77(8), 341S-349S.

[21]   W. Y. Li, T. J. Ma, S. Q. Yang, Q. Z. Xu, Y. Zhang, J. L. Li, and H. L. Liao: 'Effect of friction time on flash shape and axial shortening of linear friction welded 45 steel', Mater. Lett., 2008, 62(2), 293-296.

[22]   T. J. Ma, W. Y. Li, Q. Z. Xu, Y. Zhang, J. L. Li, S. Q. Yang, and H. L. Liao: 'Microstructure evolution and mechanical properties of linear friction welded 45 steel joint', *Adv. Eng. Mater.*, 2007, 9(8), 703-707.

[23]   W. A. Baeslack, T. F. Broderick, M. Juhas, and H. L. Fraser: 'Characterization of solid-phase welds between TI-6Al-2Sn-4Zr-2Mo-0.1Si and Ti-13.5Al-21.5Nb titanium aluminide', *Mater. Charact.*, 1994, 33(4), 357-367.

[24]   P. L. Threadgill: 'The prospects for joining titanium aluminides', *Mater. Sci. Eng. A-Struct. Mater. Prop. Microstruct. Process.*, 1995, 193, 640-646.

[25]   P. L. Threadgill: 'Solid state joining of nickel aluminides: Preliminary study', Proc. 3rd Int. Conf. on 'Synthesis, Processing and Modelling of Advanced Materials' (ed: F. H. Froes, T. Khan, and C. M. Ward-Close), Paris, France, 25-27 June1997, 1997, ASM, 153-158.

[26]   M. Corzo, O. Casals, J. Alcala, A. Mateo, and M. Anglada: 'Mechanical evaluation of linear friction welds in titanium alloys through indentation experiments', *Revista De Metalurgia*, 2005, 41(6), 403-409.

[27]   T. Ma, S. Yang, Y. Zhang, and D. Xi: 'linear rubbing jointing method of aluminium piece and steel piece', Patent: Northwestern Polytechnical University, CN101020275-A, 2007.

[28]   G. M. Workman and E. D. Nicholas: 'Friction welding aluminium and its alloys to different materials', *Metals and Materials*, 1986, 2(3), 138-140.

[29]   H. Y. Li, Z. W. Huang, S. Bray, G. Baxter, and P. Bowen: 'High temperature fatigue of friction welded joints in dissimilar nickel based superalloys', *Mater. Sci. Technol.*, 2007, 23(12), 1408-1418.

[30]   A. Mateo, M. Corzo, M. Angada, J. Mendez, P. Villechaise, J. P. Ferte, and O. Roder: 'Welding repair by linear friction in titanium alloys', *Mater. Sci. Technol.*, 2009, 25(7), 905-913.

[31]   P. L. Threadgill: 'Terminology in friction stir welding', Sci. Technol. Weld. Join., 2007, 12, 357-360.

[32]   D. Helm and G. Lutjering: 'Microstructure and properties of friction-welds in titanium alloys', Proc. 9th Int. Conf. 'Titanium '99' (ed: I. V. Gorynin and S. S. Ushkov), St Petersburg, Russia, 7-11 June 1999, CRISM, 1726-1733.

[33]   M. Karadge, M. Preuss, C. Lovell, P. J. Withers, and S. Bray: 'Texture development in Ti-6Al-4V linear friction welds', *Mater. Sci. Eng., A*, 2007, 459(1-2), 182-191.

[34]   C. Mary and M. Jahazi: 'Multi-scale analysis of IN-718 microstructure evolution during Linear Friction Welding', *Adv. Eng. Mater.*, 2008, 10(6), 573-578.

[35]   W. A. Baeslack, P. L. Threadgill, E. D. Nicholas, and T. F. Broderick: 'Linear friction welding of Ti-48Al-2Cr-2Nb (at. pct) titanium aluminide', Proc. of 'Titanium '95 - Science and Technology' (ed: P. A. Blenkinsop, W. J. Evans, and H. M. Flower), Birmingham, UK, 22-26 October 1995, 1996, Institute of Materials, 424-431.

[36]   M. M. Attallah, M. Preuss, and S. Bray: 'Microstructural development during linear friction welding of titanium alloys', Proc. 8th Int. Conf. on 'Trends in Welding Research' (ed: S. A. David), Pine Mountain, Georgia, 1-6 June 2008, 2008, ASM.

[37]   J.Romero, M.M.Attallah, M. Preuss, M. Karadge, and S.E. Bray: 'Effect of the forging pressure on the microstructure and residual stress development in Ti-6Al-4V linear friction welds', *Acta Mater.*,2009,57(18),5582-5592.

[38]   M. R. Daymond and N. W. Bonner: 'Measurement of strain in a titanium linear friction weld by neutron diffraction', *Physica B-Condensed Matter*, 2003, 325(1-4), 130-137.

[39]   P. Frankel, M. Preuss, A. Steuwer, P. J. Withers, and S. Bray: 'Comparison of residual stresses in Ti-6Al-4V and Ti-6Al-2Sn-4Zr-2Mo linear friction welds', *Mater. Sci. Technol.*, 2009, 25(5), 640-650.

[40]   M. Karadge, P. Frankel, A. Steuwer, C. Lovell, S. Bray, P. J. Withers, and M. Preuss: 'Microstructure, texture, local tensile properties and residual stress relief in Ti-6Al-4V linear friction welds', Proc. of 'Materials Science & Technology' Cincinnati, Ohio, 2006, Association for Iron and Steel Technology, 35-46.

[41]   M. Preuss, J. Quinta da Fonseca, A. Steuwer, L. Wang, P. J. Withers, and S. Bray: 'Residual stresses in linear friction welded IMI550', *Journal of Neutron Research*, 2004, 12(1), 165-173.

[42]   P. J. Withers: 'Residual stress and its role in failure', *Rep Prog Phys*, 2007, 70(12), 2211-2264.

[43]   F. P. Bowden and D. Tabor: 'The friction and lubrication of solids'; 2001, Oxford classic texts.

[44]   T. Jun, Z. Tiancang, L. Pengtao, L. Jing, and M. Yu: 'Numerical computation of a linear friction welding process', *Physical and Numerical Simulation of Materials Processing, Pts 1 and 2*, 2008, 575-578, 811-815.

[45]   A. Vairis & M. Frost: 'Modelling the linear friction welding of titanium blocks', *Mater.Sci.Eng., A*, 2000,292(1),8-17.

Experimental Investigation on Effect of Particle Sizes of Molybdenum Disulphide on Wear Under Heavy Load and Slow Speed Conditions

S. M. Muzakkir, Harish Hirani

(Department of Mechanical Engineering, Indian Institute of Technology Delhi, India)

ABSTRACT: *In the present work, experimental investigation has been carried out to identify the effectiveness of employing three different particle sizes of MoS2 (Nano-particles: 40 nm size, Technical superfine grade: 1.75 μm size and Technical grade: 53 μm size) in varying quantities (0.5, 1.0 and 1.5% by weight) on the wear of the sliding surfaces. The experiments were conducted on a conformal block and disk test setup. The running-in distance required to achieve steady state wear was determined experimentally. The wear of the block is measured as its weight loss after the test. The results of the experiments are reported.*

Keywords: *Molybdenum disulphide, Nano-particles, wear, running-in wear, steady wear.*

I. Introduction

The molybdenum disulphide (MoS_2) had been in use for quite a long time as a solid lubricant additive in oils [1] for effectively reducing the wear between contacting sliding surfaces. Under extreme operating conditions of heavy loads and low sliding velocities, the asperities of the sliding surfaces interact with each other and results in wear which may eventually cause the surface degradation/failure. Recent advancements in the technology of synthesizing nano-sized molybdenum disulphide (MoS_2) particles [2] have accelerated their use as anti-wear additive in lubricants. The molybdenum disulphide nano-particles when used as lubricant additive also enhances the load carrying capacity of the base oil in addition to reducing wear [3]. The nano-particles are shown to have superior properties than micro-sized MoS_2 particles due to high specific surface area [4], which is also the cause of their agglomeration [5]. The lubricating property of nano-sized molybdenum disulphide (MoS_2) is attributed to its layered crystal structure (as a result of strong polarization of sulfur atoms) providing easy sliding of its lamellae [6]. The amount of wear reduction is dependent on the particle size of molybdenum disulphide (MoS_2). Hu et al. [7] investigated the effect of particle size of molybdenum disulphide (MoS_2) in liquid paraffin and proved that nano-sized particles were more effective in reducing wear and friction as compared to micro-sized particles [7]. However, if the nano-particles are not properly dispersed in the lubricant they may agglomerate and cause excessive wear due to three body abrasion. Muzakkir et al [8] have proposed a lubricant containing Zinc as antiwear additive that is able to minimize wear under heavy load and slow speed conditions. In another study Muzakkir et al [9] showed that for bearings subjected to extreme operating conditions, use of a high viscosity lubricant with anti-wear additives reduces the wear and also the probability of failures.

In the present work, experimental investigations have been carried out to determine the effect of size and quantity of molybdenum disulphide (MoS_2) particles on the wear of the sliding surfaces. Three different particle sizes of molybdenum disulphide (MoS_2) namely, Nano-particles: 40 nm size, Technical superfine grade: 1.75 μm size and Technical grade: 53 μm size, were considered as additive in a commercial lubricant in varying quantities ranging from 0.5% to 1.5% by weight. In order to achieve a distinct performance, the wear during the initial running-in period was segregated from the steady state wear. The running-in distance required to achieve the steady state wear is determined experimentally. The experiments were conducted on a conformal block of phosphorus bronze material sliding against a steel disk. The wear of the block is measured as its weight loss after the test. The results of the experiments are reported.

II. Experimental Details

In the present work, wear tests were carried out on a conformal block-on-disk test setup. The photograph and schematic diagram of the conformal block-on-disk test setup is shown in fig. 1(a) and 1(b).
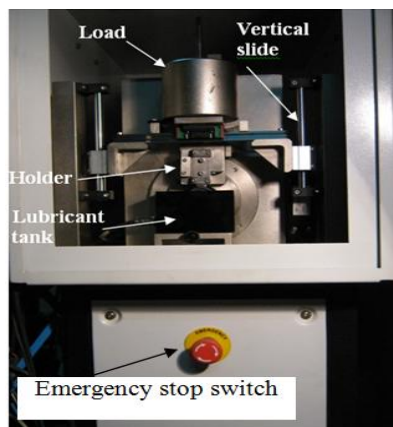
Figure 1(a) Photograph of conformal block and disk
test setup
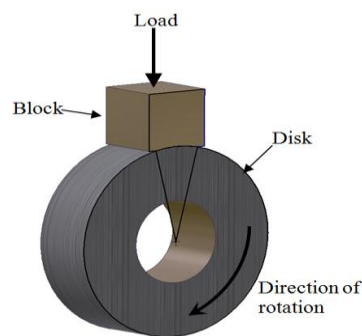
Figure 1(b) Schematic diagram

The test setup employs a conformal block (made of phosphorus bronze material) on hardened steel disk (diameter = 40 mm, width = 15mm), which is driven by induction motor. Half of the steel disk is immersed in the lubricant tank. The lubricant inside the tank is maintained at the desired temperature by the help of heaters and thermal cut-off switch. The static load is applied on the platform on which the block is fixed.

The tests were conducted at a load of 50N generating a pressure of 4.6×10^5 N/m^2 corresponding to the contact area of 1.085×10^{-4} N/m^2 of conformal block for a disk of 40 mm diameter. The disk was rotated at a speed of 25 rpm corresponding to a sliding speed of 5.23×10^{-2} N/m^2. For running-in tests, the disk was rotated at 50 rpm at a load of 50N and the wear was recorded after every 125m sliding distance corresponding to test duration of 20 minutes. The lubricant samples were prepared by dispersing the molybdenum disulphide (MoS$_2$) particles in a commercial lubricant with lithium stearate as a surfactant by ultrasonic homogenization for duration of one hour.

III. Results and Discussion

Initial experiments were conducted to determine the minimum sliding distance required to complete the running-in process. The experimental wear values were obtained after every 125m sliding distance corresponding to test duration of 20 minutes and are shown in fig. 2.
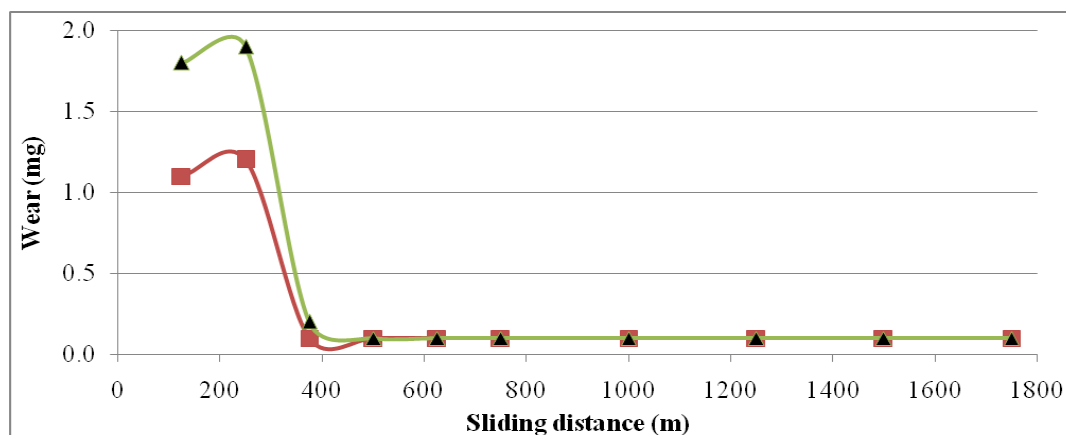
Figure 2 Wear Vs sliding distance of the conformal block during the running-in test

It is observed from figure 2 that the minimum sliding distance required to achieve the steady state wear is about 500m. Therefore, to be conservative, a value of 750m (corresponding to a test duration of 2 hours) may be taken as the minimum sliding distance for the completion of the running-in process. All the subsequent wear tests of 6 hours duration were then conducted after completing the running-in of the conformal blocks. The results of the normal tests with lubricant 1 are shown in fig. 3.
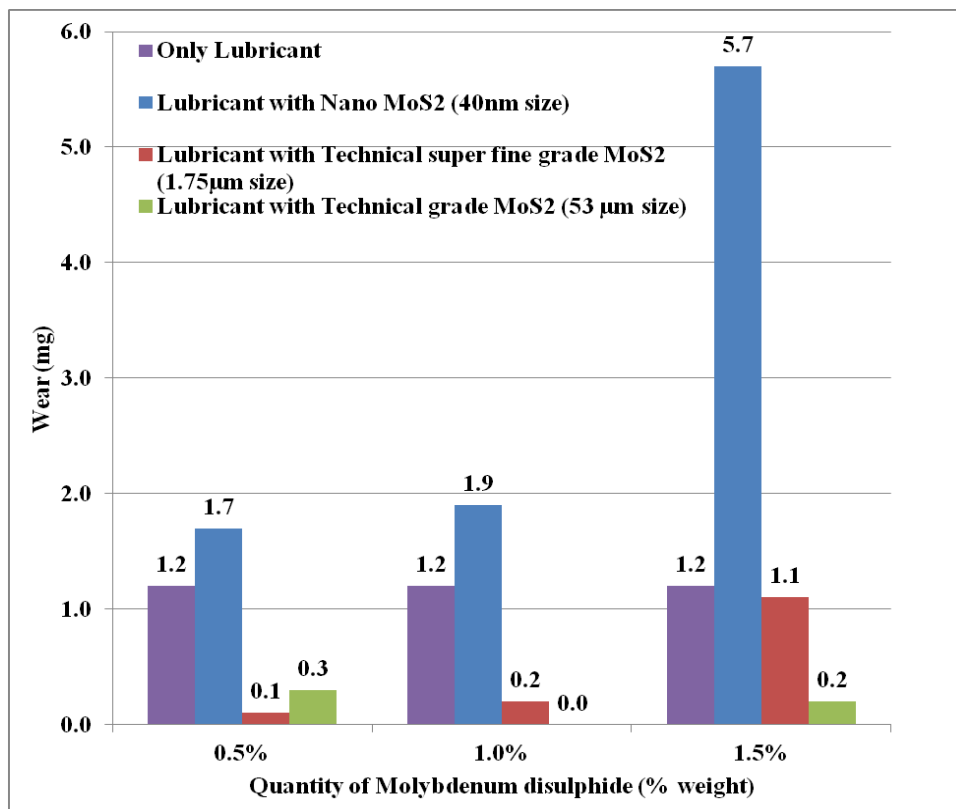
Figure 3 Wear of the conformal block after the normal test of 6 hours

It is observed from the experimental results that the wear during the normal test is highest for the MoS_2 nano-particles as compared to other particle sizes and increases with the increase in the nano-particle quantity, being the maximum when MoS_2 nano-particle quantity is 1.5%. It is observed from the experimental results that the addition of MoS_2 nano-particles results in higher wear even when compared with only oil. The wear increases with the increase in the quantity of MoS_2 nano-particles. The possible reason could be the agglomeration of nano-particles to bigger size with sharp edges. The size of the resulting nano-particles agglomerate is larger by an order of magnitude. This might have resulted in three body abrasion causing increased wear. The minimum wear was observed with the technical grade particles. In order to ascertain the reasons for increased wear with the use of MoS_2 nano-particles, the SEM images of the three molybdenum disulphide (MoS_2) particles were obtained. These SEM images of the molybdenum disulphide (MoS_2) particles are given in fig. 4, 5, and 6.
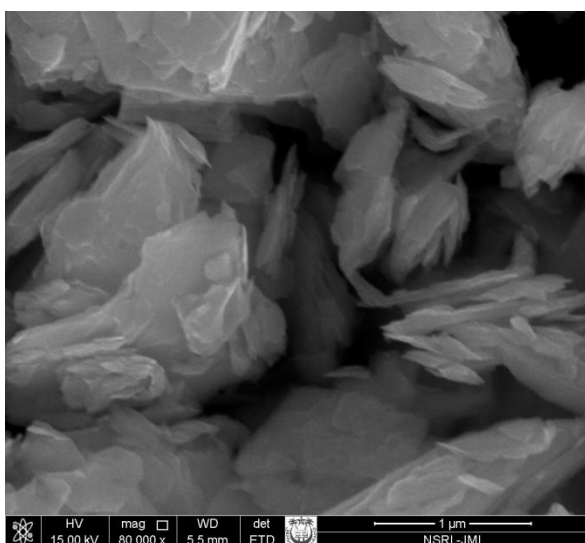
Figure 4 SEM image of MoS_2 Nano-particles
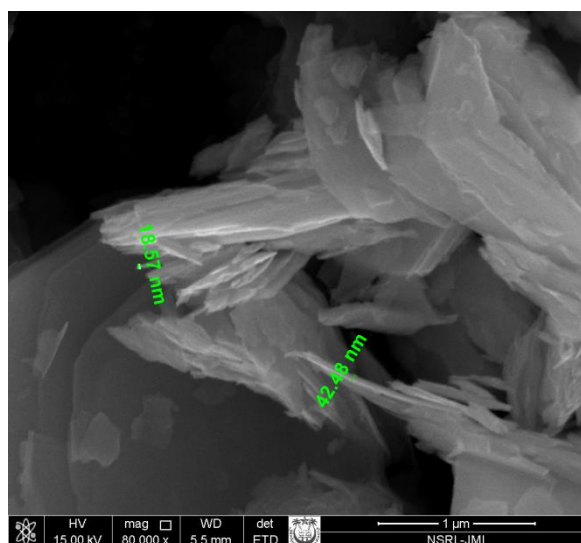
Figure 5 SEM image of MoS_2 Tech. Superfine grade particles
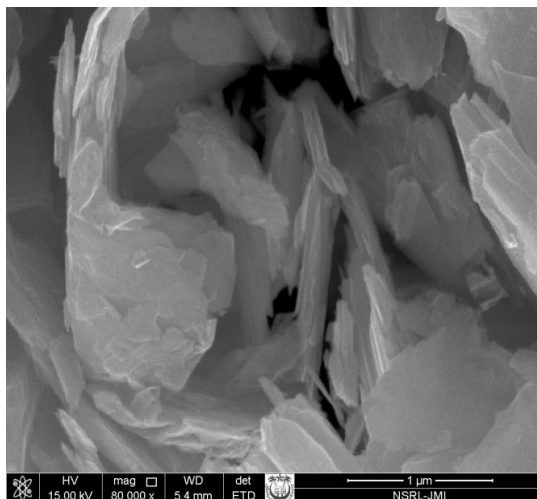
Figure 6 SEM image of MoS$_2$ Technical grade particles

It is observed from the SEM images that the molybdenum disulphide (MoS$_2$) particles are in a predominantly slices form with a distinct layered structure which is responsible for easy sliding of its lamellae that contributes in wear and friction reduction. Since nano-particles are very active, therefore there is increased adhesion of the nano-slices with each other.

IV. Conclusion

Based on the observations of the experimental studies, following conclusions are drawn:

- The wear of the sliding surfaces subjected to heavy load and slow speeds is reduced by using molybdenum disulphide (MoS$_2$) particles as additive in lubricant.
- The molybdenum disulphide (MoS$_2$) nano-particles were actually found to be detrimental to the surface as they caused increased wear.
- The increase in wear was observed with increase in nano-particles percentage in the lubricant. This could be possibly due to agglomeration of nano-particles to bigger size with sharp edges resulting in three body abrasion causing increased wear.
- The technical grade molybdenum disulphide (MoS$_2$) particles were found to reduce wear to the minimum.
- The reduction in wear increases with the increase in the percentage of technical grade molybdenum disulphide (MoS$_2$) in the lubricant. The technical grade MoS$_2$ particles have lower tendency to agglomerate.
- The reduction in wear was observed with technical superfine grade molybdenum disulphide (MoS$_2$) compared with MoS$_2$ nano-particles. The wear increased with the increase in the percentage of technical superfine grade MoS$_2$ in the lubricant.
- Further theoretical studies are needed to identify the reasons of increased wear with the use of molybdenum disulphide (MoS$_2$) nano-particles.

REFERENCES

[1]   J. P. G. Farr, Molybdenum Disulphide in Lubrication: A Review, *Wear*, *vol. 35, no. 1*, 1975, pp. 1–22.
[2]   F. A. Deorsola, N. Russo, G. A. Blengini, and D. Fino, Synthesis, Characterization and Environmental Assessment of Nanosized MoS2 Particles for Lubricants Applications, *Chem. Eng. J., vol. 195–196,* 2012,pp. 1–6.
[3]   B. Li, X. Wang, W. Liu, and Q. Xue, Tribochemistry and Antiwear Mechanism of Organic–inorganic Nanoparticles as Lubricant Additives, *Tribol. Lett., vol. 22, no. 1,* 2006, pp. 79–84.
[4]   I. M. Mahbubul, R. Saidur, and M. A. Amalina, Latest Developments on the Viscosity of Nanofluids, *Int. J. Heat Mass Transf., vol. 55, no. 4,* 2012, pp. 874–885.
[5]   D. Chu, S.-C. Chu, and M. Barigou, Qualitative Models of Particle De-agglomeration, *Powder Technol.*, vol. 195, no. 2, 2009, pp. 171–176.
[6]   Lansdown, *Molybdenum Disulphide Lubrication*. (Amsterdam, Elsevier, 1999).
[7]   K. H. Hu, X. G. Hu, Y. F. Xu, F. Huang, and J. S. Liu, The Effect of Morphology on the Tribological Properties of MoS2 in Liquid Paraffin, *Tribol. Lett., vol. 40, no. 1,* 2010, pp. 155–165.
[8]   S. M. Muzakkir, H. Hirani, and G. D. Thakre, Lubricant for Heavily Loaded Slow-Speed Journal Bearing, *Tribol. Trans.*, *vol. 56, no. 6,* 2013, pp. 1060–1068.
[9]   S. M. Muzakkir, H. Hirani, G. D. Thakre, and M. R. Tyagi, Tribological Failure Analysis of Journal Bearings used in Sugar Mills, *Eng. Fail. Anal., vol. 18, no. 8,* 2011, pp. 2093–2103.

Query Answering Approach Based on Document Summarization

Hesham Ahmed Hassan[1], Mohamed Yehia Dahab[2], Khaled Bahnassy[3],
Amira M. Idrees[4], Fatma Gamal[5]

[1]*Faculty of Computer and Information Computer Science Department, Cairo University*
[2]*Faculty of Computer and Information, Computer Science Department, King Abdulaziz University*
[3]*Faculty of Computer and Information, Computer Science Department, Ain Shams University*
[4]*Faculty of Computer and Information, Information Systems Department, Fayoum University*
[5]*Faculty of Computer and Information, Computer Science Department, Cairo University*

Abstract: *The growing of online information obliged the availability of a thorough research in the domain of automatic text summarization within the Natural Language Processing (NLP) community.The aim of this paper is to propose a novel approach for a language independent automatic summarization approach that combines three main approaches. The Rhetorical Structure Theory (RST), the query processing approach, and the Network Representationapproach (NRA). RST, as a theory of major aspect for the structure of natural text, is used to extract the semantic relation behind the text.Query processing approachclassifies the question type and finds the answer in a way that suits the user's needs. The NRA is used to create a graph representing the extracted semantic relation. The output is an answer, which not only responses to the question, but also gives the user an opportunity to find additional information that is related to the question.We implemented the proposed approach. As a case study, the implemented* approach*is applied on Arabic text in the agriculture field. The implemented approach succeeded in summarizing extension documents according to user's query. The approach results have been evaluated using Recall, Precision and F-score measures.*

Keywords: *Information Extraction, Text Summarization, Natural Language Processing.*

I. Introduction

Summarization is "a brief restatement within the document (usually at the end) of its salient findings and conclusions, and is intended to complete the orientation of a reader who has studied the preceding text" while an abstract is, according to the same standard, a "Short representation of the content of a document without interpretation or criticism". [MARTIN, 2008]. According to Mikael, in [Mikael, 2014], Automatic text summarization approaches can be classified into vector based approach, Fuzzy based approach, Genetic algorithm based approach, and Neural Network based approach.

Semantic pattern can be defined, according to [Mohamed, 2008] as "a generic format for natural language expression, to declare a specific meaning". The distinguishing of these semantic patterns are not straightforward since natural languages may have different lexical items that can be used to make reference to the same situation as well as different syntactic realization of the same arguments.

The semantic patterns elements are:

- Abstract ontological class. These classes were imported from the Agrovoc thesaurus and the publications of CLEASE as we will discuss later.
- Verb group. These groups were extracted from different lexicons like the Wordnet.
- Text constant expression.

All these elements are non-terminal element except the third element, it is a terminal element.We refer to abstract ontological class as a word between "<>" signs.

In this proposed approachwe will be working with single document summarization as an experimental study and our aim will be to produce a short summary that best suits both, the user's criteria and the writer's point of view.We will introduce some common terms in the summarization dialect: extraction is the process of detecting important segments of content and generating a new verbatim of these segments; abstraction targets to construct significant information in a new, non-verbatim way; fusion merges extracted segments coherently; and compression objects to discard unimportant segments of text [Radev et al., 2004]. Initial studieson summarizing documents proposed models for extracting weighty sentences from text using features like word or phrase frequency [Luhn, 1958], position in the text[Baxendale, 1958] and key phrases[Edmundson, 1969]. Our summary will be extractive summarization that takes benefit of three approaches, Rhetorical Structure Theory, query processing approach, and the Network Representation approach.

II. Related Work

Several automatic text summarization techniques have been proposed. These summarization techniques are classified according to [Mikael, 2014] into four categories, they are Heuristic techniques, Semantics-based techniques, Query-oriented techniques, and Cluster-based techniques. Based on these different techniques, we'll review the work done on text summarization in the last few years.

Barzilay and Elhadad in 1997 present an algorithm that computes lexical chains in a text. Based on lexical chains, they identify the nominal groups of sentences and the algorithm for segmentation by using different sources such as the part of speech tagger. Other sources may be used such as the wordnet thesaurus [Barzilay, 1997]. According to [Mikael, 2014] this method shows improvement over commercially available summarizer systems but still has two limitations. First: Sentence granularity- there is a high probability of selecting long sentences to be included in the summary. Second: the sentences that are selected and included in the summary may contain anaphor links to other parts of the text which may not be included in the summary.

In 2006 Wang and Yang [Wang, 2006] suggested a "fractal summarization technique". It uses a fractal approach for controlling the information viewed [Dolores, 2008].The fractal theory converts the text document into a tree hierarchy [Mohsen, 2012]. Their technique proposed A fractal theory to produce a summary by determining the salient features for the text and its hierarchical structure. The proposed technique used a statistical approach; therefore it can be used for multilingual text documents with minor modification of the system due to the difference of each language's features [Mikael, 2014]. Wang and Yang technique enhances the convergence of information analysis of a summary as user can control the compression ratio, and the system produces a summary that expands the information coverage and reduces the dissimilarity from the source document. Fractal theory that considers both the abstraction level of document and statistical property of the text their result shows the superior result compared to flat methods and the other structured summarization method in literature [Mohsen, 2012].

In 2007, Steinberger et al. proposed a new method for using anaphoric information in Latent Semantic Analysis (LSA) and consider its product to develop an LSA-based summarizer [Steinberger, 2013]. This method was able to attain improved performance more than the methods that don't use anaphoric information, and it also had an improvement performance by the rouge measures than all except the ones of the single-document summarizers participating in DUC-2002. The LSA has some limitation; first of which is that the word order has no effect on the syntactic relations or logic, or of morphology. Strangely, despite of this limitation the system succeeds to extract accurate reflections of segment and word implication quite well; nonetheless there would be few errors on some occasions [phiên, 2008]. Another limitation is in the resulting dimensions. The resulting dimension is not easy to interpret. This leads to results which can be acceptable on the mathematical level, but have no meaning in natural language [Steinberger, 2007]. According to [phiên, 2008] another limitation is that, LSA cannot acquire polysemy (A polysemy is different words or phrases with the same meaning). LSA treats each word as if it has the same meaning despite its context, which results to a drawback in the output, as the output will depend on the occurrence average of the words. This method of producing a summary may lead to a difficulty in performing the text comparison [Steinberger, 2007]. Therefore, another approach is introduced namely "Probabilistic latent semantic analysis", this approach based on multinomial model and it had better results than LSA [Thomas, 2007].

Based on the literature survey, the problems and challenges in the area of summarization are identified, providing the basis for the work to be carried out.

III. Proposed Approach

The aim of our proposed approach is to compose an extractive summary for a document using the previously mentioned approaches. Toreach this goal,we combined three main approaches. RST, query processing, and network representation. In our proposed approach we used RST to determine the sentence type to be either nuclear or Satellitethen we were able to decide sentence priority since Nuclear sentences have more importance to the writer; therefore the nuclear sentences must have higher priority than satellite sentences. In the final summary both nuclear and satellite sentences may be included. If a satellite sentence is having a high priority, it will still be included in the final summary and its nuclear will also be dragged to the summary to emphasize the meaning to the reader. Many relations are considered in the proposed approach, these relations are imported from many sources. These sources are:

1. Pen Discourse Tree corpus - Marcu, D., Romera, M. and Amorrortu, E. (1999b) and the relation analysis done by their PDTB Research Group. http://www.seas.upenn.edu/~pdtb/
2. Mann and Thompson paper includes 24 relations [Mann, 2006], called "Classical RST".
3. Alsanie[Al-Sanie, et. al, 2005] defined 11 Arabic relations.
4. The Leeds Arabic Discourse Treebank and the LADTB –discourse annotated Arabic Treebankhttp://www.arabicdiscourse.net/

In our proposed approach, we investigate a graph-based, language-independent approach to extractive text summarization inspired by recent developments in the area of networks. We argue that if two sentences are connected in this network they probably convey complementary information about related topics, possibly about the same topic. As our goal is to construct informative extracts, the concept of complementary sentences is crucial for the development of our summarization techniques. The document under consideration is mapped into a network representation according to the adjacency and weight matrices of order N X N (where N is the number of nodes/sentences). Table 1 is an N X N Matrix for the example in Figure 1.

Table 1: N X N Matrix

	S1	*S2*	*S3*	*Sum*
S1	-	1	1	2
S2	-	-	-	-
S3	-	1	-	1

According to this matrix, it is clear that the sentence with the highest priority is S1 followed by S3 then S2. According to RST, S1has more importance to the writer while S2 and S3 are used just to describe S1, and S2 is used just to describe S3. In all summarization approaches S1 can't be excluded, while S2 and S3 can't be included without sentence S1. In our proposed approach, S1 will be included in the final summary if S1 has a high similarity to the user's query. If S2 or S3 has a high similarity to the user's query, i.e. the answer to the user's query was in a satellite sentence, in this particular case, including the satellite sentence alone will be meaningless to the user (satellite sentences are only used by the writer to emphasize the nuclear ones). So in such situations we are not going to ignore the satellite sentences after all, but we'll have to include it's nuclear sentences as well.

IV. Proposed Framework

The proposed approach represented in Figure 1 is composed of three main phases namely document summarization phase, query processing phase and Generating Final Summary phase. The objective of the first phase - document summarization phase - is to process the user's document, to define the document rhetorical relations and to rank the document's sentences. The objective of the second phase - query processing phase - is to measure the semantic similarity between the user query and the document. The objective of the last phase - generating Final Summary phase – is to generate the final summary by selecting the sentences that are mostly related to both the user's query and the document's writer.
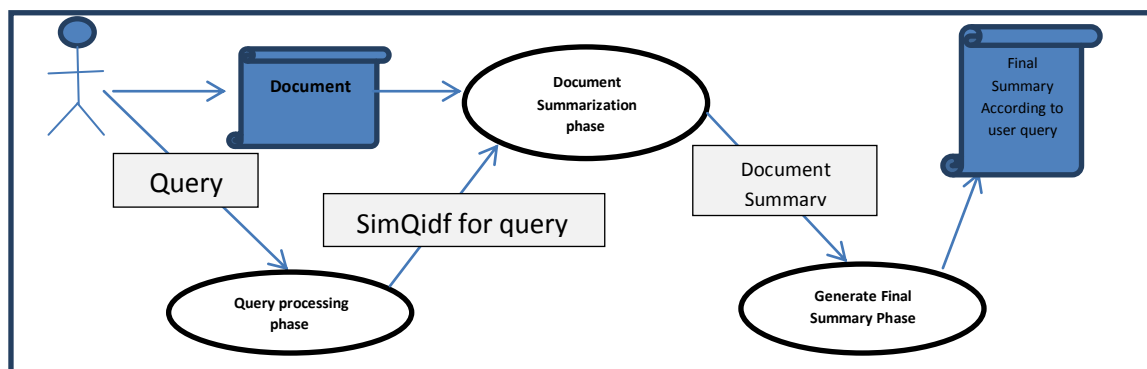
Figure 1: Proposed Approach

Query Processing Phase responds automatically to a user's query, this includes determining the relevance ranking of sentences in the document to the user's query according to a keyword search. To calculate the sentence score, the ranking is performed using "document similarities theory" [Suganya, 2014], according to [Sylvia, 2014] by comparing the deviation of angles between the document sentences' vectors and the query vector, where the query and the sentences of the document are represented as vectors, we can find the similarity between the sentences of the document and the query. This representation leads to the effectiveness in calculating the similarity between the query vector and each sentence vector in the document.

The document summarization performs the main objective which is producing the summary of the document. The first step is classifying the document submitted by the user; the classes that we used were imported from the Agrovocthesaurus [Boris, 2006]. The classification will help in the sentence ranking

component. According to the document class the sentence ranking component will determine the keywords that will raise the sentence's ranking. The second step is determining the relations between each sentence and the proceeding sentence within the same paragraph. The document is then transformed into a directed graph where an edge is drawn between each two sentences if a relation exists between these sentences. According to these relations, the sentence type is determined and a weight is given to the relation. The third step is transforming the document submitted by the user into an RST discourse graph which represents the relation between sentences in the document. The final phase namely, summary generator phase, selects the sentences that are mostly related to both the user's query and the document's writer. a rank for each sentence is measured depending on its importance to the user,elimination the similar sentences is performed, then the summary is generated according to the following rules

1- Select the highest priority sentences, the number of sentences included in summary is determined by the user.
2- If the sentence type is body then the sentence header must be included in the summary,
3- Ifthe sentence type is head and there is no body sentences underneath it are of high priority, then it is excluded.
4- If the sentence is nuclear, then it is included in the summary
5- If the RST type of the sentence is satellite then its nuclear sentence will be included even though its priority is low.

V.   Results Analysis

We present a comprehensive evaluation of the automatic text summarization methods based on rhetorical structure theory (RST), claimed to be among the best ones. We also propose a new approach and compare our results to the results of our expert. To the best of our knowledge, most of our results are new in the area and reveal very interesting conclusions.We have applied the proposed system on 15 experiments; each experiment consists of a query and a document. The results of the test cases of the experiments are listed in table 12. According to the test results the system makes accurate results in most cases. 10 cases retrieved correct results, all sentences were relevant and none of the retrieved sentences were irrelevant. These cases had an f score of 1. The cases where some relevant sentences were not retrieved, was found to be due to insufficient data exported from the Agrovoc like the diseases names, the crop names etc., in case of diseases names for example, the disease اللفحه (blight disease) was not included in the Agrovoc, which made it impossible for the engine to identify it. This situation should be handled using a defined methodology.

In other cases where some irrelevant sentences were retrieved by the engine, this was due to the problem of synonyms and antonyms that we discussed earlier; this kind of error is better handled when using the RST in combination with the Semantic patterns.The RST showed a better progress in the retrieval process, but still there were many problems. First, some relations are inclusive, not exclusive, which means that there will be no keywords to recognize them, these relations are out of the scope of our research. Secondly, the relations are some times between non coherent sentences, when we tried to handle the relation between each sentence and all other sentences within the same paragraph, the results were mostly wrong, so we considered the relation between each sentence and the proceeding sentence, but this was not completely successful, cause mainly, in Arabic sentences the relations are usually between more than two sentences, besides sometimes the relation is between two sentences that are not even coherent, sometimes the relation can be between a sentence in the beginning of the paragraph and another sentence at the end of the paragraph. These problems resulted in not being able to recognize all of the relations between the sentences and therefore the priority of the sentences was not completely accurate. The lexical chain approach can be used to solve this problem.

We faced another problem when dealing with the keywords imported from the different corpora. First we thought that stemming a word would give a better result in the similarity checking process, but unfortunately that was completely misleading. We found that not stemming the words would reduce the problem of synonyms and antonyms to a great deal. When using the semantic patterns of the terms and combining them with all their senses, the result was much more accurate. The problem of Ambiguity is varies in different languages, it is increased in the Arabic language due to the overlooking rules that combine words with clitics and affixes [grammar-lexis specifications]. Another source of confusion is that the Arabic verbs can inflect for the imperative mood and the passive voice. One final problem was the problem of readability of the summary. Mostly the summary readability was fine, only in rare situations of having a hidden pronoun, the sentences are misunderstood, the RST minimized this problem to a great deal, as the hidden pronoun in most cases is between two coherent sentences, but it was still present in a very rare situations.

Table 12: The results of the test cases

ID	relevant and retrieved (A)	relevant and not retrieved (B)	Irrelevant retrieved (c)	precision	recall	F
1	4	2	0	1	0.666666667	0.8
2	6	0	0	1	1	1
3	5	0	1	0.833333333	1	0.909090909
4	6	0	0	1	1	1
5	8	0	0	1	1	1
6	5	1	1	0.833333333	0.833333333	0.833333333
7	5	2	0	1	0.714285714	0.833333333
8	5	0	0	1	1	1
9	7	0	0	1	1	1
10	4	2	0	1	0.666666667	0.8
11	6	1	1	0.857142857	0.857142857	0.857142857
12	8	0	0	1	1	1
13	5	0	0	1	1	1
14	4	3	1	0.8	0.571428571	0.666666667
15	6	0	0	1	1	1

VI.   Conclusion

This paper shows how question answering systems—which aim at finding precise answers to questions—can be improved by exploiting summarization techniques to extract more than just the answer from the document in which the answer resides. This is done using a graph search algorithm which searches for relevant sentences in the discourse structure, which is represented as a graph. The Rhetorical Structure Theory (RST) is used to create a graph representation of a text document. The output is an extensive answer, which not only answers the question, but also gives the user an opportunity to assess the accuracy of the answer (is this what I am looking for?), and to find additional information that is related to the question, and which may satisfy an information need. This has been implemented in a working multimodal question answering system where it operates with two independently developed question answering modules. The classification process has two phases the first of which is done offline while the second one is done online.

We presented a system for document summarization satisfying user query based on RST. We proposed an approach and applied it on twenty experiments. The experiment results showed success in most cases and it triggered some problems. They are, insufficiency of data imported from different corpora, in addition to the irrelevant sentences and hidden pronoun included in the summary. The problem of synonyms and anatomies is also one of the crucial problems to be monitored.

REFERENCES

[1]   [Barzilay, 1997], Barzilay, R. and M. Elhadad, "Using lexical chains for text summarization". In Proceedings of the 35th Annual Meeting of the Association for Computational Linguistics and the 8th European Chapter Meeting of the Association for Baxendale,ГР.Г(1958).ГMachine-madeГindexГforГtechnicalГliteratureГ-ГanГexperiment.ГIBM Journal of Research

[2]   [Boris,2006], Agrovoc Web Services-Improved, real-time access to an agricultural thesaurus, 2006, Boris Lauser,. MargheritaSini, Gauri. Salokhe,

[3]   [Dolores, 2008] M. Dolores Ruiz, Antonio B. BailónEnterprise, 2008, "Summarizing Structured Documents through a Fractal Technique", springer Information SystemsLecture Notes in Business Information Processing Volume 12, 2008, pp 328-340

[4]   [Edmundson, 1969], Edmundson, H.P. 1969. "New methods in automatic abstracting". In: *Journal of the Association for Computing Machinery 16 (2).* 264-285. Reprinted in: Mani, I.; Maybury, M.T. (eds.) *Advances in Automatic Text Summarization.* Cambridge, Massachusetts: MIT Press. 21-42, 1969.

[5]   [Luhn, 1958]Luhn Hans Peter, 1958"The Automatic Creation of Literature Abstracts". IBM Journal of Research Development, 2(2):159–165.

[6]   [Mann, 2006]MaiteTaboada and William C. Mann, 2006, "Rhetorical Structure Theory: looking back and moving ahead", sage publications London.

[7]   [Martin , 2008] Martin Hassel, 2008, "Resource Lean and Portable Automatic Text Summarization", Doctoral Thesis Stockholm, Sweden.

[8]   [Mikael , 2014] Mikael Kågebäck, OlofMogren, Nina Tahmasebi, DevdattDubhashi, 2014," Extractive Summarization using Continuous Vector Space Models", published in: 2nd Workshop on Continuous Vector Space Models and their Compositionality CVSC, Gothenburg Sweden.

[9]   [Mohamed 2008] Hesham Ahmed Hassan, Hesham Ahmed Hassan, Ahmed Rafea, 2008, "TextOntoEx Automatic ontology construction from natural English text", science direct expert system with application 34 2008 1474-1480

[10]   [Mohsen, 2012] Mohsen Tofighy , OmidKashefi , Azadehamanifar, Hamid Haj, SeyyedJavadi, 2012, "Persian Text Summarization Using Fractal Theory" , University of Science and Technology, Tehran, Iran.

[11]   [phiên, 2008] ĐâyLàPhiênBảnTàiLiệuĐơnGiảnXemPhiênBảnĐầyĐủCủaTàiLiệu, 2008, "Toward Classification And Clustering In Vietnamese Web Documents", Viet Nam National University, Hanoi College Of Technology.

[12]   [Radev, et. al, 2004]Radev D. R., E. Hovy, K. McKeown, 2004, "Introduction to the special issue on summarization". Computational Linguistics. Vol 28(4). 399-408.

[13]   [Steinberger , 2013] Josef Steinberger April 2013, "Multilingual Summarization and Sentiment Analysis", Habilitation.

[14]   [Suganya1 , 2014] B. Suganya1, 2014, "Analysis on Clustering Techniques based on Similarity of Text Documents", International Journal of Advance Research in Computer Science and Management Studies Research. Available online at: www.ijarcsms.com.

[15]   [Sylvia, 2014] Sylvia Poulimenou, Sofia Stamou, SozonPapavlasopoulos, and MariosPoulos, 2014, "Keywords Extraction from Articles' Title for Ontological Purposes", Mathematics and Computers in Science and Engineering Series.

[16]   [Thomas, 2007] Thomas Landauer, Susan T. Dumais, 2007"A Solution to Plato's Problem: The Latent Semantic Analysis Theory of Acquisition, Induction, and Representation of Knowledge".

[17]   [Wang, 2006] Wang, F.L., & Yang, C.C. 2006. "The impact analysis of language differences on an automatic multilingual text summarization system", Journal of the American Society for Information Science and Technology, 57, 684–696.

[18]   http://www.arabicdiscourse.net/

[19]   http://www.medar.info/BLARK/unannotated_corpora.php

[20]   http://www.elda.org/medar_lri/monolingual_corpora.php

[21]   http://www.seas.upenn.edu/~pdtb/

[22]   http://www.arabicdiscourse.net/

[23]   [FAO]   AGROVOC Multilingual agricultural thesaurus,Food and Agriculture Organization of the United Nations (FAO), http://aims.fao.org/standards/agrovoc, URI: http://ring.ciard.net/node/1910

Parametric Characterization and Model Prediction of CBR Values of Stabilized Orukim Residual Soils, Akwa Ibom State, Nigeria

Dr. Essien Udo[1], Dr. Abidemi Ilori[2], Engr. Charles Kennedy[3]

Department of Civil Engineering, University of Uyo, Nigeria.
Department of Civil Engineering, University of Uyo, Nigeria
Department of Civil Engineering, University of Uyo, Nigeria

Abstract: *Quarry dust and lime were deployed for this stabilization experiments. Quarry dust is a by-product or sediments derived from the crushing of limestone. This soil modifying agent has a high percentage of fines. Its application increases the CBR values on a range varying from 10%, 20%, 30%, 40% residual soil against 56%, 71%, 104%, 140% CBR contents of Orukim residual soils respectively. Further increase in quarry dust content from 50% to 70% resulted in decreased values of CBR. The samples were equally devoid of plasticity hence less useful in engineering applications. Lime stabilized soil can be used for both base and sub-base materials. The oxides and hydroxides of calcium and magnesium are considered as lime, but the materials most commonly used for lime stabilization are calcium hydroxide $Ca(OH)_2$ and dolomite $Ca(OH)_2 + MgO$. The dolomite however, should not have more than thirty six percent by weight of magnesium oxide (MgO) to be acceptable as a stabilizing agent. The lime stabilized samples were soaked for ninety six hours to ascertain the contribution of curing duration on the CBR parameters. Results indicate variations along the range of 2%, 4%, 6%, 8%, 10% against 80%, 92%, 99%, 110%, 169% of lime and CBR contents respectively.These values are statistically significant. Finally multiple nonlinear regressed models were developed to aid prediction and optimization of CBR values of Orukim residual soils at various levels of stabilization.*

Keywords: *Quarry dust, Lime, Stabilization, Compaction, Residual soil*

I. Introduction

1.1 Quarry Dust Stabilization

Generally stabilization is designed to improve the physical properties of residual soils deployed for engineering applications. Several methods are used to stabilize soils such as: compaction, consolidation, grouting, admixtures, reinforcement and stone column [1]. The ability of any of these methods to improve soil properties depends on several factors, including soil type, degree of saturation, initial relative density, initial in-situ stresses, initial soil structure and special characteristics of the method used. In most cases the goal of treating the soil is increasing shear strength and loading capacity, increasing stability and settlement control[2]Quarry dust containssubstantial amount of fines. In addition to plasticity reduction, quarry dust, provides improved strength and durability. The effectiveness of quarry dust stabilization is predicated on the structural composition of the residual soil and the plastic limit which influences durability on compaction.

1.2 Lime Stabilization

One of the oldest processes of improving the engineering properties of soils is by lime stabilization. When lime is added to fine-grained soil, cat-ion exchange takes place, with the calcium and magnesium in the lime replacing the sodium and potassium in the soil. The tendency to swell as a result of increase in moisture content is therefore immediately reduced. The plasticity index value of the soil is also reduced. Pozzolanic reaction may also occur in some resulting in the formation of cementing agents that increase the strength of the soil. When silica or alumina is present in the soil, a significant increase in strength may be observed over a long period of time. An additional effect is that lime causes flocculation of the fine particles, thereby increasing the effective grain size of the soil. The percentage of lime used for any project depends on the type of soil being stabilized. The determination of the quantity of lime is usually based on an analysis of the effect that different lime percentages have on the reduction of plasticity and the increase in strength of the soil. [3]

II. Materials Selected

2.1 Orukim Residual Soil

Samples of soil selected for this research was dug with shovels at four distinct borrow pits along Orukim-Eto-Essek-Okposo Road. The samples were excavated both vertically and horizontally bearing in mind the variability of residual soil in its natural composition. The samples were conveyed in four, fifty kilogram nylon bags, carefully tagged to ensure proper identification and transported to Mothercat Limited, Materials Testing Laboratory at Uyo.

2.2 Quarry Dust

The quarry dust used in this experiment came from the limestone quarry factory in Akamkpa, Cross River State. This is the by-product or sediments derived from the crushing of limestone. This soil modifying agent has a high percentage of fines, and as expected, the CBR value of quarry dust was the minimum value from both experiments, in that it in fact increased the overall fines content of the Orukim residual soil. The material was purchased from a local supplier at Aka-Itiam street depot in Uyo.

2.3 Lime

Addition of lime helps to arrest the shrinkage and swelling behaviour of soil.[4]. This is due to the creation of chemical bonds and aggregation. The use of lime to improve the engineering properties of soil had been in practice for long in many parts of the World. The lime used in this work was purchased from Ewet market in Uyo. The primary purpose was to evaluate the behaviour of Orukim residual soil on application of various percentages of lime and compactive effort on the maximum dry densities and corresponding optimum moisture contents. Lime stabilized soil is an engineered product that must be properly evaluated, proportioned and constructed in order to obtain the good and long-term performance.[5] Generally lime reduces the plasticity of a highly expansive

III. Preparation and Testing Of Samples

3.1 UnstabilizedMechanical Compaction Tests

This test was conducted to determine the mass of dry soil per cubic meter and the soil was compacted in a specified manner over a range of moisture contents, including that giving the maximum mass of dry soil per cubic meter. For each of the samples, the Modified Proctor Compaction tests were conducted. The air-dried material was divided into five equal parts through a riffle box and weighed to 6000g each. Each sample was poured into the mixing plate. A particular percentage of distilled water was poured into each plate and thoroughly mixed with a trowel. An interval of about 60minutes was allowed for the moisture to fully permeate the soil sample. The sample was thereafter divided into five equal parts, weighed and each was poured into the compaction mould, in five layers and compacted at 61 blows each using a 4.5kg rammer falling over a height of 450mm above the top of the mould. The blows were evenly distributed over the surface of each layer. The collar of the mould was then removed and the compacted sample weighed while the corresponding moisture content was noted. The procedure was repeated with different moisture contents until the weight of compacted sample was noted to be decreasing. With the optimum moisture content obtained from the Modified Proctor test, samples were prepared and inserted into the CBR mould and values for the plain mechanical compaction were read for both top and bottom at various depths of penetration.

3.2 Quarry Dust–Residual Soil Stabilization Tests

Different percentages of quarry dust varying from 10%, 20%, 30%, 40%. 50%, 60% and 70% were added to air-dried samples 1, 2, 3 and 4. Each of the test samples was thoroughly blended with a trowel, divided into five parts with the aid of a riffle box, moisturized and weighed. Thereafter the Modified Proctor compaction test was carried out to determine the OMC and MDD. Liquid limit and plastic limit tests were conducted on each of the samples. Based on the OMC and MDD results, CBR tests were then conducted on each specimen following five equal layers of compaction with 4.5kg rammer at 61 blows each falling over 450mm height to the top of the mould. Equally the quarry dust content was varied from 10% to 70% corresponding to the OMC and MDD derived from the compacted tests.

3.3 Lime–Residual Soil Stabilization Tests

The percentage of lime used in this study varied from 2%, 4%, 6%, 8% and 10% to the air-dried weight of the residual soil. That decisionwas informed by the fact that Orukim residual soil is highly anisotropic. The percentage of residual soil on corresponding basis varies from 98%, 96%, 94%, 92% and 90% to the weight of hydrated lime. The mixture was thoroughly blended, moisturised and samples taken for liquid limit tests. Similar compaction procedures were adopted for the four soil samples. The modified proctor test was carried out on all the samples uniformly distributed with a 4.5kg rammer and height was 450mm above the soil compacted

on five equal layers of 61 blows each. With the OMC and MDD results obtained three samples each of the soil-lime specimen were prepared for CBR test. One sample was tested immediately. The remaining two samples were soaked for 96 hours by complete immersion in water. After the curing duration, the specimen was allowed to drain for 25minutes prior to CBR testing.

The lime used in this work was purchased from Ewet market in Uyo. The primary purpose was to evaluate the behaviour of Orukim residual soil on application of various percentages of lime and compactive effort on the maximum dry densities and corresponding optimum moisture contents. Lime stabilized soil is an engineered product that must be properly evaluated, proportioned and constructed in order to obtain the good and long-term performance[6]. Generally lime reduces the plasticity of a highly expansive soil, as well as improving the stress-strain behaviour.

3.4 California Bearing Ratio Tests

The CBR test [as it is commonly known] involves the determination of the load-deformation curve of the soil in the laboratory using the standard CBR testing equipment. It was originally developed by the California Division of Highways prior to World War 11 and was used in the design of some highway pavements. This test has now been modified and is standardized under the AASHTO designation of T193. With the OMC and MDD results, three specimens each were prepared for the CBR test. One specimen was tested immediately while the remaining two were wax cured for six days and thereafter soaked for 24 hours and allowed to drain for 15 minutes. After testing in CBR machine, the average of the two readings was adopted. This procedure meets the provision of clause 6228 design criteria, FMW&H [1997].

IV. Presentation of Test Results

Table 1: Orukim Residual Soil Compaction at Unstabilized Condition

Sample No	MDD Kg/m^3	NMC (%)	unsoaked CBR (%)	Fines (%)
1	1880	9.3	58	30
2	1870	8.5	53	32
3	1890	10.5	55	35
4	1860	9.6	58	33

Table 2: Orukim Residual Soil and Quarry Dust Classification– Sample no. 1

Quarry dust Content (%)	MDD Kg/m^3	OMC (%)	CBR Unsoaked (%)	LL	PL	PI	% passing Sieve No. 200	Classification	
								AASHTO	USCS
0	1880	9.3	58	32	20	12	30	A- 2 -6	SC
10	1990	8.5	56	32	23	9	28.0	A- 2 - 5	SM
20	2010	8.3	71	30	23	7	26	A- 2 -5	SM
30	2040	8.3	104	29	23	6	25	A- 2 -4	SM
40	2040	8.2	140	28	22	6	23	A- 2 – 4	SM
50	1910	6.3	99	21	NIL	NIL	30	A- 1 – b	SM
60	1960	7.6	64	19	NIL	NIL	19	A -1 - b	SM
70	1820	15.3	43	17	NIL	NIL	15	A – 1 - b	SM

Table 3: Orukim Residual Soil and Quarry Dust Classification – Sample no. 2

Quarry dust content (%)	MDD Kg/m³	OMC (%)	CBR Unsoaked (%)	LL	PL	PI	% passing Sieve 200	Classification	
								AASHTO	USCS
0	1870	8.5	53	36	22	14	32	A- 2 -6	SC
10	1900	6.2	54	34	19	15	27	A- 2 – 6	SC
20	2000	8.5	68	29	20	9	30	A- 2 -4	GM
30	1910	6.1	86	27	20	7	29	A- 2 -5	SM
40	1930	6.7	128	26	20	6	28	A- 1 – b	SM
50	1950	6.7	89	25	20	5	17	A- 1 – b	SM
60	1980	8.5	50	18	NIL	NIL	21	A -1 - b	SM
70	1780	12.6	45	18	NIL	NIL	16	A – 1 – b	SM

Table 4: Orukim Residual Soil and Quarry Dust Classification – Sample no. 3

Quarry dust Content (%)	MDD Kg/m³	OMC (%)	CBR Unsoaked (%)	LL	PL	PI	% passing Sieve 200	Classification	
								AASHTO	USCS
0	1890	10.5	55	29	25	4	35	A- 2 -4	SM
10	1920	11.5	52	30	20	10	29	A- 2 – 5	SM
20	2010	11.5	83	27	19	8	27	A- 2 -6	SC
30	2020	8.3	81	28	22	6	25	A- 2 -5	SM
40	2070	9.2	117	27	19	8	26	A- 1 – b	SM
50	2030	10.1	83	26	16	10	19	A- 1 – b	SM
60	2080	8.6	56	18	NIL	NIL	17	A -1 - b	SM
70	2040	8.1	42	16	NIL	NIL	14	A – 1 - b	SM

Table 5: Orukim Residual Soil and Quarry Dust Classification – Sample no. 4

Quarry dust Content (%)	MDD Kg/m³	OMC (%)	CBR Unsoaked (%)	LL	PL	PI	% passing Sieve 200	Classification	
								AASHTO	USCS
0	1860	9.6	58	37	21	16	33	A- 2 -6	SC
10	1890	6.2	63	31	23	8	29	A- 2 – 4	SM
20	2010	12.3	98	29	20	9	26	A- 2 – 5	SM
30	2060	7.8	101	27	19	8	29	A- 2 -4	SM
40	2050	8.4	111	20	15	5	23	A- 1 – b	SM
50	2030	11.5	88	26	20	6	21	A- 1 – b	SM
60	1990	8.2	65	16	NIL	NIL	16	A -1 - b	SM
70	1760	12.5	42	19	NIL	NIL	17	A – 1 - b	SM

Table 6: Orukim Residual Soil and Lime Classification – Sample no. 1

LIME Content (%)	MDD Kg/m³	OMC (%)	Soaked CBR (%)	LL	PL	PI	% passing Sieve 200	Classification	
								AASHTO	USCS
0	1810	8.4	26	26	21	5	22	A- 2 - 4	SM
2	1940	8.2	76	31	22	9	29	A- 2 - 4	SM
4	2100	8.9	92	28	20	8	29	A- 2 - 4	SM
6	1990	8.5	105	29	23	6	31	A- 2 - 4	SM
8	1980	8.5	98	28	23	5	32	A- 2 – 4	SM
10	1980	8.2	110	19	NIL	NIL	33	A- 2 - 4	SM

Table 7: Orukim Residual Soil and Lime Classification – Sample no. 2

LIME Content (%)	MDD Kg/m³	OMC(%)	soaked CBR (%)	LL	PL	PI	% passing Sieve 200	Classification	
								AASHTO	USCS
0	1950	11.4	26	32	23	9	28	A- 2 - 4	SM
2	1920	12.4	80	30	21	9	31	A- 2 - 4	SM
4	2060	11.5	92	25	18	7	32	A- 2 - 4	SM
6	2090	15.0	99	30	21	9	33	A- 2 - 4	SM
8	2060	14.8	110	26	21	5	34	A- 2 – 4	SM
10	2080	12.1	120	19	NIL	NIL	35	A- 2 - 4	SM

Table 8: Orukim Residual Soil and Lime Classification – Sample no. 3

LIME Content(%)	MDD Kg/m³	OMC (%)	soaked CBR (%)	LL	PL	PI	% passing Sieve 200	Classification	
								AASHTO	USCS
0	1940	10.5	32	29	25	4	35	A- 2 - 4	SM
2	2000	9.3	82	31	21	10	32	A- 2 - 4	SM
4	2050	8.5	86	27	21	6	32	A- 2 - 4	SM
6	1980	11.4	98	28	20	8	34	A- 2 - 4	SM
8	2040	10.3	92	28	21	7	34	A- 2 – 4	SM
10	2130	8.6	169	20	NIL	NIL	38	A- 2 - 4	SM

Table 9: Orukim Residual Soil and Lime Classification – Sample no. 4

Lime Content(%)	MDD Kg/m³	OMC (%)	CBR soaked (%)	LL	PL	PI	% passing Sieve 200	Classification	
								AASHTO	USCS
0	1960	10.7	26	37	21	16	33	A-2-4	SM
2	2090	6.1	80	30	20	10	33	A-2-4	SM
4	1930	11.5	85	30	22	8	34	A-2-4	SM
6	1930	10.4	98	30	24	6	35	A-2-4	SM
8	1950	12.4	140	21	NIL	NIL	36	A-2-4	SM
10	1970	8.9	145	18	NIL	NIL	39	A-2-4	SM

V.   Discussion of Test Results

Table 1 shows the result of mechanical compaction tests of Orukim residual soil at unstabilized condition. Tables'2 to 5 present Orukim residual soil and quarry dust classification incorporating the plasticity limit as well as the grain-sized distribution based systems. The samples are classified at stabilized conditions. Tables 6 to 9 present Orukim residual soil and lime stabilization. The plasticity index (PI) classification provides a soil profile over depth with the probability of belonging to different soil types, which more realistically and continuously reflects the in-situ soil characterization which involves the variability of soil type. The grain-size distribution classification emphasizes the certainty of behaviour. The advantage of combining the two classification methods is realised when dealing with the behaviour of the soil-water characteristic curve and the variability arising from the application of various percentages of stabilizers. For instance at location 1 under unstabilized condition 30% maximum residual soil sample passes the No 200 ASTM sieve, the liquid limit is 32%, plastic limit is 20% maximum and the plasticity index is 12. Based on AASHTO and USCS classifications, this is a composition of clayey sand, A-2-6 and SC respectively or clay sand mixture with appreciable amount of fines. At modified conditions, for example with 20% quarry dust, it is observed that the physical characteristics depreciate gradually to liquid limit, 30%, plastic limit, 23% and plasticity index of 7 with proper compaction.

The CBR values under quarry dust stabilization vary from a minimum of 56% to a maximum of 140% with 10% and40% quarry dust content respectively at location 1. Conversely with lime stabilization the CBR values appreciated considerably from 82% to 169% with lime content of 2% and 10% respectively at location 3.

VI.   Multiple Non-Linear Regressed Models

Based on analysis and utilizing multiple nonlinear regressed programs the following models were developed for evaluating CBRvalues of Orukim residual soils at various levels of stabilization with quarry dust and lime. The models are often used for the purposes of prediction and optimization to determine for what values of the independent variables the dependent variable is a maximum or minimum.

CBR_{Q1}= 24.896 + 1.974Q - 1.909D + .469M - .028Q^2 + .111D^2 + .747M^2 + .799QD - .373QM - .301DM……………………………………………………………………………………………………..1.1
Where Q=Quarry dust [%], D=Maximum dry density[Mg/m³], M = Optimum moisture content [%]

CBR_{Q2}= 43.927 + 3.223Q − 1.543D + 3.926M - .051Q^2 + .627D^2 - .122M^2 + .641QD - .197QM - .1O2DM……………………………………………………………………………………………………..1.2
Where Q=Quarry dust [%], D=Maximum dry densty[Mg/m³], M = Optimum moisture content [%]

CBR_{L1}= 89.318 − 2.448L + 1.199D + .669M - .538L^2 + .573D^2 + .479M^2 + .135LD - .197LM - .837DM………………………………………………………………………………………………………1.3
Where L=lime [%], D=Maximum dry density [Mg/m³], M= Optimum moisture content [%]

CBR_{L2} = 108.171 - 3.977L + 7.717D + 1.233M - .211L^2 + .346D^2 - .141M^2 - .209LD +,191LM +.464DM………………………………………………………………………………………………………1.4
Where L=lime [%], D=Maximum dry density [Mg/m³], M= Optimum moisture content [%]

Table 10: Multiple Regressed Variables for Measured and Computed CBR Values – Residual Soil and Quarry Dust Stabilization (Samples1&2)

Quarry Dust Content (%)	MDD (kg/m^3)	OMC (%)	Measured CBR (%)	Computed CBR (%)
10	1.99	8.5	56	75.538
20	2.01	8.3	71	70.321
30	2.04	8.3	104	61.762
40	2.04	8.2	140	47.517
50	1.91	6.3	99	38.145
60	1.96	7.6	64	5.323
70	1.82	15.3	43	-101.262
10	1.9	6.2	54	58.741
20	2	8.5	68	71.192
30	1.91	6.1	86	60.348
40	1.93	6.7	128	50.287
50	1.95	6.7	89	35.986
60	1.98	8.5	50	-3.226
70	1.78	12.6	45	-88.849
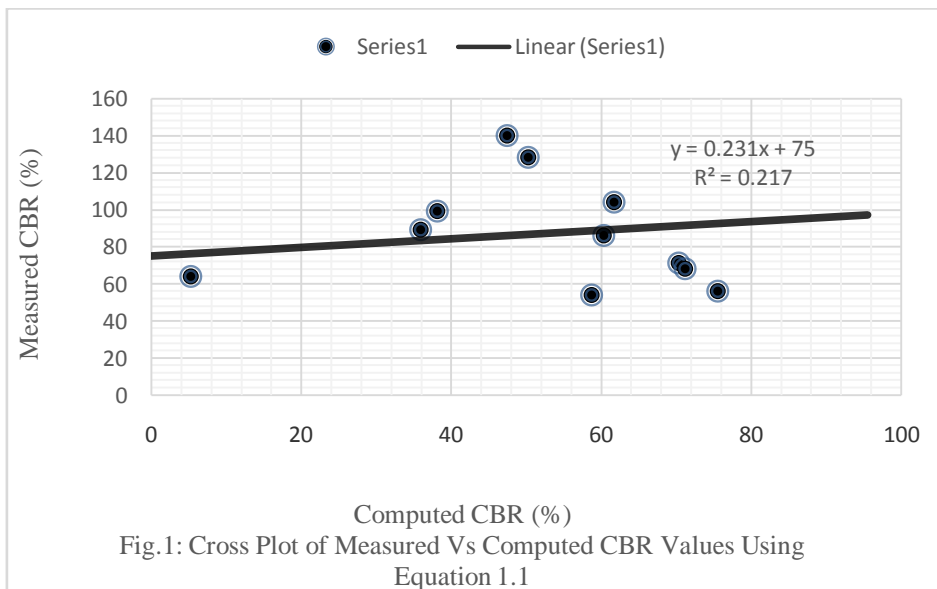
Fig.1: Cross Plot of Measured Vs Computed CBR Values Using Equation 1.1

Table 11: Multiple Regressed Variables for Measured and Computed CBR Values – Residual Soil and Quarry Dust Stabilization. (Samples 3&4)

| Quarry Dust Content (%)	MDD (kg/m^3)	OMC (%)	Measured CBR (%)	Computed CBR (%)
10	1.92	11.5	52	119.089
20	2.01	11.5	83	126.803
30	2.02	8.3	81	123.230
40	2.07	9.2	117	115.821
50	2.03	10.1	83	92.612
60	2.08	8.6	56	72.517
70	2.04	8.1	42	37.054
10	1.89	6.2	63	98.117
20	2.01	12.3	98	128.950
30	2.06	7.8	101	124.121
40	2.05	8.4	111	116.919
50	2.03	11.5	88	87.717
60	1.99	8.2	65	71.463
70	1.76	12.5	42	-8.647

Fig.2: Cross Plot of Measured Vs Computed CBR Values Using Equation 1.2
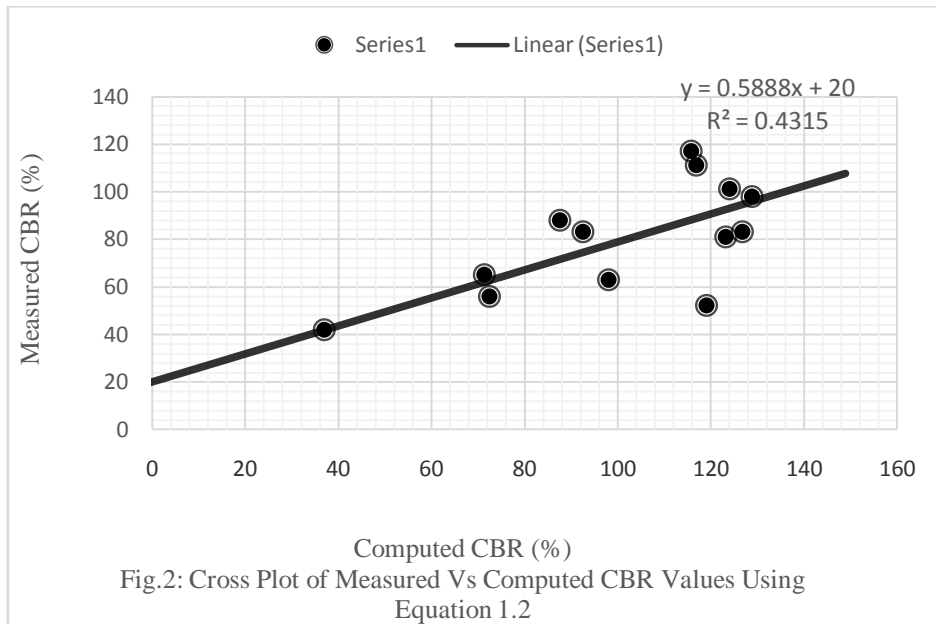
Table 12: Multiple Regressed Variables for Measured and Computed CBR Values – Residual Soil and Lime Stabilization. (Samples 1&2)

Lime Content (%)	MDD (kg/m³)	OMC (%)	Measured CBR (%)	Computed CBR (%)
2	1.94	8.2	76	108.424
4	2.1	8.9	92	98.336
6	1.99	8.5	105	77.618
8	1.98	8.5	98	54.872
10	1.98	8.2	110	26.282
2	1.92	12.4	80	144.337
4	2.06	11.5	92	119.083
6	2.09	15	99	135.804
8	2.06	14.8	110	108.406
10	2.08	12.1	120	52.142

Fig.3: Cross Plot of Measured Vs Computed CBR Values Using Equation 1.3
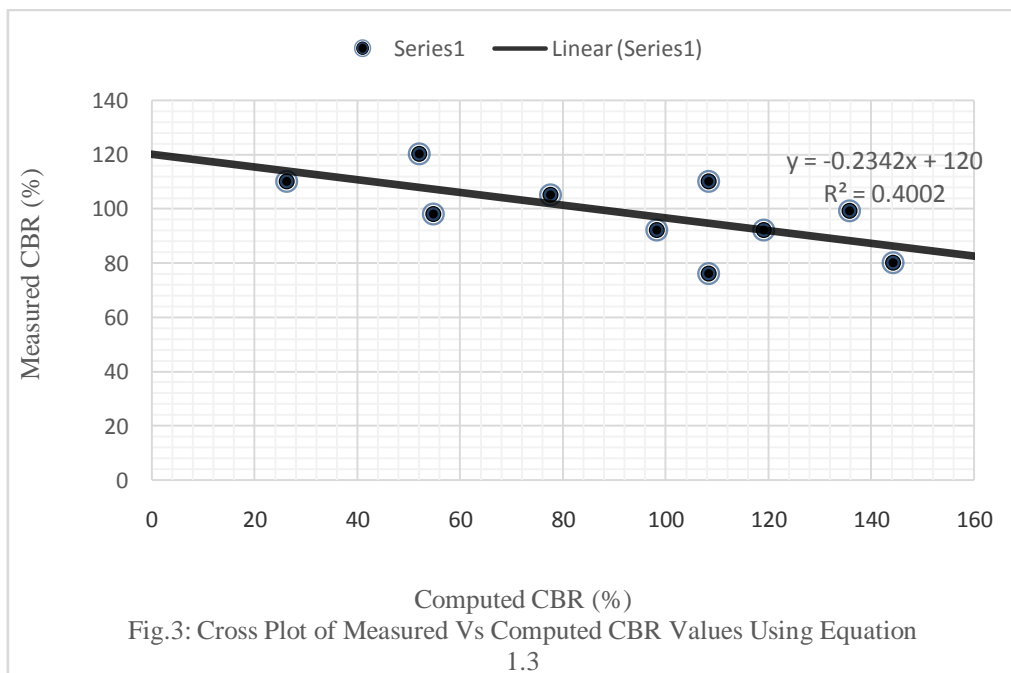
Table 13: Multiple Regressed Variables for Measured and Computed CBR Values – Residual Soil and Lime Stabilization. (Samples 3&4)

Lime Content (%)	MDD (kg/m^3)	OMC (%)	Measured CBR (%)	Computed CBR (%)
2	2	9.3	82	128.482
4	2.05	8.5	86	122.747
6	1.98	11.4	98	115.102
8	2.04	10.3	92	106.674
10	2.13	8.6	169	94.861
2	2.09	6.1	80	128.407
4	1.93	11.5	85	121.300
6	1.93	10.4	98	114.120
8	1.95	12.4	140	106.251
10	1.97	8.9	145	92.903
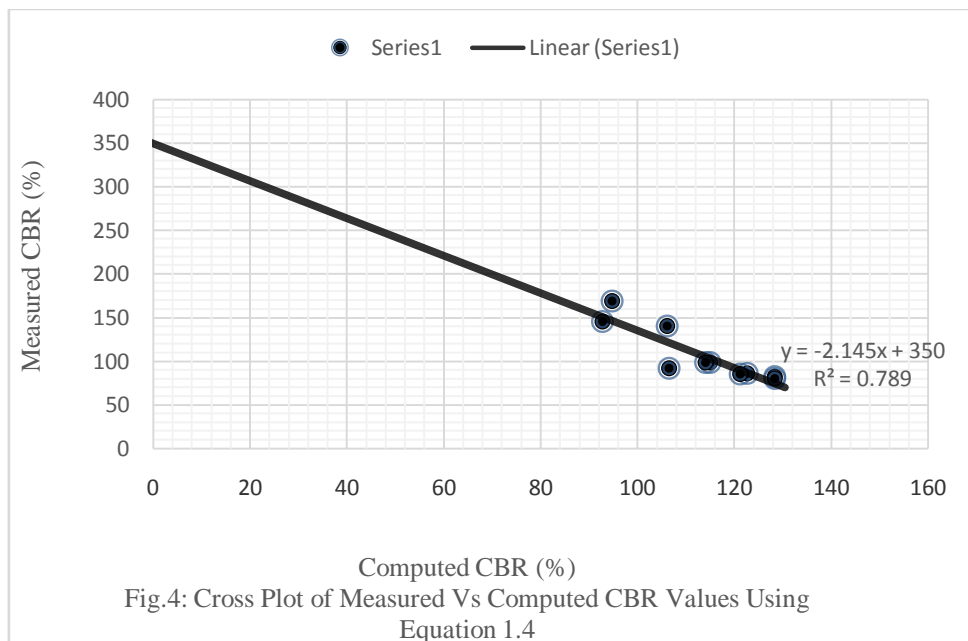
Fig.4: Cross Plot of Measured Vs Computed CBR Values Using Equation 1.4

VII. Conclusion

Tables 10 and 11 present the multiple regressed variables for measured and computed CBR values resulting from quarry dust stabilization. Results vary from 56KPa – 140KPa and 75KPa – 129KPa for measured and computed values respectively. Tables 12 and 13 present similar values resulting from lime stabilization. Results vary from 76KPa -169KPa and 108KPa – 144KPa for the measured and computed CBR values respectively.

The models 1.1 and 1.3 do not seem to generate higher correlations between the measured and computed values hence could further be optimized by subjecting the coefficients of the input variables to basic iteration.

The models 1.2 and 1.4 are adequate for this research. Model 1.2 revealed that with quarry dust content ranging from 10% - 30% of residual soil the measured and computed values vary from 63% - 101% and 98% - 124% respectively. With regards to model 1.4 it is observed that lime stabilization varying from 2% - 6% of residual soil content yielded measured and computed CBR values varying from 82% - 98% and 128% - 115% respectively. These values are adequate for both sub base and base course applications because they areabove recommended minimum specified by FMW&H [1997] code.

The accuracy and reliability of the models were checked by comparing the measured and computed values of CBR and computing the correlation coefficients. The figures I to IV illustrate the measured and computed values based on non- linear regressed models. The straight line in the figure represents the line of perfect equality where the values being compared are exactly equal.

The correlation coefficients R^2 at 95% confidence interval are 0.2175,0.4315 and 0.4002,0.7899 for CBR with quarry dust content from 10% - 70% and lime content from 2% - 10%. These values are significant statistically and suggest that the measured and computed values are compatible.

Acknowledgement

REFERENCES

[1]   Zomorodian, A. and Eslami, A. [2005] Determining the Geotechnical Parameters of Stabilized Soils by Stone Column Based on SPResults. Electronic Journal of Geotechnical Engineering, Vol.10 2005, Bundle A.

[2]   Stavridakis, E. [2005] A Proposed Classification for Anisotropic Engineering Behaviour of Cement Treated Clayey Mixtures Related to Their Strength and Durability. Electronic Journal of Geotechnical Engineering, Vol.10, 2005.

[3]   Cole, L.W. and Cepco, C. [2006] PENNDOT'S Efforts to Improve Pavement Sub-grade During Highway Reconstruction – Airfield and Highway Pavements Specialty Conference, Atlanta, Georgia , U.S.A.

[4]   Butler, R. L. and Cerato, A. B. [2007]. Stabilization of Oklahom Expansive Soils using Lime and Class C Fly-Ash. Proc. of Session of Geo Denver. Colorado, USA.

[5]   Galvero, T. C. B, Elsharief, A. and Simoes, G. F. [2004] "Effects of Lime on Permeability and Compressibility of Two Tropical Residual Soils. Journal of Envir. Engrg, Vol. 130, Issue 8, pp 881-885.

[6]   Akawi, E. and Kharabsheh, A. [2000] Lime Stabilization Effects on Geotechnical Properties of Expansive Soils in Amman, Jordan. Electronic Journal of Geotechnical Engineering, Vol. 5, 2000.

An Overview of Disarray in Vibrational Analysis of Composite Leaf Spring Subjected to Harmonic Excitation with Nonlinear Parameters

Yogesh Y. Kamble[1], Prof. Dr. S. H. Sawant[2]

[1]*PG Student Department of Mechanical Engineering, Dr. J.J. Magdum College of Engineering, Jaysingpur*
[2]*Professor Department of Mechanical Engineering, Dr. J.J. Magdum College of Engineering, Jaysingpur*

Abstract: *Most real-world phenomena exhibit nonlinear behavior. The behavior of steel leaf spring is nonlinear. It is having relatively high weight, and change in solid axle angle due to weight transfer specially during cornering of vehicle. That will lead to oversteer and directional instability under such situation it is very difficult for driver to control vehicle. These are some defect of metallic leaf spring so considering automobile development and importance of relative aspect such as fuel consumption, weight, ride quality, and handling development of new material is necessary in the automobile industry. In practice, engineering structures display a certain degree of nonlinearity, often due to a combination of nonlinear material properties, geometric effects, structural joints and nonlinear boundary conditions. Normally these effects are neglected by linearization in the intended working range. However, it becomes increasingly more important to take the nonlinear effects into account. This paper tries to give an idea about the previous researches and their finding about study of nonlinearity in spring.*
Keywords: *Composite Leaf Spring, Nonlinearity, E-Glass/ Epoxy, Tsai-Wu criterion.*

I. Introduction

Increasing competition and innovations in automobile sector tends to modify the existing products or replace old products by new and advanced material products. A suspension system of vehicle is also an area where these innovations are carried out regularly. More efforts are taken in order to increase the comfort of user. Appropriate balance of comfort riding qualities and economy in manufacturing of leaf spring becomes an obvious necessity. To improve the suspension system many modifications have taken place over the time. Inventions of parabolic leaf spring, use of composite materials for these springs are some of these latest modifications in suspension systems [1].

A leaf spring is a simple form of spring, commonly used for the suspension in vehicles. A leaf spring which is an automotive component is used to absorb vibrations induced during the motion of vehicle. Leaf springs are long and narrow plates attached to the frame of a trailer that rest above or below the trailer's axle. There are single leaf springs and multi leaf springs which are used based on the application required. It also acts as a structure to support vertical loading due to the weight of the vehicle and payload. Under operating conditions, the behavior of the leaf spring is complicated due to its clamping effects and interleafs contact, hence its analysis is essential to predict the displacement and mode frequency [2].

In order to conserve natural resources and economize energy, weight reduction has been the main focus of automobile manufacturers in the present scenario. Weight reduction can be achieved primarily by the introduction of better material, design optimization and better manufacturing processes. Leaf springs probably are the oldest automobile suspension gadgets still in active use. Their simplicity and effectiveness might be contributing to this. The fact that a staggering amount of load is managed well while reducing the subsequent discomfort substantially adds to their reliability. The suspension leaf spring is one of the potential items for weight reduction in automobiles as it accounts for 10% - 20% of the unsprung weight. This achieves the vehicle with more fuel efficiency and improved riding qualities[3, 11].

The introduction of composite materials was made it possible to reduce the weight of leaf spring without any reduction in load carrying capacity and stiffness. Since, the composite materials have more elastic strain energy storage capacity and high strength to weight ratio as compared with those of steel, multi-leaf steel springs are being replaced by mono-leaf composite springs. The composite material offer opportunities for substantial weight saving but not always be cost-effective over their steel counterparts [4].

There is an increasing awareness regarding highway traffic safety and automobile rollover accidents involving Sport Utility Vehicles (SUV'S). Among others, catastrophic rollover accidents of SUV draw

increasing attention to vehicle design and safety requirements. For this reason, accurate and efficient computer simulations of SUV models play an important role inthe design, performance evaluations and stability analysis of such vehicle systems. Most of SUV and trucks are equipped with leaf springs in either the front or rear axle suspension systems in order to improve the ride comfort and to support heavy loads. It is well known, however, that the suspension characteristics of leaf springs are highly nonlinear due to contact between spring leaves and hysteresis due to frictional effect [5].

Most real-world phenomena exhibit nonlinear behavior. There are many situations in which assuming linear behavior for physical system might provide satisfactory results. On other hand, there are circumstances or phenomena that require a nonlinear solution. A nonlinear structural behavior may arise because of geometric and material nonlinearities, as well as change in the boundary conditions and structural integrity.

II.   Free Vibration Analysis of Composite Leaf Springs

A. L. Aishwarya et al.studied that the free vibration analysis of composite leaf springs clamped on one side. This has been done using a three dimensional finite element model in ANSYS version 12. The effects caused by the variation of width, friction between the leaves of the spring, relative movement of the leaves and the changes that occur in the natural frequency of the spring when the orientation of the fiber stacks by varying leaves have been discussed.The effect of friction has been studied by varying the values of friction in augumented method with the layer specification being no separation (always) for a 0l90l90l0 angular stack arrangement of fibers. In this paper they concluded that there is no significant effect of friction coefficient, no significant variation between friction and bonding cases, frictionless surfaces causes for reduction in frequencies and increase in leaf width improves natural frequencies.

III.   Analysis of Composite Leaf Spring by Using Analytical and FEA

Ranjeet Mithari et al. [4] analyzed, a seven-leaf steel spring usedin passenger cars is replaced with a composite multi leaf spring made of glass/epoxy composites. The dimensions and the number of leaves for both steel leaf spring and composite leaf springs are considered to be the same. The primary objective is to compare their load carrying capacity, stiffness and weight savings. Finally, fatigue life of steel and composite leaf spring is also predicted using life data. The objective of the work is to calculate stresses, strength to weight ratio, dynamic loading condition, and stiffness and compare those with conventional steel leaf spring. For the accurate evaluation of above factor, they use Finite Element Method. In Static analysis, there is no variation of force with respect to time. Output in the form of stress, displacement, etc. with respect to time is not taken into account. Modal analysis of leaf spring is conducted to study the natural frequencies.

IV.   Modeling and Analysis Of Composite Leaf Spring Under The Static Load Condition by Using Fea

M. M. Patunkar and D.R.Dolas [6] done analysis of composite leaf spring. In this analysis the conventional steel leaf spring is tested for static load condition and results are compared with a virtual model of composite material leaf spring. Leaf spring is modeled in Pro-E 5.0 CAD software and it is imported and simulated in ANSYS 10.0 for better understanding. Results of Composite Leaf Spring are compared on the basis of analysis reports produced by ANSYS software.Under the same static load conditions deflection and stresses of steel leaf spring and composite leaf spring are found with the great difference. Deflection of Composite leaf spring is less as compared to steel leaf spring with the same loading condition.

V.   Analysis and Optimization of a Composite Leaf Spring

Mahmood M Shokrieh and DavoodRezaei [7] studied, a four-leaf steel spring used in passenger cars replaced with a composite spring made of glass/epoxy composites. The main objective was the shape optimization of the spring to give the minimum weight. They concluded that static loading and full bump is not sufficient to design a composite leaf spring. So, a stress analysis was performed using finite element method. All the calculations were done using the version 5.4 of ANSYS [9]. In the finite element modeling, every leaf was modeled with eight-node 3D brick elements (SOLID 45) and then five node 3D contact elements (CONTACT 49) were used to represent contact and sliding between adjacent surfaces of leaves. The focus was on to obtain a spring with minimum weight that is capable of carrying given static external forces by constraints limiting stresses (Tsai–Wu criterion) and displacements.

VI.   Experimental Investigation and Numerical Analysis of Composite Leaf Spring

K. K. Jadhao et al. [8] worked on design, fabrication, experimental testing and analysis of composite spring made up of E-glass fiber, chopped strands mat and epoxy resin (general purpose resin) with constant width and thickness throughout its length.They calculated experimental values of the stresses and deflection

by testing the leaf springs under static loading condition. These results are also compared with FEA. The weight of the leaf spring is reduced considerably about 85 % by replacing steel leaf spring with composite leaf spring. They compared performance of existing steel leaf spring with the fabricated composite leaf spring. Testing has been done for unidirectional E-Glass/Epoxy mono composite leaf spring. Since the composite leaf spring is able to withstand the static load, they concluded that there is no objection from strength point of view also, in the process of replacing the conventional leaf spring by composite leaf spring.

VII. Design and Analysis of Composite Leaf Spring

Y.N.V. Santhosh Kumar and M. Vimal Teja [9] in their paper discussed that the composite structures for conventional metallic structures has many advantages because of higher specific stiffness and strength of composite materials. The automobile industry has shown increased interest in the replacement of steel spring with fiberglass composite leaf spring due to high strength to weight ratio. There work deals with the replacement of conventional steel leaf spring with a Mono Composite leaf spring using E-Glass/Epoxy. The design parameters were selected and analyzed with the objective of minimizing weight of the composite leaf spring as compared to the steel leaf spring. The leaf spring was modeled in Pro/E and the analysis was done using ANSYS Metaphysics software.

VIII. Analysis and Comparison of Vehicle Dynamic System with Nonlinear Parameters Subjected To Actual Random Road Excitations

Prof. S. H. Sawant and Dr. J. A. Tamboli published a paper on Analysis and Comparison of Vehicle Dynamic System with Nonlinear Parameters Subjected to Actual Random Road Excitations. Paper investigates the importance of effects depend upon the degree of nonlinearity and so the effect on the response. In this paper, nonlinearity in mass, spring and damper are considered and compared for their individual and relative significance. Also, it is studied how nonlinearity affects the response compared to linear system. The theories of non-linear dynamics are applied to study non-linear model and to reveal its non-linear vibration characteristics. Thus this paper deals with comparison between simulation results obtained for passive and semiactive linear systems with nonlinear mass, spring and damper. The excitation is taken as actual random road excitation to achieve improved performance. Thus,the emphasis is to study the nonlinearities in mass, spring and damper for passive suspension system performance and compare the relative significance [10].

IX. Conclusion

From the literature survey it is seen that the Design and analysis of composite leaf spring, has started from developing theories related to design and development of composite leaf spring and is now moving towards optimizing various spring parameters according to applications. Theories are used to calculate the natural frequencies and mode shapes. In order to carryout vibrational analysis of composite leaf spring it is necessary to carryout analysis with nonlinear parameters.

References

[1]   Jaydeep J. Patil, Dr. S. A. Patil. "Design and Analysis of Composite Leaf Spring using Finite Element Methods,"- A Review, International Journal of Advanced Engineering Technology, Volume V, Issue II, 2014.
[2]   Mohansing R. Pardeshi, Dr. (Prof.) P. K. Sharma, Prof. Amit Singh "Vibration Analysis of E-Glass Fibre Resin Mono Leaf Spring used in LMV," International Journal of Advanced Technology in Engineering and Science,Volume No.02, Issue No. 05, May 2014.
[3]   A. L. Aishwarya, A. Eswara Kumar, V. Balakrishna Murthy, "Free Vibration Analysis of Composite Leaf Springs," International Journal of Research in Mechanical Engineering And Technology, Volume 4, April 2014.
[4]   Ranjeet Mithari, "Analysis of Composite Leaf Spring by using Analytical and FEA," International Journal of Engineering Science and Technology (IJEST), ISSN : 0975-5462, Volume 4, December 2012.
[5]   Hiroyuki Sugiyama, Ahmed A.Shabana, Mohamed A.Omar, Wei-Yi Loh. "Development of Nonlinear Elastic Leaf Spring Model for Multibody Vehicle Systems," Computer Methods in Applied Mechanics and Engineering, Feb. 2005.
[6]   M. M. Patunkar, D. R. Dolas. "Modelling and Analysis of Composite Leaf Spring under the Static Load Condition by Using FEA," International Journal of Mechanical and Industrial Engineering, Volume 1, Issue 1, 2011.
[7]   Mahmood M.Shokrieh, Davood Rezaei. "Analysis and Optimization of a Composite Leaf Spring," Composite Structures, 2003.
[8]   K. K. JADHAO, DR. R.S DALU. "Experimental Investigation and Numerical Analysis of Composite Leaf Spring," International Journal of Engineering Science and Technology (IJEST), Volume 3, June 2011.
[9]   Y. N. V. Santhosh Kumar, M. Vimal Teja, "Design and Analysis of Composite Leaf Spring," International Journal of Mechanical and Industrial Engineering (IJMIE), ISSN No. 2231-6477, Vol-2,Issue-1,2012.
[10]   Prof. S. H. Sawant, Dr. J. A. Tamboli "Analysis and Comparison of Vehicle Dynamic System with Nonlinear Parameters Subjected to Actual Random Road Excitations", International Journal of Mechanical Engineering and Technology (IJMET), ISSN 0976 –6340(Print), ISSN 0976 – 6359(Online) Volume 3, Issue 2, May-August 2012.

Conditioning Monitoring of Gearbox Using Different Methods: A Review

Mr. Rohit Ghulanavar[1], Mr. M. V. Kharade[2]

[1]*PG student Department of Mechanical Engineering, Dr. J.J. Magdum College of Engineering, Jaysingpur*
[2]*Asst. Professor Department of Mechanical Engineering, Dr. J.J. Magdum College of Engineering, Jaysingpur*

Abstract: *Gears are important element in a variety of industrial applications such as machine tool and gearboxes. An unexpected failure of the gear may cause significant economic losses. For that reason, fault diagnosis in gears has been the subject of intensive research. Vibration signal analysis has been widely used in the fault detection of rotation machinery. Fault diagnosis plays an important role in condition monitoring to enhance the machine time. In view of this, the present investigation focused on the development of Fault diagnosis system of gearboxes based on the vibration signatures and Artificial Neural Networks. In the present investigation to generate the vibration signatures an experimental set-up has been fabricated with sensing and measuring equipment. The prominent faults, wear, crack, broken tooth and insufficient lubrication of the gear were practically induced in the present investigation. Vibration signatures of the gearbox were collected by transmitting the motion at constant speed with gears having no fault, without applying any load. By inducing one fault at a time, vibration signatures were collected with different degrees of wear on a gear tooth, a gear with a broken tooth, tooth with crack and with insufficient lubrication. As the vibration data of maximum amplitudes was found to be inseparable, fault diagnosis based on this data was not possible. Five prominent statistical features were extracted based on data pertaining to maximum amplitudes of vibration and used fault diagnosis. Due overlapping of this data, it was decided to use ANN based fault diagnosis system for the present investigation. The set of statistical features were extracted based on data pertaining to maximum amplitudes of vibration and used them as input parameters to the ANN based fault diagnosis system designed.*
Keyword: *Gearbox, Conditioning Monitoring, Acoustic Signals, Wavelet Transform, ANN.*

I. Introduction

Today, most maintenance actions are carried out by either the predetermined preventive or the corrective approach. The predetermined preventive approach has fixed maintenance intervals in order to prevent components, sub-systems or systems to degrade. The concept of condition monitoring is to select measurable parameters on the machines, which will change as the health or condition of a machine. Regular monitoring is done and the change is detected. Once a change is detected it is possible to make a more detailed analysis of the measurements to determine what the problem is, and hence arrive at a diagnosis of the problem [1-3].

The parameters most often chosen to detect this change in conditions either vibration, which tends to increase as a machine moves away from a smooth running condition into a rough mode with development of a fault, or an analysis of machine noise or acoustics, or machine lubricants where samples are tested for items such as wear debris from a developing fault [4-6]. There are various sensors to detect and monitor the early signals of electrical, mechanical, electronic, pneumatic, hydraulic, etc. and provide an aid to fault diagnosis and to establish an effective maintenance management procedure to predict and prevent system failure just in time [9].

Typical applications of gearboxes include electric utilities, automotive industry, ships and helicopters. A practical and robust monitoring system is critically needed to provide the earliest warning of damage or malfunction in order to avoid sudden failure. Currently, there are three approaches to the detection of faults in geared system: acoustic signal analysis, debris monitoring and vibration analysis. The vibration based diagnosis has been the most popular monitoring technique because of ease of measurement. When vibration features of component are obtained, its health condition can be determined by comparing these patterns with those corresponding to its normal and failure condition [8].

In new technique, wavelet analysis possesses particular advantages for characterizing signals at different localization levels in time as well as frequency domain. It has a wide variety of applications in many engineering fields such as signal processing, image processing, pattern recognition, seismology, machine

visualization, etc. In the field of mechanical fault diagnosis, wavelet analysis has been used in gear diagnosis [7].

The time domain vibrational signal is typically proceed into frequency domain applying Fast Fourier Transform. Wavelet Transform (WT) has attracted many attention.The WT was utilized to represent all possible possibilities of transients in vibration signals generated by faults in gear box [10].

II.   Condition Monitoring using Wavelet Transform

N. Baydar & A. Ball [1], have used vibration analysis is widely used in machinery diagnostic and the wavelet transform has also been implemented in many application in the conditioning monitoring of machinery. Vibration signal to detect the various local faults in gearboxes using wavelet transform, vibration and acoustic signals for detection failure of gear. Two commonly encountered local faults, tooth breakage and tooth crack, were simulated. The results of acoustic signals were compared with vibration signals.

III.   Condition Monitoring using Acoustic Signals

Baydar and Andrew Ball [2], examines whether acoustic signals can be used to detect faults in gearbox using smoothed pseudo-winger-ville distribution. Three types of progressing local faults, broken tooth, gear crack and localized wear, were simulated and results are from acoustic signals were compared crack and localized were estimated.

IV.   Use of Time domain techniques for vibration signal for Fault Detection in Gear Box

F. A. Andrade, et al [3], introduces a new technique for early identification of spur gear tooth fatigue cracks, namely the Kolmogorov minor test. This test works on the null hypotheses that the cumulative density function (CDF) of a target distribution is statistically similar to the CDF of a reference distribution. In fact, this is a time-domain signal processing technique that compares two signals, and returns the likelihood that the two signals have the same probability distribution function. Based on this estimate, it is possible to determine whether the two signals are similar or not. Therefore, by comparing a given vibration   signature to a number of template signatures (i.e., signatures from known gear conditions) it is possible to state which is the most likely condition of the gear under analysis.

Jing Lin, et al [4], commences with technique of wavelet de-noising for mechanical fault detection. For gears and roller bearings, periodic impulses indicate that there are faults in the components. However, it is difficult to detect the impulses at the early stage of fault because they are rather weak and often immersed in heavy noise. Existing wavelets, which do not match the impulse very well and do not utilize prior information on the impulses. A new method for wavelet threshold de-noising is proposed in this paper; it not only employs the Morlet wavelet as the basic wavelet for matching the impulses, but also uses the maximum likelihood estimation for thresholding by utilizing prior information on the probability density of the impulse. This method has performed excellently when used to de-noise mechanical vibration signals with a low signal-to-noise ratio.

W. X Yang and X.M. Ren [5], studied development of an effective impulses detection technique is necessary and significant for revaluating the working condition of these machines ,diagnosing their malfunctions, and keeping them running normally over prolong periods. With the aid of wavelet transforms, a wavelet –based envelope analysis method is proposed. In order to suppress any undesired information and highlight the features of interest, an improved soft threshold method has been designed so that inspected signal is analyzed in a more exact way.

V.   Condition Monitoring using Continuous Wavelet Transform

H.Zheng, et al [6], worked on new approach of gear fault diagnosis based on continuous wavelet transform is presented. Continuous wavelet transform can provide a finer scale resolution than orthogonal wavelet transform. It is more suitable for extracting mechanical fault information. In this, the concept of time-averaged wavelet spectrum (TAWS) based on Morlet continuous wavelet transform is proposed. Two fault diagnosis methods named spectrum comparison method (SCM) and feature energy method (FEM) based on TAWS are established. The results of the application to gearbox gear fault diagnosis show that TAWS can effectively extract gear fault information.

Wilson Q. et al [7], experimentally investigates the sensitivity and robustness of the currently well-accepted techniques: phase and amplitude demodulation, beta kurtosis and wavelet transform. Four gear test cases were used: healthy gears, cracked, filed and chipped gears. The vibration signal was measured on the gearbox housing and processed, online, under three "filtering conditions: general signal average, overall residual and dominant meshing frequency residual. Test results show that beta kurtosis is a very reliable time-domain diagnostic technique.

G. Dalpiaz, et al [8], worked on the detection and diagnostic capability of some of the most effective techniques discussed and compared on the basis of experimental results, concerning a gear pair affected by a

fatigue crack. In particular, the results of new approaches based on time-frequency and cyclostationarity analysis are compared against those obtained by means of the well accepted spectrum analysis and time-synchronous average analysis. Moreover, the sensitivity to fault severity is assessed by considering two different depths of the crack. The effect of transducer location and processing options are also shown.

VI. Condition Monitoring using Discrete Wavelet Transform

S. A. Adewusi and B. O. Al. - Bedoor [9], presented an experimental study of the dynamic response of an overhang rotor with a propagating transverse crack using the discrete wavelet transform (DWT)-a joint time frequency analysis technique. Start-up and steady state vibration signatures are analyzed using Daubechies (Db6) mother wavelet and the results are presented in the form of scalograms and space-scale energy distribution graphs.

VII. Use of Spectral Analysis for Detection and Diagnosis of Shaft Faults in Gear Box

Darley Fiacrio de Arruda Santiago [10], concluded that the field of fault diagnostic in rotating machinery is vast, including the diagnosis of items such as rotating shafts, rolling element bearings, couplings, gears and so on. The different types of faults that are observed in these areas and the methods of their diagnosis are accordingly great, including vibration analysis, model-based techniques, statistical analysis and artificial intelligence techniques.

VIII. Condition Monitoring Using Artificial Neural Network

N. Saravanan, et al [11], presented the paper deals with the effectiveness of wavelet-based features for fault diagnosis of a gear box using artificial neural network (ANN) and proximal support vector machines (PSVM). Vibration signals extracted from rotating parts of machineries carries lot many information within them about the condition of the operating machine. Further processing of these raw vibration signatures measured at a convenient location of machines unravels the condition of the component or assembly under study. The statistical feature vectors from Morlet wavelet coefficients are classified using J48 algorithm and features were fed as input for training and testing ANN and their relative efficiency in classifying the faults in gear box was compared

IX. Conclusion

In this paper, authors have been presented a brief review of some current vibration based techniques used for condition monitoring in geared transmission systems. After the review of literature on gear fault analysis, the following points are concluded.

(i)   Gearbox vibration signals are usually periodic and noisy. Time-frequency domain average technique successfully removes the noise from the signal and captures the dynamics of one period of the signals.

(ii) Time domain techniques for vibration signal analysis as waveform generation, Indices (RMS value, Peak Level value, and crest factor) and overall vibration level do not provide any diagnostic information but may have limited application in fault detection in simple safety critical accessory components.The statistical moment as kurtosis is capable to identify the fault condition but skewness trend has not shown any effective fault categorization ability in this present gear fault condition.

(iii) Spectral analysis may be useful in the detection and diagnosis of shaft faults.

(iv) In frequency domain analysis, it is concluded that FFT is not a suitable technique for fault diagnosis if multiple defects are presents on gearbox. The envelope analysis and Power Spectrum Density techniques have shown a better representation for fault identification. The Hilbert Transform and PSD techniques are suitable for multiple point defect diagnostics for condition monitoring.

(v)   Synchronous signal averaging has the potential of greatly simplifying the diagnosis of shaft and gear faults (i.e., the safety critical failures) by providing significant attenuation of nonsynchronous vibrations and signals on which ideal filtering can be used. Further development needs to done on the implementation of synchronous averaging techniques and the analysis of results.

From the literature survey it is seen that the theories are developing to detect fault of gearbox. Now it is moving towards new technique like Artificial Neural Network (ANN). Expert system based on ANN and fuzzy logic can be developed for robust fault categorization with the use of extracted features from vibration signal.

REFERENCES

[1]   N. Baydar & A. Ball, "Detection Of Gear Failures Via Vibration And Acoustic Signals Using Wavelet Transform".Mechanical Systems and Signal Processing (2003), Vol. 17(4), 787–804.

[2]   Baydar and Andrew Ball have presented [3] "A Comparative Study of Acoustic and Vibration Signals in Detection of Gear Failures Naim Using Winger-Ville Distribution". 24 August 2000.

[3]   F. A. Andrade, I. Esat And M. N. M. Badi ,"A New Approach To Time Domain Vibration Condition Monitoring: Gear Tooth Fatigue Crack Detection And Identification", in Journal of Sound and vibration (2001), Vol.240(5), 909-919

[4]   Jing Lin, Ming J. Zuo, Ken R. Fyfe, "Mechanical Fault Detection Based on the Wavelet De-Noising Technique".Journal of Vibration and Acoustics Copyright 2004 by ASME JANUARY 2004, Vol. 126, 9-14.

[5]   W. X Yang and X.M. Ren, "Detecting Impulses in Mechanical Signals by Wavelets".Journal on Applied Signal Processing 2004:Vol.8, 1156–1162.

[6]   H. Zheng, Z. Li and X. Chen, "Gear Fault Diagnosis Based on Continuous Wavelet Transform".Mechanical Systems and Signal Processing (2002) 16(2–3), 447–457.

[7]   Wilson Q. Wang, Fathy Ismail and M. Farid Golnaraghi, "Assessment of Gear Damage Monitoring Technique Using Vibration Measurement".Mechanical Systems and Signal Processing (2001), Vol. 15(5), 905-922.

[8]   G. Dalpiaz, A. Rivola and R. Rubini ,"Effectiveness and Sensitivity of Vibration Processing Techniques for Local Fault Detection in Gears".Mechanical Systems and Signal Processing (2000), vol. 14(3), 387-412.

[9]   S. A. Adewusi and B. O. Al.- Bedoor ,"Wavelet Analysis of Vibration Signals of an Overhang Rotor with a Propagating Transverse Crack'. Journal of Sound and vibration (2001) ,246(5), 777-793.

[10]   Darley Fiacrio de Arruda Santiago, "Application of Wavelet Transform to Detect Faults in Rotating Machinery". ABCM Symposium of Mechatronix, Vol.1, 616-624.

[11]   N. Saravanan , V.N.S. Kumar Siddabattuni, K.I. Ramachandran "Fault Diagnosis of Spur Bevel Gear Box Using Artificial Neural Network (ANN), and Proximal Support Vector Machine (PSVM)." 9 August 2009.

Design, Analysis & Balancing of 5 Cylinder Engine Crankshaft

Yogesh S. Khaladkar[1], Lalit H. Dorik[2], Gaurav M. Mahajan[3], Anil V. Fajage[4]

[1,2,3,4] B.E. Student, Dept. of Mech. Engg. Dr.D.Y. Patil Institute of Engg. & Tech. Ambi, University of Pune, India.

Abstract: *The crankshaft is a backbone of internal combustion engine. So the design & analysis is major aspects to get high power transmission & efficiency. The selection of material is an important parameter while designing any mechanical component. The material should be high strength & capacity to absorb the shocks as well as fatigue. The material also have less wear tendency. The crankshaft should be high torque transmitting capacity. So to achieve these objectives high carbon steel are used for design & analysis purpose. This paper gives the idea about analysis as well as proper balancing of weights by using these three materials. The modelling is done by using solid work software & then analysis by using ANSYS software with Finite Element Analysis (FEA) method. The 5 cylinder engine gives the power stroke at 144 degree angle. By addition of counterweights & modified design these odd cylinders are balanced properly. The Finite Element Analysis Method is used to determine stress, strains & deflection at most stressed point which results into failure of shaft. Results obtained from analysis are used during weight optimization. The Shaft is analyzed using static analysis. For absorbing vibrations proper damping material is used to achieve the requirement of safe design. The optimization results into reduction of weight as well as cost.*

Keywords: ANSYS, Crankshaft,Damping, Finite Element Analysis, Optimization.

I. Introduction

1.1) Design:

Mechanical design includes weight optimizationas well as optimum size, shape, etc. against failureunder the application of operational loads. A good design should also minimize the cost of material and cost of production. Failures that are commonly associated with mechanical components which are broadly classified as:
(a) Failure by breaking of brittle materials and fatigue failure of ductile materials.
(b) Failure by yielding of ductile materials, subjected to non-repetitive loads.
(c) Failure by elastic deformation. The last two modes cause change of shape or size of the component rendering it useless and, therefore, refer to functional or operational failure.

Most of the design problems refer to one of these two types of failures. Designing, thus, involves estimation of stresses and deformations of the components at different critical points of a component for the specified loads and boundary conditions, so as to satisfy operational constraints.

1.2) Finite Element method:

In FEM, actual component is replaced by a simplified model, identified by a finite number of elements connected at common points called nodes, with an assumed behavior or response of each element to the set of applied loads, and evaluating the unknown field variable (displacement, temperature) at thesefinite number of points. The crankshaft is the most important moving part of internal combustion engine. It converts reciprocating motion into rotary motion. Since the crankshaft experiences a large number of load cycles during its working. The performance, durability, torque transmitting capacity, stress, strains, service life, fatigue failure and durability of this component has to be considered in the design process. It must be strong enough to take the downward force of the power stroked without excessive bending. So the reliability and life of internal combustion engine depend on the strength of the crankshaft largely. The torsional vibration appears when a power impulse hits a crankpin toward the front of the engine and the power stroke ends. If not controlled, it can break the crankshaft. Strength calculation of crankshaft becomes a key factor to ensure the life of engine. This study is about 5 cylinder engine crankshaft. The modelling of crankshaft is done by using solid work software. The Finite Element Method is used to calculate stresses & deflection of crankshaft by using ANSYS software. The main aim is to increase efficiency & balancing of crankshaft by weight optimization. Thus the reduction in weight results into material reduction. So the cost will be lower than the conventional engine. The 5 cylinder engine gives more efficiency than 4 cylinder engine. The material for crankshaft is Cast Iron. Other alternate materials on which analysis has been done are, Forged steel, high carbon steel.

II. Literature Review

V. Vijaykumar [1] presented a paper on analysis of crankshaft using finite element analysis method with ABAQUS software. The material specifications are reviewed. Paper gives idea about dynamic load acting on crankshaft during operation. To find critical stresses and maximum load for crankpin is calculated by analyzing the results obtained from ABAQUS.

Solanki et al.[2] gives the idea about the design of crankshaft depends upon dynamic loading and optimization can lead to shaft diameter to fulfil the requirement of automobile.

V. Mallikarjuna Reddy[3] this gives the invention about the problem occurs in 6 cylinder diesel engine. The model is made by using unigraphics and analyzed by using ANSYS.

III. Design Calculations for Crankshaft

The specification of diesel engine for Safari Dicor are tabulated as follows.

No. of cylinders	5
Bore(D)	85mm
Stroke	96mm
Displacement	2179cc
Compression Ratio	17.2:1
Max. Power	104.4KW @4000rpm
Max. Torque	320Nm @ 1700-2700rpm
Max. Gas Pressure	25bar

3.1) Deign of crankshaft:

When the crank is at an angle of Maximum bending moment. At this position of the crank, the maximum gas pressure on the piston will transmit maximum force on the crankpin in the plane of the crank causing only bending of the shaft.

Let 'D' be the bore diameter in mm,

P= Pressure intensity in N/mm^2

F_p= Gas load on piston in N.

Force on piston F_p= Area of bore× Max. Combustion pressure

$$= \pi/4*D^2*25*10^5$$

=14.18KN.

In order to find thrust in connecting rod, we should find out angle of inclination of connecting rod with line of stroke (i.e. angle φ)

$$Sin\varphi = Sin\theta/(l/r)$$
$$= Sin\theta/n = (sin35)/4$$
$$\varphi = 8.24^0.$$

Thrust in connecting rod $F_{CR}= F_p / cos\varphi$

$$=14.32KN.$$

Thus, thrust in C.R. is in tangential as well as radial direction which are as follows,

a)Tangential force on crankshaft, $F_T= F_{CR} \sin (\theta+ \varphi)$

$$=9.81KN.$$

b) Radial force on crankshaft, $F_R= F_{CR} \cos (\theta+ \varphi)$

$$=10.43KN.$$

Now, the reactions at bearings due to tangential force are:

$$H_{T1}= H_{T2}=F_T/2=4.9KN$$

Similarly, reactions due to radial force are:

$$H_{R1}= H_{R2}=F_R/2=5.21KN.$$

3.2) Design of crankpin:-

Let d_c be the diameter of crankpin. The bending moment at center of crankpin is given by

$$M_C=H_{R1}*b$$
$$=5.21*86=448.06Nm.$$

Twisting moment on crankpin is $T_c=170.68Nm$

The equivalent twisting moment

$$T_e=(M_c^2+ T_c^2)^{1/2}$$
$$=479.46Nm$$

Also equivalent twisting moment

Te=$(\pi/4 * d_c^3 *$Prem. Shear stress$)$

Permissible shear stress=35N/mm^2

From above equation

479.46= $\pi/4 * d_c^3 * 35$

d_c =45mm.

Diameter of crankpin=45mm.

C) Von mises stresses $M_{ev}=((K_b*M_c)+(0.5*K_t*T_c))^{1/2}$

M_{ev}=914.22N/mm^2.

IV. Modelling Of Crankshaft

The software used for modelling is Solidwork. The solidwork includes following parameters:-

1.Part Design

2. Assembly Design

3. Drafting

4.Sketch

5.3D modelling.
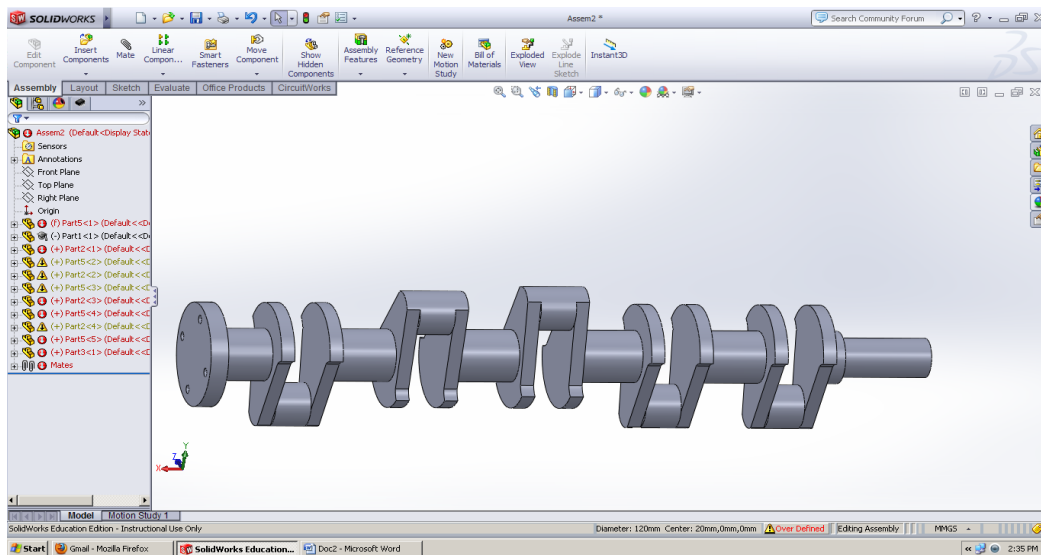
V. Meshing of crankshaft

The Meshing (Discretization) is the first step of Finite Element Method. In this step the component or part is divided into number of small parts. To analysis each element of the component meshing is done using mesh tool in ANSYS.
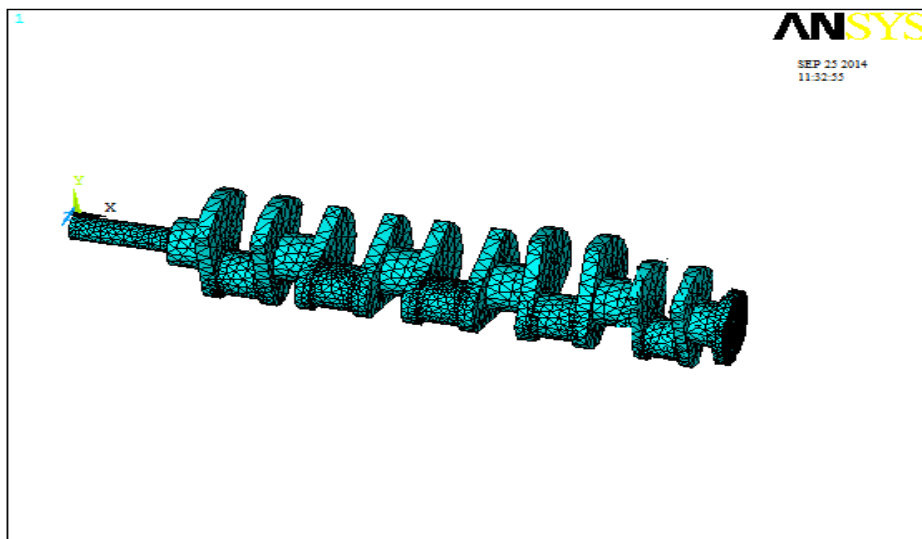
VI. Loading & Boundary Conditions

Crankshaft is a constraint with a ball bearing from one side and with a journal on the other side. The ball bearing is press fit to the crankshaft and does not allow the crankshaft to have any motion other than rotation about its main axis. Since only 180 degrees of the bearing surfaces facing the load direction constraint the motion of the crankshaft.
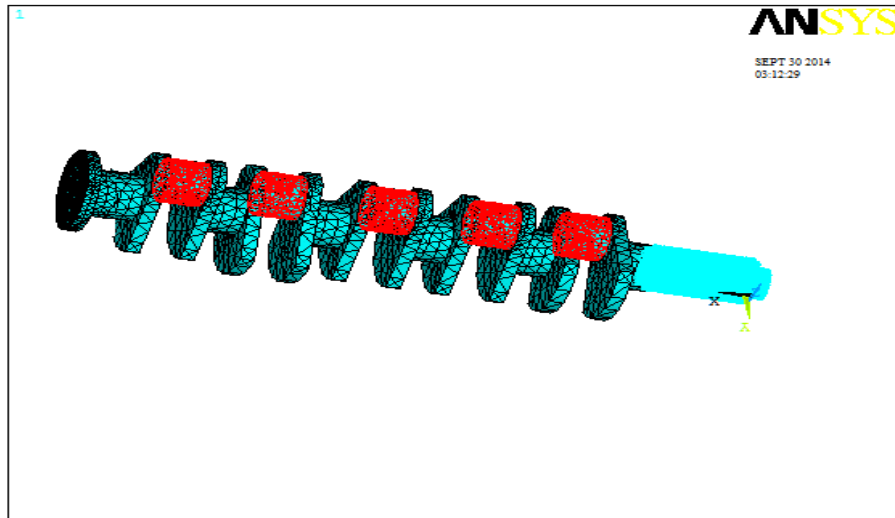
VII. Static Structural Analysis

After applying the boundary conditions & force the next step is that to perform static analysis of crankshaft. In this we are concern with deflection of crankshaft & stresses produced in crankshaft. The total deformation is shown in figure. The deformation is not same throught the length. It depends upon the load & boundary conditions. The red colour portion shows the maximum deformation while blue colour shows the minimum deformation. The maximum displacement is 5mm.
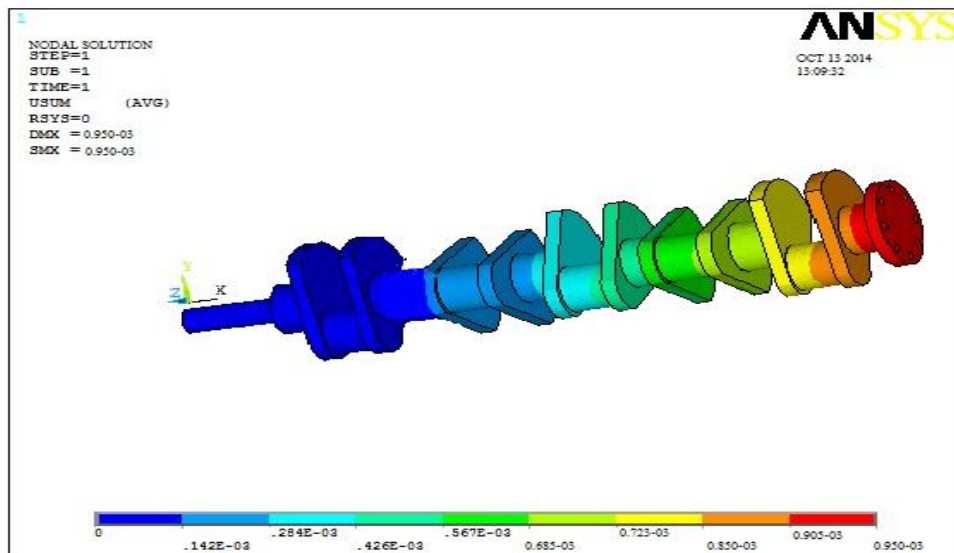
VIII. Results

By applying forces & boundary conditions, deformation of shaft generates stresses.

Sr.No.	Type Of Stresses	Theoretical	FEA Analysis
1	Von-Misses Stresses	914.22	950.0
2	Shear Stresses	110.25	120.7

IX. Conclusion

In this paper the crankshaft model is made by using solidworks and then analyzed by using ANSYS. The conclusions are made from the results are as maximum stresses occurs at the centre of crankpin. The maximum stress occurs at fillet between crank journal and crank cheeks. The edge of the crankshaft offers high stress. The practical results are matches to theoretical results, so Finite Element Analysis(FEA) is best method for analysis of permissible stresses. As there are 5 cylinders having efficiency equal to 6 cylinder, so our design gives the weight optimization as well as low cost. The materials used are appropriate having high capacity to absorb shocks and vibration with proper balancing.

REFERENCES

[1]. J. Meng, Y. Liu, R. Liu, (2011), "Finite Element analysis of 4-Cylinder Diesel Crankshaft" I.J. Image, Graphics and Signal Processing, vol 5, pp. 22-29.

[2]. Sreeraj Nair K., Kiran Robert and Shamnadh M. (2014) "Stress Analysis of IC Engine Cylinder Head". International Review of Applied Engineering Research.ISSN 2248-9967 Volume 4, Number 2 (2014), pp. 123-128.

[3]. Momin Muhammad Zia Muhammad Idris(2013)"Crankshaft Strength Analysis Using Finite Element Method". Momin Muhammad Zia Muhammad Idris / International Journal of Engineering Research and Applications (IJERA) ISSN: 2248-9622. Vol. 3, Issue 1, January -February 2013, pp.1694-1698.

[4]. V.Vijayakumar, T.Gopalakrishnan and Dr.R.Vivekananthan(2014) "Design and Contact Analysis of Crankshaft Using Abaqus". INTERNATIONAL JOURNAL OF RESEARCH IN AERONAUTICAL AND MECHANICAL ENGINEERING. vol.2, Issue.3, March 2014.

[4]. V.B. Bhandari. "Design of Machine Element" Mc Graw Hill Education.